Master's Thesis

Geotechnical characterization of the rock mass surrounding the Aljustrel mining compound

Tiago Rodrigues

Supervisors:

Univ.Prof. Dipl.-Ing. Dr.mont. Peter Moser

Prof. Dipl-Ing. Pedro Bernardo

31/10/2022

Chair of Mining Engineering and Mineral Economics
Department Mineral Resources Engineering
Montanuniversitaet Leoben

A-8700 LEOBEN, Franz Josef Straße 18
Phone: +43 3842-402-2001
Fax: +43 3842-402-2002
bergbau@unileoben.ac.at

Declaration of authorship

„I declare in lieu of oath that this thesis is entirely my own work except where otherwise indicated. The presence of quoted or paraphrased material has been clearly signaled and all sources have been referred. The thesis has not been submitted for a degree at any other institution and has not been published yet.”

Tiago Rodrigues

Preface, Dedication, Acknowledgment

This work could not have been written without the participation and assistance of a group people and entities to whom I would like to address my sincere appreciation.

To my supervisor, Professor Pedro Bernardo, for the determining scientific contribution, guidance and human support while developing this endeavor. His collaborative participation during my academic journey which has culminated with a professional opportunity in the mining industry has to be thanked particularly.

To ALMINA – Minas do Alentejo, S.A., on behalf of Engineer Daniel Rocha, for providing the data crucial to this work and giving permission to publish my dissertation. He has equally given me the opportunity to integrate a challenging project.

To Orica Mining Services Portugal, S.A. and Instituto Superior Técnico, on behalf of Manuel Rafael, for providing me with technical support while using their devices: seismograph and ultrasound equipment.

To my colleagues and friends, Diogo Mendes, Francisco Galante, Francisco Nogueira, Francisco Pinto, Gonçalo Matos, Guilherme Martins, Henrique Neves and Henrique Primitivo for the friendship and enjoyable moments.

To Helena Tello for the kindness, understanding and unconditional support while performing this dissertation.

Last but not least, I express my deepest gratitude to my parents, who have always encouraged me and directed their efforts towards my personal and academic development.

Abstract

In an underground production environment, the most evident impact from rock blasting activities are ground vibrations. In mining operations near urban areas disturbance and complaints on behalf of populations are not uncommon.

This document studies the ground surface geotechnical properties of the Aljustrel town (Alentejo province, Portugal). To achieve the objectives of this study, a database is considered compiling information relative to 2.175 vibration records measured at ten structures within different sections of Aljustrel between 2018 and 2022. These served as a basis to estimate, by means of multiple linear regression, 23 valid characteristic attenuation equations according to the mathematical expression presented by Johnson (1971). Such equations consider categorical variables like the existence of a rock mass discontinuity created by an initial production blast; section of the Aljustrel town where the records were monitored; geographical orientation between the blasting and the monitoring points; initiation pattern geometry; and time delay between adjacent holes. Results suggest that for reduced distances, the inexistence of a rock mass discontinuity directly above the blasted volume and the north-south direction influence the propagation of seismic waves released by the explosive charges, being that smaller maximum charges per delay are recommended in these situations. For great distance values, a spiral initiation geometry contributes to the measurement of greater vibration amplitudes.

A detailed study considering four structures, where the respective building materials' waves propagation velocity and geometrical parameters are measured, indicates that no significant vibration amplification caused by resonance has occurred for events registered at these locations.

Keywords:

Ground vibration, Prediction models, Natural frequency, Underground production blasting, Aljustrel mining compound

Zusammenfassung

In einer unterirdischen Produktionsumgebung sind die offensichtlichsten Auswirkungen von Felssprengungen Bodenvibrationen. Bei Bergbaubetrieben in der Nähe städtischer Gebiete sind Störungen und Beschwerden der Bevölkerung keine Seltenheit.

Dieses Dokument untersucht die geotechnischen Eigenschaften der Bodenoberfläche der Stadt Aljustrel (Provinz Alentejo, Portugal). Um die Ziele dieser Studie zu erreichen, wird eine Datenbank in Betracht gezogen, die Informationen zu 2.175 Schwingungsaufzeichnungen zusammenstellt, die zwischen 2018 und 2022 an zehn Strukturen in verschiedenen Abschnitten von Aljustrel gemessen wurden. Diese dienten als Grundlage, um mittels multipler linearer Regression 23 gültige charakteristische Dämpfungsgleichungen gemäß dem von Johnson (1971) vorgestellten mathematischen Ausdruck zu schätzen. Solche Gleichungen berücksichtigen kategoriale Variablen wie das Vorhandensein einer Diskontinuität der Gesteinsmasse, die durch eine anfängliche Produktionsexplosion verursacht wurde; Abschnitt der Stadt Aljustrel, in dem die Aufzeichnungen überwacht wurden; geografische Ausrichtung zwischen den Sprengungen und den Überwachungspunkten; Geometrie des Initiationsmusters; und Zeitverzögerung zwischen benachbarten Löchern. Die Ergebnisse deuten darauf hin, dass bei verringerten Entfernungen das Fehlen einer Diskontinuität der Gesteinsmasse direkt über dem Sprengvolumen und die Nord-Süd-Richtung die Ausbreitung der von den Sprengladungen freigesetzten seismischen Wellen beeinflussen, da in diesen Situationen kleinere maximale Ladungen pro Verzögerung empfohlen werden. Für große Abstandswerte trägt eine spiralförmige Initiationsgeometrie zur Messung größerer Schwingungsamplituden bei.

Eine detaillierte Studie unter Berücksichtigung von vier Strukturen, bei denen die Wellenausbreitungsgeschwindigkeit und die geometrischen Parameter der jeweiligen Baumaterialien gemessen werden, zeigt, dass für Ereignisse, die an diesen Orten registriert wurden, keine signifikante Schwingungsverstärkung durch Resonanz aufgetreten ist - Diskontinuität direkt über dem gesprengten Volumen und die Nord-Süd-Richtung beeinflussen die Ausbreitung von seismischen Wellen, die von den Sprengladungen freigesetzt werden, da in diesen Situationen kleinere maximale Ladungen pro Verzögerung empfohlen werden. Für große Abstandswerte trägt eine spiralförmige Initiationsgeometrie zur Messung größerer Schwingungsamplituden bei.

Stichwörtern:

Bodenvibration, Vorhersagemodelle, Eigenfrequenz, Produktionssprengung unter Tage, Bergbaukomplex Aljustrel

Table of contents

1. Introduction

The oldest records and evidence of Human activity date back to Prehistory. Examples of such evidence are rock art, ancient stone carvings, stone cores, flint tools and hammerstones. These elements have helped ancient cultures to develop themselves and to thrive in adverse conditions. As such, even before the first sedentary people, nomadic tribes have included geological materials in their daily life, fundamental to their survival. The importance of the Human dependency on natural raw materials such as stone and metals is well documented and served as an inspiration when naming the Stone, Bronze and Iron Ages. Initially, inorganic elements such as rocks, which were subject to further changes in shape and size were collected at the surface. However, after the discovery of excavation techniques, it quickly became evident that the subsurface was also rich in these components. After this discovery and subsequent development, the extraction of such materials has become an important activity for civilizations, being now known as mining.

According to some authors, mining, smelting and refining of metals has been documented since the Bronze Age (Darling, 2011). The final products of these activities were used to produce jewelry, coins, cutting and farming tools, and metal alloys.

In his work, entitled *De Re Metallica* and containing 12 books, Georgius Agricola describes mining exploitation methods, and both the smelting and refining processes which constituted the state-of-the-art in the 16th Century. This endeavor was the first one in the Mining Engineering field to be published. At this time, rock fragmentation was performed by means of picks and chisels which percussed against the rock mass disintegrating it along its discontinuities. However, if these discontinuities were inexistent, or if the rock revealed high resistance to excavation due to its hardness and/or abrasivity, bonfires would be utilized at the rockface. The increase in temperature would induce thermal expansion and workers would put out the fire by pouring cold water on it. The contact between the rock and cold water would cause a sudden contraction of the rockface, being that this abrupt variation in volume induced by a dilation-contraction cycle would form cracks and fractures within the face. After showing a vaster net of discontinuities, the rock was more easily excavated using the aforementioned percussion tools.

Until the Industrial Revolution, mining was characterized by small productivity and efficiency levels. Thereby, the emergence of new technologies such as steam machines and, later on, electric or diesel systems, has changed the paradigm in the mining industry once more rock could be excavated, transported and processed. Allied to this, pumping engines, initially developed by Thomas Newcomen in the 18th Century, permitted exploitations to work faster and for longer periods, in a safer environment and to advance in depth. Further, innovations in rock excavation techniques after the introduction of black powder into mining operations, and the inventions of the safety fuse, by William Bickford in 1831 and dynamite, by Alfred Nobel in 1867, contributed to a rapid development of the mining industry (Darling, 2011). It is worth mentioning that the advances in excavation methods have not only revolutionized Mining Engineering in the last three centuries, but also Civil Engineering, where these are necessary for the construction of dams, roadways, tunnels or water and sanitation infrastructure.

1.1. Fundamental principles of Mining Engineering

The evolution of some Engineering Sciences such as Mechanical, Civil and Electrical Engineering, has made it possible to produce even more sophisticated objects like cars, large structures such as dwellings, offices or cultural facilities, and electronic devices such as computers or sensors, respectively. Taking this into consideration, to allow the maintenance of the living standards nowadays, it is necessary to ensure a rational and sustainable management of raw materials including mineral resources. Likewise, one should also guarantee that the origin of these resources is as sustainable as possible, meaning that the extractive industry complies with its four underlying fundamental principles: safety, economy, maximized recovery of the resources and, most recently, environmental protection (Bernardo, 2004).

Like in every other activity, safety is the first and most important principle to consider in a mining exploitation. As an inspector general of mines in France, Frédéric Le Play's statement – *The most important thing to come out of a mine is the miner* –, reveals the industry's concerns over the workers occupational health and safety. Safety can be defined as the condition of safeguarding a person or an object connected to an industrial activity from a given hazard. Here, it is important to mention that the *person* is any stakeholder which is directly (workers) or indirectly (third-party) involved in this activity. An *object* may be a structure, equipment, fauna and flora, or a landscape.

The second principle (economy) is directly connected to the economic viability of an investment. Hence, the extraction of mineral resources can only take place if the unitary costs are lower than the commodity price on the market, i.e., if there is profit. One should highlight the increasing integration and internationalization of national economies that depend, most of the times, on foreign suppliers to purchase raw materials. This trend obliges companies to be competitive by pursuing state-of-the-art technology and optimizing operations, being able to lower production costs, thus maximizing the recovery of a mineral deposit. Most of the times, mine reserves change over time (dynamic process), due to commodity price fluctuations. As such, supply and demand – which influence the market price – have a direct impact on the analyzed principle.

The output products of mining activities (energetic, ore and industrial minerals, gemstones or construction materials) are characterized as non-renewable raw materials. The progressive exploitation of a mineral deposit leads to its depletion at a medium-long term. Thereby, resources have to be sustainably managed and exploited, and the recovery of a deposit has to be maximized. This maximization principle implies that companies should avoid selective mining, whereby high-grade ore is extracted and low-grade ore is left in the deposit, maximizing a company's profit. This unsustainable practice should be avoided and controlled by governments.

Lastly, with an increasing concern over ecosystems and nature degradation, most countries have created standards and legislation aiming at promoting the protection of stakeholders and societies. These mechanisms intend to encourage and oblige companies to pursuit the best available techniques and to mitigate environmental impacts that may result from the exploitation process, protecting the environment and contributing to a sustainable development of the society.

The four mentioned principles cannot be individually maximized. Likewise, a very economical operation may be hazardous and environmentally unsustainable, whereas an operation subject to stringent environmental guidelines on physical and chemical contaminants – dust and gases, respectively – may be expensive and originate a minimized recovery of the reserves. As such, a sustainable and well-dimensioned operation is one that balances the four fundamental principles and defends the interests of all stakeholders.

1.2. Dissertation subject framework

Two major classes of mining operations are common in the industry: open pit (surface) and underground mining. The first is defined as the removal of overburden from the topographic surface, if applicable, and consequent excavation of the orebody using horizontal benches. After removing overburden and waste rock, and producing tailings originated at the beneficiation plant, these subproducts are transported to a specified disposal site outside the final pit perimeter. In some cases, such as coal mining, subproducts may be disposed at the mined out area, if these do not pose a threat to the environment. This method is usually applied in shallow deposits of metallic or non-metallic minerals (including construction materials). Some advantages related to open pit mining are the following: higher productivity, lower costs and good recovery of the deposit, when compared to underground mining; and little ground support requirement. However, besides being limited to shallow deposits due to high stripping ratio values and high transportation costs for deeper operations, these require large disposal areas, tend to be associated with evident environmental impacts such as noise, dust and flyrock, and activities may be conditioned by the weather (Altiti et al., 2021). Underground mining methods, on the other hand, are used when the mineral deposit is sufficiently deep and due to technical, environmental or economic reasons open pit mining methods are not an option. If sufficiently deep, underground exploitations require complex infrastructure such as drifts, pillars, drawpoints, or shafts to transport rock and workers and to ventilate stopes and drifts. Normally, the following groups of mining methods can be applied: selective (cut-and-fill and shrinkage stoping), bulk (block caving, sublevel open stoping, sublevel caving and vertical crater retreat) and those used to mine (sub)horizontal mining deposits (room-and-pillar and longwall mining) (Abzalov, 2016). Such complex infrastructure involves greater production costs and, in some cases, lower levels of productivity. However, the main advantages of underground mining are the mitigation of environmental impacts like the ones previously addressed, lower visual impact and waste disposal areas comparing with open pit mining, and the possibility of stope backfilling. This reduces the necessity of large tailings storage facilities, improves ground stability, reduces the airflow demand and ore dilution, and provides a safer working area (Pagé et al., 2019). Nowadays, due to social (*social license to operate* – public acceptance) and environmental concerns, some companies opt for underground mining methods in shallow deposits rather than conventional open pit ones which tend to be associated with lower production costs, as mentioned before.

In underground mines, both mechanical rock excavation methods and excavation with explosives (drill and blast) are applicable. The first group comprises roadheaders, continuous miners, coal ploughs, impact hammers and backhoe excavators. In general, these are productive methods which work continuously and with lower operating costs. The possibility of automation and remote control diminish the miners exposure to hazards and the necessary workforce. In this category, roadheaders are a frequent option to some operations after its flexibility, mobility and ability to excavate selectively (Bilgin et al., 2014). Compared to drill and blast, mechanical excavation methods are responsible for less environmental impacts – less vibration, noise and rock mass damage; and most machines emit fewer toxic gases, once they include electric motors in their constitution. Furthermore, the excavation profile registers little overbreak, so floor, crown and rib surfaces are smooth. Nevertheless, competent rock masses characterized by great uniaxial compressive strength and abrasivity (usually defined by the CERCHAR Abrasivity Index – CAI) values may hinder the economic application of mechanical rock cutting methods such as excavation using roadheaders. Figure 1 summarizes three situations considering this equipment: rock mass economically cuttable by means of current mechanical excavation methods (green area); critical range where a rock mass may be economically cuttable with improved technology (new pick characteristics, design and layout – margin for research and development) and operating procedures (blue area); and rock mass that cannot be economically excavated using today's methods such as those relying on roadheaders (white region).

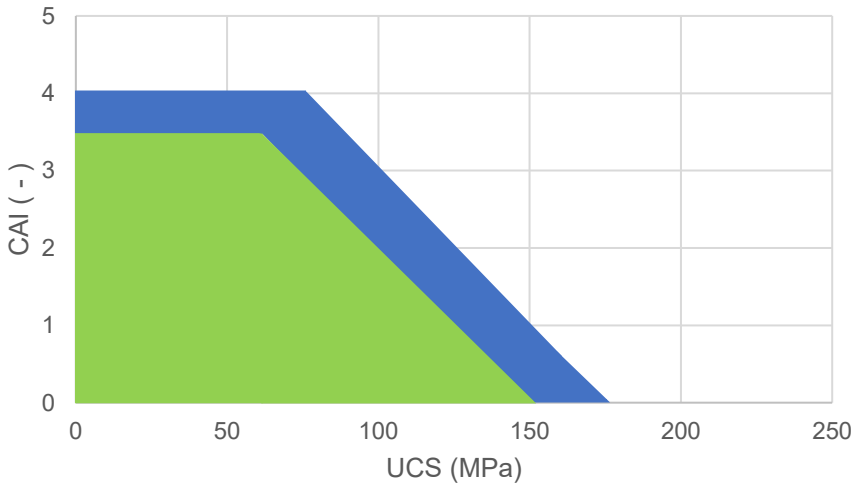

Figure 1 - Range of CERCHAR Abrasivity Index and Uniaxial Compressive Strength that define the applicability of roadheaders (adapted from Hartlieb, 2013).

Considering the uneconomical range in Figure 1, drill and blast excavation methods are a suitable alternative in this situation. Moreover, high investment costs in mechanical excavation methods and lower flexibility in terms of section to be covered (determined by the boom extension or plough surface area) may be reasons to excavate a rock mass using explosives.

Despite its cost-benefit relationship and versatility (usage in mining environments, trench excavation or underwater construction works, for example) the application of explosives, has undesirable side effects which in most cases cannot be ignored given the proximity between the blasting

point and the various parties to protect such as people, structures, equipment and ecosystems. The predominant environmental impacts that may occur as a consequence of drill and blast are rock mass instability after overbreak, flyrock, noise/air blast, dust and ground vibrations. The majority of these impacts are circumscribed to the mining operation perimeter. However, once they are perceived at a greater distance, vibrations may be a source of concern, being this a common reason for complaints and disputes between neighboring communities and mining companies.

Given the amount of energy released after a blast, which is directly proportional to the quantity of explosives employed per delay, it is necessary to register ground vibrations at a reduced distance from the blast. It is not uncommon to measure and feel vibrations more than one kilometer away from the excavation point. Hence, this phenomenon is associated with two critical aspects: disturbance of people and damage to objects like structures (dwellings or cultural heritage) and equipment located in the surroundings of the operation. Likewise, considering the damage potential of ground vibrations, most countries have created or adopted regulations and norms, suggesting limits concerning ground vibration amplitudes measured at nearby structures, to minimize damage risks. Additionally, human exposure to blast-induced vibration is also regulated in some nations.

Since 1983, there is a Portuguese technical document that recommends vibration velocity limits originated from geotechnical activities (NP 2074). The main purpose of the definition of conservative values is to protect structures (private and public) from vibrations due to blasting or similar events. This was later on updated, in 2015, with even more restrictive vibration amplitude values. Considering this technical framework and in order to comply with it, companies are recommended to design blasting patterns after predicting vibration velocities at a given distance defined by a receiver which is intended to protect, ensuring that this value does not exceed the threshold limit value. Usually, the blast design process is carried out after estimating a vibration velocity propagation model.

Lastly, given the amplification effect caused by resonance, it is important to consider the dominant frequency of the blasting event and the monitored structures natural frequency.

1.3. Study objectives and organization

This dissertation is going to analyze more in detail the use of drill and blast as an excavation method in an underground environment characterized by a complex geology, where the most relevant and perceptible secondary effect are ground vibrations. The area of study is a mining town located in southern Portugal, where two mines (Feitais and Moinho) are currently active and producing base metals employing sublevel open stoping and longitudinal bench and fill as the main methods of ore excavation. Despite the existing social license to operate and considering the proximity of the mines to residential areas, the license holder has been carrying out monitoring campaigns to assess the exploitation’s impacts like the visual one and others caused by noise and, most importantly, vibrations originated by blasting.

In the present work, data collected during a four-year period and using engineering seismographs are going to be considered and analyzed (according to structural and human response vibration standards) with the aim of modelling ground vibration amplitude prediction equations that characterize the mining area under study in a dynamic way. Multiple models will be estimated, considering different operational and geographical scenarios, and geological factors. As operations are advancing towards the urban area and closer to the surface, the existence of such tool is becoming increasingly relevant. The resulting models would then allow a more accurate blasting pattern design, considering vibration amplitudes as the dependent variable, hence ensuring a more sustainable excavation process that complies with the technical framework in force, not compromising the surrounding structures integrity or disturbing populations. Initially, two independent variables are going to be included in the model. The second stage will take into account other variables such as the section of the studied area, the initiation pattern geometry and direction between the source and the receiver. Additionally, the time delay between holes is going to be considered, pursuing a greater coefficient of determination between the experimental data and the regression models. By including some of these variables, the main goal is to determine optimal timing and initiation sequence patterns that maximize the explosives energy effectively consumed in fragmentation rather than in adverse undesired effects. Moreover, one intends to assess eventual directions and regions in space through which stress waves travel without suffering considerable attenuation. Likewise, other preventive mechanisms will be suggested as an attempt to mitigate the measured vibration velocities at a certain location, thereby ensuring that these are below the recommended limits. An additional methodology, aiming at testing the application domain of a formula to estimate some of the monitored structures natural frequency, is going to be performed. This will culminate with an assessment on the existence of resonance at the considered structural elements.

Hence, this document consists of eight chapters which can be grouped in two parts as follows. As an initial approach, the first part constitutes a theoretical framework that describes the most relevant properties of explosive substances and respective importance, concerning rock mass excavation. The most common blasting patterns and basic principles of rock and soil dynamics are addressed here. Moreover, this section analyzes one of the secondary effects of drill and blast, ground vibrations, as well as the respective mitigation and monitoring measures. Lastly, given the scope of this work, a brief introduction to ground vibration amplitude prediction models and some of the most prominent European ground vibration monitoring standards, with emphasis on structural damage and human discomfort is carried out.

The second and last part of this dissertation comprises a historical, geographical and geological framing of the studied area. The methodology used to collect real data from diverse production blasts in the two considered mines, and respective analysis and formulation of vibration prediction models are described. Finally, to achieve the proposed objectives, not only regression models are estimated, but also an optimal time delay pattern is suggested, with the purpose of decreasing the energy transmitted through the rock mass upon blasting. A study considering the effect of resonance at four different structures is also performed, after determining their respective natural frequency.

2. Application of explosive substances in rock mass excavation

Given the amount of energy released by explosive products, it is relevant to understand the hazards while applying it in geotechnical activities to avoid eventual fatalities related to an improper handling and application of explosives, and to mitigate the impact of rock blasting on descriptors in the vicinity of these operations. This is fundamental, once people often associate the intensity of secondary effects related to drill and blast with an uncontrolled or incorrect use of explosives. As such, an updated knowledge of the existing substances available on the market and best available techniques is essential to ensure a safe environment within and around mining operations, guaranteeing and maintaining the social license to operate.

In this section, a broad description of the explosive substances composition, characteristics and fields of application in geotechnical activities is performed. After discussing the importance of each blasting pattern geometrical parameter for both underground and open pit scenarios, a special emphasis is given to ground vibration. Concerning vibration amplitudes, the physical properties used to describe it and its impact on structures are mentioned. Additionally, the importance of frequency as a structural damage assessment criterion, monitoring campaigns relevant outputs and measures to mitigate vibrations are discussed. The rock fragmentation mechanism during a detonation is also addressed.

2.1. Mining operations

To work efficiently and safely, mining exploitations rely on two kinds of operations: unit and auxiliary ones. Unit operations have a direct influence on the excavation process of the rock mass, contributing to the recovery of the mineral of interest. These contribute to the mining advance and depend on auxiliary operations. The second group usually supports the production process (Bernardo, 2004). Table 1 compiles the two different types of mining operations and provides examples for both cases.

Table 1 - Typical mining unit and auxiliary operations (adapted from Bernardo, 2004).

<table>
<tr><th colspan="2">Unit operations</th><th>Auxiliary operations</th></tr>
<tr><td>Drilling</td><td rowspan="2">Mechanical excavation</td><td>Hoisting</td></tr>
<tr><td>Blasting</td><td>Pumping</td></tr>
<tr><td colspan="2">Loading</td><td>Ventilation</td></tr>
<tr><td colspan="2">Hauling</td><td>Illumination</td></tr>
<tr><td colspan="2">Primary crushing</td><td>Ground support, survey, maintenance, etc.</td></tr>
</table>

The unit operations described above constitute a cyclical process that is repeated after each advance, i.e., after removing the intended volume of rock submitted to the application of excavation mechanisms. Due to the importance of blasting to this work, this operation is going to be thoroughly analyzed in the following chapters.

Generally, open pit and underground mining methods do not reveal considerable variations with regards to the involved unit operations. Considering the underground environment, illumination and ventilation play a crucial role, whilst in open pit operations only the first may be necessary in particular situations. Stripping, on the other hand, is only observed in open pit mines or quarries, once the access to the deposit is made through the surface. The following schemes (Figures 2 and 3) aim to describe the two considered production scenarios and highlight the most evident differences between them:

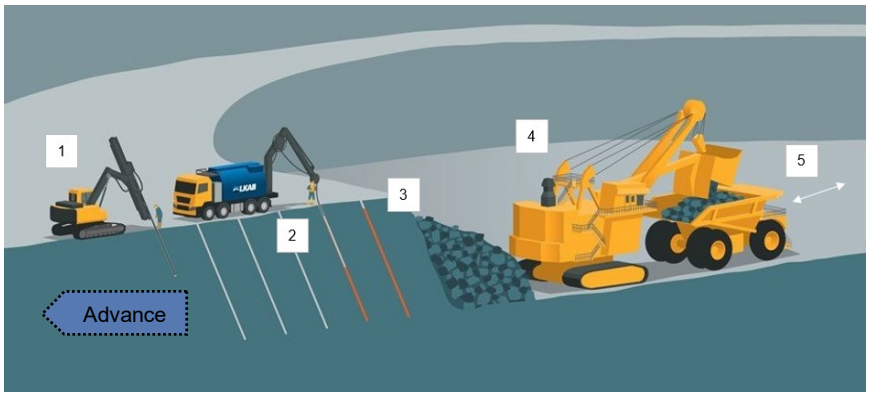

Legend:
1 - Drilling
2 - Loading the drillholes with bulk explosives
3 - Blasting
4 - Loading
5 - Hauling

Figure 2 - Open pit operations in hard rock (adapted from LKAB, 2022).

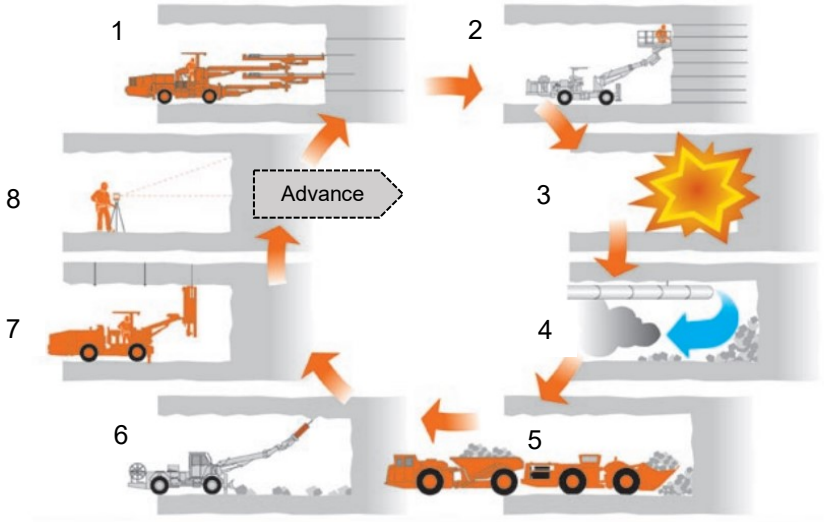

Legend:
1 - Drilling
2 - Loading the drillholes with explosives
3 - Blasting
4 - Ventilation
5 - Loading and hauling
6 - Scaling
7 - Ground support
8 - Surveying

Figure 3 - Underground (drift) operations in hard rock (adapted from Heiniö, 1999).

Apart from the aforementioned differences between both production environments, scaling is usually carried out in underground mines where the rock face is required to be as intact as possible to be further supported. In underground tunneling there is only one free face, whilst in open pit mining this number is not smaller than two. Despite not represented in Figures 2 and 3, in most cases, crushing

and beneficiation succeed loading and hauling in the production process to obtain the final sellable product (Table 1).

Considering the second principle of mining engineering (economy) and a competitive globalized market, companies have to perform an integrated and intensive study on all unit operations as a whole (Figure 4).

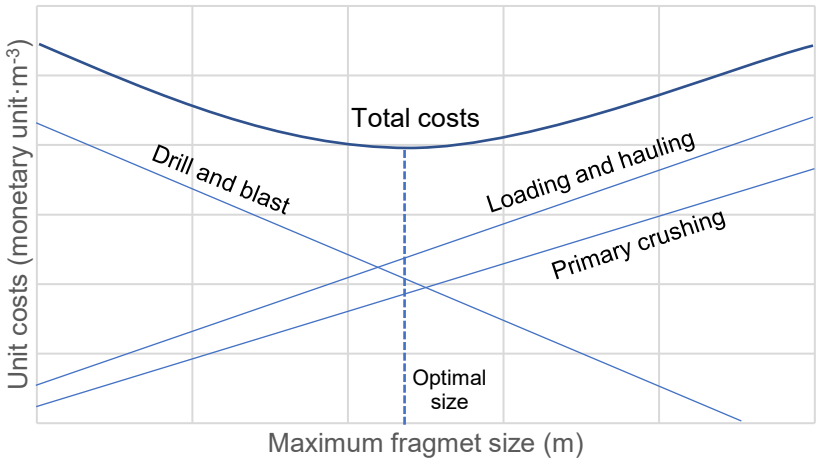

Figure 4 - Correlation between the unit and total costs and fragment size (adapted from Bernardo, 2004).

As is evident from Figure 4, the minimization of one operation does not imply that the total costs are near the optimal point (defined by an optimal fragment size). Considering this aspect, each operation has to be fully understood and adjusted on a regular basis in such a way that the integrated system is as efficient, economical and sustainable as possible. In this regard, drill and blast has to be associated with monitoring plans with the objective of registering, in real time, all the key performance indicators, allowing production managers to perform the necessary changes when sudden variations in the rock mass geology or equipment performance occur. This also contributes to the compliance of the fourth fundamental principle (environmental protection).

In the geotechnical domain, to optimize and ensure safety in rock excavation using civil explosives, it is important to understand the definition of explosive, its properties, available products on the market, how to design a blasting pattern and mitigate its environmental impacts and, most importantly, the legal and technical bases governing the use of explosives that intend to ensure the execution of an operation which is safe to both people and structures. The following sections have the objective of describing the mentioned elements.

2.2. Explosive substances properties and product selection

Explosive substances are chemical compounds or a mixture of compounds which, when initiated by friction, impact or heat, decompose very rapidly, releasing substantial amounts of energy in

the form of heat, gas and shock. Two major categories of reactions within explosives can be differentiated: deflagration and detonation. The first is characterized by a rapid combustion of the explosive, although this velocity of reaction is inferior to the sonic velocity (about 340 $m \cdot s^{-1}$). This reaction produces mainly heat and gases. On the other hand, detonation occurs when the rate of reaction exceeds the speed of sound, thus producing a shockwave (Heiniö, 1999; Bernardo, 2004; Lusk and Worsey, 2011). Usually, explosives can be used for both civil (commercial) and military purposes. Whitin the scope of this work, only civil explosives are going to be analyzed. Commercial explosives register detonation velocities that range from 1.500 $m \cdot s^{-1}$ to 7.830 $m \cdot s^{-1}$, generating a great volume of gases (around 1 liter per gram of product) at extremely high temperature (1.500 to 4.000 ºC) and pressure (2 to 40 GPa) values (Aimone, 1992; Lusk and Worsey, 2011).

Since the introduction of black powder in mining projects, more innovative explosives formulas have been discovered, revolutionizing the industry at a gradual rate. After the discovery of nitroglycerin by an Italian chemist in 1846, Alfred Nobel invented dynamite (in 1866), which would be widely used in mining endeavors later on. Since 1950, dynamite has been replaced by cheaper and safer ANFO (Ammonium Nitrate – Fuel Oil) products. This last formula, once applied in drillholes in the bulk form, poses a threat to the environment when dissolved in water, given its toxicity. As such, when drillholes containing water are loaded with ANFO products, there is the risk of contamination of the surrounding aquifers (Bernardo, 2004). Some authors mention that at high temperatures, ANFO reacts exothermally with pyrite (hot ground), originating spontaneous unplanned blasts. This reaction can be delayed by including urea and potassium in the ANFO chemical composition, nevertheless these elements do not prevent such hazard from occurring (Miron et al., 1979). These two factors contributed to the development of the most widely used explosives formula nowadays: ammonium nitrate-based emulsions. According to FEEM (as cited in Bernardo, 2017), in 2015, the emulsions, ANFO and dynamite market share in Europe represented 65,7 %, 26,8 % and 7,5 %, respectively. Usually, civil explosives are consumed in the bulk (ANFO and emulsions) or in the packaged (dynamite and emulsions) form, depending upon the blast size.

A successful blast is always supported on a proper and planned blast design. This design includes the selection of explosive, which depends upon economic, environmental and field conditions. Hence, the explosive substances chosen must ensure that the excavation unit costs are close to the lowest possible point, without disregarding the required displacement and degree of fragmentation of the rock (Figure 4) and the possible environmental impacts. According to Dick et al. (1983), the following aspects have to be considered when selecting the explosive products to be applied:

1. Explosive costs – the unit cost of explosive products is key in their selection. Ammonium nitrate-based explosives (namely ANFO) are the most competitive ones on the basis of cost per unit of energy. Depending on the proportion of nitroglycerin in dynamite, ANFO products are four to six times cheaper than the first one.
2. Charge diameter – this parameter is limited by the borehole diameter and by the critical diameter of the explosive. ANFO's efficiency increases proportionally to the charge diameter. The drillhole diameter can be changed. However, the critical diameter of the explosive cannot.
3. Rock blastability – geological and geotechnical characteristics of the rock mass must be assessed and taken into consideration. Hard and dense rocks contribute to expensive drilling activities and difficulties in the fragmentation process. Once explosives with high velocity of

detonation (VOD) are more efficient in fragmenting competent rock masses, the proportion of nitroglycerin is to be considered when blasting in such conditions, given the fact that this substance increases the VOD and thus the released energy. Aluminum, on the other hand, increases the released heat of explosion and consequently the relative effective energy, contributing to a greater detonation pressure.

4. Water conditions – when drillholes contain water, water-resistant explosives may be preferred over granular ones like ANFO. However, this explosive can be used if packaged in a plastic container forming a cartridge, or if applied into a hole lined with a water-proof liner, although this solution may have a limited effectiveness due to the possibility of rupture.
5. Fumes release – in underground environments, the release of toxic fumes after a blasting event is an occupational concern. Some explosives formulas like dynamite and emulsions are preferred over ANFO, after their oxygen balance that minimizes fumes emissions. Further to this, an improper explosive ingredient mix may cause non-optimal fumes emissions.
6. Other conditions – like ambient temperature (low temperatures may cause explosives insensitivity); propagating ground (that may cause unintended detonations between drillholes or dead pressing); storage and transportation requirements (magazines have to be designed in such a way that weather conditions or fires have a minimal impact on the stored explosives and the risk of theft is minimized); and the existence of explosive atmospheres (hot grounds), which require the usage of determined explosives to avoid unplanned blasts.

Up to this point, only secondary explosives have been described. Comparing with primary explosives, these are less sensitive to friction, impact or heat. Additionally, they require at least a primary explosive for initiation (Lusk and Worsey, 2011). Thus, initiation systems include primary explosives in their composition and examples of these products are detonating cords, detonators and boosters.

To safely initiate dynamite, in 1863 Alfred Nobel invented the detonator. This simple system consists in a slow-burning safety fuse attached to a blasting cap that contains primary and base charges. Due to the fact that a cutoff in the safety fuse or its mixture with water may leave uninitiated detonators, Nobel's invention was quickly superseded by electric detonators – invented in 1895 (Lusk and Worsey, 2011).

Electric detonators that work with millisecond delays were developed in 1950's and allow safer blasts with minimized side effects. These are initiated by an electrical resistance which heats up and initiates a pyrotechnic element. In consequence, the delay element is ignited, initiating both the primer and the base charge. They have some drawbacks attached to them, such as the limited number of delays per blast, the delay scatter which can contribute to overlaps (aggravating the blast environmental effects) and its sensitivity to stray currents, lightning events or batteries (Lusk and Worsey, 2011).

In the second half of the twentieth Century shock-tube non-electric detonators were introduced onto the market. These elements are initiated by shock and allow a larger number of delay timings, being the most cost-effective detonator available. Furthermore, this system is not sensitive to stray currents and is more resilient than electric detonators which depend on electrical wires. The usage of these detonators requires surface connectors, which determine the hole delay. However, these have some disadvantages like the inability to test the system connections, the associated delay scatter and the limited number of delays, which for drift or tunnel blasts with a considerable number of holes implies

that some detonators are initiated at the same instant, increasing the maximum charge per delay and consequently vibration amplitudes (Lusk and Worsey, 2011).

Lastly, in the 21st Century, programmable electronic detonators were developed, offering a considerable flexibility in the delay design – greater than that of non-electric detonators. These systems can be remotely initiated by a unique exploder (*blast box*) and have an incorporated chip used to control the delay timing, which uses electrical energy stored in one or more capacitors to supply power for timing clock and initiation energy. Compared to the preceding detonators, the timing error associated with electronic detonators is lower (around 1 ms or 0,01 %). Hence, it is possible to control overlaps, mitigating environmental effects such as vibrations and flyrock. These detonators also improve fragmentation, decrease overbreak and allow the frequency control of ground vibration, being this an aspect to be later described. Nevertheless, the considerable detonator costs and the necessary *blast box*, increase of the unit costs related to blasting using electronic blasting systems (Lusk and Worsey, 2011).

The second initiation element to be described is the detonating cord. Invented in the early 20th Century, the detonating cord initiates explosive charges radially, once it is placed in parallel to them along the hole, connecting different drillholes. Given its reduced linear charge, this penthrite-based explosive is frequently used in presplitting or in the contour series of underground tunnels (to be later described). The main advantages of detonating cord are its resistance to tension, abrasion and humidity (given its waxed or plastic coating), safety and ease of handling, and the available linear charges – that vary from 3 $g \cdot m^{-1}$ to 100 $g \cdot m^{-1}$ – which can be chosen depending on different site requirements. Nonetheless, the usage of this initiation system does not allow precise delay timings, may contribute to misfires due to the fact that the cord can be ripped apart, and contributes to an increase in the blasting side effects like noise, air blast, dust and flyrock (given its exposure on the surface, between drillholes) (Lusk and Worsey, 2011).

Like the detonating cord, boosters have a high VOD (around 7.000 $m \cdot s^{-1}$). They are generally used together with a detonator to initiate a low-sensitivity bulk explosives column, forming a primer. A booster is generally composed by nitroglycerine, penthrite or pentolite. It is water-resistant, safe to handle and applicable in the following temperature range: -40 ºC to 70 ºC (Lusk and Worsey, 2011).

2.3. Rock fragmentation mechanism in blasting

In rock blasting, the energy released during detonation results in rock fragmentation and in the previously mentioned five environmental side effects: overbreak, flyrock, noise/air blast, dust and ground vibrations. This chapter analyzes the rock fragmentation mechanism originated by the energy released by civil explosives.

The detonation of an explosive charge within a hole drilled in a rock mass promotes fracturing of the surrounding rock and consequent failure. According to Winzer and Ritter (1980) (as cited in Dowding and Aimone, 1992), this process is associated with two distinct phases of breakage mechanism:

1. Effect of stress waves generated from the detonation shock force – the generated shock wave travels into the rock with a velocity that depends on the rock and explosive properties, violently and dynamically disturbing the rock mass within a reduced time period. The cylindrically divergent wave gradually decays in peak pressure amplitude and is described by both a stress and radial component.
2. Effect of detonation gas pressure within the borehole – upon detonation the formed gas products increase the borehole and adjacent cracks pressures. These pressures promote the extension of the existing radial cracks and the formation of isolated blocks, increasing fragmentation. Usually, this phase occurs during a period longer than the initial one.

Figure 5 depicts the sequence of events during a rock blast close to a free face.

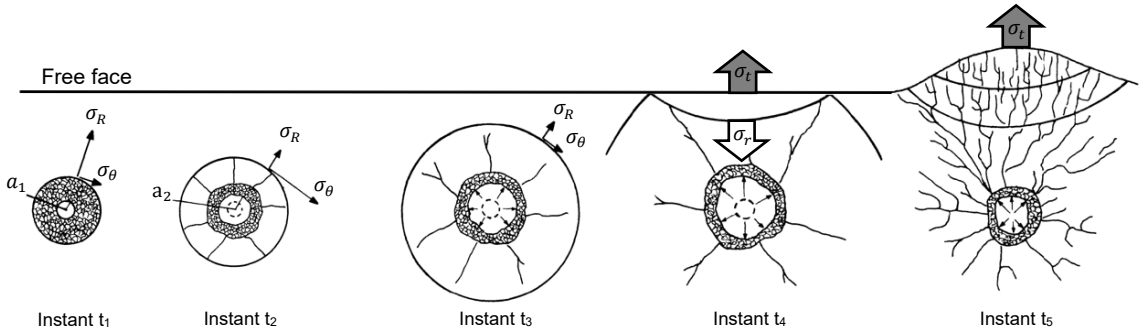

Legend: a_1, a_2 – drillhole expansion; σ_R, σ_θ – radial and tangential stress components; σ_t, σ_r – transmitted and reflected stresses

Crushing around the borehole	Radial cracking	Seismic propagation of shock wave Beginning of gas expansion	Beginning of fragmentation (after the wave reflection)	Burden movement, face slabbing and crack network formation after gas expansion
First phase				Second phase

Figure 5 - Temporal sequence of events occurring in the rock mass (near a free face) after detonation (adapted from Dowding and Aimone, 1992).

The described phases act together, promoting local pressure values greater than the rock dynamic resistance. According to Figure 5, close to the drillhole, the radial component of the stress wave (σ_R) is compressive, exceeding the dynamic compressive strength of the rock. At this stage (t_1), the rock surrounding the drillhole behaves like a fluid, showing no elastic properties. The attenuation of σ_R below the rock strength defines the end of the crushing zone, which ranges from two to four drillhole radii away from the center of the drillhole.

As the shockwave travels away from the center of the borehole σ_R is attenuated below the rock strength and the tangential stress component (σ_θ) increases, overpassing the dynamic tensile rock strength, creating a fractured area that can be extended up to 50 borehole radii away (t_2).

As the shock wave is further attenuated in such a way that the involved stresses occur below the rock elastic limit, the fractures cease and the wave travels away in a radial form as an elastic sound wave (t_3). The energy released by the explosive in the form of gases contributes to the propagation of the existing radial fractures.

Instants t_4 and t_5 are characterized by the enhancement of fracture patterns near the free face, after the transition of σ_R from a compressive to a tensile wave as it is reflected (σ_r) at the free face. Multiple reflections of transmitted and reflected waves occur, promoting successive fracturing, thus

originating new cracks in the vicinity of the drillhole. The originated fragmentation is also dependent on preexisting geological discontinuities.

Given the amount of energy released during a blasting event, the knowledge of the seismic or elastic zone is of importance, principally in the case where there is the risk of vibration-induced damage to structures. At this zone, like in natural seismic events, stress waves prevail (Bernardo, 2004).

As discussed in chapter 2.2., various aspects contribute to the selection of the explosive to be applied in an excavation activity. However, to maximize the energy efficiency and minimize the energy released to the environment in the form of noise and air pressure, some of the explosives properties have to meet the rock characteristics: impedance matching of these elements. Equation 1 denotes the calculation of the characteristic impedance (I_P) in a given medium.

$$I_P = \rho \cdot c \qquad \text{(Equation 1)}$$

Where ρ represents the medium density (kg·m^{-3}) and c its waves propagation velocity (m·s^{-1}). The characteristic impedance of a given material consists in the resistance with which the shock waves propagate through it.

As such, when considering the rock mass density and the waves propagation velocity its characteristic impedance can be calculated using Equation 1 and a given explosive is chosen in such a way that both impedance values are similar. After selecting a particular explosive product to be applied, the maximum theoretical pressure within the explosive column (detonation pressure) can be calculated (Equation 2).

$$P_D = \frac{\rho_e \cdot VOD^2}{4} \qquad \text{(Equation 2)}$$

Where the P_D is the detonation pressure (Pa), ρ_e is the explosive density (kg·m^{-3}) and *VOD* is the characteristic velocity of detonation (m·s^{-1}), as seen before. It should be noted that the detonation pressure is directly linked to the crushing pressure (fragmentation), whilst the released gases are related to the fractures propagation and displacement of the formed fragments during the blast. Given the direct proportionality between the detonation pressure and the released energy, it is expected that greater values of the first originate greater ground vibration velocities for fixed ground conditions and distance values.

2.4. Conventional blasting patterns

According to Bernardo (2004), blasting pattern is a technical document where one defines the drilling works to be carried out at the working face and the respective explosive charges to be applied, both in quantity and quality, aiming at excavating hard rock which cannot be economically or technically excavated by means of conventional mechanical excavation methods. Despite considering economical aspects and comparing the different excavation methods available, a blast design also takes into consideration environmental restrictions and assigns a determined firing sequence with a predefined

delay timing in such a way that the explosives energy is efficiently used in the excavation and undesired side effects of the blast are mitigated.

This chapter intends to describe different blasting patterns both in open pit and underground production scenarios, highlighting the geometrical parameters involved and the way these may vary according to different rock mass properties.

2.4.1. Open pit excavations

In 1963, Ash presented linear numerical relationships concerning geometrical parameters of an open pit bench blasting pattern, which are validated and widely used in quarries and mines worldwide (Hustrulid, 1999). Namely in open pit operations, empirical formulas are commonly used to describe the geometrical properties of bench blasting patterns (Figure 6).

Legend:
B – Burden
S – Spacing
H – Bench height
T' – Stemming
G – Subdrilling
L – Drillhole length
Ø – Drillhole diameter
CC – Column charge
BC – Bottom charge
TC – Total charge

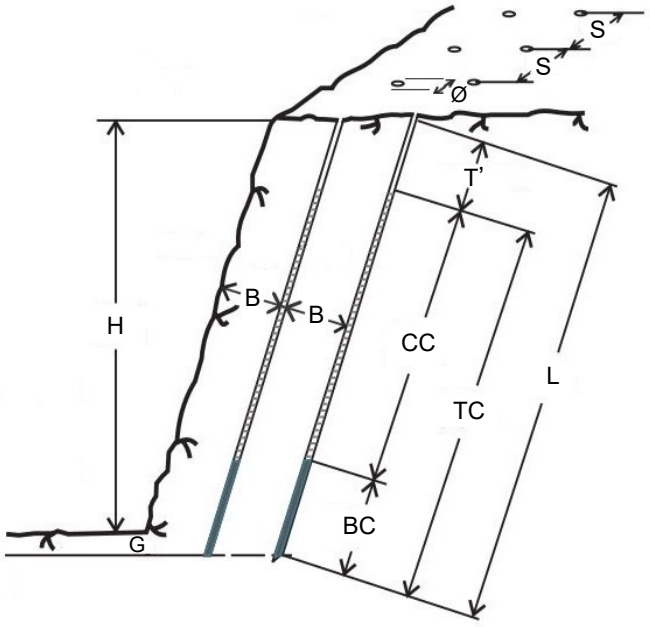

Figure 6 - Main geometrical parameters of a bench blasting pattern (adapted from Heiniö, 1999).

According to Ash's work, the geometrical parameters present in Figure 6 are dependent upon the drillhole diameter, which may vary based on production and environmental restrictions and geological conditions. As such, this author proposes the utilization of a set of empirical constants (K_i) varying within fixed range values which depend on characteristics like the explosives density, rock mass geology, timing between holes, environmental concerns (mainly on air blast and flyrock) and planned production volume (Table 2).

Table 2 - Geometrical design of a bench blasting pattern after Ash (adapted from Gama, 1998, as cited in Bernardo, 2004).

Geometrical parameter	Empirical constant	Expression	Range of variation	Depending on:
Burden (B)	K_B	$B = K_B \cdot Ø$	$25 \leq K_B \leq 40$	Explosive density and rock mass strength
Spacing (S)	K_S	$S = K_S \cdot B$	$1{,}25 \leq K_S \leq 5$	Delay interval between adjacent charges
Bench height (H)	K_H	$H = K_H \cdot B$	$1{,}5 \leq K_H \leq 4$	Production volume
Stemming (T')	$K_{T'}$	$T' = K_{T'} \cdot B$	$0{,}5 \leq K_{T'} \leq 1$	Environmental concerns on noise and flyrock
Subdrilling (G)	K_G	$G = K_G \cdot B$	$0{,}2 \leq K_G \leq 0{,}5$	Bench height and floor roughness

Table 2 shows that the burden – directly proportional to the drillhole diameter (Ø) – influences the values for the remaining geometrical parameters. As such, patterns with greater hole diameters tend to be wider (greater burden and spacing), and have longer drillholes (once subdrilling increases) and greater bench heights, being more productive. This, however, increases the average grain size resulting from the blast (which may require secondary fragmentation), the risk of flyrock and rock mass instability after overbreak, and most importantly, the risk of ground vibrations and noise. In the case of pronounced bedding at the toe bench, subdrilling may be dismissed ($K_G = 0$). In Portugal, the Decree-Law nº162/90 (Article 126) sets the maximum bench height in open pit exploitations at 15 m. After reclamation, this value cannot exceed 10 m. In several cases, given the imposed legal restrictions, *H* is defined *a priori*, conditioning the calculation of the remaining geometrical parameters.

It is worth mentioning that the empirical formulas presented in Table 2 serve as a first approximation in the design of a blasting pattern. Hence, if the calculated geometrical parameters are not economically (Figure 4) nor environmentally optimal, these should be adjusted according to the site properties and requirements to mitigate the side effects of the excavation process (with a particular emphasis on vibrations) and/or to minimize the mining operation unit costs.

In open pit blasting patterns, there is an uneven energy distribution along the explosives column (Figure 6). Given the greater confinement at the bench toe which offers more resistance to the energy released by the explosives, a denser bottom charge (with greater P_D – Equation 2) is applied in this region. As such, the stress released during the blast has to overcome the rock resistance at this part of the bench, so that failure occurs. The bottom charge has also the role of initiating the column charge, which normally has a lower density, is associated with lower costs and generates a greater volume of gases. As an initial approximation, one of the used criteria to estimate the bottom charge (BC) is based on the estimated burden (B) (Equation 3) (Bernardo, 2004).

$$BC = 1{,}3 \cdot B \qquad \text{(Equation 3)}$$

Once the burden (B) is usually determined in meters, the length of the bottom charge is estimated considering the same unit.

2.4.2. Underground excavations

Underground blasting rounds can be divided into two basic types: those with one free face and those with more than one free face. The first is used in drifts, tunnel and shaft rounds, and in certain room-and-pillar operations. Blasting rounds with more than one free face are used in open stopes, large-diameter tunnels using bench methods and sublevel caving. It is common that multiple-face rounds are designed in a similar way to surface blasting, where two to four free faces exist (Dick et al., 1983; Dowding and Aimone, 1992). For this reason, this section will only cover rounds falling under the first type. When comparing stope blasting with open pit bench excavation, the major difference may reside in the fact that drillholes within the same ring may have different rotation angles, and in the application of up-hole drilling. The confinement associated with the drift access, which can limit the jumbo drill rig positioning or the stope geometry have an influence on the drillholes orientation, and thus rotation and inclination angles. In terms of blastholes loading, these may not be charged along their full length to allow an adequate distribution of explosive within the ring. However, the distance between explosive charges should not exceed the defined spacing (usually similar to the burden), in such a way that ore recovery and fragmentation are not compromised by an inaccurate loading design.

Considering the importance of underground excavations to this work, one intends to know the involved design variables in an underground blasting pattern, which may be subject to changes to minimize ground vibration levels in surrounding structures. The design procedure is well-described in the literature (Langefors and Kihlstrom, 1978; Heiniö, 1999) by means of analytical expressions and graphical representations. This process is especially influenced by the opening cut geometry. The purpose of the cut is to create additional free faces providing relief for the rest of the blast. Two major types of opening cuts can be identified: parallel (burn cut) and angled (V-, fan and pyramid cut) hole cuts (Figure 7).

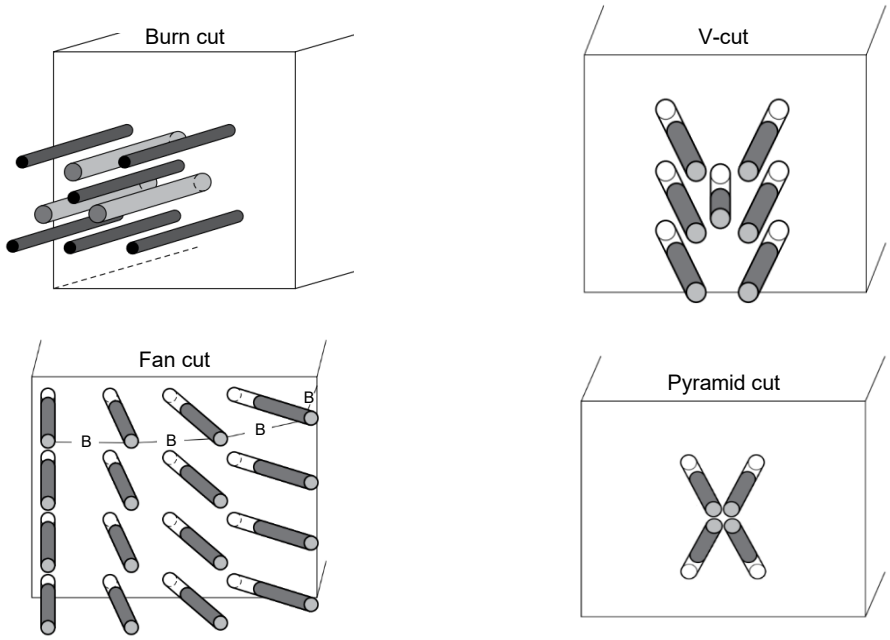

Figure 7 - Detail of different opening cut layouts in a drift round (rock's eye view) (adapted from Lusk and Worsey, 2011).

According to Figure 7, with the exception of the fan cut, the remaining layouts have cut drillholes in a specific location of the drift face, i.e., they do not cover the entire face. It should be noted that the location of the cut can vary, dictating the direction and distance of throw. In the fan cut, the distance between adjacent holes toes is the burden (B).

In burn, V- and pyramid cut designs, the drillholes can be divided into three principal series: cut, blast/stoping and perimeter holes (Figure 8). Some authors divide the perimeter holes into floor/lifter and contour (rib and back) holes (Dowding and Aimone, 1992; Heiniö, 1999).

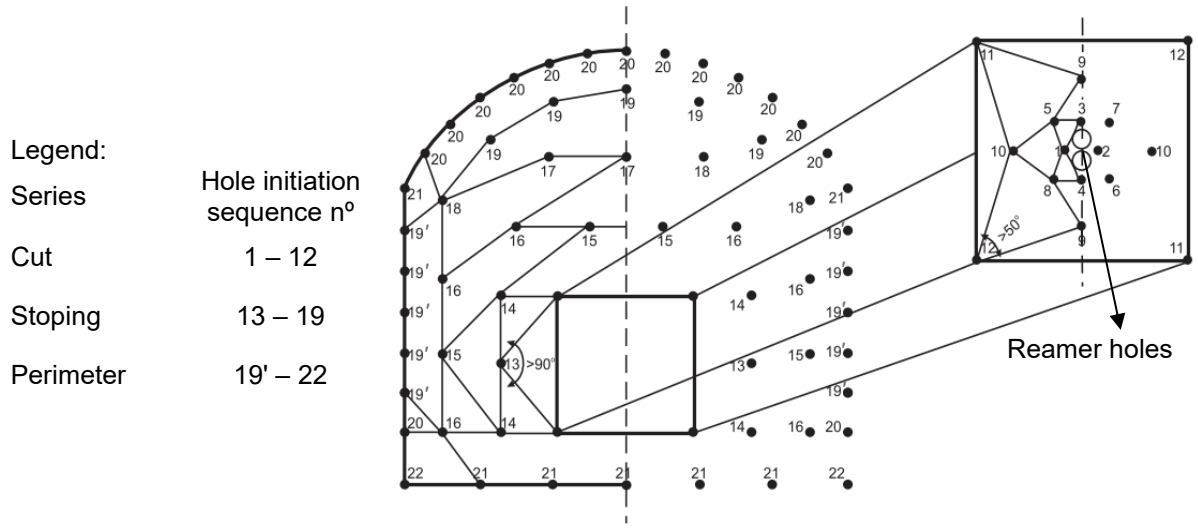

Figure 8 - Drillhole series in a drift round (adapted from Heiniö, 1999).

The series depicted in Figure 8 have the following objectives:

1. Cut – creation of additional free faces providing relief for the rest of the blast;
2. Stoping – usage of the created free faces to increase the blast efficiency, excavating most of the intended rock volume;
3. Perimeter – definition of the real excavation perimeter as close to the theoretical contour as possible.

The numbers assigned to each hole represent the firing pattern, where the cut holes are the first ones to be fired, being followed by the stoping (13 – 19) and, lastly, by the perimeter holes (19’ – 22). In the cut, it is noteworthy that long enough delay times between holes should exist, allowing the rock to suffer sufficient breakage and be thrown through the narrow empty reamer holes (represented in light grey – burn cut – in Figure 7, and in white in Figure 8).

Regarding the explosive charges to be applied, given the greater confinement in the cut, a higher specific charge (concentration) is used in this series, whilst this value decreases with the increasing distance from the cut. Considering the high number of simultaneous delays to be fired in the contour, to mitigate environmental impacts such as vibration and damage to the surrounding rock mass,

guaranteeing a smooth drift contour, the perimeter holes are the ones with the lowest linear charge. In the contour series, time delay precision is important in such a way that the simultaneously fired holes induce the creation of a regular surface defined by fractures which coalesce and provide a split, contributing to the approximation between the real excavation perimeter and the planned one. This suggests the importance of using electronic detonators in this series. Moreover, according to Figure 8, taking into consideration the greater number of stoping holes, when compared to the remaining series, if there is a considerable number of blast holes, it may not be possible to initiate each one at different instants of time using non-electric detonators, contributing to an increase of vibration amplitudes. For this reason, electronic detonators are recommended in drift blast rounds.

The confined environment associated with underground excavation activities diminishes the environmental constraints. Here, air blast, noise, flyrock and dust do not pose a hazard to surrounding structures and other descriptors such as people outside the mine operation perimeter. Thereby, rock mass instability and ground vibration have a greater importance. For this reason, like in open pit blasts, in addition to determining the geometrical parameters of the drilling pattern, one has to determine the maximum charge per delay with the objective of minimizing the mentioned impacts.

Similar to what has been described in 2.4.1., after considering the indicated influencing factors and, above all, normative restrictions in terms of blast-induced environmental impacts the empirical design process can be performed. However, the obtained blasting pattern may not be the optimal one and may be continuously corrected and adjusted, according to the results observed in the field, aiming to improve the following blast rounds.

2.5. The ground vibration phenomenon

Dynamic events such as an earthquake (natural) or blasting (anthropogenic) are transmitted through the ground and occur in the form of vibrations, which in turn propagate in the form of stress waves, until attenuation totally dissipates the initially transmitted energy. Within this context, it is important to define the concept of vibration.

According to the literature (Kramer, 1996), vibration is an oscillatory movement of any physical system (in the solid, liquid or gaseous state), which is displaced from its equilibrium condition. Within the scope of this work, vibration is considered to be the ground elastic response to the stress waves that travel through the considered medium. This phenomenon is usually described by the amplitude (expressed as a function of displacement, velocity or acceleration), period, wavelength, frequency and duration. As the stress wave travels through a three-dimensional space, it can be characterized by mutually perpendicular components: longitudinal (L), transverse (T) and vertical (V). As the name suggests, the V direction is the vertical one, L is directed along the line between the blast and the monitoring point, and T is perpendicular to the first two (Dowding, 1992).

2.5.1. Classification of stress waves

After a blasting event, the sudden release of energy into the ground (rock and/or soil mass) takes place, promoting the propagation of body and surface waves. These waves may impact nearby people and structures, having vibration amplitudes that depend on the quantity of energy released by the blast, the distance between the source and the monitoring point, the transmission and dissipation properties of the ground, and the dynamic resistance of structures as well as its weakest elements (Gama, 2003).

As mentioned before, the transmitted stress or seismic waves can be divided into body and surface waves (Figure 9). Body waves travel radially at small distances from the energy source through the rock and soil mass, until they intersect a boundary such as another rock layer or the ground surface, producing shear and surface waves. These have relatively high frequencies (10 to 40 Hz) and rapid attenuation, when compared to surface waves. Surface waves travel along surfaces and interfaces within the rock and soil mass. This last group registers, however lower propagation velocities and frequencies (2 to 8 Hz), being perceived at greater distances given the greater energy associated with them (Dowding, 1992; Bernardo, 2004).

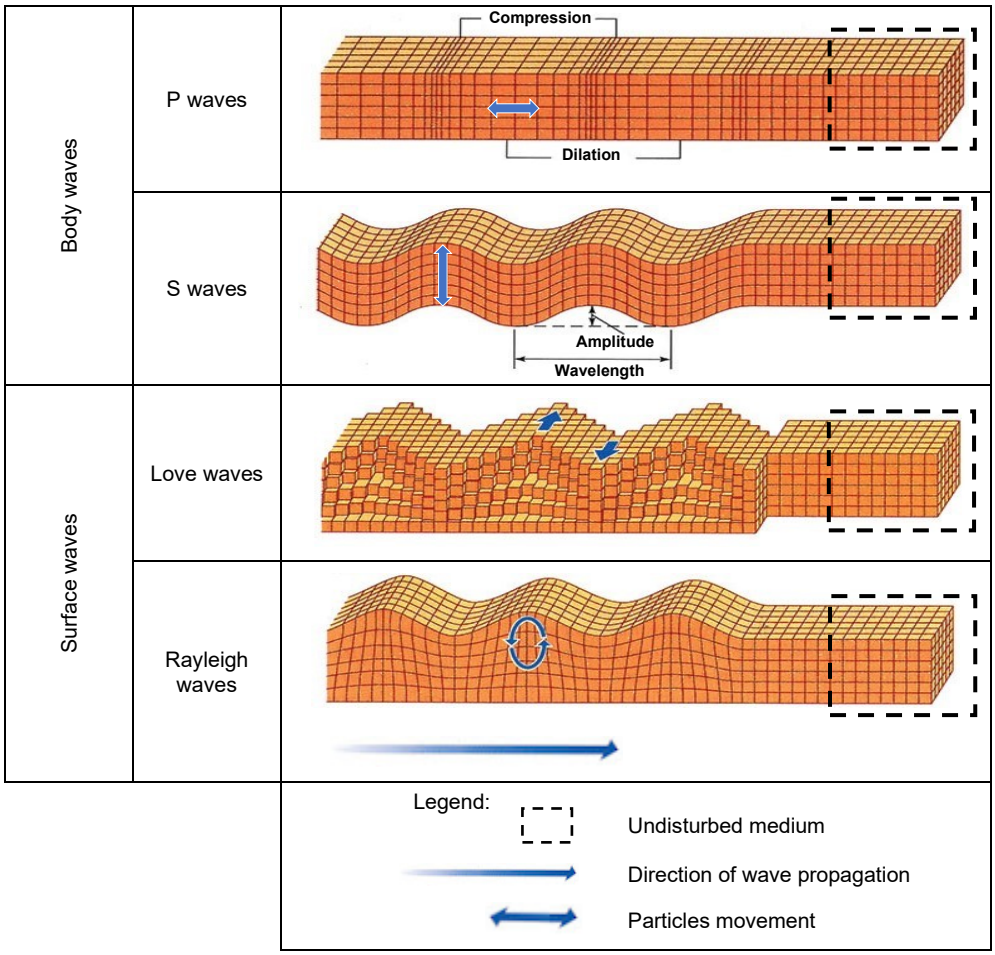

Figure 9 - Seismic waves (adapted from Das, 2022).

As illustrated in Figure 9, body waves can be divided into compressive (P) and distortional, secondary or shear (S) waves. On the other hand, Love and Rayleigh waves constitute surface waves. Also known as primary ones, P waves involve alternating compression and dilation of the ground material, promoting variations in its volume. As S waves propagate, they cause shearing in the surrounding rock or soil material, changing its shape, but not its volume. Love waves have no vertical component and the horizontal particle movement is perpendicular to the direction of the waves propagation. Lastly, Rayleigh waves involve vertical and horizontal components at the surface according to an elliptic orbit. These may contain up to 80 % of the total energy and once they are perceived at the surface and at greater distances, structures located hundreds of meters from the energy source, such as a blast, are associated with potential damage risks (Kramer, 1996; Bernardo, 2004).

2.5.2. Importance of ground vibration amplitude as a structural damage criterion

According to Dowding (2011), the response of surface structures is dependent upon peak particle velocity amplitudes and frequency of vibration. For belowground structures, waves propagation velocity and frequency determine the rock mass and founded structures response. In the two cases, cracking is originated by induced strains, being that particle velocity values are used as an index of strain. Firstly, it is important to analyze the influence of vibration on structures.

As mentioned before blast-induced vibrations may be produced by several geotechnical operations. These can be divided into three categories (Sarsby, 2013):

1. Steady-state or continuous – when an approximately constant level of vibration lasts for a substantial period of time (for example: vibrations originated from earthworks, compressors or large pumps working during a prolonged period);
2. Transient or impact – if the vibration peak levels result from a sudden impact, which is followed by a prolonged time after complete attenuation (for example: pile-driving using a drop hammer or detonation of isolated explosive charges);
3. Intermittent – when a sequence of brief vibration events is separated by intervals of considerably lower vibration amplitudes (for example: ground motion after percussion drilling or detonation of delayed explosive charges).

In this work, it is assumed that no permanent displacements on structures are caused by excavation by means of drill and blast. However, it is important to highlight some of the effects blasting events may have on structural elements. Some examples are structural distortion, faulted or displaced cracks, falling objects and cosmetic cracking of wall coverings. These are not expected to occur when vibration levels are below the recommended limits defined to prevent cosmetic cracking. Apart from structural response, excessive instrument, machine and human response, and micro disturbance may occur (Dowding, 2011).

Some authors divide excessive structural response into three categories (Northwood et al., 1963; Siskind et al., 1980a; Dowding, 2011). These are presented in order of declining severity and

increasing distance of occurrence, beginning with effects that, if observed, occur closest to the blasting area:

1. Major (permanent distortion) – compromising the structure integrity (e.g. large cracks or differential settlement of the foundations that result in the distortion or weakening of the superstructure);
2. Minor (displacement cracks) – surficial damage that does not affect the structure strength (e.g. broken windows, hairline cracks in masonry, and fissuring of interior and exterior wall plaster coatings);
3. Threshold (cosmetic cracking) – formation of new plaster cracks and extension of preexisting ones with oscillation of loose objects such as bricks and furniture).

With regards to cosmetic cracking, it is worth noting that these do not affect structure stability and are similar to those that occur during the structures natural aging. Apart from blasts, these can be caused by differential thermal expansion, structural overloading, chemical changes in construction materials, shrinkage and swelling of wood, fatigue and aging of wall coatings, and differential foundation settlement.

From the previously mentioned elements that define vibration, amplitude (normally described by velocity or acceleration) of vibration and frequency are the two most important ones to consider when it comes to its effect on structures. Structural damage is correlated with the first parameter. The expressions present in Equations 4, 5 and 6 denote the existing relationships between amplitude (expressed as velocity, v, (m·s^{-1}) and acceleration, a, (m·s^{-2})) and frequency, f, (s^{-1}).

$$f = \frac{1}{T''} \quad \text{(Equation 4)}$$

$$v = 2 \cdot \pi \cdot f \cdot \delta \quad \text{(Equation 5)}$$

$$a = 2 \cdot \pi \cdot f \cdot v \Leftrightarrow a = 4 \cdot \pi^2 \cdot f^2 \cdot \delta \quad \text{(Equation 6)}$$

Where T'' is equivalent to the wave period (s) and δ the particle displacement (m) when excited by the wave.

Ground vibrations originated by any seismic event are directly proportional to the induced dynamic stresses, σ_d, (Pa) as Equation 7 shows (Dowding, 1992). This last physical quantity can easily be correlated with the structures dynamic resistance. The constant of proportionality involved in this expression corresponds to the medium characteristic impedance I_P (Equation 1).

$$\sigma_d = \rho \cdot c \cdot v \quad \text{(Equation 7)}$$

Similar to the previous equations, v is equal to the rock mass particles vibration velocity (mm·s^{-1}) and $\rho \cdot c$ is the rock characteristic impedance, being ρ its density and c its typical wave propagation velocity. In consequence, the effect of ground vibration on structures is also dependent on the lithology on which they are founded. Thereby, it is essential to characterize and understand the ground a structure lays on, to prevent the occurrence of damage induced by blasts.

According to Rinehart (1975) (as cited in Bernardo, 2004), static stresses in rock materials may be five to thirteen times less than equivalent dynamic ones – in the case of hard and soft rock, respectively. The reason for this is that, in dynamic loads, rock mass discontinuities such as joints and microfractures are not involved in the fracturing process, given the very limited time period of the loading phase. This reasoning is depicted in Figure 10.

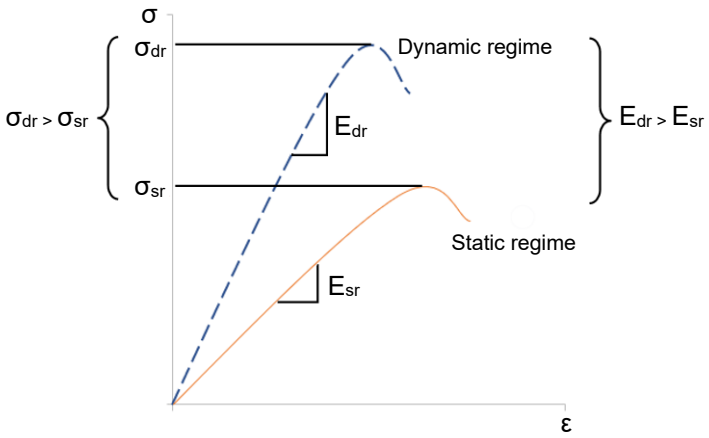

Figure 10 - Stress-strain curves in static and dynamic regimes (adapted from Bernardo, 2004, as cited in Gama, 1971).

Where the curves slopes E_{dr} and E_{sr} correspond to the elastic moduli in the dynamic and static regimes, respectively. The remaining physical quantities mentioned in this figure σ_{dr} and σ_{sr} are equivalent to the rock material dynamic and static resistance, respectively.

Once the main objective of the detonation process in geotechnical activities is rock fracturing, σ_d should exceed σ_{dr}. Fracturing will occur until the dynamic stress is lower than σ_{dr}. From that moment onwards, only rock deformation as a consequence of stress waves propagation will be verified.

In a real situation, with interest to this work, in which stress waves travel through a rock mass (which is not ideal, i.e., inelastic, anisotropic, heterogeneous and discontinuous), the energy released by a detonation is going to be dissipated with time due to energy attenuation mechanisms. This attenuation process is verified by means of decreasing vibration amplitudes (Dowding, 1992). For this reason, for increasing distance values from the blast, one should expect decreasing values of σ_d. Sarsby (2013) provides a more detailed analysis on waves attenuation; indicating that the factors influencing this phenomenon are the waves geometrical spreading; the progressive separation of surface, P and S waves components given the different propagation velocities that characterize them; the presence of discontinuities in the rock mass; and internal friction that causes frequency-dependent attenuation.

Nevertheless, in practice, stress waves may not suffer attenuation with distance. By way of example, in stratified rock masses, waves may concentrate or overlap to reflected ones (constructive interference), measuring greater ground vibrations at more distant points (Azevedo and Patrício, 2003, as cited in Bernardo, 2004). Moreover, the lithology on which the structures foundations are based, has an important influence on vibration levels measured on these constructions, as Figure 11 suggests.

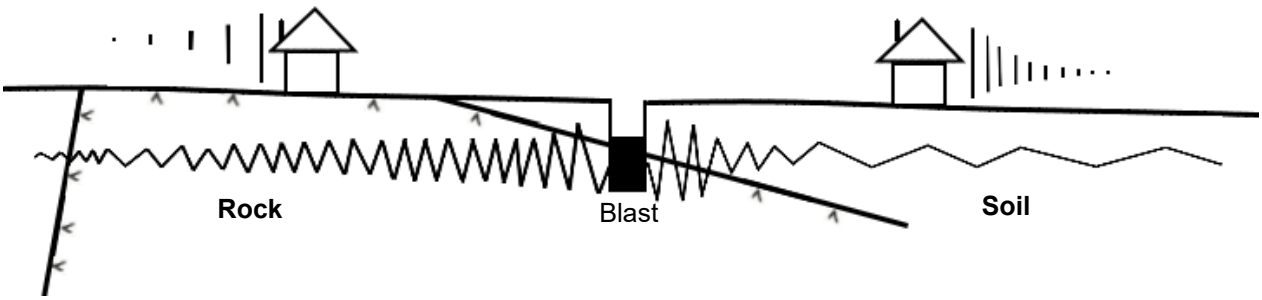

Figure 11 - Foundation lithology influence on vibration levels at two similar structures, equidistant from a blast (adapted from Lopez Jimeno et al., 1995).

According to Figure 11, the building founded on rock registers a lower vibration velocity than the one founded on soil. This is due to the fact that geological formations that have a higher wave attenuation capacity originate greater vibration velocities than those that register lower vibration energy dissipation levels, such as a competent rock mass. In reality, this phenomenon is explained by the relationship between ground vibration velocities and dynamic stresses (Equation 7), where for a constant σ_d if the characteristic impedance decreases, the vibration amplitude increases and vice versa. In other words, formations with lower impedance values (where attenuation occurs at a greater rate for a given distance interval) attenuate dynamic stresses more rapidly, though this is not the case for particle vibration velocities.

If a wave is transmitted through different media, with different I_P, its propagation is ruled by the relationship between the characteristic impedance that defines each medium. Considering Snell's law, Equation 8 shows the relationship between the amplitudes of the incident (A_i) and transmitted (A_t) waves (m) that propagate through the interface of two media as a function of their impedance. It is noteworthy that the wave travels from medium 1 to 2 (Bernardo, 2004).

$$A_t = \frac{2}{1 + \frac{\rho_1 \cdot c_1}{\rho_2 \cdot c_2}} \cdot A_i \qquad \text{(Equation 8)}$$

The quotient between the first and the second medium impedance is equivalent to the refractive index (n'). Thereby, the previous equation may be defined by the following expression (Equation 9):

$$A_t = \frac{2}{1 + n'} \cdot A_i \qquad \text{(Equation 9)}$$

As such, considering Equations 7 and 9, if the vibration velocity measured on a structure founded on rock is defined as v_r, the vibration velocity measured at a structure founded on soil is deduced by Equation 10.

$$\rho_s \cdot c_s \cdot v_s = \frac{2}{1 + n'} \cdot \rho_r \cdot c_r \cdot v_r \Leftrightarrow v_s = \frac{2 \cdot n'}{1 + n'} \cdot v_r \qquad \text{(Equation 10)}$$

According to this expression and Figure 11, if the incident wave propagates through the rock mass and reaches an interface between this lithology and a soil mass, given the fact that n' is greater than one, one can conclude that v_s is greater than v_r.

2.5.3. Importance of frequency as a structural damage criterion

As mentioned in the previous section, the analysis of possible damage to structures is carried out through amplitude of vibration and frequency. Hence, it is also convenient to define frequency and its relationship with eventual undesired effects on construction elements. This physical property is intrinsically related to the rock mass response, as it is going to be addressed below.

The proximity of the dominant frequency of rock or soil mass vibrations to one of the buildings natural frequency may generate the condition of resonance, i.e., an amplified structural vibratory response (Svinkin, 2008). Nevertheless, if only a reduced number of blast-induced motion cycles at a similar amplitude and frequency are observed, resonance vibrations are not verified. This phenomenon is not only dependent on structure stiffness, but also damping ratio (β) and mass of the main structural components (Dowding, 2011). Figure 12 represents a graphical method to determine the dynamic magnification factor, according to the frequency (f/f_n) and damping ratios, where f and f_n are the vibration event and structure natural frequency, respectively. The dynamic magnification factor (R_d) can be defined as the quantification of a structures response, when submitted to a dynamic load such as a vibratory event, i.e., the ratio of the peak to the static amplitude (Smith et al., 2007).

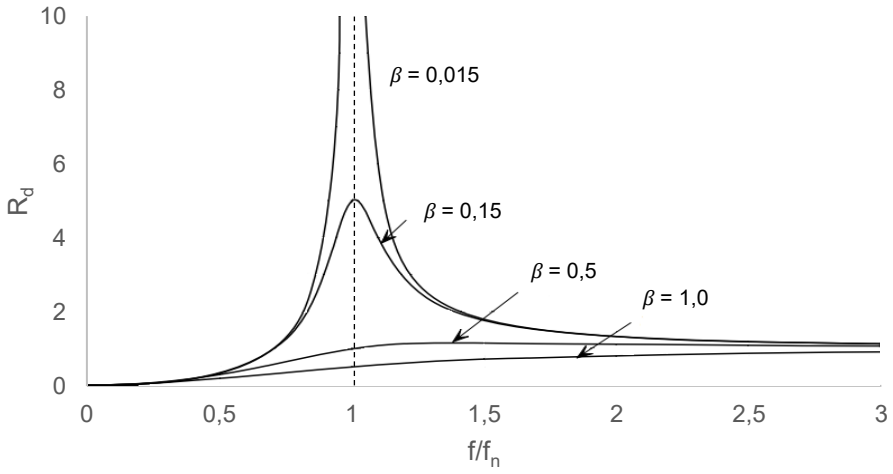

Figure 12 - Dynamic magnification functions (adapted from Smith et al., 2007).

This figure illustrates the increasing dynamic magnification factor and thus structural response when the frequency ratio is close to one. Lower damping ratios, which in turn imply longer steady-state periods, are related to greater dynamic response factors, increasing the probability of structural damage occurrence. Regarding different building materials, one may expect that lower damping ratios (for example 0,015) are associated with steel structures, whereas greater values (1,0) may characterize wooden structures. Additionally, buildings with masonry or reinforced concrete in their constitution are characterized by intermediate β, such as 0,15.

As demonstrated, the structures natural frequency is a fundamental property when estimating its response to dynamic events. This physical quantity can be estimated as an inverse function of the building's number of stories N_S (Equation 11). However, this relationship is only accurate for one- or two-story structures, indicating its limited application domain (Newmark and Hall, 1982). Notwithstanding this consideration, the simplistic approach shown below may be used in rural areas, where most mines are located, once multistory buildings are unlikely to be found in the vicinity of these operations.

$$f_n = \frac{10}{N_S} \quad \text{(Equation 11)}$$

For unusual tall structures and slender ones, its natural frequency cannot be estimated with Equation 11. Taking this into consideration, Bernardo (2004) suggests a new formula (Equation 12), where f_n is a function of the structure's height (H_S), respective building material's waves propagation velocity (C_P) and porosity (n) – ratio between volume of voids, including non-structural elements, and total volume. As such, according to this formula, the structures natural frequency is influenced by its geometrical parameters and building material physical properties.

$$f_n = \frac{C_P}{2 \cdot \pi \cdot H_S} \cdot \sqrt{1 - n} \quad \text{(Equation 12)}$$

Buildings' walls and floors register typical f_n values in the range of 12 to 20 Hz, while their superstructure responds to lower frequency values (5 Hz). Taking into consideration that low-frequency waves (like Rayleigh waves) are the most energetic ones, this response is a concern if resonance occurs, further incrementing eventual damages. Moreover, according to Equation 5, for the same velocity, low-frequency vibrations produce greater levels of displacement. Therefore, lower frequencies induce greater structural response (Dowding, 2011).

Some authors (Sarsby, 2013) argue that at a given distance from the vibration source, the ground verifies a *filtering effect* of the stress waves propagating through it, causing it to vibrate at a limited frequency range (from 5 to 100 Hz), known as dominant frequency f_d. This is equivalent to the transmitted frequency to structures founded on the considered medium and can be estimated by means of Equation 13 (Esteves, 1993).

$$f_d = \frac{C_S}{4 \cdot h} \quad \text{(Equation 13)}$$

Where C_S is the S waves propagation velocity (m·s^{-1}) and h is the layer thickness (vertical distance between the ground surface and the first geological interface). As shown in Equation 13, ground dominant frequencies depend the lithology resistance, which is directly related to the waves propagation velocity. Thus, one can conclude that a soil mass, which is considered as less competent (lower resistance) tends to register lower dominant frequency values than a continuous and homogeneous rock mass (Sarsby, 2013). The following example (Figure 13) illustrates a situation where similar buildings (with a natural frequency of 10 Hz) founded on the same rock mass (B, with C_S = 1.000 m·s^{-1}) are affected by the same seismic event showing, however, different dominant frequencies given the existing variations in h.

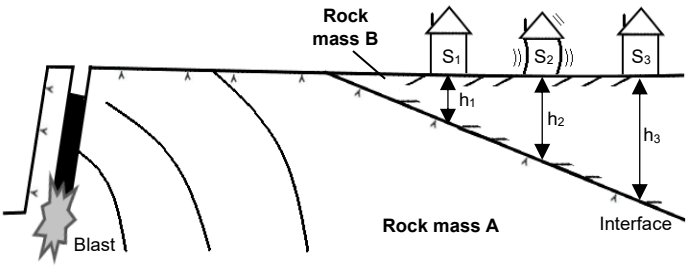

Structure	h (m)	f_n (Hz)	f_d (Hz)	Resonance
1	10	10	25	No
2	25	**10**	**10**	**Yes**
3	50	10	5	No

Figure 13 - Vibration amplification caused by resonance (adapted from Bernardo, 2004).

In this figure, f_d is estimated through the use of Equation 13. As can be concluded, regardless of the considered distance, the structures reveal distinct dynamic responses. This is justified by h, where for an intermediate layer thickness (h_2), there is an approximation of frequencies (natural and dominant), inducing an increase in the vibration amplitude verified in structure S_2, which may damage this but not the neighboring ones.

Despite the theoretical approaches previously mentioned, the dominant frequency can be estimated (taking into account the three components L, V and T) by visual inspection of a seismogram (amplitude vs. time graph) considering Equation 4, or calculated using the Fast Fourier Transform (FFT) in the three directions. In addition to lithology, Dowding (2011) states that dominant frequencies are generally inversely proportional to distance and to the size of the blast. Thereby, construction blasts, which involve smaller charge values and distances from structures tend to produce higher frequencies than mining ones, being less hazardous to adjacent structures.

In this context, electronic detonators are preferable in civil blasting, because they enable a precise control of the time delays between consecutive blastholes. In consequence, the resulting dominant frequency may be estimated (Equation 4) in such a way that an overlapping of frequencies and consequent structure resonance are avoided. This same reasoning may be considered when using non-electric detonators, despite the lower control on delay timings. Another advantage of electronic detonators is the control of potential overlaps, ensuring that the maximum charge per delay does not exceed the predetermined one, maintaining vibration levels within the expected interval.

2.6. Ground vibration monitoring

To describe ground vibration, particle velocity is the most preferable element amongst the three amplitude descriptors, once it has the best correlation with blast-induced cracking empirical formulas. Hence, it constitutes the basis of vibration monitoring. When assessing structural-response motions induced by blasting events, it is easier to consider this parameter, rather than the dynamic stress (Equation 7), given the fact that the first can be directly obtained by monitoring instruments without the need of calculation, and international standards limit vibration amplitude and not σ_d (Dowding, 1992). Although geotechnical operations assign greater importance to blast-induced effects on structures, countries like Germany or Great Britain, have published standards that recommend limits on human

exposure to vibration in buildings (DIN 4150-2 and BS 6472-2, respectively). When these standards are complied with, the vibrations produced will not normally lead to human discomfort in dwellings and similar buildings (British Standards, 2008; Deutsches Institut für Normung, 2016a). For these reasons, it is critical to measure ground motions (namely vibration velocity) and determine the associated frequency.

With regards to particle velocity, this can be measured by means of calibrated engineering seismographs endowed with triaxial geophones, which are appropriately located on the ground, considering the blast geometry. These convert mechanical vibration energy into electrical energy, directly proportional to the ground vibration amplitude and discriminate the three motion L, V and T components. At the moment of each detonation, the existing geophones (velocity transducers) receive the corresponding seismic events and register them in the case they are between the detection limits and over the trigger value. During this process, the onboard computer analyzes the data and generates event and FFT reports that can be downloaded and further analyzed on any portable computer.

Usually, an event report contains the peak acceleration and displacement, and a sensor check. Moreover, the following elements are generated: peak particle velocity, PPV, (maximum vibration velocity registered for a given component) and respective time relative to trigger, and peak vector sum (PVS), where this is the resultant vector of PPV and is considered as the maximum vibration velocity measured at the monitored location. It is mention worthy that PVS results from the calculation of the resultant vector (L, V and T) considering the three coordinates (v_L, v_V and v_T) at the same instant that yields the largest result for the considered event. As such, PVS is less than the resultant vector considering the maximum components (PPV_L, PPV_V and PPV_T) at distinct instants (Equation 14).

$$PVS = \left|\sqrt{v_L^2(t) + v_V^2(t) + v_T^2(t)}\right| < \left|\sqrt{PPV_L^2(t_1) + PPV_V^2(t_2) + PPV_T^2(t_3)}\right| \quad \text{(Equation 14)}$$

Dowding (2011) suggests that it is common to observe PVS values at the same instant as the one that corresponds to the maximum registered PPV. Moreover, the peak vector sum may be as much as 10 % greater than the maximum single-component peak.

The last element to be considered on an event report is the analysis of the registered velocity and frequency according to a specific vibration control standard that is selected by the user.

With regards to the FFT report, this contains three FFT spectra (one for each direction), where the events dominant frequency may be calculated. This frequency corresponds to the direction in which the vibration amplitude is maximum.

2.7. Ground vibration mitigation measures

To promote rock mass fracturing by dynamic actions, vibration velocities over 700 to 1.000 mm·s^{-1} are required (Holmberg and Persson, 1978). Gama (1998) indicates that only 5 to 15 % of the energy released by the detonation of explosives is effectively used to promote rock fragmentation.

Such empirical evidence highlights the relative amount of energy transmitted through the surrounding rock mass, which can impact, as seen before, neighboring structures. For this reason, to protect the different stakeholders and objects, the control of undesired blasting effects and mitigation measures have to be considered upon blasting pattern design and further optimization of this process.

In their work, Rosenthal and Morlock (1987) present diverse factors related to blasts and blasting patterns which can have varying impacts on the resultant vibration velocities (Table 3).

Table 3 - Factors which influence blast-induced vibrations (adapted from Rosenthal and Morlock, 1987).

Controllable variables	**Influence on ground vibrations**		
	Significant	**Moderately significant**	**Insignificant**
Charge weight per delay	•		
Delay interval	•		
Charge confinement	•		
Burden	•		
Specific charge	•		
Drillhole inclination	•		
Direction and type of initiation	•		
Spacing		•	
Bench height/charge depth		•	
Subdrilling		•	
Covered or uncovered detonating cord			•
Amount and type of stemming			•
Uncontrollable variables	**Significant**	**Moderately significant**	**Insignificant**
Local geology and rock mass properties	•		
Type and depth of overburden	•		
Distance from the blast	•		
Time delay error		•	
General surface terrain			•

Beginning with the uncontrollable variables, the most relevant factor influencing a blast design is local geology. This is intrinsically connected to the rock mass properties, being that these have to be known and characterized with the objective of adjusting the applied explosive charges to the required minimum to achieve the desired rock fragmentation, hence optimizing the firing pattern. Moreover, heterogeneity leads to differential waves propagation and stratified rock masses may concentrate the reflected waves, increasing vibration velocities. On the other hand, rock mass discontinuities may lead to vibration attenuation – destructive interreference.

As discussed before, one should expect to measure greater vibration values at a lower distance from the source, given direct relationship between this last variable and attenuation.

In some cases, depending on the scatter (function of the detonator type), time delay errors may originate an overlapping in time of different blastholes, thus increasing the charge per delay, or even changes in the initiation sequence. This should be accounted for, once detonators are associated with errors which can be responsible for an increase in undesired blast effects in particular ground vibration. In this case, electronic detonators are more reliable and the preferred ones, once they are more accurate timewise, and allow frequency estimation and consequent resonance prevention.

For the controllable factors, considering the geometrical pattern parameters indicated in Table 2, burden is the one that has the greatest importance to ground vibration control, due to the fact that it maximizes the efficiency of the explosive energy in terms of rock fragmentation and consequently minimizes the amount of released energy into the rock mass in the form of seismic waves. As described by Table 2, burden increases with an increasing drillhole diameter and the constant of proportionality K_B should be within the considered range. Values of this constant larger than its upper limit (40) originate significant vibration levels without proper rock breakage and displacement. On the other hand, K_B values below the suggested lower limit (25) contribute to excessive rock fragmentation and displacement, leading to flyrock, air pressure and dust hazard. This scenario, however, substantially decreases vibrations.

In bench blasting, the use of inclined drillholes influences the blast performance and the associated impacts, not only in terms of the achieved fragmentation and displacement, but also in terms of slope stability, specific charge and vibrations transmitted through the rock mass, as Figure 14 suggests.

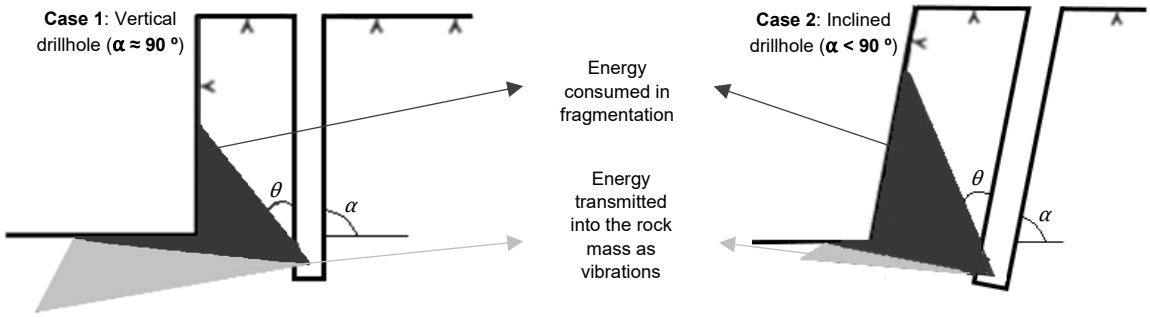

Figure 14 - Influence of drillhole inclination on blast performance and environmental impacts magnitude (adapted from Gama, 1971).

The analysis of Figure 14 indicates that the application of vertical drillholes (with inclination, α close to 90 º) is less favorable in the sense that a greater quantity of energy is transmitted into the rock mass (light grey area), while the useful energy consumed in fragmentation (influenced by θ, function of the explosive VOD) is lower, when compared to the case (2) where inclined drillholes are used. As such, inclined drillholes are recommended to mitigate impacts on different descriptors promoted by ground vibration.

An increase in the charge weight per delay may be caused by multiple factors like an increase in the bench height, subdrilling, and explosive cartridge dimensions (diameter and/or length) and confinement. As it will be further discussed, a greater charge weight per delay implies that more energy is released at a given time frame, which in turn increases vibration amplitudes.

In the case where the bench height is high in such a way that concerns associated with the charge weight may arise, several authors (Lopez Jimeno et al., 1995; Heiniö, 1999; Bernardo, 2004; Dowding, 2011) suggest two practices whose objective is to decrease the charge per delay, and consequently vibrations: division of the bench into two or more smaller benches and decking. The first consists in dividing the original bench into smaller units which are blasted separately. Decking, on the other hand, is carried out through a physical separation of the explosives column into at least two parts with stemming between them, which are initiated at different delays (Figure 15). The more decks, the more partitioned is the energy in time and along the hole. Again, this practice is important mainly when there are nearby structures to protect and there is the risk of not complying with the recommended limits, because the amount of explosive per delay is high.

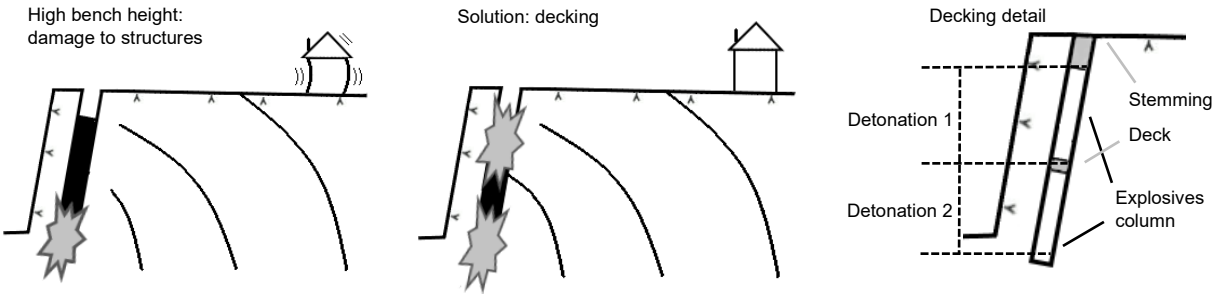

Figure 15 - Ground vibration mitigation using decking (adapted from Bastos, 2003, as cited in Bernardo, 2004).

Both the stemming and the deck (depicted in this figure) usually consist in aggregates and the adjacent charges (each one composed by bottom and column charges) are initiated at different delays by the respective detonators and not by sympathetic detonations. Here, it is noteworthy that the charge located at the upper part of the bench (detonation 1) is the first one to detonate. This diminishes the confinement associated with each charge, which is dependent upon the number of free faces, mitigating impacts like vibration and flyrock. Regarding the deck dimensions, for dry and wet holes, the thickness of this barrier should be 6 and 12 times the hole diameter, respectively (Dowding, 2011).

Taking into account blasthole initiation, top initiation generates lower vibration levels (Hagan and Kennedy, 1977). This, however, compromises stemming efficiency, aggravating other impacts like flyrock, dust and air blast.

The use of delayed charges, i.e., the distribution of the detonation process in time is of relevance, not only because of the charge reduction per timing, but also because of the successive creation of free faces, improving the fragmentation process and decreasing the amount of energy released into the rock mass, due to the lower confinement (Bernardo, 2004).

Lastly, the application of presplitting (instantaneously firing lightly-charged holes) or slot drilling can be highlighted as additional vibration mitigation measures. These aim at creating a physical

discontinuity (fracture plane) on the rock mass between the source of seismic energy and the monitoring point, decreasing overbreak and vibration levels, consequently protecting a given building from possible damage. The created void may be filled with air or water. According to Heiniö (1999), if a slot is drilled close to and along a structure's foundation, vibration velocities measured at this location can be reduced by up to 80 %. These techniques are effective and recommended principally when sensitive structures like slender ones or monuments are to be protected and the associated suggested limits are lower. Yet, it is critical to ensure their successful execution, justifying the additional involved time, costs and means of production.

3. Analysis of ground vibration monitoring standards

Regarding vibrations, generally, technical documents such as standards only consider intermittent and transient vibrations. In the United States, ground vibration monitoring standards (USBM RI 8507) are based upon the occurrence of threshold cosmetic cracking of plaster wall coverings. As such, regulatory control limits are lower than the levels at which cosmetic cracking may exist. This is simultaneously verified in similar international standards. To assess structural damage, conservative values are usually considered. These, however, may be relatively high when compared to those associated with human comfort. In fact, the human being is ten times more sensitive to vibration than structures (Dowding, 2011). The vibration perception threshold is equal to 0,3 $mm \cdot s^{-1}$ (Kiely, 1999). This justifies regular complaints on behalf of different stakeholders surrounding mining operations, once humans associate the discomfort promoted by blast-induced vibrations to cosmetic damage on structures. Furthermore, it is not uncommon that complainants associate pre-existing cosmetic cracks to blasting events, even if this form of damage is caused by non-mining factors such as differential thermal expansion or chemical changes in construction materials (as mentioned in chapter 2.5.2.).

From the existing international ground vibration monitoring standards created to protect structures from blasting-related damages, the German (DIN 4150-3) and the British (BS 7385-2) ones may be highlighted. Given the framework of this work, it is also relevant to consider the Portuguese standard (NP 2074). In this chapter, these documents are both individually and collectively analyzed, where a broad comparison is finally carried out. Lastly, a brief introduction to the British document on human exposure to vibration in buildings is performed.

3.1. Ground vibration monitoring standards with emphasis on structures

3.1.1. Portuguese standard: NP 2074

Created in 1983 and updated in 2015, the Portuguese standard NP 2074 has the objective of recommending limit values for intermittent vibrations originated from geotechnical activities (like rock blasts) to prevent any damage to structures caused by these dynamic events (Instituto Português da Qualidade, 2015). The performed updates were based on International Organization for Standardization (ISO 2041:2009 and ISO 5348:1998) and German (DIN 4150-3:1999) standards, promoting the existence of some similarities between these and the Portuguese version.

In Portugal and lusophone countries that have adopted the considered standard, intermittent vibrations occurring between 7 a.m. and 8 p.m. have to comply with this document, though they may

not be perceived by the Human Being. For time periods between 8 p.m. and 7 a.m. these events can occur, as long as they are not uncomfortable to people in the vicinity. It is noteworthy that the assessment of human discomfort and the influence on sensitive devices located at hospitals or laboratories whose limits may be more restrictive are not addressed by NP 2074.

In this standard, structures are divided into three categories, according to the degree at which they may be affected by vibrations: sensitive, current and reinforced. This classification takes into account the structures conditions (considering old buildings or those with tiles installed on mortar as sensitive), slenderness ratio (where towers and chimneys are classified as sensitive) and equity value (classifying monuments and transportation infrastructure as sensitive structures). Current structures correspond to dwellings or offices whose slenderness is not high. The last category, reinforced structures, includes those built with reinforced concrete, including metallic elements in their superstructure, or with an industrial use. Additionally, the document suggests the performance of a *previous assessment*. This constitutes an *a priori* inspection of the nearby buildings to survey eventual existing cracks and its dimensions, and compare the effect dynamic geotechnical events have on these.

To monitor ground vibrations close to structures that must be protected from blasting events, for example, NP 2074 suggests that the monitoring system must include triaxial transducers, a central processing unit and an analog-to-digital converter. Transducers must point towards the vibration source and be mounted on a surface of the structure connected to its foundation, and at a height less than 0,5 m from the yard's surface level. Furthermore, the system has to be calibrated on a yearly basis, and be able to measure frequencies from 2 to 80 Hz and PVS values ranging between 0,5 and 100 mm·s^{-1}.

For compliance analysis, both the event's dominant frequency (f_d) and the maximum vibration velocity at a given instant (PVS considering Equation 14) must be registered. After recording these physical properties and classifying the structures to be protected, the resulting PVS is compared with the standard's limit value (Table 4).

Table 4 - Recommended limit values for vibration velocity, in mm·s^{-1}, according to NP 2074 (Instituto Português da Qualidade, 2015).

Type of structure	**Dominant frequency, f_d**		
	$f_d \leq 10$ Hz	**10 Hz < $f_d \leq 40$ Hz**	**$f_d > 40$ Hz**
Sensitive	1,5	3,0	6,0
Current	3,0	6,0	12,0
Reinforced	6,0	12,0	40,0

After monitoring hundreds of blasts worldwide and correlating these with the damage probability Siskind et al. (1980b) concluded that below 12 mm·s^{-1} no cosmetic cracking or extension of hairline cracks was observed. This conclusion was taken considering a wide range of frequency values (between 2 and 400 Hz). For this reason, it is possible to verify the conservative values present in the analyzed standard where, for frequencies less than or equal to 40 Hz, the recommended vibration velocities are not greater than the suggested 12 mm·s^{-1} threshold. However, one should not disregard

resonance effects and the fact that structure classification is subjective. Hence, not all vibratory events deemed compliant with this standard will not induce visible damage to a given building. Conversely, not all vibration measurements over the recommended limit values are expected to damage a structure.

Lastly, within the scope of the Portuguese standard and for rock blasting vibrations, the creation (or use) of a vibration velocity prediction equation that depends on the charge per delay and distance between the blast and the structure is recommended. This practical tool should be used upon blasting pattern design, maximizing the probability of not exceeding the limit values. A more detailed analysis on this subject is presented in the next chapter. Moreover, in unfavorable situations such as sensitive structures to be protected from vibrations, the use of electronic detonators is proposed to control time delays and frequency.

3.1.2. German standard: DIN 4150-3

Similar to NP 2074, the German standard DIN 4150-3 (revised in 2016) considers the dominant frequency and the type of structure as determinant factors for the measured vibration limit value. This one, however, takes into account the maximum vibration velocity for a given component (PPV_L, PPV_V or PPV_T) at the foundations or uppermost story of a structure as the input value for compliance assessment (Table 5).

Table 5 - Recommended limit values for vibration velocity, in $mm \cdot s^{-1}$, according to DIN 4150-3 (Deutsches Institut für Normung, 2016b).

	Dominant frequency, f_d				
	Short-term				**Long-term**
Type of structure	**At the foundations**			**Uppermost story**	**Uppermost story**
	$f_d \leq 10$ Hz	**10 Hz < $f_d \leq 50$ Hz**	**50 Hz < $f_d \leq 100$ Hz**	**Any frequency**	**Any frequency**
Commercial/ industrial	20,0	20,0 to 40,0	40,0 to 50,0	40,0	10,0
Dwellings	5,0	5,0 to 15,0	15,0 to 20,0	15,0	5,0
Sensitive/ historical	3,0	3,0 to 8,0	8,0 to 10,0	8,0	2,5

According to the previous table, dynamic loads originate short-term and long-term vibrations. The first do not occur frequently enough to cause fatigue on structures and are not prone to be amplified by resonance. If these conditions are not verified, vibrations are classified as long-term ones. For this reason, due to the greater probability of damage, the recommended limit values for this category are more restrictive.

3.1.3. British standard: BS 7385-2

Contrary to the Portuguese and German documents, the British ground vibration standard BS 7385-2 establishes limit values for continuous, transient and intermittent vibrations, with the objective of mitigating damages to structures after such dynamic events. The definition of maximum vibration velocity follows the same reasoning as the one in DIN 4150-3. However, this standard suggests that the monitoring point should be located on the yard's surface and not on the structure's ground floor (Bacci et al., 2003). Alternatively, transducers may be buried if there is no founded hard surface close to the building. Regarding the compliance assessment criteria, these are the dominant frequency and type of structure (reinforced or framed structures such as industrial and heavy commercial buildings, and unreinforced or light framed structures like residential or light commercial type buildings). The suggested vibration limits are shown in Table 6.

Table 6 - Recommended limit values for vibration velocity, in $mm \cdot s^{-1}$, according to BS 7385-2 (British Standards, 1993).

Type of structure	Dominant frequency, f_d		
	4 Hz < f_d ≤ 15 Hz	**15 Hz < f_d ≤ 40 Hz**	**f_d > 40 Hz**
Reinforced	50,0	50,0	50,0
Unreinforced	15,0 to 20,0	20,0 to 50,0	50,0

When comparing the British standard to NP 2074 and DIN 4150-3, one can conclude that the first is more permissive, mainly for frequency values below 40 Hz. With regards to possible damage to structures, this document distinguishes between cosmetic, minor and major damages (classification concomitant to the one addressed in 2.5.2.).

3.1.4. Comparative analysis of different European ground vibration monitoring standards

In Europe, most international norms make a distinction between different types of structures, where vibration velocity limits are dependent on this category and on the dominant frequency. However, as is evident from the individual analysis carried out for of each document, there are some particularities and differences between them (Table 7).

As mentioned in Table 7, for compliance assessment, NP 2074 includes PVS as the input value, contrary to DIN 4150-3 and BS 7385-2. Moreover, the first and the last register the same upper dominant frequency threshold (40 Hz). Regarding this physical property, one can notice that as it increases, so does the frequency range. In other words, the difference between the frequency extreme values that characterize a soil mass is lower than the one associated with competent rock masses, which tend to filter out lower frequencies (Equation 13). The British standard, distinguishes between reinforced and unreinforced structures, being this a simpler structure classification criterion. Finally, for all types of

structures, the Portuguese document registers more conservative maximum limits for a high-frequency range (over 40 Hz).

Table 7 - Summary of the analyzed standards in force and respective particularities (adapted from Luz, 2017).

Standard	Type of structure	Maximum recommended vibration limit	Corresponding frequency range	Particularity
Portuguese (NP 2074)	Sensitive	6,0 mm·s^{-1}	f_d > 40 Hz	The use of electronic detonators is recommended in unfavorable cases such as sensitive structures to be protected from vibrations. Consideration of PVS
	Current	12,0 mm·s^{-1}	f_d > 40 Hz	
	Reinforced	40,0 mm·s^{-1}	f_d > 40 Hz	
German (DIN 4150-3)	Commercial/ industrial	50,0 mm·s^{-1}	50 Hz < f_d ≤ 100 Hz	Consideration of short- and long-term vibrations and monitoring at the foundations and/or uppermost story
	Dwellings	20,0 mm·s^{-1}	50 Hz < f_d ≤ 100 Hz	
	Sensitive/ historical	10,0 mm·s^{-1}	50 Hz < f_d ≤ 100 Hz	
British (BS 7385-2)	Reinforced	50,0 mm·s^{-1}	f_d > 40 Hz	The monitoring point should be on the yard's surface and only two structure categories are considered
	Unreinforced	50,0 mm·s^{-1}	f_d > 40 Hz	

The following graph (Figure 16) intends to compare, in a graphical way the three analyzed standards, considering the vibration velocity limits for reinforced/industrial structures:

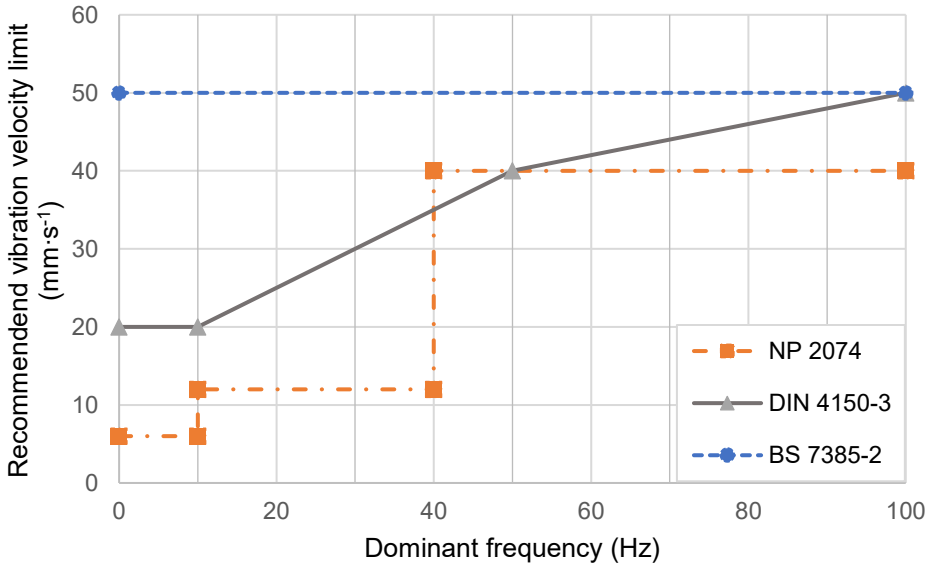

Figure 16 - Recommended vibration velocity limits for the updated analyzed standards for reinforced/industrial structures.

Figure 16 confirms the greater frequency range, typically verified in the high-frequency domain. Additionally, for lower dominant frequency values, the three norms show a more pronounced difference regarding the vibration limits. The Portuguese document is more conservative, recommending vibration

limits than can be up to eight times lower than the ones suggested by the remaining standards – comparing the NP 2074 6 mm·s^{-1} with the BS 7385-2 50 mm·s^{-1} limit. Conversely, BS 7385-2 is the least restrictive one. It should be mentioned that the limits for DIN 4150-3 illustrated in this figure are the ones relative to short-term vibrations measured at the structure foundations. Additionally, it is noteworthy that the presented limits in NP 2074 correspond to PVS, whereas the remaining standards suggest limits for PPV values.

Lastly, it is important to consider the differences between PPV- and PVS-based standards. Table 8 depicts six scenarios with different PPV and PVS values. The last is calculated according to Equation 14. It should be noted that both physical quantities are registered at instant t_1.

Table 8 - Different scenarios where PPV and PVS, in mm·s^{-1}, occur at the same instant.

Scenario	$PPV_L(t_1)$	$PPV_V(t_1)$	$PPV_T(t_1)$	$PVS(t_1)$
1	11,0	0,0	0,0	11,0
2	0,0	11,0	0,0	11,0
3	0,0	0,0	11,0	11,0
4	11,0	11,0	0,0	15,6
5	11,0	11,0	11,0	19,1
6	18,0	4,8	4,0	19,1

When analyzing this table, one can conclude that although scenarios 1 to 3 register the same PPV and PVS the effect dynamic events have on a given structure is different. In the second case, once slabs present in a building have a greater degree of freedom according to the vertical direction, this event could induce a greater damage to such element, whilst in the remaining scenarios, pillars – that register a greater response according to the longitudinal and transverse directions – could crack when vibration amplitudes are greater in the horizontal plane – 1 and 3.

The comparison of scenarios 1 to 3 with 4 and 5 shows that, in this case, PPV-based ground vibration standards are more favorable when assessing vibratory events than those that consider PVS. The second type of technical documents focus on the impact on structures as a combination of the vibration components at the same instant rather than the different directions individually. Hence, for the fifth scenario, the PPV is equal to 11,0 mm·s^{-1}, while the PVS is equivalent to 19,1 mm·s^{-1}, disregarding the most critical direction to structures.

Regarding the impact a vibratory event has on pillars, although the PVS values are similar in scenarios 5 and 6, the potential damage to this element is greater in the event that registers a PPV closer to the PVS: 6. In conclusion, PVS-based standards do not differentiate between the impact stress waves have on a particular structural element, while those that consider PPV do.

3.2. Ground vibration monitoring standards with emphasis on human exposure: BS 6472-2

The previously addressed standards do not focus on the impact rock blasting has on other elements such as people in the vicinity of mining or construction activities. As mentioned before, Great Britain and Germany have published documents specifying concrete recommendations in terms of vibration limits perceived by humans inside buildings. The International Organization for Standardization has also composed a standard on this subject: ISO 2631-2, being its most recent version updated in 2003. Currently, this document is being adapted for further publication in Portugal.

Initially published in 1984, BS 6472-2 aims at establishing specific and *satisfactory* vibration velocity limits to mitigate the impact on one of the descriptors not covered by BS 7385-2: humans. It should be noted that the compliance of this standard is not mandatory within the Portuguese territory. Its most recent version entitled *Guide to evaluation of human exposure to vibration in buildings – Part 2: Blast-induced vibration* was amended in 2008 and is chiefly applicable to blasting related to mineral extraction, construction works and demolition activities that register temporally spaced detonations.

Apart from ground vibrations, the considered standard addresses the air overpressure phenomenon which is defined as the combination of *both audible (noise) and inaudible (concussion) energy produced by a detonation of explosives*, propagating in the form *pressure wave in the atmosphere*. With regards to this topic, BS 6472-2 suggests that the sound level meter used to measure air overpressure has a low frequency response (2 Hz high-pass system) to fully capture the dominant low frequency component. Additional to the measurement of air overpressure, its prediction and suggested limit values are discussed. For 150 dB(lin), it is demonstrated that poorly mounted windows can crack, although most windows crack when air overpressure levels reach 170 dB(lin). Structures are not expected to suffer any damage for air overpressure levels below 180 dB(lin). According to this standard, the highest air blast levels associated with mineral extraction measured in the United Kingdom are less than 1 % of those that start to induce structural damage. (British Standards, 2008).

Regarding blast-induced ground vibration, BS 6472-2 suggests the same procedure for measuring this phenomenon as BS 7385-2 does. The standard assumes that the external measured levels are defined in such a way that vibration amplitudes inside the buildings are deemed satisfactory. Seismographs should measure PPV values between 0,1 and 100 $mm \cdot s^{-1}$, by means of transducers, over the frequency range 4,5 to 250 Hz. Similarly to air overpressure, the estimation of vibration prediction models (equation on the plane PPV ($mm \cdot s^{-1}$) vs. scaled distance ($m \cdot kg^{-0,5}$)) is mentioned.

Lastly, the suggested vibration magnitudes for up to three daily blast events are presented below (Table 9). These should not be exceeded by more than 10 % of the events. Here, special attention should be given to the place where people are located at, the period between the blasts and the number of blasts in a given time period, once these aspects could influence the perception of the satisfactory magnitude. For blasting activities related to the mining industry, the normal working period (daytime) can be considered as 8 a.m. to 6 p.m. Monday to Friday and 8 a.m. to 1 p.m. on Saturday, with no

detonation events on Sundays or Public Holidays. The night period ranges between 11 p.m. and 7 a.m. During this time, it is recommended that no vibration or air overpressure should be perceptible at residential structures. Routine blasting is not considered on Sundays or Public Holidays. *Other times*, excluding the night-time, cover the period outside the working day.

Table 9 - Recommended limit values for vibration velocity, in mm·s^{-1}, with respect to human response for up to three daily blast vibration events, according to BS 6472-2 (British Standards, 2008).

Place	Time	Satisfactory PPV magnitude
Residential	Day	6,0 to 10,0[B)]
	Night	2,0
	Other times	4,5
Offices and workshops [A)]	Any time	14,0

A) *Critical working areas where delicate tasks impose more stringent criteria than human comfort are outside the scope of this standard.*

B) *Within residential properties people exhibit a wide variation of tolerance to vibration. Specific values are dependent upon social and cultural factors, psychological attitudes and the expected degree of intrusion. In practice the lower satisfactory magnitude should be used with the higher magnitude being justified on a case-by-case basis*.

If more than three blasts occur in a working day, then a factor F should be multiplied to the suggested limits present in Table 9, reducing them. This multiplication factor can be calculated according to Equation 15.

$$F = 1{,}7 \cdot N^{-0,5} \cdot {T_b}^{-d} \quad \text{(Equation 15)}$$

Where N is the number of blast events per day (greater than 3); T_b (s) is the blast event duration typical for the site; and constant d is equal to 0,32 for wooden floors, 1,22 for concrete floors, and 0 if T_b is less than 1 second.

According to Goldman (1948), notwithstanding humans are sensitive to vibration velocities, frequency is also an influencing factor. As such, disturbance caused by vibratory events decreases with frequency. The analyzed standard, however, does not recommend vibration amplitude limits that depend on the frequency of the event.

Despite differing in the field of application, when comparing BS 6472-2 with the Portuguese document, the first is broader with regards to the covered time period. During the period at which the second is valid (7 a.m. to 8 p.m.) it can be concluded that it proposes more conservative limits. It is important to mention that the values considered in the British standard are corresponding to PPV, whereas NP 2074 takes into account the peak vector sum. Both norms establish specific limits depending on the type of structure. Nevertheless, in BS 6472-2 these values are also suggested according to time and daily number of blasts, and not dominant frequency.

4. Ground vibration amplitude prediction models

After characterizing the structures to protect, understanding the ground on which these are founded and determining the vibration velocity limits (based upon ruling standards similar to those addressed in chapter 3.), it is necessary to determine a vibration amplitude prediction model capable of extrapolating the maximum charge per delay to be applied, knowing the distance between the monitoring point and the blasting event properties. These tools are usually created taking into account experimental data collected in the area of study, given the fact that there is a high degree of complexity associated with each soil and rock mass. The present chapter intends to briefly mention some of the existing prediction models and how these may be influenced by the blasting (controllable) and geological (uncontrollable) conditions.

In 1927, Rockwell concluded that the best physical quantity that describes the structures resistance to ground motion is the displacement its particles suffer after a given dynamic event. Under this premise, Morris (1950) proposed one of the initial wave attenuation models where the building's particle displacement is directly proportional to the detonated charge and inversely correlated with the distance from the energy source. Later, Heelan (1953), Blair and Duvall (1954), Duvall and Fogelson (1962), and Langefors and Kihlstrom (1963) suggested similar expressions – valid for cylindrical charges – that correlate the maximum vibration velocity with the explosives charge and the distance (Bernardo, 2004; Ainalis et al., 2017). Several authors included additional variables in their models like thermodynamic properties of the explosives (Louro, 2009), average burden (Pires, 2021), time delay between adjacent blastholes (Bernardo and Negreira, 2015; Urbano, 2020) and rock mass rating (Luz, 2017).

To date, the scientific community has not defined a universal vibration attenuation expression that is able to predict blast-induced vibration amplitudes. Nevertheless, Lopez Jimeno et al. (1995) and Hustrulid (1999) state that Johnson's mathematical formula (1971) (Equation 16) is the one that has been widely used in the construction and mining sectors (Bernardo and Torres, 2005).

$$v = a \cdot Q^b \cdot D^c \qquad \text{(Equation 16)}$$

According to Equation 16 the resulting vibration velocity v (mm·s^{-1}) is a function of the explosives charge per delay Q (kg) and distance between the detonation and the monitoring points D (m). The dimensionless constants a, b and c are dependent upon the blast design (burden, spacing, stemming, charge weight, etc.) and the *in situ* parameters (geological discontinuities and respective orientation, rock formation, etc.). These constants are determined by multiple linear regression, usually by means of a statistical software or programming language. Therefore, one requires an experimental database with vibration velocity and frequency values registered at different monitoring points near the blasting area, and respective Q and D. It should be noted that several regression attempts, excluding a maximum number of events of 10 % may be carried out in order to obtain the greatest possible coefficient of determination (Bernardo and Torres, 2005). The constants that correspond to the maximized

adjustment, i.e., to the greatest coefficient of determination define de model. After computing the characteristic attenuation equation and, according to the vibration control standard in force, determining the maximum vibration velocity at a given distance, it is possible to estimate the maximum charge per delay, minimizing, hence the potential hazard to structures. Figure 17 synthetizes a modelling methodology suggested by Bernardo and Torres (2005), where after creating an initial database and estimating a vibration velocity prediction model, the determination of the maximum charge per delay becomes possible.

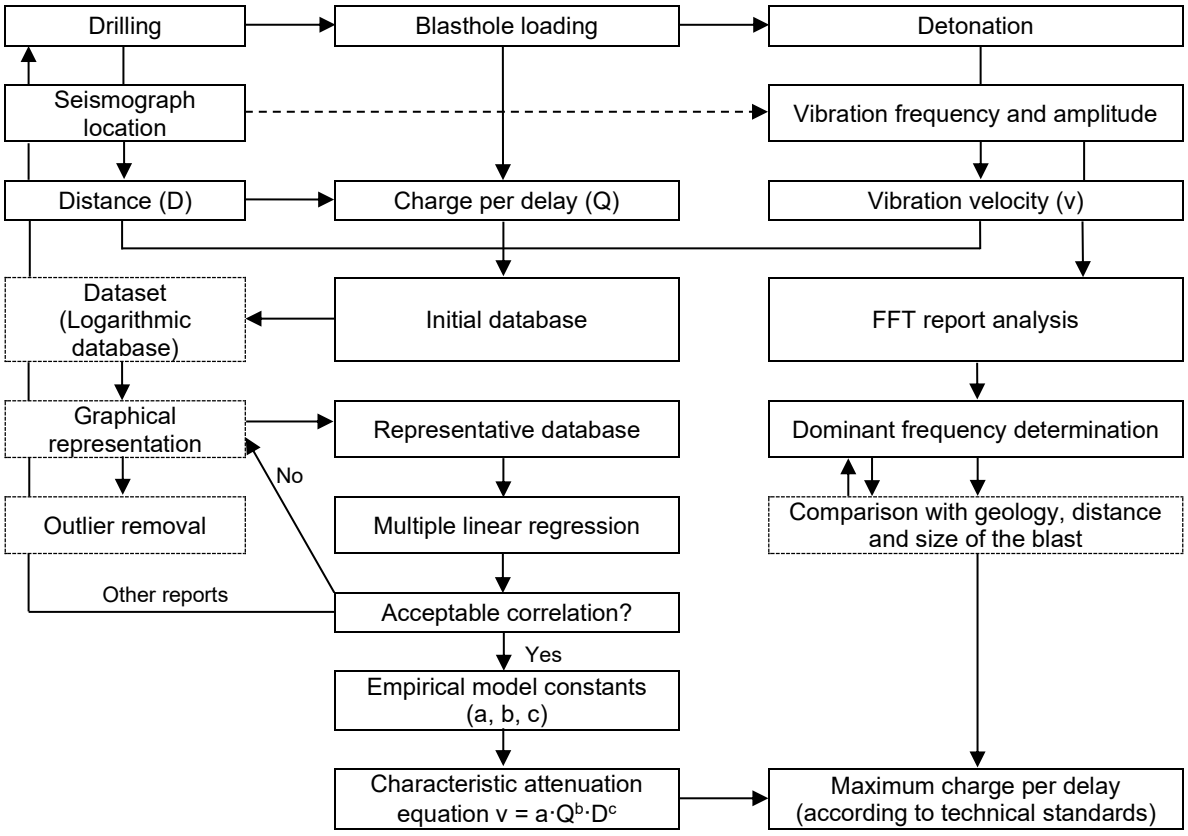

Figure 17 - Control methodology of ground vibration induced by rock blasting events (adapted from Bernardo and Torres, 2005).

Considering the procedure illustrated in Figure 17, it is noteworthy that the vibration velocity is dependent upon both controllable (charge per delay) and uncontrollable variables (distance between the structure and the monitoring point). As mentioned before, the first may be influenced by dividing the bench into smaller units or decking. At a preliminary phase of a mining operation, where no model has been defined, it is recommendable to use models suggested in the literature (Table 10), with the objective of designing the blasting pattern (as a function of the charge weight per time delay – Q). As the operation progresses and event reports are gathered, the three variables can be conjugated, creating an initial database which allows the formulation of the area's characteristic attenuation equation (Equation 16). This may be updated with time, as more data are acquired. Lastly, after attaining a satisfactory model with an acceptable coefficient of determination which fits the experimental data, Q

may be determined with a greater accuracy. This type of approach minimizes the probability of damaging structures in the surrounding area and, most importantly, the risk of not complying with the technical recommendations defined by national standards.

Table 10 - Johnson's model constants for different lithologies (adapted from Bernardo and Torres, 2005).

Lithology	Source	a	b	c
Basalt	Gama (1997)	2.000	0,70	-1,90
Limestone (unspecified)	Gama (1997)	580	0,60	-1,40
Limestone (unspecified)	Bernardo and Torres (2005)	1.271	0,32	-1,37
Pisolitic limestone	VISA Consultores (1999)	500	0,42	-1,22
Granite, gneiss and pegmatite	Holmberg (1982)	700	0,70	-1,50
Hematite	Gama (1979)	380	0,73	-1,87
Schist-greywacke	Remísio (1994)	1.598	0,88	-2,06

According to Table 10, different rock types tend to be characterized by different models. Within a given lithology, the constants a, b and c may vary, after different geomechanical properties of a specific rock mass, its alteration state or the existence of discontinuities. Nevertheless, the estimated constants should not differ considerably from those suggested in the literature. Moreover, one should verify positive b and negative c coefficients, once the vibration velocity is expected to decrease with distance, and increase with the maximum charge per delay, as previously discussed. This physical quantity is null or positive and hence, a has to be positive.

The isokinetic curves of the presented models can be projected on the Q vs. D plane and serve as an expeditious tool to estimate the maximum charge per delay, in such a way that the considered vibration velocity at a given distance is not likely exceeded (Figure 18):

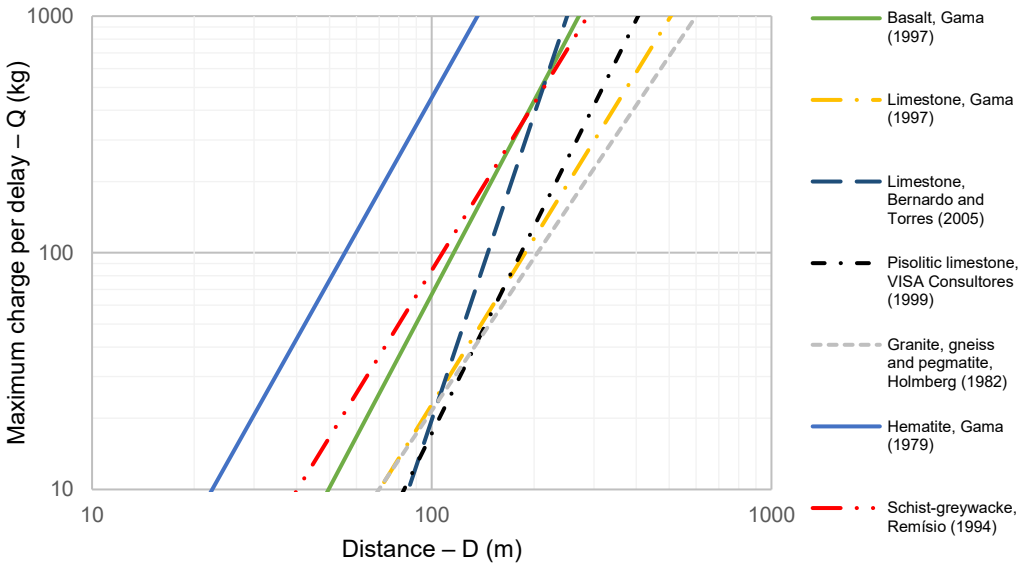

Figure 18 - Isokinetic curves corresponding to different lithologies considering v = 6 mm·s^{-1}.

According to this figure, for distances over 100 m, the most conservative models are the ones relative to pisolitic limestone (VISA Consultores, 1999), limestone (Gama, 1997), and granite, gneiss and pegmatite (Holmberg, 1982). As such, for a fixed distance and vibration velocity, a lower Q value may be applied. Conversely, the least restrictive model, suggested by Gama (1994) corresponds to hematite. It can also be highlighted that the depicted curves have different slopes. The model with the greatest gradient (limestone – Bernardo and Torres, 2005) indicates that for a constant variation in D, a greater differential is verified in Q, suggesting that the analyzed rock mass attenuates vibrations at a greater rate when compared to the remaining models. Contrary to this, the equation with the lowest gradient (granite, gneiss and pegmatite – Holmberg 1982) indicates that the rock mass is more competent and thus, attenuates stress waves at a lower rate. The remaining propagation laws have similar slopes, being that the attenuation degree of the rock mass is intermediate compared to the two indicated scenarios.

As previously mentioned, other variables may be included in ground vibration amplitude models. In fact, NP 2074 suggests the consideration of an energy weighting factor that takes into account the bottom and column charge mass and thermodynamic properties. This expression is shown below (Equation 17) and was studied by Louro (2009).

$$v = a \cdot W^b \cdot D^c \qquad \text{(Equation 17)}$$

Where W (kg) is equivalent to the weighted maximum charge per delay considering the properties of the applied explosive products. This factor may be calculated according to different characteristics such as the detonation pressure or effective energy. The following formula (Equation 18) expresses the calculation of W according to the detonation pressure of the column and bottom charges (P_{dCC} and P_{dBC}, respectively), and to the maximum total charge per delay (Q_{TC}) considering the differentiation between column and bottom charges (Q_{CC} and Q_{BC}, respectively):

$$W = Q_T \cdot \left(\frac{P_{dCC}}{P_{dCC}} \cdot \frac{Q_{CC}}{Q_{TC}} + \frac{P_{dBC}}{P_{dCC}} \cdot \frac{Q_{BC}}{Q_{TC}}\right) \qquad \text{(Equation 18)}$$

As such, once the bottom charge releases more energy per unit of mass of explosive – expressed as a function of P_d –, this expression highlights the greater contribution of this type of explosive to the weighted maximum charge per delay when compared to column charge products.

5. Case study mines and respective framing

The underground mines, object of analysis in this work, are located in southern Portugal (Alentejo province), more precisely in the town of Aljustrel. This case study has provided real data from stope blasts with the final objective of creating models similar to the one suggested by Johnson (Equation 16) that are able to estimate ground vibration amplitudes in the vicinity of a detonation. The inexistence of propagation equations adjusted to the studied area has motivated the development of this work.

5.1. Geographical and geological framework

Initially exploited by the Phoenicians during the Bronze Age, and then by the Romans which named the town *Vipasca* and, later on, *Metallum Vipacensis*, Aljustrel has an important mining history that started more than four millennials ago (Schermerhorn et al., 1987). These populations were responsible for the extraction of ore minerals from surface gossans, producing gold, silver and other metals. In this area, modern mining started in the mid-19th Century by Companhia de Mineração da Transtagana and after successive alterations in ownership, ALMINA – Minas do Alentejo, S.A. is currently the lease owner. In 2019, the mining industry in Aljustrel was responsible for 327 direct and 691 indirect jobs within ALMINA's industrial facilities.

Until 1980's the Aljustrel deposits were mined for pyrite. Soon after the extraction of this commodity became uneconomic, the production of base metals such as copper, lead and zinc started. Precious metals like gold and silver are also present in the orebody, despite at lower grades. This endeavor involved the construction of a 1,2 Mtpa processing plant and other infrastructure like an underground crushing station and a shaft (Chilcott and Owen, 2007). Later on, the processing unit was expanded, reaching its actual capacity: 6 Mtpa. Currently, ALMINA produces zinc, copper, silver and lead concentrates sold to China, Spain, Belgium and Sweden.

Today, six orebodies are well documented in an area of 6 x 2 km belonging to the Aljustrel mining district: Feitais, Estação, Gavião, Moinho, Algares and São João, being distributed across two major zones. The first two deposits are located on the normal limb of the Feitais anticline, whereas the remaining ones are lined along the Southwest anticline. These geological occurrences are located at the Iberian Pyrite Belt, hosting the largest concentration of massive sulfides deposits worldwide. This metallogenic province is estimated to hold 800 million tons of reserves, from which 250 million are located in the Aljustrel area (Carvalho et al., 1976; Sousa and Oliveira, 1983; Schermerhorn et al., 1987). The most relevant ore minerals are pyrite (more than 70 % of the total reserves), sphalerite, galena, chalcopyrite, arsenopyrite and tetrahedrite. The prevailing gangue minerals are barite, carbonates and quartz. The existing deposits were formed between the Late Devonian and the Early Carboniferous (Chilcott and Owen, 2007). At present, only the Feitais and Moinho deposits are being exploited.

Aljustrel geology and the orebodies known to date have been extensively studied and described by authors like Schermerhorn and Stanton (1969), Schermerhorn (1971), Barriga and Fyfe (1988), Chilcott and Owen (2007), Barrett et al. (2008), Leitão (2014), and Morais et al. (2020). Some have divided the area stratigraphy into six main units, from the oldest to the most recent one: Phyllite Quartzite Group (composed by slate, quartzite, limestone and conglomerate), Lower Rhyolite unit, Massive Sulfide horizon (containing mainly zinc, pyrite and copper facies), Upper Rhyolite unit, Lower Sedimentary unit (where chert siltstone and argillite are often present), and Upper Sedimentary unit (mainly composed by wacke, schist and argillite).

Regarding the region tectonics, faults, folds, thrust faults and verging folds may be observed. The most relevant structures are the Messejana, Moinho, Castelo, Represa and Feitais faults. It is noteworthy that a thrust contact is commonly verified between the Lower and Upper Sedimentary units. The mentioned elements suggest the existing heterogeneity in the Aljustrel mine area, which influences the propagation of energy through the ground in the form of vibrations. Figure 19 illustrates the existing orebodies (with the exception of Gavião – located 2,5 km southwest of the São João deposit), geotechnical features of the region, the mining concession boundaries (a), and area where structures are founded on, with the respective use type (b). Here, the proximity between the urban area and the blasts carried out at the two active mines is evident. For this reason, vibrations are frequently perceived by local people, eventually causing their discomfort and, ultimately, originating complaints.

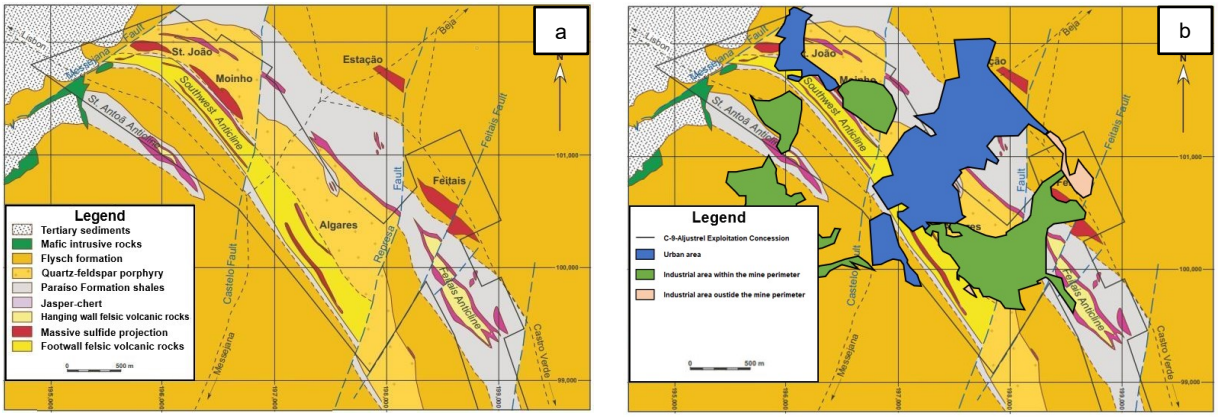

Figure 19 - a. Geology of the Aljustrel mining area and surface projection of the known orebodies. b. Aljustrel town structures use map (adapted from Barrett et al., 2008; Oliveira et al., 2009).

According to Figure 19 (b), the C-9-Aljustrel Exploitation Concession comprises both urban and industrial areas. The last group includes facilities which are mainly within the mine perimeter.

5.1.1. Feitais mine

In the Aljustrel mining area, the deposits are usually zoned with zinc-rich and high-grade copper zones near the hanging and footwall, respectively, being separated by a sterile to low-grade pyrite.

The Feitais orebody, represented in Figure 20, occurs in stratiform and lenticular beds on the normal limb of the anticline with the same designation. The Feitais anticline axis strikes 315 º and reveals a moderate dip northeast. A second phase of intense compressive stresses has induced the first phase fold axes to plunge moderately to northwest and southeast, resulting in axial planes that run perpendicular to each other. Feitais genesis is related to felsic vulcanism and hydrothermal activity, which promoted the concentration of metal rich hot fluids. The orebody is a mass of complex sulfides with a length of 1.000 meters, width of 700 meters and thickness of 100 meters, striking 305 º and dipping 50 º northeast. The deposit does not outcrop, however the mineralized area starts 50 meters below surface (Chilcott and Owen, 2007).

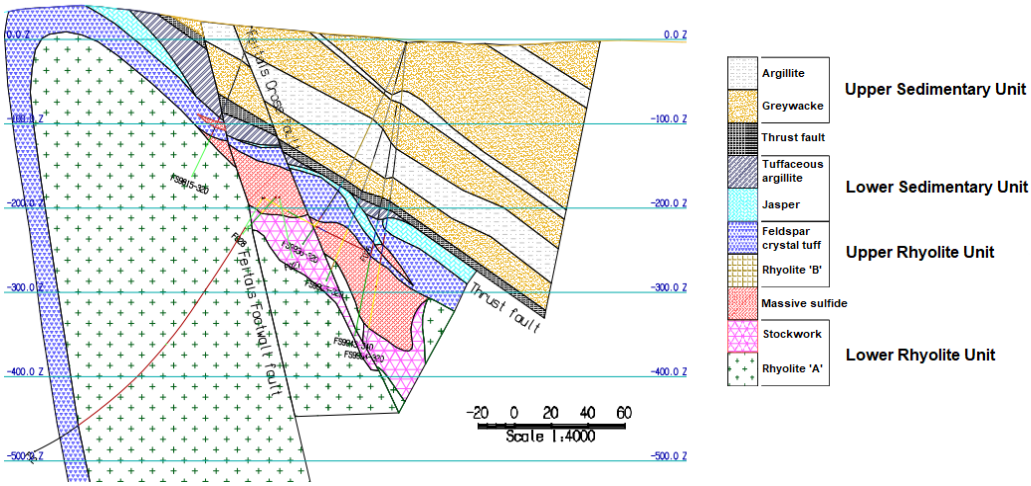

Figure 20 - Feitais orebody SW-NE cross-section (units in meters) (adapted from EuroZinc Mining Corporation, 2000).

The copper-rich footwall zone of the orebody is not only associated with massive sulfides, but also with a stockwork formation revealing pyrite and chalcopyrite veins. The deposit contains fine-grained sulfide minerals such as pyrite, the most abundant one, sphalerite, galena, chalcopyrite, tetrahedrite, arsenopyrite and trace amounts of lead antimony sulfides like bournonite, boulangerite and meneghinite. The aforementioned lithological subgroups that are observed in the Aljustrel mining area are equally verified in the described orebody, where the Late Devonian's Lower Rhyolite unit and the Carboniferous' Upper Sedimentary unit are the oldest and youngest formations, respectively (Chilcott and Owen, 2007). Feitais is characterized by several discontinuities such as the Feitais footwall, cross and thrust faults and Represa fault (Figures 19 (a) and 20).

5.1.2. Moinho mine

Considering the Moinho orebody, it has suffered a higher degree of deformation and has been exploited for a longer period than Feitais – mining activities started in the mid-19th Century and in the late 20th Century, respectively. The deposit known as Moinho is located on the normal limb of the Southwest anticline and in the northern part of the Aljustrel mining area (Figure 19 (a)). Cleavage

associated with this deformation strikes northwest and southeast, being that later compressive stresses have forced the fold axes to plunge northwest and southeast. Geological surveys have proven that Moinho has many similarities to the Feitais orebody, namely with regards to the existing lithological units. Additionally, these studies have indicated that this deposit strikes 315 º, dips 60 to 70 º to the northeast, and reveals a length of 700 meters, width of 700 meters and thickness that varies from 1 to 100 meters (Chilcott and Owen, 2007). The described geological formation is depicted in Figure 21.

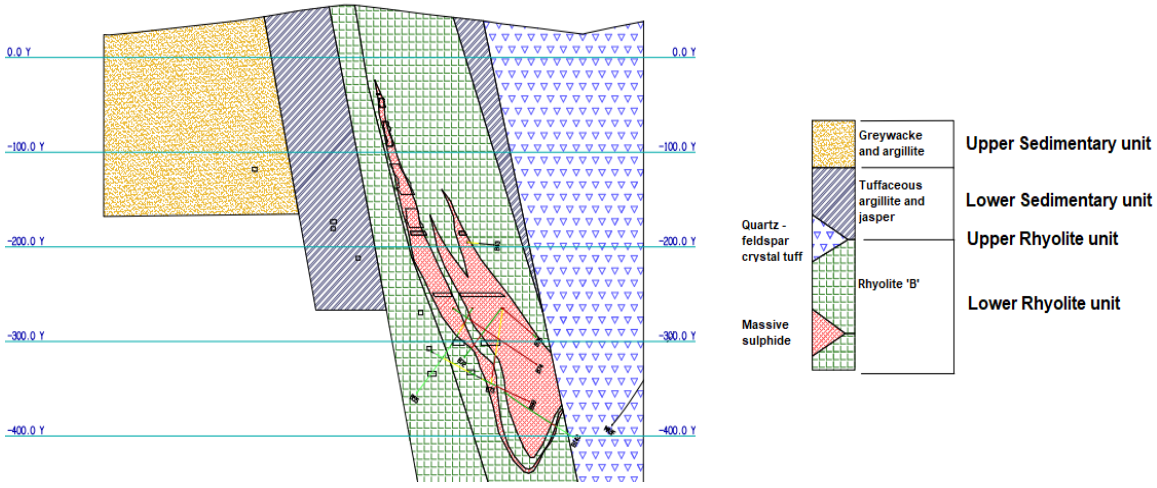

Figure 21 - Moinho orebody SW-NE cross-section (units in meters) (adapted from EuroZinc Mining Corporation, 2000).

The deposit is associated with several structural features such as the Southwest anticline and the Moinho cross faults. According to Chilcott and Owen (2007), the deposit is *truncated down-dip by the northwest-southeast striking Moinho hanging wall fault*. An additional feature known as the Footwall fault records a similar orientation and coincides with the axial plane of the Southwest anticline. The hanging wall and footwall stratigraphy is strongly foliated and a certain degree of movement is revealed by the majority of the contacts. Lastly, other faults sub-parallel to the axial plane of the folds limit the massive sulfide and include the volcanic units, forming a physical barrier to ground vibrations, promoting consequent reflection, refraction, diffraction and dispersion of vibration-related stress waves. The anisotropy caused by foliation and the stratigraphic sequence that includes the same units as the Feitais orebody are additional factors contributing to an eventual attenuation or constructive interference of stress waves.

The Moinho orebody is, in its majority, fine-grained massive sulfides such as pyrite (more than 70 %), sphalerite, galena, chalcopyrite, tetrahedrite, arsenopyrite and other sulfosalts.

Despite the heterogeneity and anisotropy that characterize the Aljustrel mining area, which was severely deformed by geological phenomena, both mines are, at first, studied individually, considering the surrounding rock mass as a continuous, homogeneous, isotropic, linear and elastic entity, discarding the effect of different lithologies and geotechnical structures. Later on, a more detailed examination on the existence of an eventual anisotropy is carried out.

5.2. Mining method

5.2.1. Feitais mine

Both mines apply bulk mining methods, characterized by high productivity and low costs due to the stopes dimensions. At Feitais mine, the orebody is mined using sublevel open stoping with backfilling. It is noteworthy that the stope is blasted in two phases: an initial lower volume followed by the upper part. Both phases are approximately 20 meters high. From the footwall, drawpoints are driven on 40 m intervals (stope height), approximately 5 by 5 m. After reaching the end of the stope, the drifts are enlarged in both directions by 10 m, reaching a total width of 15 meters. Then, a slot raise is mechanically excavated or drilled using parallel drillholes between consecutive sublevels to create an initial free face. Afterwards, up-hole benching is used to enlarge the existing free face and further enable blasting of the remaining rings belonging to the lower 20-meter portion of the stope. At this phase, drillholes are usually charged with an adhesive bulk emulsion and primed with boosters combined with programmable electronic detonators. Lastly, after the stope is remotely mucked, its upper portion is drilled downwards, charged with packaged emulsion explosives (primed with electronic detonators) and blasted, where blastholes that belong to rings closer to the slot raise are the first ones to be initiated. In most cases, bottom and column charge explosives are used. The remaining rings are then blasted until the planned ore volume is excavated. Figure 22 illustrates the described sequence of the stopes excavation process. Drillholes with 89 mm in diameter are parallel or fanned, depending on factors like the stope shape or the drawpoints relative position. Primary and secondary stopes are later backfilled with paste and uncemented waste from underground development, respectively.

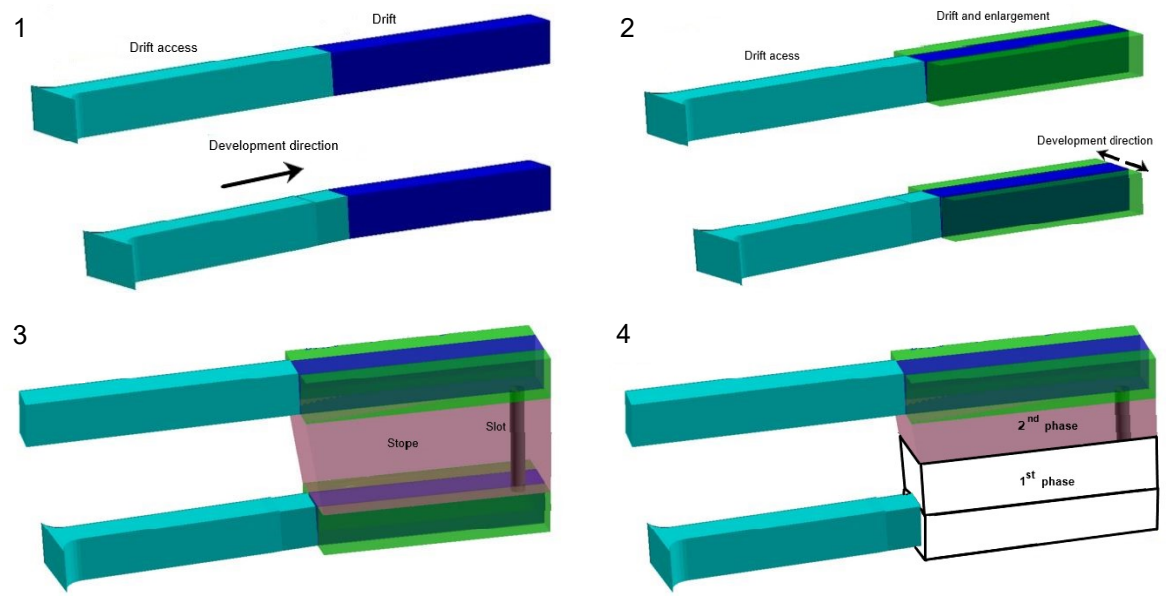

Figure 22 - Stope development sequence (adapted from ALMINA – Minas do Alentejo, S.A., n.d.).

It should be mentioned that, in particular circumstances, due to mine planning considerations, stopes are 20 meters high. These rare cases may involve up-hole, downhole benching, or a combination of both. At Feitais mine, an additional geometry is verified, where stopes between the 160 m and the

210 m levels are 50 meters high. Regarding ground vibrations, these are a concern given their proximity to the surface and the extension of the explosives column, motivated by the stopes dimensions, which may involve greater charge per delay values. Once in the first phase of the stope blast, the rock mass is more continuous and confinement is greater, this is prone to generate greater vibration velocity amplitudes than downhole bench detonations, where a discontinuity created by the previously excavated lower part decreases the energy transmitted into the rock mass. This will be studied and assessed in chapter 7.

5.2.2. Moinho mine

Regarding the older Moinho mine, the employed mining method is longitudinal bench and fill with loose rockfill. Stopes are developed in the longitudinal direction and are 20 meters high. As such, drawpoints are driven every 20 meters. Depending upon planning considerations, these may register widths of up to 15 meters. Due to geotechnical concerns, a pillar is left between adjacent stopes.

The development sequence of the stopes at Moinho is similar to the one shown in Figure 22, corresponding to the Feitais mine. However, some changes can be highlighted. Usually, 76 and 89 mm diameter drillholes are drilled downwards using long-hole drilling rigs, being that their orientation depends on the stopes geometry. Blastholes are charged with packaged emulsion explosives (typically bottom and column charge) and primed with electronic detonators. The initial rings to be blasted are the ones closer to the slot raise and the remaining ones are then blasted until the planned volume is excavated. Here, it is important to consider that the stope is only blasted in one phase. Thus, with regards to ground vibrations, these are not attenuated by the lower confinement promoted by an existing discontinuity in the rock mass, created by the initial up-hole blasted volume, as verified at Feitais. In limited situations, stopes are blasted using up-hole benching, or a combination of this one and downhole benching. In this case, due to the jumbo drill rigs characteristics, blast holes have a diameter of 89 mm.

Considering environmental impacts mitigation measures, with emphasis on vibrations, ALMINA applies the following measures: multiple initiation for blast holes more than 20 meters long and slot raise excavation by means of mechanical excavation, rather than conventional and drill and blast methods which are less frequent for this stope element. Electronic detonators are used, rather than non-electric ones, reducing the probability of delay overlapping and ensuring a wider range of available delay timings.

It is necessary to add that the company carries out permanent monitoring campaigns to assess the compliance of NP 2074 and optimize the blasting pattern with regards to the vibration impact on nearby descriptors. This procedure includes seven Instantel engineering seismographs strategically placed at five different monitoring points (located at the industrial area within and outside the mining area, and within the urban perimeter). Such devices are verified by a certified institution on a yearly basis, ensuring that the measured values do not have considerable deviations. The transducers placement, orientation, and PVS and frequency detection intervals are compliant with the recommendations provided by NP 2074. Between 2018 and 2020, four other structures were monitored during different periods. The majority of the records collected from 2018 to 2022 are considered in the present work.

6. Methodology

The present section intends to describe the process of data collection and consequent compilation, fundamental to achieve the objectives proposed in chapter 1.3. This step can be divided into two parts: analysis of information collected during ALMINA's systematic vibration monitoring campaign and fieldwork. An additional description of a particular stope blast is carried out.

6.1. Database organization

Regarding the first stage, the license holder is responsible for the real-time monitoring of blast-induced ground vibrations at structures within the Aljustrel town, originated by development and production blasting activities. Once the last category of blasts is more relevant concerning environmental impacts, given the greater explosive charge per delay, these are the only ones to be considered in this work. In terms of production blasts responsible for generating vibration velocities over the trigger, the monitored data are then added into a database that includes the stope designation; used seismograph and respective geophone; monitored structures location; event date; maximum vibration amplitude in the FFT spectrum; dominant frequency; and PVS. The stope designation includes a letter (F and M for stopes located at the Feitais and Moinho mines, respectively), level identification, type of ore and respective number within the level at issue. By way of example, the zinc ore stope number 027 located at the 270 m level at Feitais is designated as F270SZ027.

The contribution of the present dissertation to the database, which involved the consultation of stope holes charging records (example in Annex A), is the addition of complementary parameters to the existing records such as type of blast (up-hole or downhole benching); the maximum real explosive charge per delay (including the explosive substance designation and quantity in the considered blast hole) and respective hole theoretical geographical coordinates; orientation angle between the blast and the receiver; time delay between adjacent holes and rings; seismographs geographical coordinates; and initiation geometry. To estimate the blast hole coordinates, georeferenced AutoCAD drilling patterns were considered, whilst the determination of the monitoring points absolute position was carried out using Global Navigation Satellite Systems survey equipment. The considered reference system (geodetic datum) was the Lisbon Datum. Once the coordinates between the two points are known, it becomes possible to estimate the respective distance – last parameter to be included in the database. The orientation of the waves path between the energy source and the monitored points is considered for anisotropy assessment of the rock mass surrounding the studied area. For azimuth angles between 45 and 135 º, and 225 and 315 º, the orientation is equivalent to north-south (N-S), whereas the complementary angles correspond to east-west (E-W). Apart from the regular monitoring campaign, additional seismographs were placed at points of interest, being this detailed in the following section.

The described database is present in Annex B and includes 2.362 records from 1.078 production blasts (2.359 of which are part of the original monitoring campaing and the remaining three constitute additional records) from a period between February 2018 – period at which the mining methods were reviewed and updated – and August 2022. During this time frame, a total of 1.215 stope blasts was carrried out, suggesting that 137 events (11 %) did not generate vibration amplitudes over the trigger level (0,51 mm·s^{-1}). Once multiple seismographs were placed at different locations during coincident time periods, it is common to monitor vibrations originated by the same blast at distinct points. Additionally, the compilation of events includes 111 trim blasts. This technique is usually carried out after the schedulled production blasts in a given stope have taken place and when a considerable mineralized volume such as pillars is not excavated as initially planned (underbreak), therefore aiming at maximizing ore recovery. Under this condition, given the fact that the rock mass reveals to be less continuous when compared to ring blasts, events associated with trim blasts are discarded from this work. For the same reason, secondary fragmentation of oversize material in the muckpile that generate vibration amplitudes over the trigger is not considered. Lastly, 76 events are discarded from this study once it was not possible to determine the maximum charge per delay (Q). As such, the total of valid events present in the database is equal to 2.175.

6.2. Fieldwork

The second step consisted in the development of fieldwork, which included two distinct activities. The initial one corresponded to the placement of an engineering seismograph at a public structure (Aljustrel Town Hall), within the urban area of Aljustrel, following the procedure suggested by NP 2074 and described in detail in chapter 3.1.1. A second seismograph was placed at a residential structure. Considering the additional activity, this one included the calculation of relevant elements from several structures such as height, building material's waves propagation velocity and porosity to test the validity of an expeditious formula, given by Equation 12, to estimate one of the structures dynamic response properties: natural frequency.

6.2.1. Ground vibration monitoring within the Aljustrel mining area

The location of the monitored buildings, where seismographs were installed in the previous four years is present in Figure 23 that corresponds to an orthophoto of the Aljustrel town. It is relevant to note the strategic relative position of the monitoring points that cover a wide area, including different directions, between the town and the location of the blasting events.

Figure 23 - Surface projection of the Feitais and Moinho orebodies and location of the monitored points within the Aljustrel mining compound.

Regarding this figure, the location of the ten monitored structures is identified with letters and color coded according to their respective type. The classification criteria used are the ones described in NP 2074. This code is described as follows:

1. Sensitive structures are identified in red: A and B;
2. Current structures are presented in yellow: C, D, E and F;
3. Reinforced structures are shown in green: G, H, I and J.

The blasting events considered in this work (production ones) are circumscribed to the illustrated surface projection of both orebodies, being that the proximity between these and descriptors like humans and structures at the Aljustrel town, sensitive to ground vibrations is evident.

It is important to note that the seismographs were strategically placed between the mines perimeter, equivalent to the blasting source, and elements to protect such as constructions located within the Aljustrel mining compound and people inside them, trying to cover multiple surface distance range values and directions. Structures H and J are within the mine perimeter, whereas the remaining ones are located outside this perimeter (within the industrial area – B, G and I – and within the urban area A, C, D, E and F). The structures monitored in parallel with the previously addressed ALMINA's campaign are depicted by letter C and E and ground vibration recording was started on July 12th and July 25th, respectively, and ended on August 8th, 2022. In 2020 a monitoring campaign was carried out at structure E, being that data previously obtained here were also considered in this study. It is noteworthy that the trigger level was set to 0,3 mm·s^{-1}, corresponding to the human vibration perception threshold (Kiely, 1999). Figure 24 represents the first location, where a verified Instantel Micromate®

engineering seismograph coupled with a DIN triaxial was placed. The second location included an Instantel Minimate® seismograph coupled with an ISEE geophone (Figure 25).

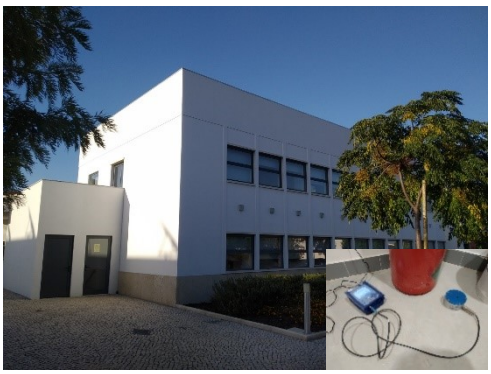

Figure 24 - Structure C: Aljustrel Town Hall.

Figure 25 - Structure E: residential building.

Figures 26 to 33 illustrate the remaining monitored structures relevant to this work.

Figure 26 - Structure A: church.

Figure 27 - Structure B: gas station.

Figure 28 - Structure D: swimming pool ancillary facilities.

Figure 29 - Structure F: residential building.

Figure 30 - Structure G: workshop.

Figure 31 - Structure H: primary ventilation fan ancillary facility.

Figure 32 - Structure I: workshop.

Figure 33 - Structure J: primary ventilation fan ancillary facility.

Finally, after the end of the monitoring campaign at structures C and E, the recorded vibration events were uploaded from the seismographs to a computer and latter processed using a specific software developed by Instantel (THOR™) to obtain PVS and dominant frequency values from the generated event and FFT reports, respectively. Apart from the three registered events (two at structure C and one at E), additional two were recorded. These, however were characterized by anomalous PVS values and FFT reports, which could be justified by spurious energy released during the activity of people and equipment located near the two monitored structures. Annex C depicts an example of generated event and FFT valid reports. These reports correspond to the production blast that took place at Feitais mine, more specifically at the 510 m level and longitudinal stope 027L (F510SZ027L), on August 1st, 2022. The event was registered at structure E.

To provide an objective example of a production blast and consequent result in terms of fragmentation, production volume and specific explosives consumption, the stope F410SZ041 is going to be analyzed. The considered blast involved a secondary stope from the Feitais mine at the 410 m level. The blast took place on August 22nd, 2022, and contained five parallel rings (R7 to R11). These are illustrated in Figure 34.

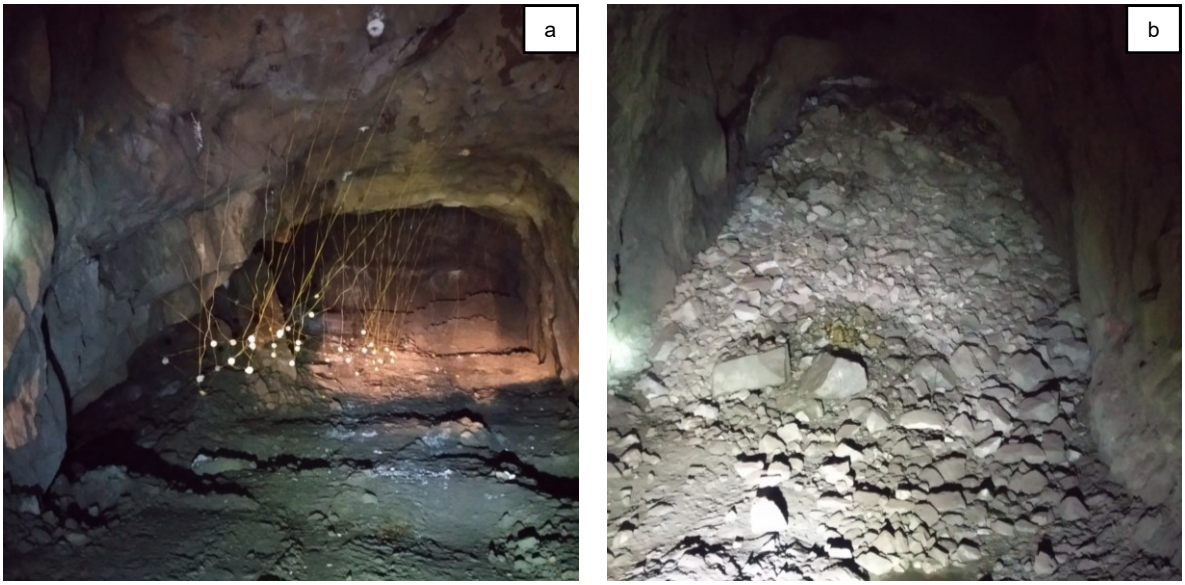

Figure 34 - Stope F410SZ041 before (a) and after (b) blasting rings 7 to 11.

As is evident from Figure 34 (a), the blast involved loading up-holes with adhesive bulk emulsion which is visible around some holes collars. In total, 3.134 kg of explosive were used to blast 2.127 m^3 (9.228 tons) of ore – equivalent to a powder factor of 1,47 kg/m^3 (0,34 kg/ton). The estimated value is similar to the one obtained for hard rock production blasts carried out on granite.

When considering Figure 34 (b), one can notice that the explosive energy was efficiently used in rock fragmentation, due to the inexistence of oversize material in the muckpile. It should be noted that the drawpoint represented in the right figure is a 5 by 5 m drift.

6.2.2. Estimation of structures geometrical parameters and respective building materials waves propagation velocities

To complement the study on ground vibrations in the Aljustrel mining area, one considers relevant the estimation of the monitored structures natural frequency, allowing the identification of eventual resonance phenomena and consequent performance of changes in the blasting pattern aiming at protecting the considered buildings. At this stage of the fieldwork, the analyzed structures are A, C, D and E given their importance in terms of ground vibrations control. It should be remembered that the buildings in cause are classified as sensitive and current ones – according to NP 2074 –, and once they are located at the urban area and it is expected that sensitive descriptors such as humans may be within these elements during the blasting period, more attention should be given to them. Structure F, a residential one, is not considered because no permission was granted to carry out the intended descriptive study.

Thus, to apply the formula present in Equation 12, it is necessary to determine the monitored buildings height, the respective porosity (dependent on its geometrical parameters), and C_P. To complete the determination of the first two elements, a tape measure is used, whereas the last physical property is estimated by means of an ultrasound device equipped with two piezoelectric transducers (one receiver and one transmitter) with predominant frequencies of 55 kHz. In some cases where the respective floor plan is available, this document is observed and considered, once it provides a better understanding of the building's characteristics, such as its geometry, area and possible location of most structural elements.

Initially, the buildings and respective levels height is estimated. Afterwards, the product of this variable and the area corresponds to the volume of the building. The next step consists in determining the structural elements location and corresponding volume. Such elements are essentially pillars and slabs. Lasty, the structures porosity, defined by Equation 19, is estimated.

$$n = \frac{volume\ of\ voids\ of\ the\ structure}{total\ structure\ volume} = \\ = \frac{total\ structure\ volume\ -\ volume\ of\ structural\ elements}{total\ structure\ volume} \quad \text{(Equation 19)}$$

As can be inferred from the equation, a void is considered as a volume in the structure which does not correspond to a resistant element of the building such as pillars or slabs, therefore transmitting a reduced amount of seismic energy.

The estimation of the building materials' waves propagation velocity was carried out as Figure 35 illustrates.

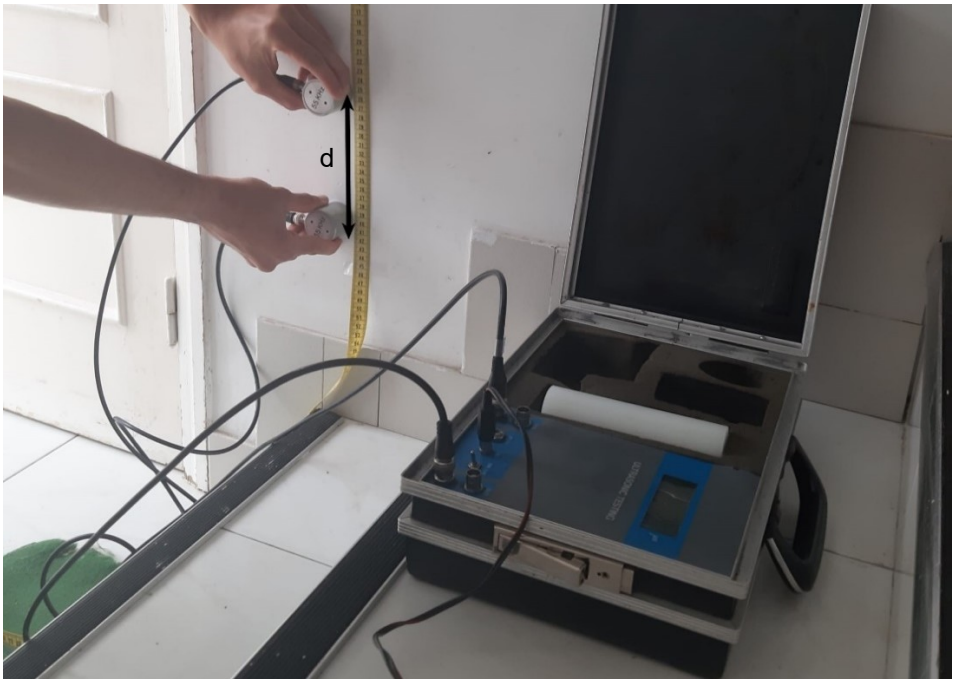

Figure 35 - Estimation of the building material's waves propagation velocity for structure C.

After calibrating the ultrasound equipment and placing the two transducers at a known distance (d) on the same surface of a structural element, one can estimate C_P by the division between the distance and the travel time of the transmitted signal. Ideally, the transducers are placed at a wall on a surface that contains structural elements such as pillars. Several distances from 5 to 30 cm and according to an interval of 5 cm were considered. Nevertheless, it should be mentioned that for structure A no accurate readings were obtained for distances of 25 and 30 cm. The geometrical parameters were however, determined for the intended elements.

Table 11 synthetizes the values measured in the field regarding the estimation of the mean C_P value – $\overline{C_P}$ – , structures height and porosity. Annex D compiles information regarding each of the studied structures, relevant to determine the respective building materials' propagation velocity and porosity.

Table 11 - Results of the building materials' waves propagation velocity, structures height and porosity estimation.

Structure	Sample material	$\overline{C_P}$ (m·s^{-1})	Height (m)	Porosity (-)
A	Masonry	3.152,2	8,7	0,64
C	Reinforced concrete	2.189,7	8,1	0,91
D	Reinforced concrete	2.030,9	10,5	0,87
E	Wood	2.383,0	2,7	0,99

Similar studies developed for buildings with characteristics similar to structure A have determined that the waves propagation velocity for masonry ranges between 1.050 and 3.050 m·s^{-1} (Zielińska and Rucka, 2018). The estimated velocity is similar to the interval upper limit. This is greater than the C_P that characterizes reinforced concrete, which according to the bibliography is about 2.140 m·s^{-1} (Feng and Yi, 2017). Such difference may be justified by the compaction degree of the structure and the geological material that characterizes the structural element (masonry), which for structure A is unknown. It should be mentioned that the propagation velocities estimated for structures A and E are deemed relatively high, being unexpected. Lastly, Fabisiak et al. (2007) have concluded that the C_P of pine wood varies between 4.000 and 5.800 m·s^{-1}. This diverges from the values measured in the field, suggesting that the possible aging and treatment the wood has suffered may contribute to a decrease in this physical quantity values.

7. Analysis of the obtained data and results

After the fieldwork, a database was created, compiling the initial and additional information regarding each blasting event. The data present in this compilation were thereafter analyzed, verified, and finally processed. As it will be described later on in detail in this chapter, a preliminary investigation of the variables distribution is performed. This is followed by a compliance assessment regarding two different ground vibration monitoring standards. The present chapter ends with a detailed study of the compilation of vibration events with the objective of determining the variables relevance and performing the removal of outliers. This process culminates in the creation of ground vibration propagation models for both Feitais and Moinho mines considering Johnson's mathematical formula (Equation 16) and additional relevant variables – geographical and operational ones. The estimation of these models is performed by means of a commercial statistical software (SPSS), more specifically, utilizing a multiple linear regression tool.

As mentioned before and according to Figure 22 that describes the development sequence of a stope, two operational conditions that affect the propagation of vibrations through the ground can be highlighted: one where there is no considerable void adjacent to the blast (i.e. first phase of the production blasts), and another one characterized by a direct discontinuity under the remaining blasted volume (second phase). Figure 36 illustrates these scenarios.

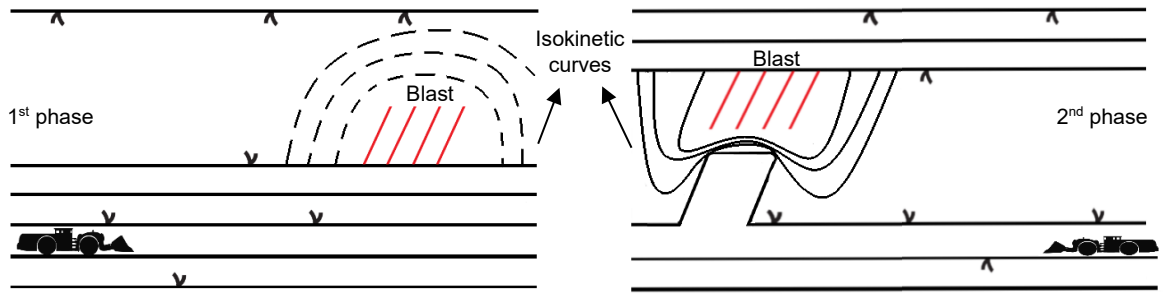

Figure 36 - Influence of the void created by previous production blasts on the propagation of ground vibrations.

Under this condition, it is expected that in the first phase of the blast, given the greater rock mass continuity between the source of energy and the receiver, vibration amplitudes registered at the monitored structures are greater than in its subsequent stage. Conversely, after the discontinuity imposed by the initial blasts, stress waves are deviated by this void, suffering successive reflections before reaching the surface. Nevertheless, this hypothesis is going to be tested later on. Hence, three operational scenarios will be considered: vibration events registered after blasts from the Feitais mine without an existing discontinuity (FWOD) and with an existing discontinuity (FWD), and from the Moinho mine without an existing discontinuity (MWOD). Once it is not possible to integrate in a simple model the influence of the existing voids such as drifts, open stopes and other infrastructure on the propagation of stress waves these will not be considered in this study. It is noteworthy that the reduced number of

blasting events carried out at 20-meter high stopes at the Feitais mine – excavated in one phase – are considered in FWOD.

7.1. Exploratory data analysis

Firstly, one should perform an exploratory data analysis where simple statistical elements of the most relevant variables are calculated and discussed. As such, it becomes possible to identify the respective measures of central location (arithmetic mean and median) and dispersion (standard deviation, maximum, minimum and range). Additionally, this procedure provides information on the possible correlation between variables, allowing the creation of preliminary assumptions.

After calculating simple statistical elements of the most relevant variables PVS, Q, D, f_d, and time delay between adjacent holes (T) these values are summarized in Table 12. As previously mentioned, the number of valid samples is equivalent to 2.175 from which 1.203 contain information about T (discrete variable). The ones that contain this variable were originated after 542 production blasts.

Table 12 - Statistical description of the five considered variables for the three operational scenarios.

		Minimum	$P_{25\%}$	Mean	Median	$P_{75\%}$	Maximum	Standard deviation	Range	Number of samples
MWOD	PVS (mm·s^{-1})	0,52	0,64	1,09	0,77	1,27	3,66	0,69	3,13	40
	Q (kg)	21,42	54,91	79,08	70,12	98,70	162,50	31,34	141,08	
	D (m)	512,67	547,39	678,72	589,73	781,08	1.476,78	192,61	964,11	
	T (ms)	50,00	75,00	73,04	75,00	75,00	75,00	5,50	25,00	
	f_d (Hz)	2,13	26,73	38,62	40,00	49,96	73,50	17,37	71,38	
FWD	PVS (mm·s^{-1})	0,30	1,20	2,55	1,97	3,26	16,70	2,06	16,40	1.011
	Q (kg)	16,07	87,28	107,78	100,01	125,01	254,57	39,71	238,51	
	D (m)	161,79	380,06	488,35	447,94	540,89	1.912,53	199,00	1.750,75	
	T (ms)	50,00	50,00	58,99	50,00	65,00	75,00	10,28	25,00	
	f_d (Hz)	2,25	20,00	32,88	26,75	40,10	146,00	19,81	143,75	
FWOD	PVS (mm·s^{-1})	0,36	1,05	2,25	1,77	2,90	12,80	1,70	12,64	1.124
	Q (kg)	10,71	113,75	140,89	152,00	171,00	281,00	49,13	270,29	
	D (m)	179,26	411,42	520,84	478,33	576,16	1.922,29	203,79	1.743,04	
	T (ms)	25,00	50,00	60,20	50,00	75,00	75,00	11,39	50,00	
	f_d (Hz)	2,13	20,00	33,42	28,90	40,07	120,00	17,12	117,88	
								Total		2.175

According to the previous table, most of the samples were recorded after blasts at the Feitais mine, justifying its higher productivity. Given the lower minimum and mean values for D considering FWOD and FWD, both the mean and maximum PVS measured at the monitored structures are greater than in MWOD. Despite the reduced difference, the mean dominant frequencies associated with the events from Feitais are lower than the one calculated for Moinho (38,62 Hz), suggesting that the rock mass has different characteristics, revealing a different filtering effect in both cases. Regarding T, the

most frequented values for this variable are 50, 65 and 75 ms. However, in limited cases other time delay sequences were used (25, 42 and 60 ms).

7.2. Preliminary analysis of the monitored events

Once the existing standards addressed in chapter 3. indicate vibration limits below which it is not likely to observe cosmetic, minor or major structural damage, it is pertinent to analyze the monitored events taking into consideration such technical bases. Moreover, given the geographical framework of the mining operation under study that is characterized by the relative proximity between geotechnical activities – dependent upon explosives to successfully excavate the rock mass – and the surrounding populations, one cannot disregard a technical approach on human exposure to blast-induced vibrations.

7.2.1. Study of the obtained ground vibration records according to NP 2074

Motivated by the vast number of samples, to simplify the study of the obtained results considering the national standard in force, records measured at both sensitive and current structures are analyzed separately from those belonging to industrial ones.

Firstly, it should be mentioned that all the records are deemed compliant according to the national legislation. The initial group to be studied is the one that compiles records registered at sensitive and current structures, including a total of 122 samples. As such, comparing the obtained data with the most unfavorable and conservative ground vibration limits present in NP 2074 (equivalent to sensitive structures, according to Table 4) the results are shown in Figure 37. This figure corresponds to a projection of the samples on the PVS vs. Q and PVS vs. D planes, and the suggested vibration velocity limits.

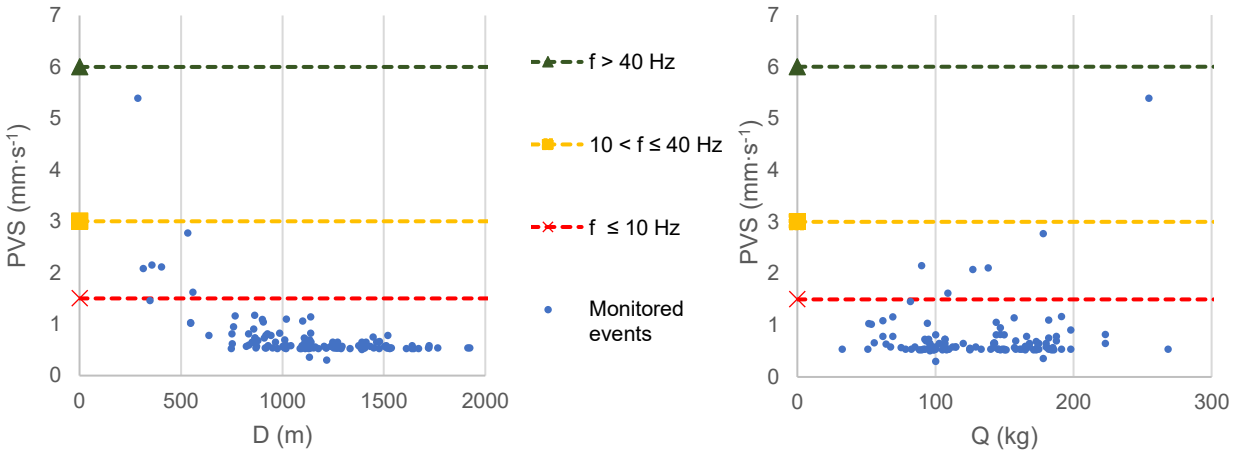

Figure 37 - Projection of the samples measured at sensitive and current structures, and comparison with ground vibration amplitude limits suggested by NP 2074 for sensitive structures.

The observation of Figure 37 suggests that the majority of the records (116 in total – 95 % of the samples) are below the most restrictive limit (represented by the red dashed line). The six points located above this limit were recorded at structure B, which is within the industrial area outside the mine perimeter (Figure 23). The reduced distance (less than 558 m) and great charge per delay (between 90 and 255 kg) associated with these observations justify the high PVS values, when compared with the remaining points. The mean PVS of the considered samples is equal to 0,74 mm·s^{-1}, which is equivalent to half of the lower limit. It is possible to conclude that if the structures addressed in this analysis (A, B, C, D, E and F) were classified as sensitive ones, most of the projected records would be below the 1,5 mm·s^{-1} threshold and thus, regardless of the dominant frequency, these events would comply with the standard. As mentioned before, there were no events registering PVS values over the respective limit. Hence, it is unlikely that the blasting events were responsible for direct damage verified in the studied buildings.

In this graph, the representation of the samples coordinates is not performed, once it would make the plot unreadable. It is more relevant, however, to consider the group as a whole in such a way that anomalous and alarming vibration values are detected and studied more in detail. Additionally, the inverse relationship between PVS and D and the direct proportionality between the dependent variable and Q can be verified.

Now, the representation of the remaining class that includes reinforced structures is carried out (Figure 38).

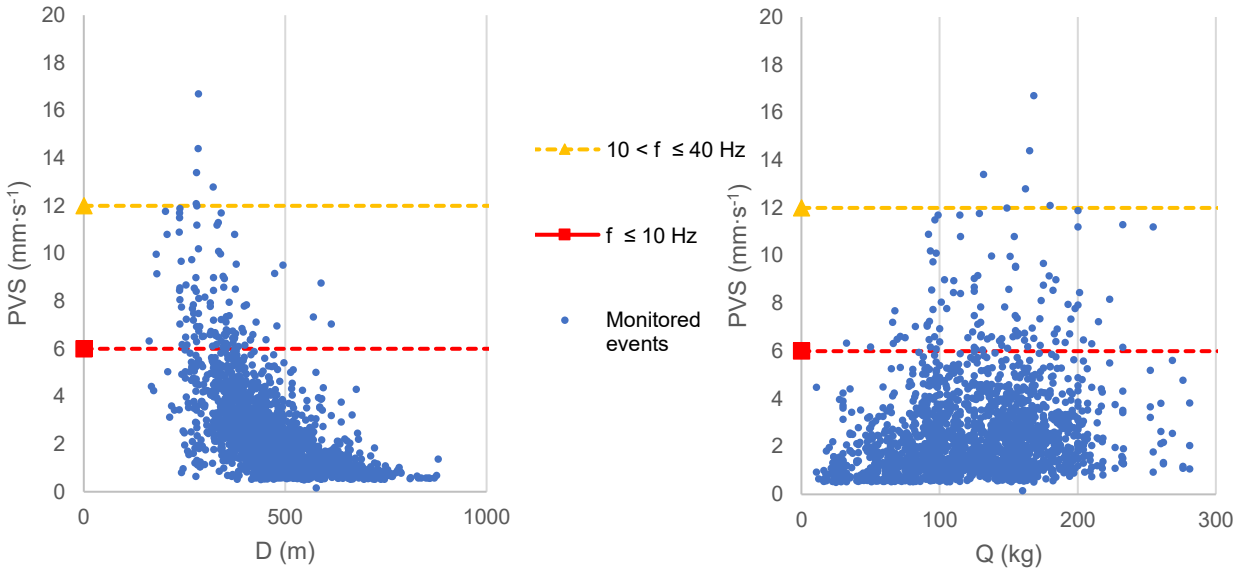

Figure 38 - Projection of the samples measured at reinforced structures, and comparison with ground vibration amplitude limits suggested by NP 2074 for sensitive structures.

Motivated by the considerable number of observations (2.053), an individual study of the projected elements is not possible. Nevertheless, it is evident that the greatest PVS monitored at a reinforced structure corresponds to 16,7 mm·s^{-1}. This is less than half of the upper vibration limit for this class of buildings, which is not depicted in Figure 38, once it would increase the density of the

represented points. In this situation, the lower distance values imply greater PVS recorded at structures G, H, I and J, where the mean vibration amplitude is equal to 2,47 mm·s^{-1}. Almost 94,7 % of the samples are below the most conservative limit. The remaining 5,0 % – PVS between 6 and 12 mm·s^{-1} (102 observations) – and 0,3 % (PVS above 12 mm·s^{-1}: 6 samples) were monitored at lower distances, as illustrated in the figure.

In conclusion, under the premise that the considered records comply with the Portuguese standard and that in both situations 95 % of the observations are located below the most restrictive limits for the respective structure categories, the license holder blasting activities are safe and are not expected to damage the surrounding structures. This does not invalidate a continuous effort to follow the best available techniques and mitigate ground vibration amplitudes by optimizing blasting patterns, protecting different stakeholders and reducing the likelihood of possible complaints.

7.2.2. Study of the obtained ground vibration records according to BS 6472-2

Once there is no Portuguese standard suggesting maximum limits concerning human exposure to blast-induced vibrations, an analysis considering the British document BS 6472-2 is going to be performed. Taking into account that blasts in Aljustrel mines occur between 7 p.m. and 8 p.m. (which according to Table 9 fall into the *other times* period), and that the majority of the people living in the town are within residential structures during this time, the recommended vibration limit is equal to 4,5 mm·s^{-1}. Additionally, they are more susceptible and sensitive, and less tolerant to ground vibrations, being this the principal reason for assessing the impact blasting events have on them. The data collected at the remaining current structures that are not deemed residential are also included in this study. This grouping is performed, because of the structures location (urban area). Consequently, only records relative to structures C, D, E and F are subject to study in this case. The projection of the considered samples, along with the mentioned velocity limit is illustrated in Figure 39.

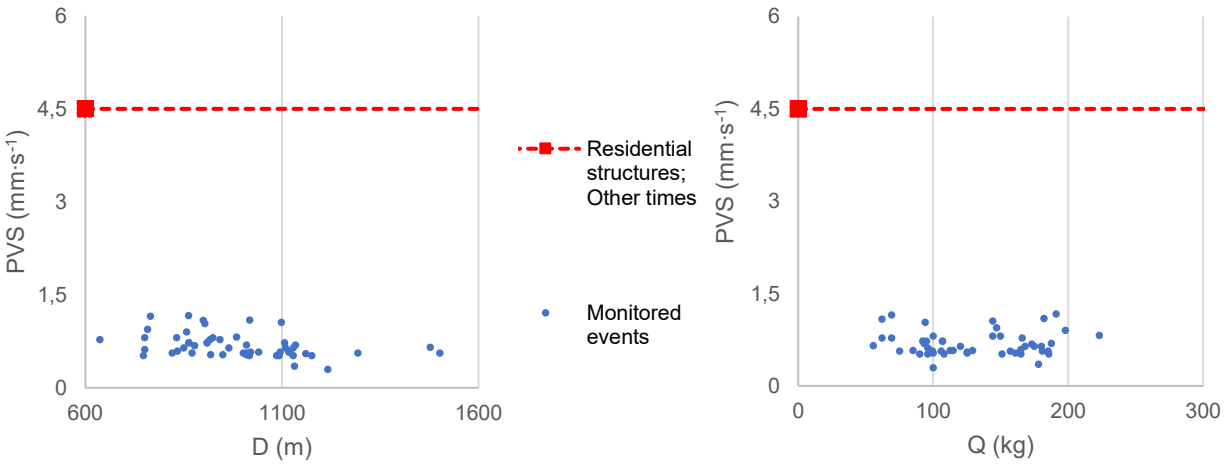

Figure 39 - Projection of the samples measured at current structures, and comparison with ground vibration amplitude limits suggested by BS 6472-2 for residential structures.

According to this figure, the projected samples register PVS values below 1,5 mm·s^{-1} (at least one third of the suggested limit of 4,5 mm·s^{-1}). As such, in this situation and during the studied period, BS 6472-2 is complied with. Although the recorded PVS values are over the human perception threshold (0,3 mm·s^{-1}), these are not excessive and the considered blasts had a reduced impact on humans. When analyzing Figures 37 and 39, it is possible to verify the greater vibration amplitudes measured at structures A and B in relation to the rest, once they are not depicted in the second graph.

Now, taking into account the expression present in Equation 15, one intends to estimate the maximum number of blast vibration events per day, in such a way that the vibration limit is equivalent to the previously considered value of 4,5 mm·s^{-1}. Therefore, rearranging this equation to solve it for N yields the following expression (Equation 20):

$$PVS_{max} = 4{,}5 \cdot F \Leftrightarrow PVS_{max} = 4{,}5 \cdot 1{,}7 \cdot N^{-0{,}5} \cdot {T_b}^{-d} \Rightarrow N = \left(\frac{4{,}5 \cdot 1{,}7 \cdot {T_b}^{-d}}{PVS_{max}}\right)^2 \quad \text{(Equation 20)}$$

Considering the mentioned limit and that the structures floor is made of concrete (d equal to 1,22); T_b = 2,175 s, for the case where 30 equally delayed in time holes are blasted with a timing difference of 75 ms; and the maximum vibration velocity (PVS_{max}) recorded which is equal to 1,171 mm·s^{-1}, the obtained value for N, according to this equation, is 6,41. Hence, under the assumed conditions, no more than six blasts can be carried out per day. During the studied period – between February 2018 and August 2022 – a maximum of four production blasts were carried out daily. Thus, it is equally verified that the standard in study would be complied with considering this more restrictive scenario.

After addressing different normative scenarios, the main conclusion is that ground vibration limits suggested by the technical documents are complied with and that no significant disturbance to humans located at residential structures and damage to buildings caused by rock blasting in the studied structures are expected to occur.

Although the maximum PVS recorded at structures C, D, E and F is 1,171 mm·s^{-1}, for these structures, it is recommended that BS 6472-2 is also taken into consideration when designing blasting patterns, minimizing the impact stope blasting has on humans and, consequently, on structures – if the suggested limit according to this standard is more conservative than the one indicated by NP 2074.

7.3. Geotechnical modelling of the studied area

The statistical and normative study of the samples compiled in the database serves as a preliminary mechanism to identify different hypotheses to be further tested and verified. In this work, it is expected that the performance of models considering groups with different characteristics allows one to test the validity of such hypotheses and take further conclusions.

7.3.1. Outliers: detection and removal

Firstly, before performing any modelling task it is important to consider the samples most relevant variables (PVS, Q and D), assessing their eventual relationship and removing anomalous values. This process minimizes the risk of developing a model which is not accurate in estimating the true value of the dependent variable (PVS). In other words, it guarantees more reliable models, with an expected increase in the coefficient of determination (R^2). According to Dodge (2009), this coefficient assesses the ability of a linear regression model to predict a dependent variable after the input of one or more independent ones. As such, R^2 measures the strength of the linear relationship between the involved variables, ranging from 0 to 1. Greater values of R^2 indicate a better adjustment of the model to the data points.

To minimize the impact of anomalous values on the calculated models, experimental data have to be analyzed and filtered out to identify and remove them, respectively. These are usually known as outliers and, as mentioned in chapter 4., not more than 10 % of the samples should be removed. The existence of such samples may be due to innumerous reasons such as an incorrect orientation of the geophone towards the blasting point or inadequate coupling of this device to the monitored structures surface, constructive or destructive interference of the stress waves caused by the existing heterogeneities of the rock mass, differences in the transmission of energy into the rock mass after the stemming quality, etc.

Given the considerable number of elements present in the database, it is not recommended nor accurate to remove the existing outliers by means of a visual inspection of the data, as Figure 40 suggests.

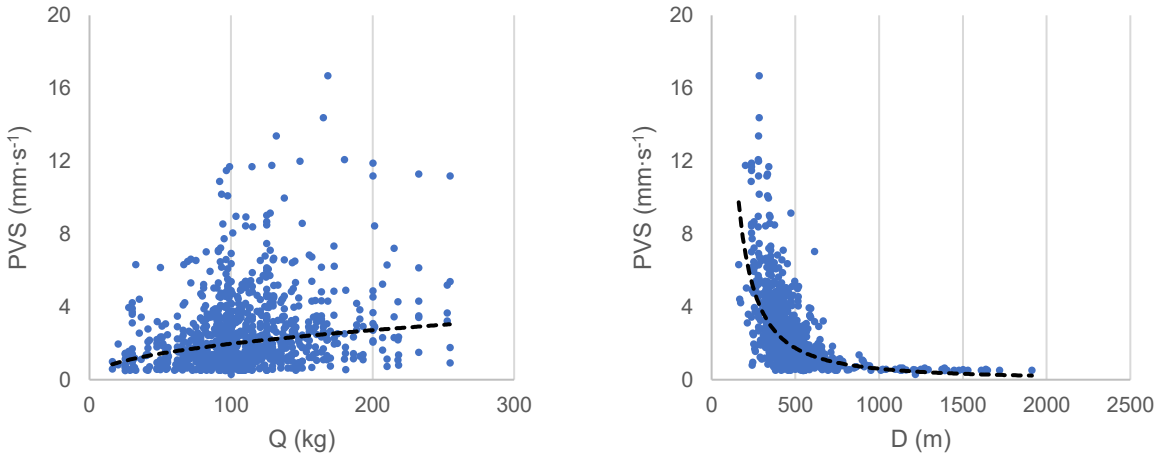

Figure 40 - Projection of the samples corresponding to the FWD scenario with outliers.

Consequently, after the projection of 1.011 samples – represented in blue – on the depicted planes, one can notice the density of points which makes the task of individually removing a maximum

of 101 samples (10 % of the events belonging to the considered class) a difficult one. The dark dashed lines correspond to the power regression curves for each scatter plot.

As such, an alternative method to identify outliers has to be tested. In this case, an initial Johnson's model is estimated for each group: FWOD, FWD and MWOD. This step is performed using multiple linear regression in SPSS. To estimate the models constants a, b and c by means of a regression tool and obtain an expression equivalent to the one presented in Equation 16, it is important to previously determine the logarithm of the variables PVS (v), Q and D, so that the following expression is obtained (Equation 21):

$$v = a \cdot Q^b \cdot D^c \Leftrightarrow \log(v) = \log(a) + b \cdot \log(Q) + c \cdot \log(D) \equiv y = b_0 + b_1 \cdot x_1 + b_2 \cdot x_2 \quad \text{(Equation 21)}$$

As such, after obtaining a linear relationship between the three variables, the rock mass constants can be determined by the following formulas:

- a = 10^{b_0};
- b = b_1;
- c = b_2.

After estimating the coefficients a, b and c for the three cases, the dependent variable is estimated for all samples ($\widehat{PVS}$) by means of the application of the respective inferred model. This is followed by the calculation of the absolute value of the residuals, corresponding to the modulus of the difference between the observed and the estimated/predicted PVS value (Equation 22).

$$|Residual| = |Observed\ value - Predicted\ value| = \left|PVS - \widehat{PVS}\right| \quad \text{(Equation 22)}$$

After determining the modulus of the residuals, an equivalent to 10 % of the samples with the greatest residual value are considered as outliers and, thus removed from the analysis that follows. Figure 41 illustrates the scatter plots that combine the two independent variables (Q and D) with the dependent one (PVS) after performing this removal.

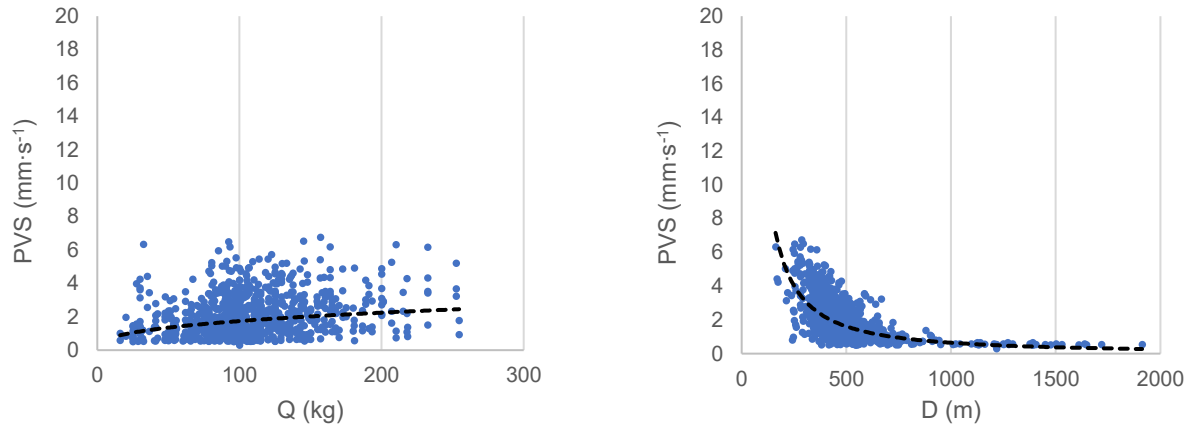

Figure 41 - Projection of the samples corresponding to the FWD scenario without outliers.

When comparing Figures 40 and 41, it is possible to verify that the removal of outliers (101 in total) has created a denser concentration of points around the power regression. Table 13 summarizes the changes in the three production scenarios after removing the respective outliers.

Table 13 - Johnson's model constants for the three operational scenarios before and after the removal of outliers.

Operational scenario		Number of samples	a	b	c	R^2	Number of outliers
MWOD	With outliers	40	8.549	-0,05	-1,38	0,43	4
	Without outliers	**36**	**788**	**0,05**	**-1,08**	**0,41**	
FWOD	With outliers	1.124	3.729	0,50	-1,63	0,60	112
	Without outliers	**1.012**	**1.315**	**0,49**	**-1,46**	**0,64**	
FWD	With outliers	1.011	2.379	0,63	-1,63	0,61	101
	Without outliers	**910**	**992**	**0,57**	**-1,45**	**0,62**	

It is important to note that, for both cases at the Feitais mine, R^2 has increased (4 % for FWOD and 1 % for FWD) after removing the outliers – one tenth of the samples. Nevertheless, for MWOD the coefficient of determination has decreased 2 %. This is due to the low correlation between variables in the initial scenario, originating a negative b coefficient (positive after removing four anomalous values), which contradicts the theory. As such, to allow a more detailed study of this category, despite having a lower value for R^2, the group with 36 samples is going to be considered. For FWD and FWOD, the posterior analysis is going to consider the dataset without the identified outliers.

7.3.2. Determination of ground vibration attenuation equations after Johnson's model

Although three operational cases are considered, given the distance range between each of the monitored structures and the location of the blasts, events monitored at structures located at the industrial area within and outside the mine perimeter (IA Mine and IA Outside the Mine, respectively), and at the urban area (Urban area) are going to be studied separately. The main objective of this differentiation is to assess the heterogeneity of the rock mass at different sections of the Aljustrel town in terms of ground vibrations propagation.

According to Figure 19 (a), the studied region reveals a complex geology at the surface. The predominant stratigraphic unit is the Upper Sedimentary one, mainly composed by greywacke, wacke, schist and argillite. To compare the obtained models with the ones inferred in previous studies and assess the validity of the results, the equation present in the literature for schists and greywackes is going to the deemed as the theoretical model for the region in analysis (Table 10). As such, considering

the mentioned categories, the estimated equations (using SPSS) and respective coefficients of correlation are compiled in Table 14.

Table 14 - Johnson's model constants for the three operational scenarios and sections within the Aljustrel town.

Operational scenario	Section	Number of samples	a	b	c	R^2
MWOD	IA Mine	30	24.003	0,21	-1,73	0,43
	Urban area	**6**	**0,2**	**-0,09**	**0,22**	**0,50**
FWOD	IA Mine	296	9.300	0,55	-1,83	0,76
	IA Outside the Mine	657	7.695	0,49	-1,75	0,53
	Urban area	59	10	0,07	-0,45	0,20
FWD	IA Mine	276	4.673	0,64	-1,78	0,68
	IA Outside the Mine	586	3.597	0,57	-1,66	0,51
	Urban area	**48**	**32**	**-0,26**	**-0,39**	**0,33**

This table shows that some models are not valid, due to the respective coefficients which contradict the expected direct proportionality between PVS and Q and the inverse relationship between PVS and D. For this reason, these will not be considered hereinafter. Such equations are highlighted and are the following: MWOD and FWD Urban area. The coefficient of determination of the models estimated for the Feitais mine, indicate that increasing distances tend to generate less accurate equations, which may be due to the greater probability of the waves being reflected and refracted on the existing rock mass interfaces (constructive or destructive interference). Figures 20 and 21 highlight the existence of such discontinuities that affect the propagation of stress waves before these reach the surface. For this reason, the value of R^2 for FWOD Urban area, IA Outside the Mine and IA Mine suggest a weak, moderate and strong relationship between the variables, respectively (according to the classification suggested by Landis and Koch (1977)). For MWOD, given the reduced number of samples and the previously mentioned weak correlation between variables, R^2 does not follow this trend. Comparing the different propagation laws with the one present in the literature (Table *10*) – deducted by Remísio (Bernardo and Torres, 2005) –, the ones that have a weaker adjustment to the experimental data (below 51 %) show a greater deviation in the rock mass coefficients than those with greater R^2.

It is also important to project the isokinetic curves on the Q vs. D plane, to compare the different laws, assessing the ones that are more restrictive. As such, taking into consideration the mean and median dominant frequencies for the three operational scenarios (Table 12) – which according to NP 2074 fall under the intermediate frequency class – and the type of structure that is subject to more conservative vibration limits, it is reasonable to consider vibration velocity values equal to 3 $mm \cdot s^{-1}$. Figure 42 corresponds to the projection of the determined models present in the previous table. The theoretical model is also included in this representation.

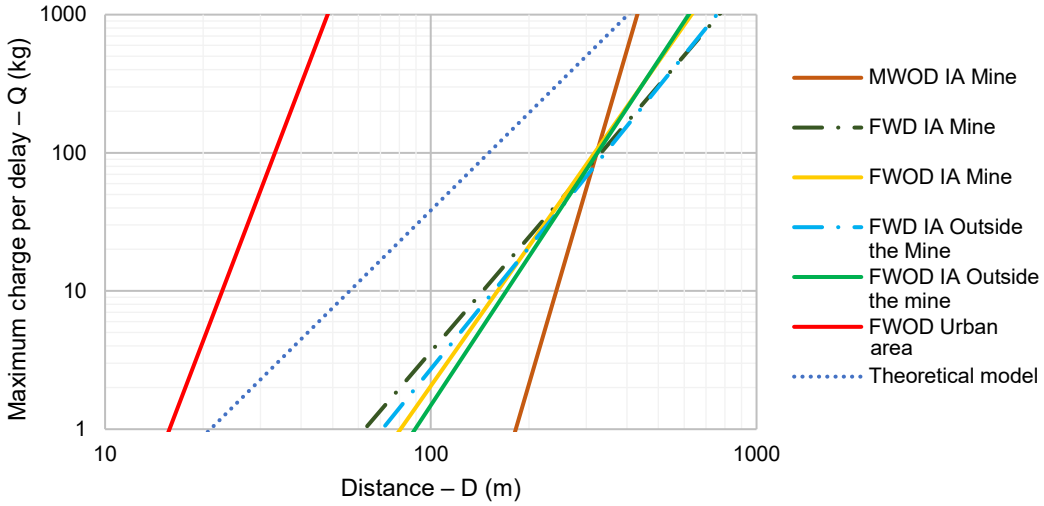

Figure 42 - Isokinetic curves corresponding to the theoretical and inferred models for each operational scenario and section of the town considering v = 3 mm·s^{-1}.

According to this figure, if the distance D is less than 300 m, the rock mass attenuates stress waves originated from blasts carried out at the Moinho mine at a lower rate. One possible reason for this may be the fact that the mine in consideration has a lower production rate and, consequently the rock mass has less discontinuities induced by the existing voids such as excavated drifts and stopes. For events belonging to FWD IA Mine and IA Outside the Mine, and D over 300 m, these models show an evident convergence and are the most conservative ones (more than those that describe FWOD). The least restrictive law is FWOD Urban. The reason for this may be related to the greater distance between the blasting and monitoring points, which increases the probability and impact of destructive interference after the contact between vibration waves and rock mass discontinuities including lithological transitions and geotechnical accidents.

Considering distance values below 300 m, FWD equations for IA Mine and IA Outside the Mine allow greater maximum charges per delay than FWOD (for the same sections), suggesting the influence of the previously blasted volume within the proximity of the blast, which may attenuate part of the released energy. Consequently, at greater distance values, it is expected that more relevance is assigned to the rock mass heterogeneities than to physical barriers artificially created, such as previous excavations.

For increasing distance values, the equations developed for Feitais (excluding FWOD Urban) converge to the theoretical model. This may indicate that, as the stress waves propagation becomes progressively less impacted by the existing voids, the geotechnical characteristics of the studied rock mass approximate to those that define the geology studied by Remísio (Bernardo and Torres, 2005). However, the disparity between the inferred and the theoretical laws highlight the importance of the formulation of different models that have a better adjustment to the samples measured at an area characterized by a complex geology and where previously developed formulas do not have much applicability and accuracy.

Now, considering the most conservative models that characterize each of the mines (regarding Feitais, both FWOD and FWD IA Outside the Mine are going to be addressed), one intends to create an expeditious auxiliary tool in the design of a charging diagram, taking into account fixed Q and D values for a determined velocity limit. To estimate Q and D, it is necessary to solve Equation 16 for each variable, respectively, as Equations 23 and 24 suggest. Given the aforementioned criteria, the limit is equivalent to 3 mm·s^{-1}. The Q values to consider correspond to the respective mean for this variable at both mines, whereas the D reference values are equal to the minimum for each case (Table 12).

$$Q = \left(\frac{v}{a \cdot D^{c}}\right)^{\frac{1}{b}} \quad \text{(Equation 23)}$$

$$D = \left(\frac{v}{a \cdot Q^{b}}\right)^{\frac{1}{c}} \quad \text{(Equation 24)}$$

Thereby, the application of both expressions yields the results present in Table 15 as follows:

Table 15 - Estimated maximum charge per delay and distance for each operational scenario and respective most conservative model considering v = 3 mm·s^{-1}.

		For a defined D		For a defined Q	
Operational scenario	**Section**	**D (m)**	**Estimated Q (kg)**	**Q (kg)**	**Estimated D (m)**
MWOD	IA Mine	160	0,3	80	314,5
		510	3.904,1	125	332,4
FWD	IA Outside the Mine	160	8,0	80	305,2
		510	500,8	125	345,8
FWOD	IA Outside the Mine	160	10,7	80	318,2
		510	317,3	125	370,8

The analysis of this table and Figure 42 suggest that for MWOD IA Mine, for reduced D values (below 160 m) blasts are impracticable, once Q should not exceed 0,3 kg. However, for distances over 510 m, this value may be greater than 3.904 kg. The minimum distance verified in blasts at Moinho is equal to 500 m (Table 12). Thus, no concerns on excessive vibrations at the monitored structures are expected to occur, considering a maximum vibration amplitude of 3 mm·s^{-1}. Regarding the Feitais mine, the minimum registered distance is 160 m, which according to the estimated laws, demands some attention during charging planning for values close to this reference.

Lastly, for the three addressed operational scenarios and Q around 80 kg, it is important to take into account the distance, which should not be inferior to 305 m. If blastholes require charges over this limit, one suggests the implementation of multiple initiation (decking). An alternative option would be to reduce the stope height, or to divide this volume into more than one stope in such a way that this charge per delay limit is respected.

It is important to note that in up-hole blasts, given the rockfall hazard while charging blast holes and the complexity associated with this process, it is not advisable to perform decking. In fact, according to Table 12, the maximum Q value for the registered events is equal to 281 kg. Hence, the reduction of the up-holes length is recommended as a ground vibration mitigation measure, in such a way that

multiple initiation is carried out at the upper portion (second phase) of the stope, therefore reducing ground vibration amplitudes.

An additional hypothesis to consider as an influencing factor of ground vibrations is the orientation between the blasting and monitoring points. Taking into account the binary orientation classification system mentioned in chapter 6.1., for the different operational scenarios, samples were divided into two categories (N-S and E-W) and the respective characteristic attenuation equations calculated. These are summarized in Table 16, as follows:

Table 16 - Johnson's model constants for the three operational scenarios and according to the orientation.

Operational scenario	Orientation	Number of samples	a	b	c	R^2
MWOD	N-S	27	220	0,07	-0,90	0,22
	E-W	9	1.973	0,03	-1,22	0,42
FWOD	N-S	724	7.893	0,52	-1,78	0,59
	E-W	288	687	0,46	-1,31	0,78
FWD	N-S	685	3.482	0,59	-1,68	0,54
	E-W	225	484	0,57	-1,32	0,80

In this case, all the models can be validated, given the positive a and b, and negative c coefficients. It can also be verified that R^2 is greater in E-W models in all operational scenarios. This may indicate the lower impact rock mass discontinuities have on stress waves propagation in terms of constructive or destructive interference according to this direction, influencing the measured PVS.

For a velocity limit of 3 mm·s^{-1}, the six obtained models can be projected on the Q vs. D plane (Figure 43).

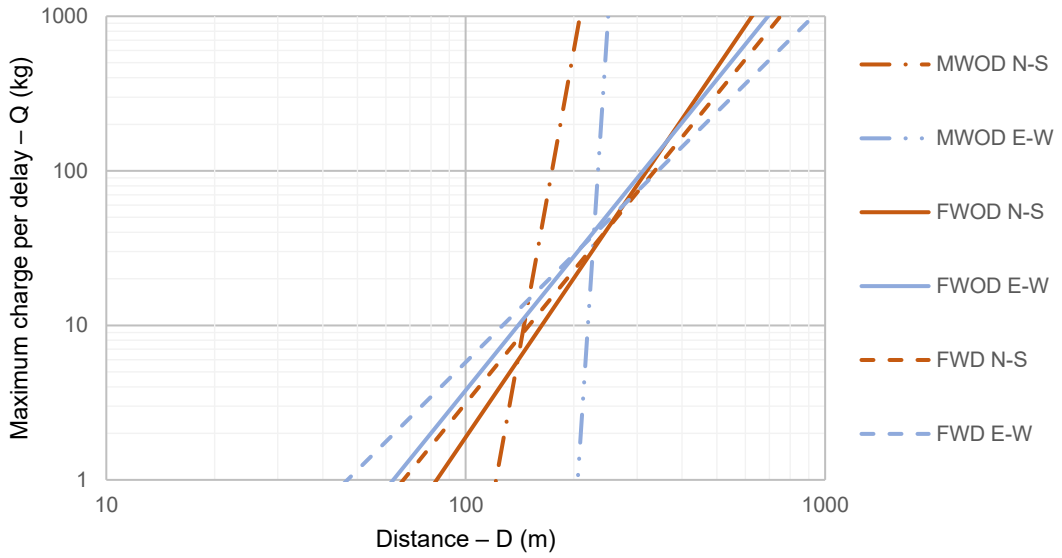

Figure 43 - Isokinetic curves corresponding to the inferred models for each operational scenario and orientation considering v = 3 mm·s^{-1}.

The results suggest that for the Moinho mine, in the E-W direction, the rock mass is more competent, offering less resistance to ground vibration propagation, involving thus more restrictive limits in terms of Q, at a given distance. For D below 275 m, the N-S direction implies more conservative models at Feitais. Over this threshold, a consistent pattern is not observed, although FWD models are the most restrictive ones, when compared to those with the same orientation.

In underground production situations, depending on the period at which stopes are blasted, the firing or initiation pattern geometry may vary. At the enlargement phase, where the free face area is more reduced and rings adjacent to the slot raise are blasted, the initiation sequence is similar to a spiral. Here, with the objective of expanding the free face, blast holes closer to the raise are initiated following this spiral pattern. The charging record present in Annex A serves as an example of this initiation geometry. Considering the greater confinement and energy concentration required to enlarge the free face, more energy may be transmitted into the rock mass in the form of ground vibrations. The additional geometry to be included in this study is the one where a regular free face, parallel to the rings is present, as Figure 6 suggests. In this last case, the blast holes initiation direction is parallel to the free face and, after a ring is completely excavated, holes belonging to the adjacent ring are detonated. The considered variable, which is going to be tested, includes therefore two categories: spiral and parallel initiation geometry and after individualizing both classes, the estimated vibration propagation laws are the following (Table 17):

Table 17 - Johnson's model constants for the three operational scenarios and according to the initiation geometry.

Operational scenario	Initiation geometry	Number of samples	a	b	c	R^2
MWOD	Parallel	31	1.065	0,03	-1,11	0,40
	Spiral	**5**	**3**	**-0,27**	**-0,01**	**0,99**
FWOD	Parallel	763	2.443	0,43	-1,51	0,64
	Spiral	249	360	0,53	-1,28	0,65
FWD	Parallel	678	1.448	0,47	-1,44	0,60
	Spiral	232	1.047	0,64	-1,52	0,69

As can be noted in this table, the b coefficient associated with the model MWOD spiral is negative. This equation is not going to be taken into consideration in the posterior description. Additionally, laws estimated for parallel initiation have lower coefficients of determination.

Figure 44 shows the isokinetic curves for the valid equations.

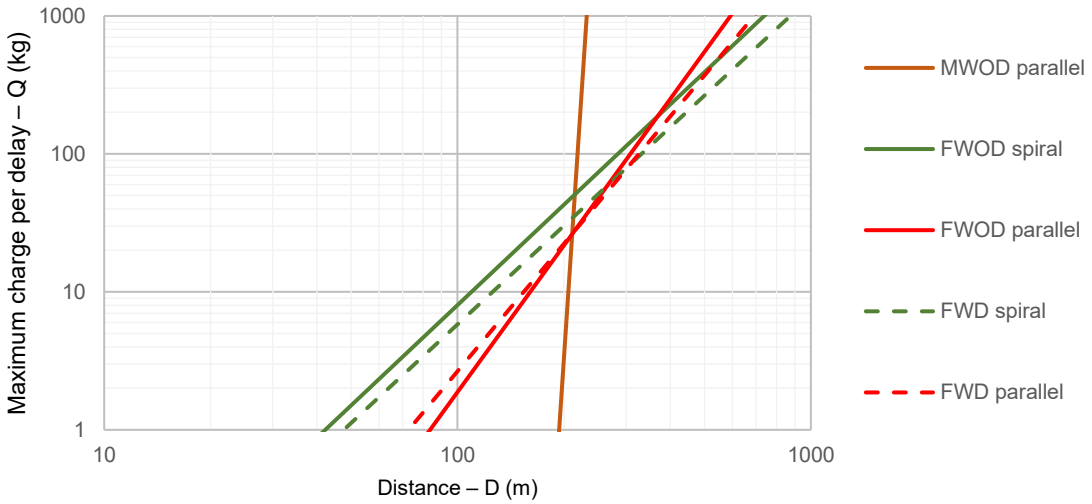

Figure 44 - Isokinetic curves corresponding to the inferred models for each operational scenario and initiation geometry considering v = 3 mm·s^{-1}.

By analyzing the influence of the initiation geometry on the Q vs. D plane it is verified that MWOD does not have practical utility in terms of ground vibration prediction given the low absolute value of the b coefficient. It is noteworthy that all the obtained models were estimated using the same mathematical approach: multiple linear regression. Nevertheless, within the interval considered in this figure, MWOD parallel does not have significance and, as such, should not be used. A possible reason may be the low number of considered events, suggesting that more samples have to be collected in future monitoring campaigns. For D below 250 m, FWD and FWOD parallel suggest that a lower charge per delay may be applied when comparing with the models developed for spiral initiation. Over this threshold, for the same initiation pattern, rock mass continuity is directly related to less restrictive models. If the distance is greater than 500 m, both equations defined by spiral initiation are more conservative. Considering spiral initiation, FWD is more restrictive regardless of the distance, as both curves are almost parallel to each other. Lastly, FWOD parallel is the most conservative equation at reduced distances – below 200 m.

To complete this study, a fourth variable – time delay between adjacent holes – is going to be included in the Johnson's mathematical formula, as Equation 25 suggests.

$$v = a \cdot Q^b \cdot D^c \cdot T^d \qquad \text{(Equation 25)}$$

The inclusion of a weighting factor that considers timing between blast holes involves the estimation of a fourth coefficient. If the initiation of adjacent holes is more spaced in time, it is expected that the explosives column promotes a greater expansion of a new free face, reducing hence the confinement around the next blasthole to be detonated. Furthermore, greater time delays contribute to a lower constructive interference between waves released after the initiation of adjacent holes, reducing ground vibration amplitudes. Therefore, the d coefficient should be negative. This, however implies more flyrock and compromises fragmentation once if breakage occurs and free face movement (associated with the consequent fragments displacement) takes place before the next holes are initiated, the energy

released by consecutive rings and holes does not act constructively, requiring therefore a narrower drilling pattern.

As such, the models obtained for MWOD, FWOD and FWD are the present in Table 18.

Table 18 - Johnson's model constants for the three operational scenarios considering the time delay between adjacent holes.

Operational scenario	Number of samples	a	b	c	d	R^2
MWOD	**25**	**169**	**0,098**	**-1,115**	**0,366**	**0,432**
FWD	447	1.693	0,582	-1,462	-0,132	0,613
FWOD	**628**	**1.502**	**0,489**	**-1,483**	**0,003**	**0,656**

This table indicates that the only model that respects the conditions imposed by theory, i.e., positive a and b, and negative c and d coefficients is FWD. For this reason, this is the only equation that is deemed valid. Although positive, the d value associated with FWOD is almost null, suggesting that the consideration of T has a negligible influence on this model. When comparing Tables 13 (models created without the consideration of outliers) and 18, it is possible to verify that the addition of a third independent variable (T) increases the coefficient of determination by 2 % for MWOD and decreases R^2 for FWD and FWOD at about 1 % and 2 %, respectively. Two models (FWOD and FWD) suggest that the T has a lower weight on vibrations than Q and D, because of the absolute value of the d coefficient. Taking into consideration the three time delays between holes most frequently used (present in 99 % of the charging records) – 50, 65 and 75 ms – the isokinetic curves associated with FWD and the respective values are illustrated in Figure 45. The considered velocity is 3 mm·s^{-1}.

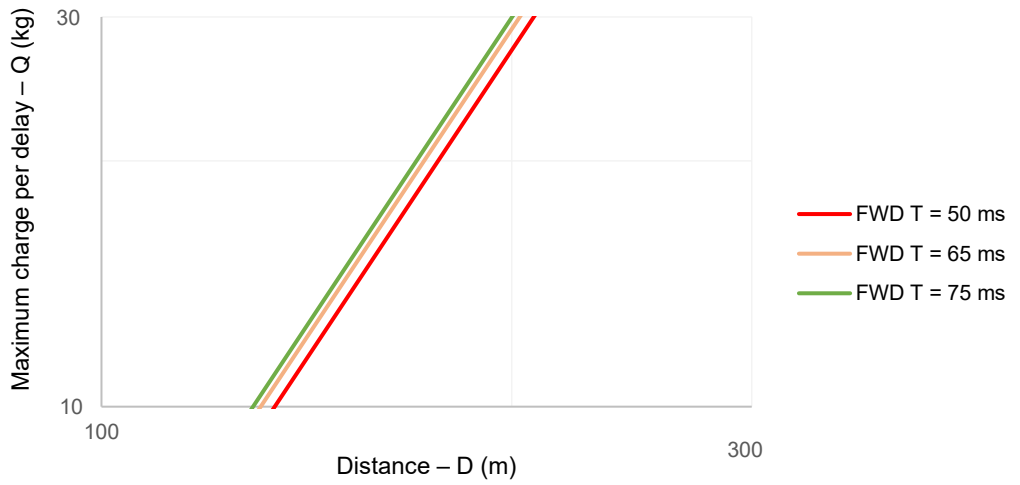

Figure 45 - Isokinetic curves corresponding to the inferred model for FWD and the most frequent time delays between adjacent holes considering v = 3 mm·s^{-1}.

The results of the projection confirm the negative d coefficient, where greater time delays are responsible for less conservative equations. Nevertheless, due to its low absolute value (0,132) its influence on the maximum recommended charge per delay is reduced. For distance values equal to 200 m, the Q variation when using 50 and 75 ms is equal to 2,5 kg. As such, despite the optimal delay

time is 75 ms in terms of ground vibration, this may not be the recommended value in terms of flyrock and fragmentation. Similar to what has been described in Figure 4, it is important to pursuit a time delay that does not compromise subsequent operations such as loading and hauling nor the compliance of ground vibration standards such as NP 2074 or DIN 4150-3. According to Andrews (1981) (as cited in Dowding and Aimone, 1992), in multiple-ring blasting, 3,3 to 16,4 ms·m^{-1} within the same ring and 6,6 to 49,2 ms·m^{-1} of burden between rings are suggested, improving fragmentation and safety – reducing the risk of misfires and the impact of flyrock or ground vibration. Thereby, once the burden that characterizes production blasts at Feitais and Moinho mines is 2,5 m, time delays of 8 to 41 ms between adjacent holes and 16 to 123 ms between rings are recommended. A combination of values within the mentioned ranges may be tested, to conclude if the delays used are deemed optimal and, eventually suggest ones that optimize production blasts. It should be noted, however, that if the burden is not constant between rings, i.e., if they have different inclinations due to design considerations, an average burden that considers the center of gravity of the charges within the ring should be taken into account.

In total, 29 models considering the previously mentioned variables were estimated, from which 23 were deemed valid ones. Due to coefficients that contradict theoretical principles, the remaining six were not validated. From the valid models, those that were associated with the greatest and the lowest coefficients of correlation are, respectively: FWD E-W (R^2 = 80 %) and FWOD Urban area (R^2 = 20 %).

7.4. Estimation of structures natural frequency

Considering the data present in chapter 6.2.2. and Equation 12 the yielded results for the structures natural frequency (f_n), along with a simple statistical description of the variable dominant frequency (f_d) of the registered events are present in Table 19.

Table 19 - Estimated natural frequency and statistical description of the variable dominant frequency for the considered structures, in Hz.

Structure	Number of samples	Estimated f_n	Dominant frequency, f_d		
			Mean	Minimum	$P_{25\%}$
A	61	34,9	12,1	2,3	3,0
C	1	13,2	50,0	50,0	50,0
D	33	11,2	28,6	2,1	13,4
E	11	14,5	54,2	33,0	46,7

Structure	Dominant frequency, f_d				
	Median	$P_{75\%}$	Maximum	Standard deviation	Range
A	13,0	13,5	40,0	9,8	37,8
C	50,0	50,0	50,0	0,0	0,0
D	26,8	40,0	66,8	20,5	64,6
E	53,3	60,1	80,0	13,8	47,0

When analyzing this table, one can conclude that the mean dominant frequency registered at each structure diverges from the respective estimated natural frequency. As such, no significant resonance is excepted to occur. However, it is possible to verify that for structures A and D, the minimum f_d is less than f_n. Therefore, a more conservative study addressing these two elements can be performed.

As can be seen from Figure 12, for a damping ratio of 0,015 (below the 0,05 value suggested by Dowding (1985) for one- to two-story buildings) the frequency ratio that may originate a significant increase in the structures dynamic response (and thus possible damage to them) varies between 0,9 and 1,2 – R_d over 3. If this frequency ratio interval is deemed as a resonance hazard threshold, from samples registered at structures A and D, only four records are within this limit. Table 20 compiles information about these records.

Table 20 - Records within the resonance hazard limit.

Monitored structure	Dominant frequency (Hz)	f_d/f_n (Hz)	PVS (mm·s^{-1})
A	40	1,15	0,539
A	40	1,15	0,568
A	40	1,15	0,648
D	13,38	1,19	0,648

Once A and D are sensitive and current structures, respectively, and given the dominant frequency associated with the events present in this table, according to NP 2074, the most conservative recommended PVS threshold is 3 mm·s^{-1}. This indicates that the records vibration amplitudes are at least four times lower than the suggested limit. In this case, for dynamic magnification factors over four, vibration events monitored at this structure could induce potential damage. However, although β is not known, a graphical analysis of Figure 12 indicates that amplification factors for the events present in this table are likely below four. Thereby, damage to structures A, C, D and E caused by blast-induced vibration it is not expected to occur, suggesting that the records present in the database show no evidence of noncompliance with the Portuguese standard on ground vibration monitoring nor damage to the monitored structures.

8. Conclusions and recommendations

8.1. Conclusions

Although the subject of ground vibrations has been studied for more than 90 years, the scientific community has not reached a consensus on the most effective vibration attenuation expression. The principal reasons underlying this are the complexity and singularity associated with each rock and soil mass, indicating that different ground vibration equations have to be adjusted for different regions of study.

In the state of the art, the most recent technologies concerning blasting pattern design and rock excavation using civil explosives were addressed. A brief description of the ground vibration phenomenon, normative documents related to this side effect and respective mitigation measures was performed. In underground production scenarios associated with sublevel open stoping and longitudinal bench and fill, the underlying principles of blasting pattern design are similar to those applied in open pit bench blasting, being that these were also mentioned in this chapter. Such theoretical bases are not recent, however they constitute the best available techniques to date.

The present dissertation had two main objectives: to model ground vibration amplitude prediction equations and to estimate the natural frequency by means of a theoretical formula, assessing then the existence of resonance at the considered structures.

The objectives proposed for this study were accomplished. In total, using a multiple linear regression tool in SPSS software, 29 models were estimated considering relevant variables v, Q and D, as suggested by Johnson (1971). From these, six were deemed invalid ones. These equations were deducted based on a database that included information relative to 2.175 real ground vibration records originated after production blasts at the Aljustrel mines (Alentejo province, Portugal). The records were registered at ten different structures between February 2018 and August 2022. Other variables such as the existence of a rock mass discontinuity imposed by an initial production blast, section of the town where the events were monitored, orientation between the blasting and monitoring points, initiation pattern geometry and time delay between adjacent holes were tested. Such models allow the estimation of ground vibration amplitudes and may be considered when performing blasting pattern designs according to the adequate operational scenarios and variables one intends to consider, and ground vibration standards.

The analysis of the compiled records indicate that NP 2074 and BS 6472-2 are complied with. Allied to this, the fact that no resonance is expected at the considered structures within the Aljustrel urban area indicate that descriptors exposed to ground vibrations such as humans and buildings are not significantly affected by blast-induced vibrations from geotechnical activities carried out at the

studied mines. When designing blasting patterns, the consideration of ground vibration limits suggested by BS 6472-2 is also relevant, protecting both descriptors.

Additional conclusions provided by the analysis of the valid models suggest that, considering the section of the Aljustrel mining area, increasing distance values tend to be associated with lower coefficients of determination. The reason for this may be the influence of the rock mass heterogeneities and lithological interfaces that contribute to local attenuation or amplification of the seismic waves generated by blasting events. For distance values below 300 m, models developed for the Feitais mine without an existing discontinuity are more conservative, highlighting the influence of the previously excavated stope volume on vibrations attenuation. At Feitais, within a 275 m radius centered at the blasting point, the north-south direction is less resistant to vibration propagation. For distances over 500 m, the initiation of blastholes according to a spiral pattern generates vibration amplitudes greater than those originated by a standard pattern where holes within the ring closer and parallel to the free face are the first ones to be detonated. Lastly, vibration propagation models that include time delay as the third independent variable attribute a low weight to this factor, when comparing with the remaining ones. From the tested values, the optimal delay regarding ground vibration is 75 ms. However, such timing may not be recommended once it compromises fragmentation and increases other undesired side effects such as flyrock, negatively influencing subsequent operations.

From the set of valid models, those that registered the greatest and lowest coefficients of correlation are the following ones, respectively:

- Feitais mine with an existing discontinuity considering the east-west direction: $v = 484 \cdot Q^{0,57} \cdot D^{-1,32}$, with R^2 = 80 %;
- Feitais mine without an existing discontinuity considering the urban area: $v = 10 \cdot Q^{0,07} \cdot D^{-0,45}$, with R^2 = 20 %.

After testing the most restrictive models considering the town section, for a maximum vibration velocity equal to 3 mm·s^{-1} and distances equal to 305 m, a charge per delay equivalent to 80 kg should not be exceeded. For values below this distance or over this charge, decking is recommended.

To mitigate the impact of ground vibration, the following measures are recommended: reduction of the stopes height or division into smaller stopes, and reduction of the up-holes length, i.e., the volume associated with the first excavation phase, once here the application of decking is a hazardous task. This last measure would allow the performance of multiple initiation when charging downholes, reducing hence the maximum charge per delay.

8.2. Recommendations for future work

Motivated by the reduced number of samples measured at the urban area, mostly after blasts carried out at the Moinho mine, some models could not be validated. To overcome this limitation, the

reinforcement of the monitoring campaign with the installation of more seismographs within this section of the Aljustrel town is suggested.

It should be noted that the developed models did not take into account the drillholes deviation nor mean burden. Once these factors significantly influence ground vibrations, the inclusion of such variables in new models is recommended. These parameters may be estimated with the conjugation of topographic surveys of the free face and Boretrak® inclinometers. Additionally, the inclusion of an energy weighting factor to attenuation equations, rather than the maximum charge per delay that does not consider different thermodynamical properties of the explosives, is of relevance. Such properties may be the detonation energy and pressure. Furthermore, by varying the column-to-bottom charge ratio, it would be possible to estimate the optimal charge proportion with regards to ground vibrations.

To diversify the monitoring locations and consider lower distances from the blast, vibration monitoring within underground infrastructure such as drifts adjacent to the blasts should be performed. This would allow the integration of the collected data to the existing database and consequent creation of a new model, and an eventual quantification of the influence underground infrastructure and stopes have on ground vibration amplitudes. Possibly, this experimental data would allow the formulation of a model with a greater coefficient of correlation given the greater rock mass continuity between the blasting and monitoring points.

To assess if the time delays between adjacent holes frequently used (50, 65 and 75 ms) are optimal, other values may be tested. As such, according to theory, one suggests testing time delays of 8 to 41 ms between adjacent holes and 16 to 123 ms between rings, comparing the results obtained after each test taking into consideration the production blasts side effects, namely ground vibration amplitudes and flyrock, and resulting fragmentation.

Lastly, as a ground vibration mitigation measure, the implementation of slot drilling, i.e., the creation of a discontinuity imposed by a series of drillholes between the blasting and monitoring points is recommended. To quantify its influence on ground vibrations, records before and after performing this measure at different stopes could be considered.

Bibliography

Abzalov, M., 2016, *Applied Mining Geology,* Springer International Publishing, 443 pp.

Agricola, G., 1556, *De Re Metallica*.

Aimone, C.T., 1992, "Rock Breakage: Explosives - Blast Design," *SME Mining Engineering Handbook. Vol.1*, H. Hartman, ed., Littleton, Colorado, pp. 722–746.

Ainalis, D., Kaufmann, O., Tshibangu, J., Verlinden, O., and Kouroussis, G., 2017, "Modelling the Source of Blasting for the Numerical Simulation of Blast-Induced Ground Vibrations: A Review," *Rock Mechanics and Rock Engineering*, Vol. 50, No. 1, pp. 171–193.

ALMINA – Minas do Alentejo, S.A., n.d., "Longitudinal Sublevel Open Stopes Method: Unpublished report".

Altiti, H., Alrawashdeh, R., and Alnawafleh, H., 2021, "Open Pit Mining," *Mining techniques*: *Past, present and future*, A. Soni, ed., London, IntechOpen.

Andrews, A.B., ed., 1981, *Design Criteria for Sequential Blasting,* Ohio, U.S.A.

Azevedo, F., and Patrício, J., 2003, "Critérios de Danos e de Incomodidade no Domínio das Vibrações Ambientes," *Ingenium, Ordem dos Engenheiros Magazine,* January 2003, pp. 85–88.

Bacci, D.C., Landim, P.M.B., Eston, S.M., and Iramina, W.S., 2003, "Principais Normas e Recomendações Existentes para o Controle de Vibrações Provocadas pelo Uso de Explosivos em Áreas Urbanas: Parte I," *Escola de Minas Magazine*, Vol. 56, No. 1, pp. 51–57.

Barrett, T.J., Dawson, G.L., and MacLean, W.H., 2008, "Volcanic Stratigraphy, Alteration, and Sea-Floor Setting of the Paleozoic Feitais Massive Sulfide Deposit, Aljustrel, Portugal," *Economic Geology*, Vol. 103, No. 1, pp. 215–239.

Barriga, F., and Fyfe, W.S., 1988, "Giant pyritic base-metal deposits: The example of Feitais (Aljustrel, Portugal)," *Chemical Geology*, Vol. 69, 3-4, pp. 331–343.

Bastos, M.J.N., ed., 2003, *Impactes Ambientais Associados à Utilização de Explosivos - 1ª Parte,* Lisbon, Portugal.

Bernardo, P., 2004, "Impactes Ambientais do Uso de Explosivos na Escavação de Rochas, com Ênfase nas Vibrações". PhD Thesis, Lisbon, Portugal.

Bernardo, P., Implicações da Directiva (UE) 2017/164 em Desmontes com Recurso a Explosivos, Segurança em Ambiente Subterrâneo – O Futuro Próximo, 2017, Lisbon, Portugal.

Bernardo, P., and Negreira, F., eds., 2015, *A delay timing between explosive charges as a new parameter to predict and control vibrations,* European Federation of Explosives Engineers.

Bernardo, P., and Torres, V., eds., 2005, *Metodologia para a Prevenção de Danos e Controle Ambiental de Vibrações Causadas por Detonações em Maciços Rochosos,* Ordem dos Engenheiros.

Bilgin, N., Copur, H., and Balci, C., 2014, *Mechanical Excavation in Mining and Civil Industries,* 1st Edition, Baton Rouge, Taylor & Francis Group, 378 pp.

British Standards, 1993, "Evaluation and Measurement for Vibration in Buildings. Guide to Damage Levels from Groundborne Vibration," BS 7385-2.

British Standards, 2008, “Guide to Evaluation of Human Exposure to Vibration in Buildings - Blast-induced Vibration,” BS 6472-2.

Carvalho, D., Goinhas, J., and Schermerhorn, L., eds., 1976, *Principais jazigos minerais do Sul de Portugal*: *Livro-Guia da Excursão,* Direcção Geral de Geologia e Minas e Serviços Geológicos, 94 pp.

Chilcott, D., and Owen, M., 2007, *Technical Report on the Aljustrel Mine, Southern Portugal,* Cornwall, United Kingdom.

Darling, P., 2011, “Mining: Setting the Scene,” *SME Mining Engineering Handbook*, P. Darling, ed., Society for Mining, Metallurgy, and Exploration, Inc., pp. 1–36.

Das, R.K.L., 2022, “Earthquake: Body Waves & Surface Waves,” constructionanddesign.blogspot.com/2016/02/earthquake-body-waves-surface-waves.html, accessed March 03, 2022.

Deutsches Institut für Normung, 2016a, “Erschütterungen im Bauwesen - Teil 2: Einwirkungen auf Menschen in Gebäuden,” DIN 4150-2.

Deutsches Institut für Normung, 2016b, “Erschütterungen im Bauwesen - Teil 3: Einwirkungen auf bauliche Anlagen,” DIN 4150-3.

Dick, R., Fletcher, L.R., and D’Andrea, D.V., 1983, “Explosives and blasting procedures manual”.

Dodge, Y., 2009, *The Concise Encyclopedia Of Statistics,* Dordrecht, London, Springer.

Dowding, C.H., 1985, *Blast Vibration Monitoring and Control,* Dowding, 297 pp.

Dowding, C.H., 1992, “Production Operations: Monitoring and Control of Blast,” *SME Mining Engineering Handbook. Vol.1*, H. Hartman, ed., Littleton, Colorado, pp. 746–760.

Dowding, C.H., 2011, “Impacts and Control of Blasting,” *SME Mining Engineering Handbook*, P. Darling, ed., Society for Mining, Metallurgy, and Exploration, Inc., pp. 1689–1704.

Dowding, C.H., and Aimone, C.T., 1992, “Production Operations: Rock breakage: explosives,” *SME Mining Engineering Handbook. Vol.1*, H. Hartman, ed., Littleton, Colorado, pp. 722–746.

Esteves, J.M., 1993, *Controlo de Vibrações Provocadas por Explosões na Indústria da Construção,* LNEC - Laboratório Nacional de Engenharia Civil.

EuroZinc Mining Corporation, 2000, “Drill hole plan - Feitais deposit: Unpublished report”.

Fabisiak, E., Moliński, W., and Roszyk, E., 2007, “The propagation velocity of ultrasound waves along the grain in the juvenile and mature, normal and reaction wood of pine (Pinus sylvestris L.),” *Forestry and Wood Technology*, pp. 200–206.

FEEM, http://www.feem-europe.org/fr.

Feng, H., and Yi, W., 2017, “Propagation characteristics of acoustic emission wave in reinforced concrete,” *Results in Physics*, Vol. 7, pp. 3815–3819.

Gama, C.D., 1971, “Otimização do Arranque de Rochas com Explosivos”. PhD Thesis, Luanda, Angola.

Gama, C.D., ed., 1998, *Ruídos e Vibrações Ligados à Utilização dos Explosivos e Equipamentos*.

Gama, C.D., ed., 2003, *Elementos de Dinâmica das Rochas,* Lisbon, Portugal.

Goldman, D., 1948, “A review of subjective responses to vibratory motion of the human body in the frequency range 1 to 70 cycles per second”.

Hagan, T.N., and Kennedy, B.J., 1977, “Practical Approach to the Reduction of Blasting Nuisances from Surface Operations,” *International Journal of Rock Mechanics and Mining Sciences & Geomechanics Abstracts*, Vol. 15, No. 3, pp. 36–46.

Hartlieb, P., 2013, “Investigations on the effects of microwaves on hard rock”. PhD Thesis, Leoben, Austria.

Heiniö, M., 1999, “Rock Excavation Handbook”.

Holmberg, R., and Persson, P.A., 1978, “The Swedish Approach to Contour Blasting,” *Proceedings of the 4th Conference on Explosives and Blasting Techniques*, pp. 113–127.

Hustrulid, W., 1999, *Blasting Principles for Open Pit Mining,* Rotterdam, Netherlands, Balkema.

Instituto Português da Qualidade, 2015, “Norma Portuguesa - Avaliação da influência de vibrações impulsivas em estruturas,” NP 2074.

Kiely, G., 1999, *Ingeniería Ambiental – Fundamentos, Entornos, Tecnologias y Sistemas de Gestión*: *(Edición Española – tradución y revisión técnica de Veza, J.M.),* McGraw-Hill Interamericana de España.

Kramer, S., 1996, *Geotechnical Earthquake Engineering,* New Jersey, U.S.A., Prentice-Hall, Inc., 673 pp.

Landis, J.R., and Koch, G.G., 1977, “The measurement of observer agreement for categorical data,” *Biometrics*, Vol. 33, No. 1, pp. 159–174.

Langefors, U., and Kihlstrom, B., 1978, *The Modern Technique of Rock Blasting,* 3rd Edition, Uppsala, Sweden, John Wiley & Sons.

Leitão, J., 2014, “Architecture of the Aljustrel volcanic-sedimentary basin,” *Comunicações Geológicas, No.* 101, pp. 469–474.

LKAB, 2022, “Our open-pit mines,” https://www.lkab.com/en/about-lkab/from-mine-to-port/mining/our-open-pit-mines/, accessed February 20, 2022.

Lopez Jimeno, C., Lopez Jimeno, E., and Carcedo, F.J.A., 1995, *Drilling and blasting of rocks,* Rotterdam, Netherlands, A.A. Balkema.

Louro, A., 2009, “Novas Formulações para Leis de Propagação de Vibrações, em Maciços Rochosos, Baseadas nas Propriedades Termodinâmicas dos Explosivos”. MSc Thesis, Lisbon, Portugal.

Lusk, B., and Worsey, P., 2011, “Rock Breaking Methods: Explosives and Blasting,” *SME Mining Engineering Handbook*, P. Darling, ed., Society for Mining, Metallurgy, and Exploration, Inc., pp. 443–458.

Luz, C., 2017, “Contribuição para o Desenvolvimento de Novos Modelos de Previsão das Amplitudes de Vibrações Produzidas por Detonações em Maciços Rochosos”. MSc Thesis, Lisbon, Portugal.

Miron, Y., Ruhe, T., and Watson, R., 1979, “Reactivity of AN-FO with Pyrite Containting Weathering Products”.

Morais, I., Albardeiro, M., Matos, J., Solá, R., Oliveira, D., Salgueiro, R., Araújo, V., and Pacheco, N., 2020, “Geochemistry of Iberian Pyrite Belt Portuguese sector massive sulfide deposits-related volcanic rocks. Considerations on hydrothermal alteration, petrology and tectonic evolution,” *Comunicações Geológicas, No.* 107, pp. 133–149.

Newmark, N.M., and Hall, W.J., 1982, *Earthquake Spectra and Design,* Berkeley, Calif., Earthquake Engineering Research Institute.

Northwood, T.D., Crawford, R., and Edwards, A.T., 1963, "Blasting vibrations and building damage," *The Engineer,* 215(5601), pp. 973–978.

Oliveira, J.T., Pereira, Z., Matos, J., and Fernandes, P., 2009, "Palinostratigrafia de Aljustrel: Relatório Final," LNEG - Laboratório Nacional de Geologia e Energia IP.

Pagé, P., Li, L., Yang, P., and Simon, 2019, "Numerical investigation of the stability of a base-exposed sill mat made of cemented backfill," *International Journal of Rock Mechanics and Mining Sciences*, Vol. 114, pp. 195–207.

Pires, M., 2021, "Conjugação de métodos de controlo de vibrações em desmontes de rocha com explosivos". MSc Thesis, Lisbon, Portugal.

Rinehart, J.S., 1975, *Stress Transients in Solids,* New Mexico, U.S.A., Hyper Dynamics.

Rosenthal, M., and Morlock, G., 1987, *Blasting Guidance Manual,* Office of Surface Mining Reclamation and Enforcement, U.S. Deptartment of the Interior.

Sarsby, R.W., 2013, *Environmental geotechnics,* 2nd Edition, London, ICE Publishing.

Schermerhorn, L., 1971, "An outline stratigraphy of the Iberian Pyrite Belt," pp. 239–268.

Schermerhorn, L., and Stanton, W., 1969, "Folded overthrusts at Aljustrel (South Portugal)," *Geological Magazine,* 106(2), pp. 130–141.

Schermerhorn, L., Zbyszewski, G., and Veiga Ferreira, O., 1987, *Notícia explicativa da folha 42-D - Aljustrel*: *Carta Geológica de Portugal,* Lisbon, Portugal, Serviços Geológicos de Portugal.

Siskind, D.E., Stachura, V.J., Stagg, M.S., and Kopp, J.W., 1980a, *Structures Response and Damage Produced by Airblast from Surface Mining*: *Report of Investigations 8485,* Washington D.C., U.S.A., U.S. Bureau of Mines.

Siskind, D.E., Stagg, M.S., Kopp, J.W., and Dowding, C.H., 1980b, *Structure Response and Damage Produced by Ground Vibrations from Surface Blasting*: *Report of Investigations 8507,* Washington D.C., U.S.A., U.S. Bureau of Mines.

Smith, A.L., Hicks, S.J., and Devine, P.J., 2007, *Design of Floors for Vibration: A New Approach,* Steel Construction Institute.

Sousa, M., and Oliveira, J., 1983, "The Carboniferous of Portugal," p. 211.

Svinkin, M.R., ed., 2008, *Soil and Structure Vibrations from Construction and Industrial Sources,* Missouri, U.S.A., Missouri University of Science and Technology, 15 pp.

Urbano, J., 2020, "Comparison of vibration amplitudes with non-electrical and electronic initiation systems". MSc Thesis, Lisbon, Portugal.

Winzer, S.R., and Ritter, A.P., 1980, *The Role of Stress Waves and The Role of Stress Waves and Discontinuities in Rock Fragmentation: A Study of Fragmentation in Large Limestone Blocks,* Missouri, U.S.A.

Zielińska, M., and Rucka, M., 2018, "Non-destructive assessment of masonry pillars using ultrasonic tomography," *Materials (Basel, Switzerland)*, Vol. 11, No. 12.

List of Figures

List of Tables

List of Abbreviations and Symbols

All the abbreviations and symbols are described as they are mentioned in the text, as well as their respective units according to the International System of Units. This table serves as an auxiliary and expeditious tool to identify the majority of the physical quantities and abbreviations present in the document.

Abbreviation	Designation	Unit
α	Drillholes inclination	°
β	Damping ratio	%
δ	Displacement	m
ε	Strain	dimensionless
ρ	Density	$kg \cdot m^{-3}$
ρ_e	Explosives density	$kg \cdot m^{-3}$
σ_{dr}	Dynamic resistance	Pa
σ_{sr}	Static resistance	Pa
σ_d	Dynamic stress	Pa
Ø	Drillhole diameter	m
a, b, c	Johnson's model coefficients	dimensionless
a	Acceleration	$m \cdot s^{-2}$
A_i	Incident wave amplitude	m
A_t	Transmitted wave amplitude	m
ANFO	Ammonium Nitrate - Fuel Oil	-
B	Burden	m
BC	Bottom charge	m
c	Waves propagation velocity	$m \cdot s^{-1}$
CC	Column charge	m
CAI	CERCHAR Abrasivity Index	dimensionless
C_P	Building material's waves propagation velocity	$m \cdot s^{-1}$
C_s	S waves propagation velocity	$m \cdot s^{-1}$
D	Distance	m
E_{dr}	Elastic moduli in the dynamic regime	Pa
E_{sr}	Elastic moduli in the static regime	Pa
f	Vibration frequency	Hz
f_n	Structures natural frequency	Hz
f_d	Dominant frequency	Hz
F	Multiplication factor	dimensionless
FFT	Fast Fourier Transform	-
FWOD	Feitais mine without an existing discontinuity	-

Abbreviation	Designation	Unit
FWD	Feitais mine with an existing discontinuity	-
G	Subdrilling	m
H	Bench height	m
H_S	Structure's height	m
h	Layer thickness	m
I_P	Characteristic impedance	$kg \cdot m^{-2} \cdot s^{-1}$
K_i	Ash's constants	dimensionless
L, V, T	Space directions (longitudinal, vertical, transverse)	-
L	Drillhole length	m
MWOD	Moinho mine without an existing discontinuity	-
N	Number of blast events per day	dimensionless
n	Porosity	dimensionless
n'	Refractive index	dimensionless
N_S	Building's number of stories	dimensionless
PPV	Peak particle velocity	$mm \cdot s^{-1}$
PVS	Peak vector sum	$mm \cdot s^{-1}$
P_D	Detonation pressure	Pa
Q	Maximum charge per delay	kg
R_d	Dynamic magnification factor	dimensionless
R^2	Coefficient of determination	dimensionless
S	Spacing	m
T	Time delay between adjacent holes	ms
T'	Stemming	m
T''	Period	s
T_b	Blast event duration	s
TC	Total charge	m
UCS	Uniaxial Compressive Strength	Pa
v	Vibration velocity	$mm \cdot s^{-1}$
VOD	Velocity of detonation	$m \cdot s^{-1}$
W	Weighted maximum charge per delay	kg

Annex A - Example of a production blast charging record

Charging record corresponding to stope F270SZ027 (downhole benching). Rings 1 to 5 depicted in this record were blasted on May 11th, 2022. The slot raise is identified in the diagram and blastholes adjacent to it are charged with Senatel™ Pulsar™ and/or Senatel™ Magnafrac™. The remaining holes are charged with a bottom charge – Senatel™ Magnafrac™ – which has a lower energy concentration, when compared with Senatel™ Pulsar™. Relevant translation is provided in the report.

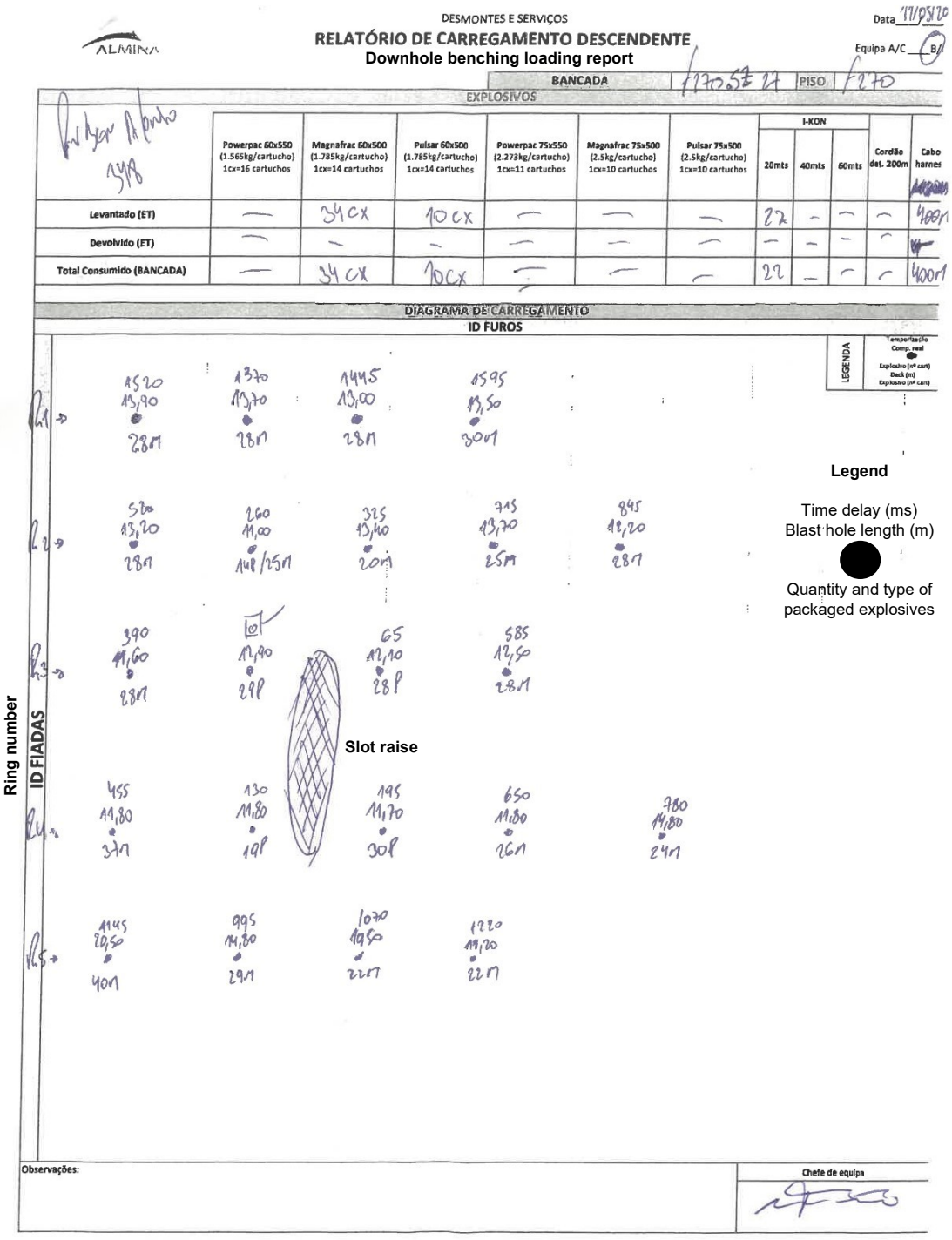

Annex B - Database containing information relative to production blasts and respective monitored events

Database compiling information relative to the considered monitored events:

Legend:

Data considered as outliers

WD Data included in models with discontinuity

WOD Data included in models without discontinuity

Date	Monitored structure	Slope	Dominant frequency (Hz)	PVS (mm·s⁻¹)	Maximum charge per delay (kg)	Delay between adjacent holes (ms)	Operational scenario	Initiation pattern geometry	Distance (m)	Orientation	Type of blast
05/02/2018	G	F43/SZ/39A	33,0	0,568	17,9		WOD	Spiral	473	N-S	Downhole
05/02/2018	I	F43/SZ/39A	54,3	0,684	17,9		WOD	Spiral	447	E-W	Downhole
06/02/2018	G	F43/SZ/39A	76,3	0,783	30,3		WOD	Spiral	468	N-S	Downhole
06/02/2018	I	F43/SZ/39A	55,5	0,833	30,3		WOD	Spiral	442	E-W	Downhole
06/03/2018	G	F31/SZ/44	74,3	1,770	64,3		WOD	Parallel	449	N-S	Up-hole
06/03/2018	I	F31/SZ/44	19,5	0,648	64,3		WOD	Parallel	366	N-S	Up-hole
08/03/2018	G	F31/SZ/44	48,0	1,580	69,6	50	WOD	Parallel	450	N-S	Up-hole
08/03/2018	I	F31/SZ/44	19,9	0,696	69,6	50	WOD	Parallel	367	N-S	Up-hole
09/03/2018	G	F31/SZ/26	40,0	2,450	194,1		WOD	Spiral	449	E-W	Downhole
09/03/2018	I	F31/SZ/26	15,6	5,760	194,1		WOD	Spiral	414	E-W	Downhole
10/03/2018	G	F43/SZ/39A	79,8	1,320	55,3	50	WOD	Spiral	463	N-S	Up-hole
10/03/2018	I	F43/SZ/39A	60,0	2,080	55,3	50	WOD	Spiral	437	E-W	Downhole
14/03/2018	I	F31/SZ/26	60,1	6,370	190,9		WOD	Parallel	413	E-W	Downhole
14/03/2018	G	F31/SZ/26	20,0	3,200	190,9		WOD	Parallel	448	E-W	Downhole
16/03/2018	I	F43/SZ/39A	59,8	2,250	57,1	50	WOD	Parallel	437	E-W	Downhole
16/03/2018	G	F43/SZ/39A	79,5	1,630	57,1	50	WOD	Parallel	466	N-S	Downhole
18/03/2018	I	F43/SZ/39A	60,0	3,260	55,9	50	WOD	Parallel	437	E-W	Downhole
18/03/2018	G	F43/SZ/39A	35,3	2,450	55,9	50	WOD	Parallel	460	N-S	Downhole
20/03/2018	I	F31/SZ/26	15,8	6,400	194,1		WOD	Parallel	413	E-W	Downhole
20/03/2018	G	F31/SZ/26	40,0	3,940	194,1		WOD	Parallel	451	E-W	Downhole
22/03/2018	I	F31/SZ/64	40,0	0,684	62,0	25	WOD	Parallel	514	N-S	Up-hole
23/03/2018	I	F43/SZ/39A	59,9	3,250	46,2	50	WOD	Parallel	440	E-W	Downhole
23/03/2018	G	F43/SZ/39A	39,9	2,750	46,2	50	WOD	Parallel	464	N-S	Downhole
10/04/2018	I	F31/SZ/44	20,0	2,280	153,0	50	WD	Spiral	340	N-S	Downhole
10/04/2018	G	F31/SZ/44	39,9	1,550	153,0	50	WD	Spiral	435	N-S	Downhole
11/04/2018	I	F31/SZ/62L	30,3	1,590	231,8		WOD	Parallel	482	N-S	Downhole
11/04/2018	G	F31/SZ/62L	30,8	1,330	231,8		WOD	Parallel	610	N-S	Downhole
12/04/2018	I	F31/SZ/44	20,0	4,890	200,0	50	WD	Parallel	339	N-S	Downhole
12/04/2018	G	F31/SZ/44	40,0	2,730	200,0	50	WD	Parallel	433	N-S	Downhole
13/04/2018	I	F41/SZ/39A	27,5	1,160	80,0	25	WOD	Parallel	449	E-W	Up-hole
13/04/2018	G	F41/SZ/39A	79,5	1,560	80,0	25	WOD	Parallel	478	N-S	Up-hole
15/04/2018	I	F31/SZ/64	40,0	1,790	190,7	50	WD	Parallel	506	N-S	Downhole
15/04/2018	G	F31/SZ/64	20,3	1,470	190,7	50	WD	Parallel	636	N-S	Downhole
20/04/2018	G	F31/SZ/48	20,8	1,050	111,0	42	WOD	Parallel	469	N-S	Up-hole
20/04/2018	I	F31/SZ/48	20,5	1,450	111,0	42	WOD	Parallel	377	N-S	Up-hole
20/04/2018	J	F31/SZ/66	21,3	0,648	161,0	50	WOD	Spiral	666	N-S	Up-hole
20/04/2018	I	F31/SZ/66	21,1	1,110	161,0	50	WOD	Spiral	543	N-S	Up-hole
27/04/2018	J	F31/SZ/48	19,9	1,890	151,0	50	WOD	Parallel	379	N-S	Up-hole
27/04/2018	J	F31/SZ/48	40,0	1,170	151,0	50	WOD	Parallel	463	N-S	Up-hole
27/04/2018	G	F31/SZ/48	26,8	1,450	151,0	50	WOD	Parallel	473	N-S	Up-hole
03/05/2018	I	F31/SZ/66	20,3	0,933	194,0	50	WOD	Parallel	542	N-S	Up-hole
03/05/2018	J	F31/SZ/66	40,0	6,730	194,0	50	WOD	Parallel	358	N-S	Up-hole
03/05/2018	G	F31/SZ/66	20,0	0,762	194,0	50	WOD	Parallel	664	N-S	Up-hole
08/05/2018	J	F31/SZ/66	20,0	0,648	60,0	50	WOD	Parallel	543	N-S	Up-hole
08/05/2018	J	F31/SZ/66	40,0	2,570	60,0	50	WOD	Parallel	357	N-S	Up-hole
10/05/2018	J	F31/SZ/42	20,0	3,950	195,0	50	WOD	Parallel	374	N-S	Up-hole
10/05/2018	J	F31/SZ/42	40,0	1,930	195,0	50	WOD	Parallel	520	N-S	Up-hole
10/05/2018	I	F31/SZ/42	20,0	2,770	195,0	50	WOD	Parallel	459	N-S	Up-hole
11/05/2018	J	F31/SZ/64	40,3	8,450	201,2	50	WD	Parallel	321	N-S	Downhole
11/05/2018	G	F31/SZ/64	20,1	2,930	201,2	50	WD	Parallel	638	N-S	Downhole
16/05/2018	G	F31/SZ/66	20,0	0,524	152,0	50	WOD	Parallel	662	N-S	Up-hole
16/05/2018	J	F31/SZ/66	20,0	2,800	152,0	50	WOD	Parallel	358	N-S	Up-hole
16/05/2018	J	F31/SZ/66	20,0	0,907	152,0	50	WOD	Parallel	539	N-S	Up-hole
18/05/2018	J	F31/SZ/66	40,3	3,620	152,0	50	WOD	Parallel	359	N-S	Up-hole
18/05/2018	I	F31/SZ/66	20,3	0,933	152,0	50	WOD	Parallel	544	N-S	Up-hole
18/05/2018	G	F31/SZ/66	20,0	0,933	152,0	50	WOD	Parallel	666	N-S	Up-hole
19/05/2018	J	F31/SZ/48	108,0	1,750	41,1	65	WD	Parallel	435	N-S	Downhole
19/05/2018	I	F31/SZ/48	30,8	2,790	41,1	65	WD	Parallel	350	N-S	Downhole
19/05/2018	G	F31/SZ/48	30,8	2,090	41,1	65	WD	Parallel	452	N-S	Downhole
21/05/2018	J	F41/SZ/39A	20,0	1,090	169,0	50	WOD	Parallel	657	N-S	Up-hole
21/05/2018	G	F41/SZ/39A	40,0	1,960	169,0	50	WOD	Parallel	477	N-S	Up-hole
22/05/2018	J	F31/SZ/44	60,0	0,959	52,3		WD	Parallel	476	N-S	Downhole
22/05/2018	J	F31/SZ/44	20,0	1,950	52,3		WD	Parallel	343	N-S	Downhole
24/05/2018	J	F31/SZ/42	20,1	1,110	52,3		WD	Parallel	438	N-S	Downhole
24/05/2018	J	F31/SZ/42	30,8	1,760	125,0	65	WD	Spiral	497	N-S	Downhole
24/05/2018	I	F31/SZ/42	15,4	4,580	125,0	65	WD	Spiral	340	N-S	Downhole
24/05/2018	G	F31/SZ/42	30,9	2,880	125,0	65	WD	Spiral	430	N-S	Downhole
25/05/2018	J	F41/SZ/39A	20,0	1,200	217,0	50	WOD	Parallel	657	N-S	Up-hole
25/05/2018	I	F41/SZ/39A	23,3	4,420	217,0	50	WOD	Parallel	449	E-W	Up-hole
25/05/2018	G	F41/SZ/39A	20,0	3,690	217,0	50	WOD	Parallel	478	N-S	Up-hole
26/05/2018	J	F31/SZ/48	19,8	3,210	156,0	50	WOD	Parallel	463	N-S	Up-hole
26/05/2018	I	F31/SZ/48	20,1	4,490	156,0	50	WOD	Parallel	381	N-S	Up-hole
26/05/2018	G	F31/SZ/48	20,1	3,830	156,0	50	WOD	Parallel	476	N-S	Up-hole
28/05/2018	J	F31/SZ/26L	60,0	5,140	173,0	50	WOD	Spiral	384	N-S	Up-hole
28/05/2018	I	F31/SZ/26L	60,0	2,080	173,0	50	WOD	Spiral	460	N-S	Up-hole
28/05/2018	G	F31/SZ/26L	38,3	1,930	173,0	50	WOD	Spiral	573	N-S	Up-hole
29/05/2018	I	F31/SZ/54	20,1	1,330	262,0	50	WOD	Parallel	411	N-S	Up-hole
29/05/2018	G	F31/SZ/54	40,0	2,180	262,0	50	WOD	Parallel	512	N-S	Up-hole
30/05/2018	J	F31/SZ/54	60,0	2,180	262,0	50	WOD	Parallel	421	N-S	Up-hole
30/05/2018	I	F31/SZ/48	19,9	3,200	175,0	50	WOD	Parallel	383	N-S	Up-hole
30/05/2018	G	F31/SZ/48	20,0	2,790	175,0	50	WOD	Parallel	479	N-S	Up-hole
30/05/2018	J	F31/SZ/48	20,0	2,150	175,0	50	WOD	Parallel	458	N-S	Up-hole
01/06/2018	I	F31/SZ/42	19,9	4,210	110,0		WD	Parallel	348	N-S	Downhole
01/06/2018	G	F31/SZ/42	19,9	2,730	110,0		WD	Parallel	442	N-S	Downhole
01/06/2018	J	F31/SZ/42	39,9	2,700	110,0		WD	Parallel	491	N-S	Downhole
02/06/2018	I	F31/SZ/54	19,9	2,450	111,0		WOD	Spiral	413	N-S	Up-hole
02/06/2018	G	F31/SZ/54	19,6	2,190	111,0		WOD	Spiral	517	N-S	Up-hole
02/06/2018	J	F31/SZ/54	19,8	2,350	111,0		WOD	Spiral	417	N-S	Up-hole
04/06/2018	I	F41/SZ/39A	19,9	3,860	90,9	50	WD	Parallel	414	E-W	Downhole
04/06/2018	J	F41/SZ/39A	20,0	3,320	90,9	50	WD	Parallel	447	N-S	Downhole
04/06/2018	J	F41/SZ/39A	38,3	2,310	51,2	50	WD	Parallel	629	N-S	Downhole
08/06/2018	I	F31/SZ/48	20,0	2,960	51,2	50	WD	Parallel	441	N-S	Downhole
08/06/2018	G	F31/SZ/48	20,0	2,350	51,2	50	WD	Parallel	446	N-S	Downhole
11/06/2018	J	F31/SZ/42	40,1	3,050	110,2	50	WD	Parallel	489	N-S	Downhole
11/06/2018	I	F31/SZ/42	20,0	8,960	110,2	50	WD	Parallel	349	N-S	Downhole
11/06/2018	G	F31/SZ/42	20,1	5,070	110,2	50	WD	Parallel	444	N-S	Downhole
12/06/2018	I	F31/SZ/26L	20,3	1,660	178,0	50	WOD	Spiral	460	N-S	Up-hole
12/06/2018	J	F31/SZ/26L	56,5	2,550	178,0	50	WOD	Spiral	384	N-S	Up-hole
12/06/2018	G	F31/SZ/26L	39,5	1,330	178,0	50	WOD	Spiral	574	N-S	Up-hole
14/06/2018	I	F31/SZ/54	20,1	1,760	150,0		WOD	Parallel	415	N-S	Up-hole
14/06/2018	J	F31/SZ/54	60,0	2,500	150,0		WOD	Parallel	416	N-S	Up-hole
15/06/2018	G	F31/SZ/26L	39,9	0,933	139,0		WOD	Parallel	576	N-S	Up-hole
15/06/2018	I	F31/SZ/26L	22,4	1,140	139,0		WOD	Parallel	463	N-S	Up-hole
15/06/2018	J	F31/SZ/26L	60,0	2,900	139,0		WOD	Parallel	393	N-S	Up-hole
16/06/2018	G	F31/SZ/48	20,0	3,030	188,7		WD	Parallel	455	N-S	Downhole
16/06/2018	J	F31/SZ/48	19,9	4,200	188,7		WD	Parallel	382	N-S	Downhole
18/06/2018	J	F31/SZ/48	19,9	2,750	188,7		WD	Parallel	435	N-S	Downhole
18/06/2018	G	F41/SZ/39A	20,0	2,440	147,7	50	WD	Parallel	449	N-S	Downhole
18/06/2018	I	F41/SZ/39A	28,5	2,120	147,7	50	WD	Parallel	415	E-W	Downhole
18/06/2018	J	F41/SZ/39A	20,0	0,933	147,7	50	WD	Parallel	630	N-S	Downhole
23/06/2018	I	F31/SZ/26L	30,8	2,460	150,0	65	WD	Spiral	441	N-S	Downhole
23/06/2018	J	F31/SZ/26L	59,0	8,580	150,0	65	WD	Spiral	346	N-S	Downhole
23/06/2018	G	F31/SZ/26L	30,9	1,800	150,0	65	WD	Spiral	563	N-S	Downhole
25/06/2018	I	F31/SZ/54	20,1	2,630	260,0		WOD	Parallel	416	N-S	Up-hole
25/06/2018	J	F31/SZ/54	60,0	3,820	260,0		WOD	Parallel	415	N-S	Up-hole
25/06/2018	G	F31/SZ/54	20,1	2,130	260,0		WOD	Parallel	520	N-S	Up-hole
27/06/2018	J	F31/SZ/66	108,0	3,240	105,0	65	WD	Parallel	323	N-S	Downhole
27/06/2018	I	F31/SZ/66	30,8	1,370	105,0	65	WD	Parallel	524	N-S	Downhole
28/06/2018	G	F31/SZ/48	20,1	4,210	127,3	50	WD	Parallel	462	N-S	Downhole
28/06/2018	J	F31/SZ/54	20,1	4,600	127,3	50	WD	Parallel	431	N-S	Downhole
28/06/2018	I	F31/SZ/48	20,1	5,740	127,3	50	WD	Parallel	357	N-S	Downhole
28/06/2018	J	F31/SZ/54	32,5	1,200	200,0	50	WOD	Parallel	524	N-S	Up-hole
30/06/2018	G	F31/SZ/54	40,3	2,460	200,0	50	WOD	Parallel	413	N-S	Up-hole
30/06/2018	I	F31/SZ/54	20,4	2,100	200,0	50	WOD	Parallel	418	N-S	Up-hole
30/06/2018	J	F41/SZ/39A	20,1	3,350	190,9	50	WD	Parallel	450	N-S	Downhole
03/07/2018	J	F41/SZ/39A	29,0	3,860	190,9	50	WD	Parallel	415	E-W	Downhole
03/07/2018	I	F41/SZ/39A	20,0	1,300	190,9	50	WD	Parallel	626	N-S	Downhole
03/07/2018	G	F31/SZ/66	40,0	0,660	147,7		WD	Parallel	652	N-S	Downhole
05/07/2018	J	F31/SZ/66	40,0	4,510	147,7		WD	Parallel	321	N-S	Downhole
05/07/2018	I	F31/SZ/66	20,0	0,933	147,7		WD	Parallel	523	N-S	Downhole
06/07/2018	J	F31/SZ/66	39,9	3,450	186,0	50	WOD	Parallel	389	N-S	Up-hole
06/07/2018	I	F31/SZ/66	20,1	3,310	186,0	50	WOD	Parallel	453	N-S	Up-hole
06/07/2018	G	F31/SZ/66	29,6	2,120	186,0	50	WOD	Parallel	565	N-S	Up-hole
07/07/2018	J	F31/SZ/48	46,1	1,850	91,4	50	WD	Parallel	428	N-S	Downhole
07/07/2018	I	F31/SZ/48	30,8	1,990	91,4	50	WD	Parallel	359	N-S	Downhole
07/07/2018	G	F31/SZ/48	30,6	1,350	91,4	50	WD	Parallel	467	N-S	Downhole
09/07/2018	G	F41/SZ/62	20,3	1,050	99,0	50	WOD	Parallel	650	N-S	Up-hole
09/07/2018	J	F41/SZ/62	40,0	3,310	99,0	50	WOD	Parallel	480	N-S	Up-hole
10/07/2018	G	F31/SZ/28	30,8	2,350	160,0	65	WOD	Spiral	482	E-W	Up-hole
10/07/2018	I	F31/SZ/28	46,1	1,120	160,0	65	WOD	Spiral	682	E-W	Up-hole
10/07/2018	J	F31/SZ/28	29,8	2,960	160,0	65	WOD	Spiral	424	E-W	Up-hole
11/07/2018	G	F31/SZ/70	31,3	0,664	166,0	65	WOD	Spiral	704	N-S	Up-hole
11/07/2018	J	F31/SZ/70	45,9	4,180	166,0	65	WOD	Spiral	382	E-W	Up-hole
11/07/2018	I	F31/SZ/70	30,5	1,180	166,0	65	WOD	Spiral	582	N-S	Up-hole
13/07/2018	G	F31/SZ/54	20,0	1,770	185,0	50	WOD	Parallel	661	N-S	Up-hole
13/07/2018	J	F31/SZ/54	39,9	2,670	176,0	50	WOD	Parallel	393	N-S	Up-hole
13/07/2018	I	F31/SZ/54	27,4	3,080	176,0	50	WOD	Parallel	448	N-S	Up-hole
14/07/2018	G	F31/SZ/48	40,0	1,090	55,0	50	WD	Parallel	472	N-S	Downhole
14/07/2018	J	F31/SZ/48	120,0	0,950	55,0	50	WD	Parallel	427	N-S	Downhole
14/07/2018	I	F31/SZ/48	19,9	1,420	55,0	50	WD	Parallel	363	N-S	Downhole
19/07/2018	I	F41/SZ/62	20,0	2,140	185,0	50	WOD	Parallel	564	N-S	Up-hole
19/07/2018	G	F41/SZ/62	20,0	1,770	185,0	50	WOD	Parallel	661	N-S	Up-hole
20/07/2018	I	F31/SZ/54	29,1	2,630	115,0	50	WD	Parallel	395	N-S	Downhole
20/07/2018	G	F31/SZ/54	20,1	2,100	115,0	50	WD	Parallel	510	N-S	Downhole

Legend:

Data considered as outliers

WD Data included in models with discontinuity

WOD Data included in models without discontinuity

Date	Monitored structure	Stope	Dominant frequency (Hz)	PVS (mm·s⁻¹)	Maximum charge per delay (kg)	Delay between adjacent holes (ms)	Operational scenario	Initiation pattern geometry	Distance (m)	Orientation	Type of blast	Date	Monitored structure	Stope	Dominant frequency (Hz)	PVS (mm·s⁻¹)	Maximum charge per delay (kg)	Delay between adjacent holes (ms)	Operational scenario	Initiation pattern geometry	Distance (m)	Orientation	Type of blast
21/07/2018	I	F310S2056	30,0	0,884	51,8	50	WD	Parallel	525	N-S	Downhole	03/09/2018	I	F310S2052	19,8	2,360	162,0	50	WOD	Spiral	400	N-S	Up-hole
25/07/2018	I	F310S2054	20,3	1,370	97,3		WD	Parallel	504	N-S	Downhole	04/09/2018	G	F310S2046	20,0	3,030	192,9	50	WOD	Parallel	455	N-S	Up-hole
25/07/2018	I	F310S2054	20,0	2,460	97,3		WD	Parallel	391	N-S	Downhole	04/09/2018	J	F310S2046	52,1	2,580	192,9	50	WOD	Parallel	483	N-S	Up-hole
26/07/2018	G	F410S2062	30,9	2,000	175,0	65	WD	Spiral	635	N-S	Downhole	05/09/2018	I	F310S2046	20,0	4,950	192,9	50	WOD	Parallel	369	N-S	Up-hole
26/07/2018	I	F410S2062	30,8	2,540	175,0	65	WD	Spiral	531	N-S	Downhole	05/09/2018	I	F310S2052	20,0	2,330	148,3	50	WOD	Parallel	402	N-S	Up-hole
27/07/2018	G	F310S2058L	29,4	2,280	103,4	50	WD	Parallel	551	N-S	Downhole	05/09/2018	J	F310S2052	120,0	3,810	148,3	50	WOD	Parallel	428	N-S	Up-hole
27/07/2018	I	F310S2058L	20,1	3,150	103,4	50	WD	Parallel	432	N-S	Downhole	05/09/2018	G	F310S2052	20,3	1,370	148,3	50	WOD	Parallel	504	N-S	Up-hole
29/07/2018	G	F310S2054	20,0	2,460	121,6	50	WD	Parallel	499	N-S	Downhole	06/09/2018	I	F410S2042	20,0	3,110	148,0		WOD	Spiral	447	N-S	Up-hole
29/07/2018	I	F310S2054	30,1	3,530	121,6	50	WD	Parallel	388	N-S	Downhole	06/09/2018	J	F410S2042	50,5	1,630	148,0		WOD	Spiral	621	N-S	Up-hole
01/08/2018	G	F310S2070	20,0	0,554	161,0	50	WOD	Parallel	705	N-S	Up-hole	06/09/2018	G	F410S2042	20,3	2,240	148,0		WOD	Spiral	486	N-S	Up-hole
01/08/2018	I	F310S2070	19,8	1,020	161,0	50	WOD	Parallel	582	N-S	Up-hole	07/09/2018	I	F310S2046	19,8	6,640	156,0	50	WOD	Parallel	376	N-S	Up-hole
02/08/2018	I	F310S2054	40,0	3,360	125,0	50	WD	Parallel	387	N-S	Downhole	07/09/2018	J	F310S2046	60,0	2,450	156,0	50	WOD	Parallel	477	N-S	Up-hole
02/08/2018	G	F310S2054	20,0	2,250	125,0	50	WD	Parallel	497	N-S	Downhole	07/09/2018	G	F310S2046	19,9	4,080	156,0	50	WOD	Parallel	468	N-S	Up-hole
02/08/2018	J	F310S2054	20,0	3,450	125,0	50	WD	Parallel	387	N-S	Downhole	08/09/2018	I	F310S2052	20,0	1,840	148,0	50	WOD	Parallel	397	N-S	Up-hole
03/08/2018	I	F310S2028	60,0	2,810	190,0	50	WOD	Parallel	415	E-W	Up-hole	08/09/2018	J	F310S2052	100,0	2,600	148,0	50	WOD	Parallel	435	N-S	Up-hole
03/08/2018	G	F310S2028	20,0	1,530	190,0	50	WOD	Parallel	453	E-W	Up-hole	08/09/2018	G	F310S2052	20,3	1,580	148,0	50	WOD	Parallel	497	N-S	Up-hole
03/08/2018	J	F310S2028	60,0	0,907	190,0	50	WOD	Parallel	675	N-S	Up-hole	10/09/2018	J	F310S2052	40,5	2,760	149,0		WOD	Parallel	437	N-S	Up-hole
05/08/2018	I	F310S2072	19,5	1,260	145,0	50	WOD	Spiral	600	N-S	Up-hole	10/09/2018	G	F310S2052	20,3	1,330	149,0		WOD	Parallel	493	N-S	Up-hole
05/08/2018	G	F310S2072	22,0	0,741	145,0	50	WOD	Spiral	721	N-S	Up-hole	10/09/2018	I	F310S2052	20,5	1,620	149,0		WOD	Parallel	395	N-S	Up-hole
05/08/2018	J	F310S2072	39,9	5,570	145,0	50	WOD	Spiral	369	E-W	Up-hole	10/09/2018	J	F410S2042	60,1	1,360	159,0		WOD	Parallel	625	N-S	Up-hole
06/08/2018	I	F310S2070	20,0	0,969	144,0	50	WOD	Parallel	585	N-S	Up-hole	10/09/2018	G	F410S2042	20,1	3,020	159,0		WOD	Parallel	483	N-S	Up-hole
06/08/2018	G	F310S2070	20,0	0,884	144,0	50	WOD	Parallel	706	N-S	Up-hole	10/09/2018	I	F410S2042	20,0	4,040	159,0		WOD	Parallel	447	E-W	Up-hole
06/08/2018	J	F310S2070	40,0	4,520	144,0	50	WOD	Parallel	366	E-W	Up-hole	11/09/2018	I	F310S2072	20,0	0,852	95,2	42	WD	Parallel	588	N-S	Downhole
07/08/2018	I	F410S2062	29,6	1,460	53,6	50	WD	Parallel	534	N-S	Downhole	12/09/2018	G	F430S2038	19,8	0,582	32,1	42	WOD	Spiral	481	N-S	Downhole
07/08/2018	J	F410S2062	60,0	3,080	53,6	50	WD	Parallel	438	N-S	Downhole	12/09/2018	I	F430S2038	60,0	0,660	32,1	42	WOD	Spiral	442	E-W	Downhole
07/08/2018	G	F410S2062	20,0	1,560	53,6	50	WD	Parallel	638	N-S	Downhole	13/09/2018	J	F310S2052	40,0	2,730	162,0	50	WOD	Parallel	432	N-S	Up-hole
08/08/2018	I	F310S2054	30,4	3,250	111,4	50	WD	Parallel	385	N-S	Downhole	13/09/2018	G	F310S2052	20,0	1,820	162,0	50	WOD	Parallel	498	N-S	Up-hole
08/08/2018	G	F310S2054	20,1	2,330	111,4	50	WD	Parallel	492	N-S	Downhole	13/09/2018	I	F310S2052	20,0	2,040	162,0	50	WOD	Parallel	399	N-S	Up-hole
08/08/2018	J	F310S2054	59,9	3,660	111,4	50	WD	Parallel	390	N-S	Downhole	14/09/2018	J	F410S2042	60,0	1,400	154,0	50	WOD	Parallel	619	N-S	Up-hole
09/08/2018	G	F310S2072	19,5	0,823	145,0	50	WOD	Spiral	724	N-S	Up-hole	14/09/2018	G	F410S2042	20,0	2,490	154,0	50	WOD	Parallel	486	N-S	Up-hole
09/08/2018	I	F310S2072	19,5	0,933	145,0	50	WOD	Spiral	603	N-S	Up-hole	14/09/2018	I	F410S2042	20,0	3,610	154,0	50	WOD	Parallel	447	N-S	Up-hole
09/08/2018	J	F310S2072	40,3	6,240	146,0	50	WOD	Spiral	370	E-W	Up-hole	15/09/2018	J	F270S2064	61,4	6,120	148,0	65	WOD	Spiral	319	N-S	Up-hole
10/08/2018	G	F310S2058L	20,0	3,530	134,0		WOD	Parallel	553	N-S	Up-hole	15/09/2018	G	F270S2064	31,0	0,783	149,0	65	WOD	Spiral	624	N-S	Up-hole
10/08/2018	I	F310S2058L	24,5	4,360	134,0		WOD	Parallel	444	N-S	Up-hole	15/09/2018	I	F270S2064	30,8	1,180	149,0	65	WOD	Spiral	495	N-S	Up-hole
10/08/2018	J	F310S2058L	40,0	4,640	134,0		WOD	Parallel	395	N-S	Up-hole	17/09/2018	G	F310S2046	20,0	1,370	144,0	50	WOD	Parallel	469	N-S	Up-hole
11/08/2018	G	F310S2070	16,3	0,648	135,0	65	WD	Spiral	689	N-S	Downhole	17/09/2018	I	F310S2046	20,0	1,910	144,0	50	WOD	Parallel	376	N-S	Up-hole
11/08/2018	I	F310S2070	27,3	1,230	135,0	65	WD	Spiral	562	N-S	Downhole	17/09/2018	J	F310S2046	100,0	1,180	144,0	50	WOD	Parallel	478	N-S	Up-hole
11/08/2018	J	F310S2070	108,0	4,250	135,0	65	WD	Spiral	327	E-W	Downhole	18/09/2018	I	F270S2064	20,5	0,950	127,0	50	WOD	Parallel	501	N-S	Up-hole
14/08/2018	J	F310S2072	40,0	4,780	276,0	50	WOD	Parallel	371	E-W	Up-hole	18/09/2018	B	F270S2064	20,3	2,080	127,0	50	WOD	Parallel	313	N-S	Up-hole
14/08/2018	G	F310S2072	20,0	1,180	276,0	50	WOD	Parallel	729	N-S	Up-hole	18/09/2018	J	F270S2064	60,1	5,500	127,0	50	WOD	Parallel	318	N-S	Up-hole
14/08/2018	I	F310S2072	20,3	1,090	276,0	50	WOD	Parallel	608	N-S	Up-hole	20/09/2018	B	F310S2072	51,0	2,150	90,0	50	WD	Parallel	355	N-S	Downhole
15/08/2018	J	F310S2028	45,5	3,230	252,5	65	WD	Spiral	665	N-S	Downhole	20/09/2018	J	F310S2072	43,8	3,260	90,0	50	WD	Parallel	331	E-W	Downhole
15/08/2018	G	F310S2028	30,5	3,670	252,5	65	WD	Spiral	441	E-W	Downhole	20/09/2018	I	F310S2072	27,0	1,000	90,0	50	WD	Parallel	586	N-S	Downhole
15/08/2018	I	F310S2028	17,0	5,200	252,5	65	WD	Spiral	399	E-W	Downhole	20/09/2018	J	F410S2042	40,0	1,490	146,0	50	WOD	Parallel	617	N-S	Up-hole
16/08/2018	G	F410S2062	19,9	1,330	95,5	50	WD	Parallel	641	N-S	Downhole	20/09/2018	I	F410S2042	19,8	2,360	146,0	50	WOD	Parallel	448	N-S	Up-hole
16/08/2018	J	F410S2062	60,3	2,950	95,5	50	WD	Parallel	437	N-S	Downhole	20/09/2018	G	F410S2042	20,0	1,640	146,0	50	WOD	Parallel	488	N-S	Up-hole
16/08/2018	I	F410S2062	20,0	1,460	95,5	50	WD	Parallel	536	N-S	Downhole	21/09/2018	J	F270S2064	100,0	5,640	148,0	50	WOD	Parallel	317	N-S	Up-hole
17/08/2018	G	F310S2028	20,0	2,300	206,8	50	WD	Parallel	436	E-W	Downhole	21/09/2018	I	F270S2064	20,0	0,925	148,0	50	WOD	Parallel	507	N-S	Up-hole
17/08/2018	J	F310S2028	99,9	1,630	206,8	50	WD	Parallel	655	N-S	Downhole	21/09/2018	G	F270S2064	40,0	0,884	148,0	50	WOD	Parallel	638	N-S	Up-hole
17/08/2018	I	F310S2028	60,0	5,260	206,8	50	WD	Parallel	392	E-W	Downhole	22/09/2018	B	F310S2070	20,0	1,460	81,8		WD	Parallel	346	N-S	Downhole
18/08/2018	J	F310S2070	40,3	4,600	79,6	50	WD	Parallel	329	E-W	Downhole	22/09/2018	J	F310S2070	40,0	2,680	81,8		WD	Parallel	327	E-W	Downhole
18/08/2018	I	F310S2070	20,0	1,110	79,6	50	WD	Parallel	563	N-S	Downhole	22/09/2018	I	F310S2070	20,0	0,684	81,8		WD	Parallel	570	N-S	Downhole
20/08/2018	G	F310S2072	15,6	1,510	232,5		WD	Spiral	712	N-S	Downhole	24/09/2018	B	F310S2046	40,0	2,110	138,0		WOD	Parallel	403	E-W	Up-hole
20/08/2018	J	F310S2072	55,6	11,300	232,5		WD	Spiral	333	E-W	Downhole	24/09/2018	J	F310S2046	19,9	1,220	138,0		WOD	Parallel	477	N-S	Up-hole
20/08/2018	I	F310S2072	27,0	3,520	232,5		WD	Spiral	585	N-S	Downhole	24/09/2018	I	F310S2046	20,0	2,880	138,0		WOD	Parallel	376	N-S	Up-hole
22/08/2018	G	F410S2062	20,0	1,400	100,0		WD	Parallel	638	N-S	Downhole	24/09/2018	G	F310S2046	20,0	2,150	138,0		WOD	Parallel	470	N-S	Up-hole
22/08/2018	J	F410S2062	100,0	2,380	100,0		WD	Parallel	437	N-S	Downhole	25/09/2018	B	F430S2038	36,5	1,030	51,8		WOD	Parallel	546	N-S	Downhole
22/08/2018	I	F410S2062	20,0	1,260	100,0		WD	Parallel	533	N-S	Downhole	25/09/2018	J	F430S2038	92,5	0,682	51,8		WOD	Parallel	633	N-S	Downhole
23/08/2018	G	F310S2028	20,0	1,440	113,3		WD	Parallel	440	E-W	Downhole	25/09/2018	I	F430S2038	61,5	1,570	51,8		WOD	Parallel	437	E-W	Downhole
23/08/2018	J	F310S2028	100,0	1,930	113,3		WD	Parallel	656	N-S	Downhole	25/09/2018	G	F430S2038	30,8	1,820	51,8		WOD	Parallel	479	N-S	Downhole
23/08/2018	I	F310S2028	20,0	3,960	113,3		WD	Parallel	395	E-W	Downhole	27/09/2018	B	F430S2038	37,6	1,020	53,6		WOD	Parallel	546	N-S	Downhole
24/08/2018	G	F310S2070	21,5	0,524	105,2		WD	Parallel	695	N-S	Downhole	27/09/2018	J	F430S2038	61,5	0,968	53,6		WOD	Parallel	631	N-S	Downhole
24/08/2018	J	F310S2070	95,0	4,160	105,2		WD	Parallel	327	E-W	Downhole	27/09/2018	I	F430S2038	61,5	1,360	53,6		WOD	Parallel	439	E-W	Downhole
24/08/2018	I	F310S2070	26,8	1,000	105,2		WD	Parallel	567	N-S	Downhole	27/09/2018	G	F430S2038	30,8	1,140	53,6		WOD	Parallel	484	N-S	Downhole
26/08/2018	G	F310S2058L	20,0	2,320	120,5	50	WD	Parallel	536	N-S	Downhole	28/09/2018	J	F410S2042	40,0	1,150	178,0	50	WOD	Parallel	619	N-S	Up-hole
26/08/2018	J	F310S2058L	40,0	2,880	120,5	50	WD	Parallel	361	N-S	Downhole	28/09/2018	B	F410S2042	40,0	2,770	178,0	50	WOD	Parallel	533	N-S	Up-hole
26/08/2018	I	F310S2058L	25,5	3,100	120,5	50	WD	Parallel	418	N-S	Downhole	28/09/2018	I	F410S2042	20,0	1,770	178,0	50	WOD	Parallel	447	N-S	Up-hole
28/08/2018	G	F310S2046	31,0	2,480	152,0	65	WOD	Spiral	461	N-S	Up-hole	28/09/2018	G	F410S2042	40,0	1,360	178,0	50	WOD	Parallel	489	N-S	Up-hole
28/08/2018	J	F310S2046	92,3	2,290	152,0	65	WOD	Spiral	484	N-S	Up-hole	30/09/2018	J	F310S2052	107,0	2,800	130,0	65	WD	Spiral	400	N-S	Downhole
28/08/2018	I	F310S2046	30,8	3,990	152,0	65	WOD	Spiral	372	N-S	Up-hole	30/09/2018	I	F310S2052	30,8	2,750	130,0	65	WD	Spiral	375	N-S	Downhole
31/08/2018	G	F310S2046	20,0	2,960	113,0	50	WOD	Parallel	464	N-S	Up-hole	30/09/2018	G	F310S2052	31,0	1,570	130,0	65	WD	Spiral	485	N-S	Downhole
31/08/2018	J	F310S2046	40,3	3,060	113,0	50	WOD	Parallel	482	N-S	Up-hole	01/10/2018	J	F310S2052	108,0	2,920	154,6	65	WD	Parallel	397	N-S	Downhole
31/08/2018	I	F310S2046	20,0	4,310	113,0	50	WOD	Parallel	373	N-S	Up-hole	01/10/2018	I	F310S2052	30,8	3,190	154,6	65	WD	Parallel	378	N-S	Downhole
02/09/2018	G	F310S2046	39,9	3,310	150,0	50	WOD	Parallel	462	N-S	Up-hole	01/10/2018	G	F310S2052	30,8	1,840	154,6	65	WD	Parallel	490	N-S	Downhole
02/09/2018	J	F310S2046	20,0	4,600	150,0	50	WOD	Parallel	480	N-S	Up-hole	03/10/2018	I	F310S2052	20,0	4,600	163,7	50	WD	Parallel	380	N-S	Downhole
03/09/2018	I	F310S2052	29,9	1,460	162,0	50	WOD	Spiral	372	N-S	Up-hole	03/10/2018	G	F310S2052	20,1	2,360	163,7	50	WD	Parallel	492	N-S	Downhole
03/09/2018	J	F310S2052	50,9	2,410	162,0	50	WOD	Spiral	431	N-S	Up-hole	04/10/2018	B	F270S2064	59,9	5,360	254,6		WD	Parallel	286	N-S	Downhole

Legend:

Data considered as outliers

WD Data included in models with discontinuity

WOD Data included in models without discontinuity

Date	Monitored structure	Stope	Dominant frequency (Hz)	PVS (mm·s⁻¹)	Maximum charge per delay (kg)	Delay between adjacent holes (ms)	Operational scenario	Initiation pattern geometry	Distance (m)	Orientation	Type of blast
04/10/2018	G	F270SZ064	40,0	0,933	254,6		WD	Parallel	629	N-S	Downhole
04/10/2018	J	F270SZ064	59,8	11,200	254,6		WD	Parallel	280	N-S	Downhole
04/10/2018	I	F270SZ064	20,0	1,780	254,6		WD	Parallel	493	N-S	Downhole
06/10/2018	B	F430SZ038	40,0	1,620	109,0	50	WOD	Parallel	558	N-S	Up-hole
06/10/2018	G	F430SZ038	20,0	1,400	109,0	50	WOD	Parallel	495	N-S	Up-hole
06/10/2018	J	F430SZ038	60,0	0,925	109,0	50	WOD	Parallel	643	N-S	Up-hole
06/10/2018	I	F430SZ038	60,0	2,350	109,0	50	WOD	Parallel	453	E-W	Up-hole
09/10/2018	J	F270SZ064	60,0	13,400	131,8	50	WD	Parallel	280	N-S	Downhole
09/10/2018	G	F270SZ064	20,0	1,370	131,8	50	WD	Parallel	630	N-S	Downhole
09/10/2018	I	F270SZ064	20,0	2,630	131,8	50	WD	Parallel	493	N-S	Downhole
10/10/2018	J	F430SZ038	60,0	0,783	109,0	50	WOD	Parallel	639	N-S	Up-hole
10/10/2018	G	F430SZ038	40,0	1,730	109,0	50	WOD	Parallel	498	N-S	Up-hole
10/10/2018	I	F430SZ038	60,0	2,330	109,0	50	WOD	Parallel	454	E-W	Up-hole
11/10/2018	G	F310SZ052	20,0	2,330	120,5	50	WD	Parallel	480	N-S	Downhole
11/10/2018	I	F310SZ052	20,0	4,420	120,5	50	WD	Parallel	372	N-S	Downhole
11/10/2018	J	F310SZ052	59,9	3,660	120,5	50	WD	Parallel	403	N-S	Downhole
13/10/2018	I	F310SZ068	30,8	1,750	193,0	65	WOD	Spiral	558	N-S	Up-hole
13/10/2018	J	F310SZ068	64,8	7,980	193,0	65	WOD	Spiral	361	E-W	Up-hole
15/10/2018	G	F310SZ068	31,0	1,020	114,0	65	WOD	Parallel	674	N-S	Up-hole
15/10/2018	I	F310SZ068	30,8	1,090	114,0	65	WOD	Parallel	553	N-S	Up-hole
15/10/2018	J	F310SZ068	41,8	4,270	114,0	65	WOD	Parallel	360	E-W	Up-hole
17/10/2018	I	F310SZ068	20,0	1,480	200,0	50	WOD	Parallel	562	N-S	Up-hole
18/10/2018	J	F270SZ064	60,1	12,000	148,7	50	WD	Parallel	280	N-S	Downhole
18/10/2018	G	F270SZ064	20,0	0,959	148,7	50	WD	Parallel	625	N-S	Downhole
18/10/2018	I	F270SZ064	20,0	1,910	148,7	50	WD	Parallel	488	N-S	Downhole
19/10/2018	J	F410SZ023L	106,0	0,898	44,6	50	WOD	Spiral	779	N-S	Downhole
19/10/2018	G	F430SZ038	20,1	0,907	114,0	50	WOD	Parallel	639	N-S	Up-hole
19/10/2018	G	F430SZ038	20,0	1,460	114,0	50	WOD	Parallel	498	N-S	Up-hole
19/10/2018	I	F430SZ038	60,0	2,010	114,0	50	WOD	Parallel	454	E-W	Up-hole
20/10/2018	J	F310SZ052	102,0	3,480	137,5	50	WD	Parallel	402	N-S	Downhole
20/10/2018	G	F310SZ052	20,0	2,380	137,5	50	WD	Parallel	479	N-S	Downhole
20/10/2018	I	F310SZ052	20,0	3,910	137,5	50	WD	Parallel	372	N-S	Downhole
20/10/2018	G	F410SZ023L	26,5	0,582	28,6	50	WOD	Spiral	530	E-W	Downhole
20/10/2018	I	F410SZ023L	23,0	0,684	28,6	50	WOD	Spiral	510	E-W	Downhole
24/10/2018	G	F410SZ023L	40,1	1,470	112,5		WOD	Spiral	529	E-W	Downhole
24/10/2018	I	F410SZ023L	80,0	1,280	112,5		WOD	Spiral	509	E-W	Downhole
25/10/2018	J	F310SZ068	40,0	5,290	188,0	50	WOD	Parallel	358	E-W	Up-hole
25/10/2018	G	F310SZ068	20,0	1,090	188,0	50	WOD	Parallel	679	N-S	Up-hole
25/10/2018	I	F310SZ068	20,0	1,110	188,0	50	WOD	Parallel	556	N-S	Up-hole
26/10/2018	G	F410SZ042	26,6	2,730	65,9	50	WD	Parallel	457	N-S	Downhole
26/10/2018	I	F410SZ042	20,0	4,120	65,9	50	WD	Parallel	413	N-S	Downhole
26/10/2018	I	F410SZ042	100,0	1,330	65,9	50	WD	Parallel	413	N-S	Downhole
27/10/2018	G	F310SZ046	27,8	2,160	138,7	50	WD	Parallel	452	N-S	Downhole
27/10/2018	I	F310SZ046	19,8	3,070	138,7	50	WD	Parallel	350	N-S	Downhole
27/10/2018	I	F310SZ046	99,9	2,250	138,7	50	WD	Parallel	350	N-S	Downhole
29/10/2018	G	F410SZ023L	20,0	1,370	62,5	50	WOD	Parallel	527	E-W	Downhole
29/10/2018	I	F410SZ023L	20,0	1,280	62,5	50	WOD	Parallel	507	E-W	Downhole
30/10/2018	G	F310SZ068	26,3	1,000	195,0	50	WOD	Parallel	693	N-S	Up-hole
30/10/2018	I	F310SZ068	19,8	1,200	195,0	50	WOD	Parallel	569	N-S	Up-hole
30/10/2018	I	F310SZ068	40,0	7,340	195,0	50	WOD	Parallel	569	N-S	Up-hole
01/11/2018	G	F410SZ060	17,5	1,510	193,0		WOD	Spiral	636	N-S	Up-hole
01/11/2018	I	F410SZ060	30,5	1,980	193,0		WOD	Spiral	541	N-S	Up-hole
01/11/2018	I	F410SZ060	40,1	3,210	193,0		WOD	Spiral	541	N-S	Up-hole
02/11/2018	G	F410SZ023L	20,0	1,950	90,9	50	WOD	Spiral	524	E-W	Downhole
02/11/2018	I	F410SZ023L	20,0	1,330	90,9	50	WOD	Spiral	503	E-W	Downhole
03/11/2018	I	F410SZ042	20,0	2,110	170,0	50	WOD	Parallel	448	N-S	Up-hole
04/11/2018	G	F310SZ046	25,8	3,780	120,5	50	WD	Parallel	453	N-S	Downhole
04/11/2018	I	F310SZ046	19,8	6,560	120,5	50	WD	Parallel	351	N-S	Downhole
04/11/2018	I	F310SZ046	19,8	2,290	120,5	50	WD	Parallel	351	N-S	Downhole
08/11/2018	G	F410SZ023L	20,0	2,340	150,0	50	WOD	Parallel	520	E-W	Downhole
08/11/2018	I	F410SZ023L	60,0	1,480	150,0	50	WOD	Parallel	497	E-W	Downhole
09/11/2018	J	F410SZ042	40,0	1,240	110,2		WD	Parallel	590	N-S	Downhole
09/11/2018	G	F410SZ042	20,0	2,300	110,2		WD	Parallel	458	N-S	Downhole
09/11/2018	I	F410SZ042	20,0	2,880	110,2		WD	Parallel	413	N-S	Downhole
12/11/2018	G	F310SZ046	20,0	2,350	147,7	50	WD	Parallel	458	N-S	Downhole
12/11/2018	I	F310SZ046	20,0	4,070	147,7	50	WD	Parallel	354	N-S	Downhole
15/11/2018	G	F410SZ023L	20,0	1,460	64,8		WOD	Parallel	521	E-W	Downhole
15/11/2018	I	F410SZ023L	60,0	1,050	64,8		WOD	Parallel	496	E-W	Downhole
16/11/2018	J	F410SZ060	46,1	2,240	122,0		WOD	Parallel	482	N-S	Up-hole
16/11/2018	G	F410SZ060	30,8	0,813	122,0		WOD	Parallel	637	N-S	Up-hole
16/11/2018	I	F410SZ060	30,8	0,976	122,0		WOD	Parallel	543	N-S	Up-hole
17/11/2018	J	F410SZ060	46,1	2,780	191,0		WOD	Parallel	480	N-S	Up-hole
17/11/2018	G	F410SZ060	30,8	1,530	191,0		WOD	Parallel	641	N-S	Up-hole
17/11/2018	I	F410SZ060	30,8	1,820	191,0		WOD	Parallel	546	N-S	Up-hole
18/11/2018	J	F310SZ068	20,0	2,280	64,1		WD	Parallel	323	E-W	Downhole
18/11/2018	G	F310SZ068	20,0	0,648	64,1		WD	Parallel	673	N-S	Downhole
18/11/2018	I	F310SZ068	20,0	0,916	64,1		WD	Parallel	544	N-S	Downhole
20/11/2018	J	F310SZ046	20,0	1,470	125,0	50	WD	Parallel	446	N-S	Downhole

Date	Monitored structure	Stope	Dominant frequency (Hz)	PVS (mm·s⁻¹)	Maximum charge per delay (kg)	Delay between adjacent holes (ms)	Operational scenario	Initiation pattern geometry	Distance (m)	Orientation	Type of blast
20/11/2018	I	F310SZ046	20,0	1,630	125,0	50	WD	Parallel	463	N-S	Downhole
20/11/2018	I	F310SZ046	20,0	2,660	125,0	50	WD	Parallel	357	N-S	Downhole
22/11/2018	I	F410SZ023L	100,0	1,330	80,7	50	WOD	Parallel	492	E-W	Downhole
22/11/2018	G	F410SZ023L	20,0	2,070	80,7	50	WOD	Parallel	518	E-W	Downhole
22/11/2018	J	F410SZ023L	59,5	0,524	80,7	50	WOD	Parallel	746	N-S	Downhole
24/11/2018	I	F310SZ060	19,8	4,810	203,0		WOD	Spiral	387	N-S	Up-hole
24/11/2018	G	F310SZ060	20,1	2,950	203,0		WOD	Spiral	485	N-S	Up-hole
24/11/2018	J	F310SZ060	39,9	3,490	203,0		WOD	Spiral	447	N-S	Up-hole
25/11/2018	I	F310SZ068	20,0	1,330	123,7		WD	Parallel	547	N-S	Downhole
25/11/2018	G	F310SZ068	20,0	0,803	123,7		WD	Parallel	676	N-S	Downhole
25/11/2018	J	F310SZ068	20,0	4,030	123,7		WD	Parallel	322	E-W	Downhole
26/11/2018	I	F270SZ066	30,5	2,020	200,0		WOD	Spiral	524	N-S	Up-hole
26/11/2018	G	F270SZ066	28,0	1,510	200,0		WOD	Spiral	655	N-S	Up-hole
27/11/2018	J	F270SZ066	40,0	7,930	200,0		WOD	Spiral	313	N-S	Up-hole
27/11/2018	G	F310SZ050	20,0	4,200	196,0	50	WOD	Parallel	386	N-S	Up-hole
27/11/2018	G	F310SZ050	20,1	3,400	196,0	50	WOD	Parallel	462	N-S	Up-hole
27/11/2018	J	F310SZ050	40,1	3,520	196,0	50	WOD	Parallel	450	N-S	Up-hole
28/11/2018	I	F310SZ046	20,0	2,580	76,1	50	WD	Parallel	357	N-S	Downhole
28/11/2018	G	F310SZ046	20,0	1,530	76,1	50	WD	Parallel	464	N-S	Downhole
28/11/2018	J	F310SZ046	40,1	1,180	76,1	50	WD	Parallel	447	N-S	Downhole
29/11/2018	I	F270SZ066	20,0	1,400	183,0	50	WOD	Parallel	518	N-S	Up-hole
29/11/2018	G	F270SZ066	40,1	1,370	183,0	50	WOD	Parallel	648	N-S	Up-hole
30/11/2018	J	F270SZ066	40,0	6,730	183,0	50	WOD	Parallel	315	N-S	Up-hole
01/12/2018	I	F410SZ023L	60,0	1,530	98,9		WOD	Parallel	490	E-W	Downhole
01/12/2018	G	F410SZ023L	40,0	2,420	98,9		WOD	Parallel	515	E-W	Downhole
03/12/2018	I	F410SZ042	20,0	2,060	139,8		WD	Parallel	414	N-S	Downhole
03/12/2018	G	F410SZ042	20,0	3,060	139,8		WD	Parallel	461	N-S	Downhole
03/12/2018	J	F410SZ042	40,0	1,050	139,8		WD	Parallel	591	N-S	Downhole
05/12/2018	I	F310SZ030	46,1	1,660	197,0	65	WOD	Spiral	656	N-S	Up-hole
05/12/2018	J	F310SZ030	61,5	3,300	197,0	65	WOD	Spiral	409	E-W	Up-hole
05/12/2018	G	F310SZ030	16,6	2,790	197,0	65	WOD	Spiral	454	E-W	Up-hole
07/12/2018	I	F410SZ023L	20,0	1,370	80,0	50	WOD	Parallel	487	E-W	Downhole
07/12/2018	G	F410SZ023L	40,0	2,210	80,0	50	WOD	Parallel	514	E-W	Downhole
08/12/2018	J	F310SZ050	40,0	2,690	194,0	50	WOD	Parallel	446	N-S	Up-hole
08/12/2018	I	F310SZ050	20,0	3,230	194,0	50	WOD	Parallel	386	N-S	Up-hole
09/12/2018	J	F270SZ066	20,0	2,830	194,0	50	WOD	Parallel	481	N-S	Up-hole
09/12/2018	I	F270SZ066	40,0	7,790	198,0		WOD	Parallel	313	N-S	Up-hole
09/12/2018	I	F270SZ066	20,0	1,530	198,0		WOD	Parallel	531	N-S	Up-hole
09/12/2018	G	F270SZ066	40,0	1,090	198,0		WOD	Parallel	662	N-S	Up-hole
10/12/2018	G	F310SZ030	40,0	1,730	171,0		WOD	Parallel	658	N-S	Up-hole
10/12/2018	I	F310SZ030	20,3	4,100	171,0		WOD	Parallel	408	E-W	Up-hole
10/12/2018	G	F310SZ030	40,1	2,620	171,0		WOD	Parallel	452	E-W	Up-hole
13/12/2018	J	F410SZ023L	100,0	0,648	80,7	50	WOD	Parallel	724	N-S	Downhole
13/12/2018	I	F410SZ023L	20,0	1,280	80,7	50	WOD	Parallel	478	E-W	Downhole
13/12/2018	G	F410SZ023L	99,9	1,850	80,7	50	WOD	Parallel	508	E-W	Downhole
16/12/2018	J	F310SZ050	30,8	3,180	200,0	65	WOD	Parallel	440	N-S	Up-hole
16/12/2018	G	F310SZ050	30,8	4,340	200,0	65	WOD	Parallel	392	N-S	Up-hole
16/12/2018	G	F310SZ050	30,8	3,870	200,0	65	WOD	Parallel	492	N-S	Up-hole
17/12/2018	I	F410SZ054	18,8	3,350	193,0		WOD	Spiral	490	N-S	Up-hole
17/12/2018	G	F410SZ054	16,3	1,810	193,0		WOD	Spiral	566	N-S	Up-hole
17/12/2018	J	F410SZ054	40,6	1,890	193,0		WOD	Spiral	522	N-S	Up-hole
20/12/2018	G	F310SZ030	20,0	2,570	186,0		WOD	Parallel	455	E-W	Up-hole
20/12/2018	I	F310SZ030	60,0	2,980	186,0		WOD	Parallel	408	E-W	Up-hole
20/12/2018	J	F310SZ030	39,9	1,370	186,0		WOD	Parallel	651	N-S	Up-hole
21/12/2018	I	F410SZ054	59,9	2,520	207,0	50	WOD	Parallel	570	N-S	Up-hole
21/12/2018	I	F410SZ054	20,0	3,810	207,0	50	WOD	Parallel	494	N-S	Up-hole
21/12/2018	J	F410SZ054	40,1	3,530	207,0	50	WOD	Parallel	520	N-S	Up-hole
22/12/2018	G	F410SZ023L	40,0	0,950	62,5	50	WOD	Parallel	509	E-W	Downhole
22/12/2018	I	F410SZ023L	20,3	1,230	62,5	50	WOD	Parallel	477	E-W	Downhole
29/12/2018	G	F270SZ066	60,0	0,813	115,0	50	WD	Spiral	640	N-S	Downhole
29/12/2018	I	F270SZ066	30,5	1,480	115,0	50	WD	Spiral	503	N-S	Downhole
29/12/2018	J	F270SZ066	120,0	8,410	115,0	50	WD	Spiral	279	N-S	Downhole
30/12/2018	G	F410SZ060	20,0	3,200	143,9	50	WD	Parallel	614	N-S	Downhole
30/12/2018	I	F410SZ060	20,0	5,010	143,9	50	WD	Parallel	513	N-S	Downhole
30/12/2018	J	F410SZ060	20,0	3,010	143,9	50	WD	Parallel	446	N-S	Downhole
04/01/2019	J	F410SZ054	40,0	2,130	200,0	50	WOD	Parallel	516	N-S	Up-hole
04/01/2019	G	F410SZ054	20,0	1,890	200,0	50	WOD	Parallel	574	N-S	Up-hole
04/01/2019	I	F410SZ054	20,0	1,800	200,0	50	WOD	Parallel	495	N-S	Up-hole
05/01/2019	J	F410SZ023L	60,0	0,648	106,0	50	WOD	Parallel	714	N-S	Up-hole
05/01/2019	G	F410SZ023L	60,0	1,500	106,0	50	WOD	Parallel	517	E-W	Up-hole
05/01/2019	I	F410SZ023L	60,0	2,010	106,0	50	WOD	Parallel	483	E-W	Up-hole
07/01/2019	J	F270SZ066	52,8	12,100	180,0	50	WD	Parallel	278	N-S	Downhole
07/01/2019	G	F270SZ066	19,9	1,140	180,0	50	WD	Parallel	642	N-S	Downhole
07/01/2019	I	F270SZ066	19,8	2,530	180,0	50	WD	Parallel	505	N-S	Up-hole
08/01/2019	G	F270SZ054	27,5	1,840	194,0	65	WOD	Spiral	496	N-S	Up-hole
08/01/2019	I	F270SZ054	15,5	3,250	194,0	65	WOD	Spiral	382	N-S	Up-hole
08/01/2019	J	F270SZ054	61,5	4,310	194,0	65	WOD	Spiral	379	N-S	Up-hole
09/01/2019	G	F310SZ043	30,8	3,340	181,0	65	WOD	Spiral	458	N-S	Up-hole

Legend:

Data considered as outliers

WD — Data included in models with discontinuity

WOD — Data included in models without discontinuity

Date	Monitored structure	Stope	Dominant frequency (Hz)	PVS (mm·s⁻¹)	Maximum charge per delay (kg)	Delay between adjacent holes (ms)	Operational scenario	Initiation pattern geometry	Distance (m)	Orientation	Type of blast	Date	Monitored structure	Stope	Dominant frequency (Hz)	PVS (mm·s⁻¹)	Maximum charge per delay (kg)	Delay between adjacent holes (ms)	Operational scenario	Initiation pattern geometry	Distance (m)	Orientation	Type of blast
09/01/2019	I	F310SZ043	30.8	5,870	181,0	65	WOD	Spiral	372	N-S	Up-hole	13/02/2019	J	F270SZ052	107,0	2,580	162,0	65	WOD	Spiral	389	N-S	Up-hole
09/01/2019	J	F310SZ043	15,3	1,810	181,0	65	WOD	Spiral	507	N-S	Up-hole	14/02/2019	I	F310SZ043	30,5	7,230	215,0	65	WD	Spiral	340	N-S	Downhole
10/01/2019	J	F270SZ074	20,0	0,524	78,4	50	WD	Parallel	737	N-S	Downhole	14/02/2019	G	F310SZ043	30,6	3,470	215,0	65	WD	Spiral	433	N-S	Downhole
10/01/2019	I	F270SZ074	20,0	1,140	78,4	50	WD	Parallel	603	N-S	Downhole	14/02/2019	J	F310SZ043	30,6	2,330	215,0	65	WD	Spiral	483	N-S	Downhole
10/01/2019	J	F270SZ074	40,0	4,730	78,4	50	WD	Parallel	302	E-W	Downhole	15/02/2019	I	F270SZ052	20,0	2,980	177,0	50	WOD	Parallel	375	N-S	Up-hole
11/01/2019	G	F310SZ060	21,5	1,580	125,0	65	WD	Spiral	471	N-S	Downhole	15/02/2019	G	F270SZ052	20,0	1,260	177,0	50	WOD	Parallel	469	N-S	Up-hole
11/01/2019	I	F310SZ060	18,3	3,280	125,0	65	WD	Spiral	363	N-S	Downhole	15/02/2019	J	F270SZ052	40,0	2,620	177,0	50	WOD	Parallel	389	N-S	Up-hole
11/01/2019	J	F310SZ060	49,8	1,750	125,0	65	WD	Spiral	418	N-S	Downhole	16/02/2019	I	F410SZ040A	20,0	3,200	181,0	50	WOD	Parallel	446	E-W	Up-hole
12/01/2019	G	F270SZ054	20,1	1,870	204,0		WOD	Parallel	505	N-S	Up-hole	16/02/2019	G	F410SZ040A	60,0	2,550	181,0	50	WOD	Parallel	478	N-S	Up-hole
12/01/2019	I	F270SZ054	20,3	2,410	204,0		WOD	Parallel	380	N-S	Up-hole	16/02/2019	J	F410SZ040A	40,0	0,925	181,0	50	WOD	Parallel	642	N-S	Up-hole
12/01/2019	J	F270SZ054	44,9	3,060	204,0		WOD	Parallel	374	N-S	Up-hole	18/02/2019	I	F270SZ052	20,0	3,430	165,0	50	WOD	Parallel	369	N-S	Up-hole
16/01/2019	J	F310SZ050	31,0	2,440	86,0	65	WD	Parallel	416	N-S	Downhole	18/02/2019	G	F270SZ052	20,0	1,900	165,0	50	WOD	Parallel	481	N-S	Up-hole
16/01/2019	I	F310SZ050	31,0	3,640	86,0	65	WD	Parallel	365	N-S	Downhole	18/02/2019	J	F270SZ052	40,1	3,380	165,0	50	WOD	Parallel	391	N-S	Up-hole
16/01/2019	G	F310SZ050	30,9	2,010	86,0	65	WD	Parallel	474	N-S	Downhole	20/02/2019	I	F370SZ064	20,0	3,830	281,0	65	WOD	Spiral	553	N-S	Up-hole
18/01/2019	J	F270SZ066	40,1	8,990	103,4	50	WD	Parallel	277	N-S	Downhole	20/02/2019	G	F370SZ064	20,1	2,050	281,0	65	WOD	Spiral	660	N-S	Up-hole
18/01/2019	I	F270SZ066	20,0	2,420	103,4	50	WD	Parallel	510	N-S	Downhole	20/02/2019	J	F370SZ064	20,0	1,060	281,0	65	WOD	Spiral	428	N-S	Up-hole
18/01/2019	G	F270SZ066	20,0	0,933	103,4	50	WD	Parallel	648	N-S	Downhole	20/02/2019	I	F410SZ040A	23,0	1,980	227,0	50	WOD	Parallel	447	E-W	Up-hole
18/01/2019	J	F410SZ023L	40,0	0,660	105,0	50	WOD	Parallel	711	N-S	Up-hole	20/02/2019	G	F410SZ040A	30,5	1,090	227,0	50	WOD	Parallel	481	N-S	Up-hole
18/01/2019	I	F410SZ023L	60,3	1,440	105,0	50	WOD	Parallel	492	E-W	Up-hole	20/02/2019	J	F410SZ040A	45,9	3,760	227,0	50	WOD	Parallel	638	N-S	Up-hole
18/01/2019	G	F410SZ023L	59,9	1,260	105,0	50	WOD	Parallel	517	E-W	Up-hole	22/02/2019	J	F270SZ064	99,9	5,990	125,0	50	WD	Parallel	352	N-S	Downhole
19/01/2019	J	F310SZ032	31,0	0,933	205,0	65	WOD	Spiral	629	N-S	Up-hole	22/02/2019	G	F270SZ064	20,1	1,800	125,0	50	WD	Parallel	481	N-S	Downhole
19/01/2019	I	F310SZ032	16,5	2,200	205,0	65	WOD	Spiral	399	E-W	Up-hole	23/02/2019	J	F310SZ043	40,0	1,750	138,7	50	WD	Parallel	478	N-S	Downhole
19/01/2019	G	F310SZ032	16,4	1,610	205,0	65	WOD	Spiral	453	E-W	Up-hole	23/02/2019	G	F310SZ043	20,0	2,940	138,7	50	WD	Parallel	436	N-S	Downhole
20/01/2019	J	F310SZ030	40,1	0,751	170,0		WD	Spiral	642	N-S	Downhole	25/02/2019	J	F270SZ052	40,1	3,710	167,0	50	WOD	Parallel	391	N-S	Up-hole
20/01/2019	I	F310SZ030	19,8	2,680	170,0		WD	Spiral	384	E-W	Downhole	25/02/2019	G	F270SZ052	40,1	1,980	167,0	50	WOD	Parallel	480	N-S	Up-hole
20/01/2019	G	F310SZ030	19,6	1,200	170,0		WD	Spiral	432	E-W	Downhole	26/02/2019	J	F370SZ064	46,1	4,620	122,0		WOD	Parallel	429	N-S	Up-hole
21/01/2019	J	F310SZ050	20,1	2,680	158,0	50	WD	Parallel	411	N-S	Downhole	26/02/2019	G	F370SZ064	30,8	0,660	122,0		WOD	Parallel	658	N-S	Up-hole
21/01/2019	I	F310SZ050	20,0	3,440	158,0	50	WD	Parallel	368	N-S	Downhole	27/02/2019	J	F270SZ072	46,1	6,520	145,0	65	WD	Spiral	294	E-W	Downhole
21/01/2019	G	F310SZ050	20,0	1,400	158,0	50	WD	Parallel	478	N-S	Downhole	27/02/2019	G	F270SZ072	61,5	0,933	145,0	65	WD	Spiral	705	N-S	Downhole
23/01/2019	I	F310SZ043	20,0	5,280	185,0	65	WOD	Parallel	369	N-S	Up-hole	28/02/2019	J	F310SZ056	34,9	3,140	186,0	65	WOD	Spiral	404	N-S	Up-hole
23/01/2019	G	F310SZ043	20,0	3,150	185,0	65	WOD	Parallel	455	N-S	Up-hole	28/02/2019	G	F310SZ056	20,0	2,140	186,0	65	WOD	Spiral	537	N-S	Up-hole
23/01/2019	J	F310SZ043	37,0	1,820	185,0	65	WOD	Parallel	506	N-S	Up-hole	02/03/2019	J	F270SZ054	66,8	6,080	126,2	65	WD	Parallel	345	N-S	Downhole
24/01/2019	G	F270SZ054	40,0	1,680	174,0	50	WOD	Parallel	497	N-S	Up-hole	02/03/2019	G	F270SZ054	33,4	2,820	126,2	65	WD	Parallel	491	N-S	Downhole
24/01/2019	J	F270SZ054	40,0	2,650	174,0	50	WOD	Parallel	379	N-S	Up-hole	03/03/2019	J	F310SZ032	20,0	1,440	121,6	50	WD	Parallel	611	N-S	Downhole
24/01/2019	I	F270SZ054	20,0	2,320	174,0	50	WOD	Parallel	384	N-S	Up-hole	03/03/2019	G	F310SZ032	20,0	1,680	121,6	50	WD	Parallel	432	E-W	Downhole
27/01/2019	J	F310SZ030	40,0	1,050	114,8	60	WD	Parallel	639	N-S	Up-hole	04/03/2019	J	F310SZ056	39,9	4,490	210,0		WOD	Parallel	400	N-S	Up-hole
27/01/2019	I	F310SZ030	20,0	3,470	114,8	60	WD	Parallel	387	E-W	Downhole	04/03/2019	G	F310SZ056	21,8	2,040	210,0		WOD	Parallel	543	N-S	Up-hole
27/01/2019	G	F310SZ030	20,0	1,090	114,8	60	WD	Parallel	438	E-W	Downhole	05/03/2019	J	F270SZ052	40,0	2,560	130,0	50	WOD	Parallel	395	N-S	Up-hole
28/01/2019	J	F410SZ060	33,4	3,030	89,8	60	WD	Parallel	444	N-S	Downhole	05/03/2019	G	F270SZ052	40,0	1,710	130,0	50	WOD	Parallel	477	N-S	Up-hole
28/01/2019	I	F410SZ060	16,8	2,540	89,8	60	WD	Parallel	515	N-S	Downhole	07/03/2019	J	F310SZ043	40,1	2,530	103,4	50	WD	Parallel	481	N-S	Downhole
28/01/2019	G	F410SZ060	16,8	1,370	89,8	60	WD	Parallel	618	N-S	Downhole	07/03/2019	G	F310SZ043	20,1	2,350	103,4	50	WD	Parallel	438	N-S	Downhole
30/01/2019	J	F410SZ054	20,0	0,950	66,4	50	WD	Parallel	487	N-S	Downhole	09/03/2019	J	F310SZ034	30,9	1,460	197,0	65	WOD	Spiral	608	N-S	Up-hole
30/01/2019	I	F410SZ054	20,0	1,200	66,4	50	WD	Parallel	464	N-S	Downhole	09/03/2019	G	F310SZ034	30,9	2,450	197,0	65	WOD	Spiral	447	E-W	Up-hole
30/01/2019	G	F410SZ054	20,0	1,080	66,4	50	WD	Parallel	547	N-S	Downhole	12/03/2019	G	F270SZ072	20,0	0,596	145,5	50	WD	Parallel	707	N-S	Downhole
31/01/2019	J	F310SZ050	40,0	2,560	82,3	50	WD	Parallel	417	N-S	Downhole	12/03/2019	J	F270SZ072	40,1	5,350	145,5	50	WD	Parallel	291	E-W	Downhole
31/01/2019	I	F310SZ050	20,0	3,330	82,3	50	WD	Parallel	362	N-S	Downhole	13/03/2019	J	F310SZ034	40,1	1,200	214,0		WOD	Parallel	600	N-S	Up-hole
31/01/2019	G	F310SZ050	40,0	1,840	82,3	50	WD	Parallel	468	N-S	Downhole	13/03/2019	I	F310SZ034	20,3	3,000	214,0		WOD	Parallel	368	E-W	Up-hole
01/02/2019	J	F270SZ064	40,0	2,280	119,0	50	WOD	Parallel	383	N-S	Up-hole	13/03/2019	G	F310SZ034	20,0	2,370	214,0		WOD	Parallel	451	N-S	Up-hole
01/02/2019	I	F270SZ064	40,0	2,290	119,0	50	WOD	Parallel	380	N-S	Up-hole	13/03/2019	J	F410SZ040A	30,8	1,330	167,5	65	WD	Spiral	616	N-S	Downhole
01/02/2019	G	F270SZ064	40,0	1,550	119,0	50	WOD	Parallel	491	N-S	Up-hole	13/03/2019	I	F410SZ040A	30,8	3,080	167,5	65	WD	Spiral	413	E-W	Downhole
02/02/2019	J	F270SZ074	40,1	4,240	67,1	50	WD	Parallel	301	E-W	Downhole	13/03/2019	G	F410SZ040A	30,8	2,190	167,5	65	WD	Spiral	449	N-S	Downhole
02/02/2019	I	F270SZ074	20,3	1,170	67,1	50	WD	Parallel	605	N-S	Downhole	14/03/2019	J	F270SZ070	40,3	8,990	184,0	50	WOD	Spiral	321	E-W	Up-hole
04/02/2019	J	F310SZ032	30,6	1,030	181,0	65	WOD	Parallel	628	N-S	Up-hole	14/03/2019	I	F270SZ070	29,5	2,310	184,0	50	WOD	Spiral	561	N-S	Up-hole
04/02/2019	I	F310SZ032	30,8	2,470	181,0	65	WOD	Parallel	397	E-W	Up-hole	14/03/2019	G	F270SZ070	60,1	1,370	184,0	50	WOD	Spiral	689	N-S	Up-hole
04/02/2019	G	F310SZ032	15,4	1,570	181,0	65	WOD	Parallel	451	E-W	Up-hole	17/03/2019	J	F310SZ032	60,0	0,950	80,7	50	WD	Parallel	609	N-S	Downhole
05/02/2019	G	F310SZ030	20,0	1,200	80,7		WD	Parallel	442	E-W	Downhole	17/03/2019	I	F310SZ032	20,0	3,240	80,7	50	WD	Parallel	377	E-W	Downhole
05/02/2019	I	F310SZ030	20,0	3,910	80,7		WD	Parallel	389	E-W	Downhole	17/03/2019	G	F310SZ032	40,0	1,040	80,7	50	WD	Parallel	439	E-W	Downhole
05/02/2019	J	F310SZ030	40,0	0,976	80,7		WD	Parallel	637	N-S	Downhole	18/03/2019	J	F370SZ064	61,5	6,860	155,0	65	WD	Spiral	392	N-S	Downhole
06/02/2019	I	F410SZ040A	15,5	2,300	174,0		WOD	Spiral	447	N-S	Up-hole	18/03/2019	I	F370SZ064	30,8	2,790	155,0	65	WD	Spiral	524	N-S	Downhole
06/02/2019	G	F410SZ040A	61,6	1,980	174,0		WOD	Spiral	476	N-S	Up-hole	18/03/2019	G	F370SZ064	46,1	1,230	155,0	65	WD	Spiral	637	N-S	Downhole
06/02/2019	J	F410SZ040A	30,8	1,180	174,0		WOD	Spiral	643	N-S	Up-hole	19/03/2019	J	F270SZ070	40,3	3,990	112,0	50	WOD	Parallel	322	E-W	Up-hole
07/02/2019	I	F270SZ072	31,0	1,570	197,0	65	WOD	Spiral	582	N-S	Up-hole	19/03/2019	I	F270SZ070	20,0	1,000	112,0	50	WOD	Parallel	563	N-S	Up-hole
07/02/2019	G	F270SZ072	24,5	0,898	197,0	65	WOD	Spiral	710	N-S	Up-hole	19/03/2019	G	F270SZ070	60,0	0,622	112,0	50	WOD	Parallel	691	N-S	Up-hole
07/02/2019	J	F270SZ072	38,3	5,640	197,0	65	WOD	Spiral	325	E-W	Up-hole	20/03/2019	J	F310SZ056	40,8	3,320	145,5		WD	Spiral	368	N-S	Downhole
08/02/2019	I	F310SZ050	20,0	3,500	61,8	50	WD	Parallel	360	N-S	Downhole	20/03/2019	I	F310SZ056	25,8	2,850	145,5		WD	Spiral	408	N-S	Downhole
08/02/2019	G	F310SZ050	40,0	1,820	61,8	50	WD	Parallel	465	N-S	Downhole	20/03/2019	G	F310SZ056	20,6	1,470	145,5		WD	Spiral	525	N-S	Downhole
08/02/2019	J	F310SZ050	40,0	2,250	61,8	50	WD	Parallel	419	N-S	Downhole	23/03/2019	J	F310SZ056	45,8	3,510	163,7	65	WD	Parallel	365	N-S	Downhole
09/02/2019	I	F270SZ054	20,0	3,480	136,4		WD	Spiral	357	N-S	Downhole	23/03/2019	I	F310SZ056	15,8	3,350	163,7	65	WD	Parallel	413	N-S	Downhole
09/02/2019	G	F270SZ054	40,0	2,550	136,4		WD	Spiral	478	N-S	Downhole	23/03/2019	G	F310SZ056	15,3	1,540	163,7	65	WD	Parallel	529	N-S	Downhole
09/02/2019	J	F270SZ054	60,0	4,450	136,4		WD	Spiral	354	N-S	Downhole	24/03/2019	I	F370SZ024L	30,5	2,090	157,0	50	WOD	Spiral	499	E-W	Up-hole
10/02/2019	I	F410SZ040A	20,0	3,460	165,0	50	WOD	Parallel	446	E-W	Up-hole	24/03/2019	G	F370SZ024L	20,5	1,540	157,0	50	WOD	Spiral	522	E-W	Up-hole
10/02/2019	G	F410SZ040A	60,0	2,280	165,0	50	WOD	Parallel	477	N-S	Up-hole	26/03/2019	I	F410SZ038	20,0	1,870	182,0	50	WOD	Parallel	460	E-W	Up-hole
10/02/2019	J	F410SZ040A	40,1	1,030	165,0	50	WOD	Parallel	637	N-S	Up-hole	26/03/2019	G	F410SZ038	20,1	1,580	182,0	50	WOD	Parallel	512	N-S	Up-hole
12/02/2019	I	F270SZ072	33,5	1,030	133,0	60	WOD	Parallel	585	N-S	Up-hole	26/03/2019	J	F410SZ038	19,8	0,823	182,0	50	WOD	Parallel	634	N-S	Up-hole
12/02/2019	G	F270SZ072	33,4	0,718	133,0	60	WOD	Parallel	713	N-S	Up-hole	27/03/2019	I	F270SZ070	21,0	0,698	105,0		WOD	Parallel	562	N-S	Up-hole
12/02/2019	J	F270SZ072	66,6	4,330	133,0	60	WOD	Parallel	327	E-W	Up-hole	27/03/2019	J	F270SZ070	100,0	2,950	105,0		WOD	Parallel	321	E-W	Up-hole
13/02/2019	I	F270SZ062	15,5	1,990	162,0	65	WOD	Spiral	375	N-S	Up-hole	28/03/2019	G	F270SZ062	20,1	1,780	125,0		WD	Spiral	470	N-S	Downhole
13/02/2019	G	F270SZ062	46,0	1,090	162,0	65	WOD	Spiral	489	N-S	Up-hole	28/03/2019	J	F270SZ062	140,0	4,670	125,0		WD	Spiral	364	N-S	Downhole

Legend:

Data considered as outliers

WD Data included in models with discontinuity

WOD Data included in models without discontinuity

Date	Monitored structure	Stope	Dominant frequency (Hz)	PVS (mm·s⁻¹)	Maximum charge per delay (kg)	Delay between adjacent holes (ms)	Operational scenario	Initiation pattern geometry	Distance (m)	Orientation	Type of blast	Date	Monitored structure	Stope	Dominant frequency (Hz)	PVS (mm·s⁻¹)	Maximum charge per delay (kg)	Delay between adjacent holes (ms)	Operational scenario	Initiation pattern geometry	Distance (m)	Orientation	Type of blast
29/03/2019	G	F310SZ056	40,1	2,440	143,2	50	WD	Parallel	517	N-S	Downhole	31/05/2019	I	F270SZ056	26,8	2,060	155,0	50	WOD	Parallel	407	N-S	Up-hole
29/03/2019	J	F310SZ056	40,1	6,430	143,2	50	WD	Parallel	373	N-S	Downhole	31/05/2019	G	F270SZ056	20,0	1,400	155,0	50	WOD	Parallel	525	N-S	Up-hole
30/03/2019	I	F370SZ024L	39,8	1,280	172,0		WOD	Parallel	518	E-W	Up-hole	02/06/2019	I	F410SZ042	146,0	1,000	16,1	50	WD	Spiral	424	N-S	Downhole
03/04/2019	J	F370SZ064	114,0	4,450	105,0	50	WD	Parallel	392	N-S	Downhole	02/06/2019	G	F410SZ042	20,3	0,596	16,1	50	WD	Spiral	462	N-S	Downhole
03/04/2019	G	F370SZ064	20,0	0,889	105,0	50	WD	Parallel	638	N-S	Downhole	04/06/2019	I	F270SZ056	20,3	3,510	151,0	50	WOD	Parallel	402	N-S	Up-hole
03/04/2019	I	F370SZ064	20,0	1,440	105,0	50	WD	Parallel	524	N-S	Downhole	04/06/2019	G	F270SZ056	39,9	2,360	151,0	50	WOD	Parallel	518	N-S	Up-hole
04/04/2019	G	F370SZ024L	19,9	1,110	157,0	50	WOD	Parallel	515	E-W	Up-hole	04/06/2019	I	F370SZ024L	11,5	6,970	167,0		WOD	Parallel	479	E-W	Up-hole
04/04/2019	I	F370SZ024L	29,8	1,310	157,0		WOD	Parallel	491	E-W	Up-hole	04/06/2019	G	F370SZ024L	40,0	3,710	167,0		WOD	Parallel	508	E-W	Up-hole
05/04/2019	J	F370SZ064	41,3	2,080	183,0	50	WOD	Spiral	486	N-S	Up-hole	05/06/2019	I	F270SZ044	15,6	4,550	200,0		WD	Spiral	329	N-S	Downhole
05/04/2019	G	F370SZ064	60,0	2,610	183,0		WOD	Spiral	536	N-S	Up-hole	05/06/2019	G	F270SZ044	46,1	3,100	200,0		WD	Spiral	444	N-S	Downhole
05/04/2019	I	F370SZ064	20,0	3,120	183,0		WOD	Spiral	453	N-S	Up-hole	05/06/2019	I	F410SZ042	42,0	0,582	60,7	50	WD	Spiral	420	N-S	Downhole
08/04/2019	J	F370SZ064	40,0	3,220	186,0	50	WOD	Parallel	481	N-S	Up-hole	07/06/2019	I	F410SZ042	3,0	0,524	28,6	50	WD	Spiral	416	N-S	Downhole
08/04/2019	G	F370SZ064	39,9	2,280	186,0	50	WOD	Parallel	544	N-S	Up-hole	07/06/2019	G	F410SZ063	39,9	1,420	175,2		WOD	Parallel	646	N-S	Downhole
08/04/2019	I	F370SZ064	20,0	2,370	186,0	50	WOD	Parallel	460	N-S	Up-hole	07/06/2019	I	F410SZ063	20,1	4,280	175,2		WOD	Parallel	542	N-S	Downhole
09/04/2019	G	F370SZ024L	40,1	1,200	159,0	50	WOD	Parallel	515	E-W	Up-hole	08/06/2019	G	F410SZ040	32,8	1,360	163,0		WOD	Spiral	502	N-S	Up-hole
09/04/2019	I	F370SZ024L	20,0	1,580	159,0	50	WOD	Parallel	490	E-W	Up-hole	08/06/2019	I	F410SZ040	30,5	1,820	163,0		WOD	Spiral	453	E-W	Up-hole
11/04/2019	G	F410SZ040A	20,0	3,180	160,2	50	WD	Parallel	456	N-S	Downhole	09/06/2019	G	F270SZ056	40,0	1,550	116,0	50	WOD	Parallel	523	N-S	Up-hole
11/04/2019	I	F410SZ040A	20,0	3,510	160,2	50	WD	Parallel	413	E-W	Downhole	09/06/2019	I	F270SZ056	20,3	2,580	116,0	50	WOD	Parallel	407	N-S	Up-hole
12/04/2019	G	F370SZ064	20,3	1,450	146,0	50	WOD	Parallel	539	N-S	Up-hole	10/06/2019	G	F410SZ040	40,0	1,840	159,0	50	WOD	Parallel	504	N-S	Up-hole
12/04/2019	I	F370SZ064	20,3	1,730	146,0	50	WOD	Parallel	455	N-S	Up-hole	10/06/2019	I	F410SZ040	20,0	2,140	159,0	50	WOD	Parallel	453	E-W	Up-hole
13/04/2019	G	F270SZ070	60,0	1,020	150,0	50	WD	Spiral	675	N-S	Downhole	11/06/2019	G	F410SZ042	40,3	0,813	53,6		WD	Spiral	449	N-S	Downhole
13/04/2019	I	F270SZ070	28,5	1,780	150,0	50	WD	Spiral	542	N-S	Downhole	11/06/2019	I	F410SZ042	99,8	1,180	53,6		WD	Spiral	412	E-W	Downhole
14/04/2019	G	F270SZ052	20,0	1,930	118,2	50	WD	Parallel	468	N-S	Downhole	12/06/2019	G	F270SZ044	20,3	3,220	163,7		WD	Parallel	441	N-S	Downhole
14/04/2019	I	F270SZ052	20,0	3,770	118,2	50	WD	Parallel	347	N-S	Downhole	12/06/2019	I	F270SZ044	20,0	6,190	163,7		WD	Parallel	328	N-S	Downhole
16/04/2019	G	F310SZ034	20,0	2,670	143,2	50	WD	Parallel	366	E-W	Downhole	13/06/2019	G	F410SZ040	20,0	1,370	158,0	50	WOD	Parallel	507	N-S	Up-hole
16/04/2019	I	F310SZ034	20,0	1,770	143,2	50	WD	Parallel	436	N-S	Downhole	13/06/2019	I	F410SZ040	20,0	2,190	158,0	50	WOD	Parallel	455	E-W	Up-hole
20/04/2019	J	F270SZ070	40,1	6,750	156,8		WD	Parallel	285	E-W	Downhole	14/06/2019	G	F410SZ042	61,5	1,310	55,3	65	WD	Parallel	454	N-S	Downhole
20/04/2019	I	F270SZ070	21,0	1,230	156,8		WD	Parallel	550	N-S	Downhole	14/06/2019	I	F410SZ042	30,8	1,780	55,3	65	WD	Parallel	413	N-S	Downhole
20/04/2019	G	F270SZ070	20,0	0,684	156,8		WD	Parallel	684	N-S	Downhole	15/06/2019	G	F370SZ024L	40,0	2,360	166,0		WOD	Parallel	507	E-W	Up-hole
21/04/2019	J	F370SZ024L	20,0	1,090	217,8		WD	Spiral	748	N-S	Downhole	15/06/2019	I	F370SZ024L	20,0	2,900	166,0		WOD	Parallel	477	E-W	Up-hole
21/04/2019	I	F370SZ024L	29,3	4,290	217,8		WD	Spiral	474	E-W	Downhole	16/06/2019	G	F270SZ068L	20,1	1,220	170,0	50	WOD	Spiral	645	N-S	Up-hole
21/04/2019	G	F370SZ024L	20,0	2,200	217,8		WD	Spiral	496	E-W	Downhole	16/06/2019	I	F270SZ068L	20,3	2,200	170,0	50	WOD	Spiral	519	N-S	Up-hole
24/04/2019	J	F310SZ063	45,4	7,390	156,0	65	WOD	Spiral	360	N-S	Up-hole	17/06/2019	I	F270SZ042	30,8	4,610	137,5		WD	Spiral	326	N-S	Downhole
24/04/2019	I	F310SZ063	30,0	2,070	156,0	65	WOD	Spiral	515	N-S	Up-hole	17/06/2019	G	F270SZ042	46,0	2,280	137,5		WD	Spiral	433	N-S	Downhole
24/04/2019	G	F310SZ063	15,3	1,330	156,0	65	WOD	Spiral	637	N-S	Up-hole	18/06/2019	G	F410SZ042	19,9	0,959	54,7	50	WD	Parallel	454	N-S	Downhole
25/04/2019	J	F410SZ038	19,9	1,040	75,8	50	WD	Parallel	610	N-S	Downhole	18/06/2019	I	F410SZ042	20,0	1,510	54,7	50	WD	Parallel	413	N-S	Downhole
25/04/2019	I	F410SZ038	20,0	1,940	75,8	50	WD	Parallel	427	E-W	Downhole	19/06/2019	G	F270SZ068L	20,0	1,490	162,0	50	WOD	Parallel	650	N-S	Up-hole
25/04/2019	G	F410SZ038	20,0	1,200	75,8		WD	Parallel	482	N-S	Downhole	19/06/2019	I	F270SZ068L	27,3	3,190	162,0	50	WOD	Parallel	524	N-S	Up-hole
26/04/2019	I	F310SZ063	20,0	1,750	173,0		WOD	Parallel	510	N-S	Up-hole	19/06/2019	J	F270SZ068L	42,8	12,800	162,0	50	WOD	Parallel	320	E-W	Up-hole
26/04/2019	G	F310SZ063	40,0	1,300	173,0		WOD	Parallel	632	N-S	Up-hole	20/06/2019	G	F270SZ056	46,1	1,470	97,5		WD	Spiral	502	N-S	Downhole
27/04/2019	I	F310SZ034	20,0	1,570	77,3	50	WD	Parallel	371	E-W	Downhole	20/06/2019	I	F270SZ056	30,8	3,180	97,5		WD	Spiral	379	N-S	Downhole
27/04/2019	G	F310SZ034	20,0	0,833	77,3	50	WD	Parallel	442	N-S	Downhole	20/06/2019	J	F270SZ056	123,0	10,100	97,5		WD	Spiral	334	N-S	Downhole
29/04/2019	I	F270SZ070	40,0	1,140	166,0	50	WOD	Parallel	569	N-S	Up-hole	21/06/2019	G	F270SZ042	20,0	2,880	130,0		WD	Parallel	434	N-S	Downhole
29/04/2019	G	F270SZ070	40,0	0,648	166,0	50	WOD	Parallel	698	N-S	Up-hole	21/06/2019	I	F270SZ042	20,0	6,680	130,0		WD	Parallel	325	N-S	Downhole
30/04/2019	I	F370SZ054	20,0	2,510	114,6	50	WD	Spiral	428	N-S	Downhole	21/06/2019	J	F270SZ042	40,0	4,600	130,0		WD	Parallel	461	N-S	Downhole
30/04/2019	G	F370SZ054	40,0	2,420	114,6	50	WD	Spiral	518	N-S	Downhole	23/06/2019	G	F410SZ040	20,0	1,330	156,0	50	WOD	Parallel	511	N-S	Up-hole
30/04/2019	I	F270SZ054	23,3	3,990	144,3	50	WD	Parallel	369	N-S	Downhole	23/06/2019	I	F410SZ040	20,0	2,160	156,0	50	WOD	Parallel	457	E-W	Up-hole
02/05/2019	G	F270SZ054	19,9	2,680	144,3	50	WD	Parallel	495	N-S	Downhole	23/06/2019	J	F410SZ040	60,0	1,100	156,0	50	WOD	Parallel	618	N-S	Up-hole
02/05/2019	I	F310SZ063	28,0	1,820	171,0	50	WOD	Parallel	512	N-S	Up-hole	24/06/2019	G	F270SZ068L	39,5	0,568	66,0	50	WOD	Parallel	656	N-S	Up-hole
04/05/2019	G	F310SZ063	20,0	0,925	171,0	50	WOD	Parallel	635	N-S	Up-hole	24/06/2019	I	F270SZ068L	40,0	0,925	66,0	50	WOD	Parallel	530	N-S	Up-hole
06/05/2019	I	F370SZ024L	60,0	2,320	122,7	50	WD	Parallel	468	E-W	Downhole	24/06/2019	J	F270SZ068L	59,9	7,210	66,0	50	WOD	Parallel	321	E-W	Up-hole
06/05/2019	G	F370SZ024L	40,0	1,650	122,7	50	WD	Parallel	494	E-W	Downhole	26/06/2019	J	F410SZ042	100,0	0,823	67,1	50	WD	Parallel	597	N-S	Downhole
08/05/2019	I	F370SZ054	20,0	2,160	112,5	50	WD	Parallel	430	N-S	Downhole	26/06/2019	I	F410SZ042	20,0	1,450	67,1	50	WD	Parallel	413	N-S	Downhole
08/05/2019	G	F370SZ054	40,0	1,750	112,5	50	WD	Parallel	524	N-S	Downhole	26/06/2019	G	F410SZ042	20,0	0,813	67,1	50	WD	Parallel	454	N-S	Downhole
11/05/2019	I	F270SZ070	24,6	0,898	182,0	50	WOD	Parallel	570	N-S	Up-hole	27/06/2019	I	F430SZ037A	50,3	0,538	16,1	50	WOD	Spiral	447	E-W	Downhole
11/05/2019	G	F270SZ070	20,0	0,568	182,0	50	WOD	Parallel	700	N-S	Up-hole	27/06/2019	G	F430SZ037A	40,0	0,635	16,1	50	WOD	Spiral	477	N-S	Downhole
14/05/2019	I	F310SZ063	20,0	2,050	142,5		WD	Spiral	495	N-S	Downhole	28/06/2019	J	F430SZ037A	42,3	0,635	26,8	50	WOD	Spiral	653	N-S	Downhole
14/05/2019	G	F310SZ063	40,0	1,050	142,5		WD	Spiral	623	N-S	Downhole	28/06/2019	I	F430SZ037A	80,3	0,751	26,8	50	WOD	Spiral	442	E-W	Downhole
15/05/2019	I	F370SZ024L	20,3	2,640	155,0	50	WD	Parallel	462	E-W	Downhole	28/06/2019	G	F430SZ037A	40,0	0,652	26,8	50	WOD	Spiral	472	N-S	Downhole
15/05/2019	G	F370SZ024L	40,0	2,180	155,0	50	WD	Parallel	491	E-W	Downhole	30/06/2019	J	F270SZ056	59,9	11,200	200,0	50	WD	Parallel	330	N-S	Downhole
18/05/2019	I	F270SZ042	19,5	3,420	141,0	50	WOD	Spiral	346	N-S	Up-hole	30/06/2019	I	F270SZ056	20,0	3,690	200,0	50	WD	Parallel	384	N-S	Downhole
18/05/2019	G	F270SZ042	20,3	1,470	141,0	50	WOD	Spiral	444	N-S	Up-hole	30/06/2019	G	F270SZ056	20,0	2,080	200,0	50	WD	Parallel	509	N-S	Downhole
18/05/2019	I	F310SZ063	27,8	1,510	102,3	50	WD	Parallel	493	N-S	Downhole	03/07/2019	J	F410SZ040	49,0	1,120	121,4		WD	Spiral	596	N-S	Downhole
18/05/2019	G	F310SZ063	20,0	0,813	102,3	50	WD	Parallel	622	N-S	Downhole	03/07/2019	I	F410SZ040	20,3	2,300	121,4		WD	Spiral	420	E-W	Downhole
19/05/2019	I	F270SZ044	16,8	4,250	141,0		WOD	Spiral	353	N-S	Up-hole	03/07/2019	G	F410SZ040	39,9	1,380	121,4		WD	Spiral	475	N-S	Downhole
19/05/2019	G	F270SZ044	33,3	2,790	141,0		WOD	Spiral	458	N-S	Up-hole	08/07/2019	I	F270SZ068L	30,8	1,710	165,0	65	WD	Spiral	506	N-S	Downhole
19/05/2019	I	F270SZ070	19,8	0,813	102,3	50	WD	Parallel	546	N-S	Downhole	08/07/2019	G	F270SZ068L	30,9	1,110	165,0	65	WD	Spiral	639	N-S	Downhole
21/05/2019	I	F270SZ042	20,0	6,610	153,0		WOD	Parallel	348	N-S	Up-hole	08/07/2019	J	F270SZ068L	108,0	14,400	165,0	65	WD	Spiral	283	E-W	Downhole
21/05/2019	G	F270SZ042	20,0	4,180	153,0		WOD	Parallel	447	N-S	Up-hole	10/07/2019	J	F270SZ042	140,0	1,200	31,7	50	WD	Parallel	463	N-S	Downhole
22/05/2019	I	F270SZ044	30,8	4,810	167,0	50	WOD	Parallel	350	N-S	Up-hole	10/07/2019	I	F270SZ042	20,3	1,200	31,7	50	WD	Parallel	319	N-S	Downhole
22/05/2019	G	F270SZ044	30,9	2,720	167,0	50	WOD	Parallel	453	N-S	Up-hole	10/07/2019	G	F270SZ042	60,0	0,696	31,7	50	WD	Parallel	425	N-S	Downhole
23/05/2019	I	F310SZ063	19,8	1,620	118,2	50	WD	Parallel	500	N-S	Downhole	11/07/2019	J	F410SZ040	48,6	1,150	127,5	50	WD	Parallel	594	N-S	Downhole
23/05/2019	G	F310SZ063	20,0	1,040	118,2	50	WD	Parallel	630	N-S	Downhole	11/07/2019	I	F410SZ040	20,0	1,700	127,5	50	WD	Parallel	422	E-W	Downhole
26/05/2019	I	F270SZ070	20,0	1,030	150,0	50	WD	Parallel	556	N-S	Downhole	11/07/2019	G	F410SZ040	20,0	1,530	127,5	50	WD	Parallel	479	N-S	Downhole
26/05/2019	G	F270SZ070	20,0	0,648	150,0	50	WD	Parallel	692	N-S	Downhole	15/07/2019	J	F270SZ056	100,0	6,560	75,0	50	WD	Parallel	327	N-S	Downhole
27/05/2019	G	F370SZ024L	40,0	1,230	124,0	50	WOD	Parallel	512	E-W	Up-hole	15/07/2019	I	F270SZ056	20,0	1,400	75,0	50	WD	Parallel	388	N-S	Downhole
29/05/2019	I	F270SZ056	24,8	3,250	163,0	65	WOD	Spiral	403	N-S	Up-hole	15/07/2019	G	F270SZ056	20,0	1,000	75,0	50	WD	Parallel	515	N-S	Downhole
29/05/2019	G	F270SZ056	46,1	2,040	163,0	65	WOD	Spiral	521	N-S	Up-hole	18/07/2019	J	F370SZ024L	100,0	1,210	114,8	50	WD	Parallel	721	N-S	Downhole

Legend:

Data considered as outliers

WD — Data included in models with discontinuity

WOD — Data included in models without discontinuity

Date	Monitored structure	Stope	Dominant frequency (Hz)	PVS (mm·s⁻¹)	Maximum charge per delay (kg)	Delay between adjacent holes (ms)	Operational scenario	Initiation pattern geometry	Distance (m)	Orientation	Type of blast	Date	Monitored structure	Stope	Dominant frequency (Hz)	PVS (mm·s⁻¹)	Maximum charge per delay (kg)	Delay between adjacent holes (ms)	Operational scenario	Initiation pattern geometry	Distance (m)	Orientation	Type of blast
18/07/2019	I	F370S2024L	20.0	4,830	114,8	50	WD	Parallel	458	E-W	Downhole	03/09/2019	G	F160SZ071R	19,3	0,783	115,0		WOD	Spiral	739	N-S	Up-hole
18/07/2019	G	F370S2024L	40,0	3,330	114,8	50	WD	Parallel	467	E-W	Downhole	04/09/2019	J	F370S2066L	60,3	2,940	193,2	50	WD	Spiral	385	E-W	Downhole
21/07/2019	J	F410S2040	100,0	0,880	113,6	50	WD	Parallel	564	N-S	Downhole	04/09/2019	I	F370S2066L	20,0	1,400	193,2	50	WD	Spiral	571	N-S	Downhole
21/07/2019	G	F410S2040	20,0	1,020	113,6	50	WD	Parallel	488	N-S	Downhole	04/09/2019	G	F370S2066L	20,5	1,110	193,2	50	WD	Spiral	689	N-S	Downhole
21/07/2019	I	F410S2040	20,0	2,220	113,6	50	WD	Parallel	425	E-W	Downhole	05/09/2019	J	F230SZ074L	40,0	4,910	155,0	50	WOD	Parallel	306	E-W	Up-hole
24/07/2019	J	F370S2024L	40,0	0,689	135,2	50	WD	Parallel	700	N-S	Downhole	05/09/2019	I	F230SZ074L	20,1	1,530	155,0	50	WOD	Parallel	626	N-S	Up-hole
24/07/2019	G	F370S2024L	40,0	1,450	135,2	50	WD	Parallel	481	E-W	Downhole	05/09/2019	G	F230SZ074L	40,0	0,684	155,0	50	WOD	Parallel	760	N-S	Up-hole
24/07/2019	I	F370S2024L	20,1	1,990	135,2		WD	Parallel	447	E-W	Downhole	07/09/2019	J	F270S2050	117,0	2,910	159,3		WD	Spiral	379	N-S	Downhole
25/07/2019	J	F410S2061	39,8	4,360	150,6		WOD	Parallel	439	N-S	Downhole	07/09/2019	I	F270S2050	16,8	4,360	159,3		WD	Spiral	338	N-S	Downhole
25/07/2019	G	F410S2061	20,0	2,120	150,6		WOD	Parallel	632	N-S	Downhole	07/09/2019	G	F270S2050	33,4	1,810	159,3		WD	Spiral	458	N-S	Downhole
25/07/2019	I	F410S2061	19,9	3,270	150,6		WOD	Parallel	528	N-S	Downhole	08/09/2019	J	F310SZ041L	33,1	1,970	172,7		WD	Spiral	499	N-S	Downhole
26/07/2019	J	F310SZ065	46,0	3,830	150,0	65	WOD	Spiral	358	N-S	Up-hole	08/09/2019	I	F310SZ041L	16,8	6,240	172,7		WD	Spiral	352	N-S	Downhole
26/07/2019	G	F310SZ065	46,1	1,030	150,0	65	WOD	Spiral	652	N-S	Up-hole	08/09/2019	G	F310SZ041L	16,8	2,280	172,7		WD	Spiral	446	N-S	Downhole
26/07/2019	I	F310SZ065	15,3	2,290	150,0	65	WOD	Spiral	529	N-S	Up-hole	10/09/2019	J	F230SZ074L	40,0	3,010	146,0		WOD	Parallel	304	E-W	Up-hole
27/07/2019	J	F370S2066L	61,4	2,050	153,0	65	WOD	Spiral	422	E-W	Up-hole	10/09/2019	I	F370S2066L	28,6	1,370	218,2		WD	Parallel	558	N-S	Downhole
27/07/2019	I	F370S2066L	25,8	1,530	153,0	65	WOD	Spiral	589	N-S	Up-hole	10/09/2019	G	F370S2066L	40,0	0,813	218,2		WD	Parallel	676	N-S	Downhole
28/07/2019	J	F270S2068L	41,8	16,700	168,2	50	WD	Parallel	284	E-W	Downhole	10/09/2019	J	F370S2066L	60,0	2,350	218,2		WD	Parallel	385	N-S	Downhole
28/07/2019	G	F270S2068L	21,8	2,220	168,2	50	WD	Parallel	647	N-S	Downhole	12/09/2019	I	F270S2050	20,0	2,880	92,1	50	WD	Parallel	341	N-S	Downhole
28/07/2019	I	F270S2068L	27,8	4,330	168,2	50	WD	Parallel	515	N-S	Downhole	12/09/2019	G	F270S2050	20,0	1,250	92,1	50	WD	Parallel	462	N-S	Downhole
29/07/2019	J	F160SZ074R	113,0	3,430	63,0	50	WOD	Spiral	224	N-S	Up-hole	12/09/2019	J	F270S2050	120,0	2,560	92,1	50	WD	Parallel	379	N-S	Downhole
30/07/2019	G	F370S2066L	20,0	0,783	152,0	50	WOD	Parallel	696	N-S	Up-hole	14/09/2019	J	F270S2032	46,4	3,430	232,5		WD	Spiral	591	N-S	Downhole
30/07/2019	J	F370S2066L	60,1	2,100	152,0	50	WOD	Parallel	423	E-W	Up-hole	14/09/2019	G	F270S2032	20,3	4,330	232,5		WD	Spiral	427	E-W	Downhole
30/07/2019	I	F370S2066L	22,3	1,140	152,0	50	WOD	Parallel	585	N-S	Up-hole	14/09/2019	I	F270S2032	16,8	6,160	232,5		WD	Spiral	357	E-W	Downhole
01/08/2019	J	F310SZ041L	59,9	2,200	155,0	50	WOD	Spiral	525	N-S	Up-hole	14/09/2019	J	F310SZ041L	40,0	2,380	137,5	50	WD	Parallel	510	N-S	Downhole
01/08/2019	G	F310SZ041L	20,3	3,660	155,0	50	WOD	Spiral	463	N-S	Up-hole	14/09/2019	G	F310SZ041L	20,0	2,830	137,5	50	WD	Parallel	444	N-S	Downhole
01/08/2019	I	F310SZ041L	20,0	9,550	155,0	50	WOD	Spiral	378	N-S	Up-hole	14/09/2019	I	F310SZ041L	20,1	6,600	137,5	50	WD	Parallel	352	E-W	Downhole
02/08/2019	J	F310SZ065	39,9	5,590	204,0		WOD	Parallel	357	N-S	Up-hole	17/09/2019	G	F270S2032	120,0	1,470	130,0	50	WD	Parallel	432	E-W	Downhole
02/08/2019	G	F310SZ065	39,9	1,310	204,0		WOD	Parallel	657	N-S	Up-hole	17/09/2019	I	F270S2032	80,0	5,190	130,0	50	WD	Parallel	361	E-W	Downhole
02/08/2019	I	F310SZ065	20,0	2,090	204,0		WOD	Parallel	534	N-S	Up-hole	18/09/2019	G	F370S2066L	40,0	2,460	159,0	50	WOD	Parallel	679	N-S	Up-hole
03/08/2019	J	F430SZ037A	19,8	1,050	60,7		WOD	Spiral	647	N-S	Downhole	18/09/2019	I	F370S2066L	26,6	2,180	159,0	50	WOD	Parallel	569	N-S	Up-hole
03/08/2019	G	F430SZ037A	79,8	1,280	60,7		WOD	Spiral	467	N-S	Downhole	19/09/2019	J	F270S2050	40,0	2,470	125,0	50	WD	Parallel	382	N-S	Downhole
03/08/2019	I	F430SZ037A	59,6	2,670	60,7		WOD	Spiral	435	E-W	Downhole	19/09/2019	I	F270S2050	19,9	4,970	125,0	50	WD	Parallel	341	N-S	Downhole
07/08/2019	G	F310SZ041L	20,1	2,060	204,0	50	WOD	Parallel	457	N-S	Up-hole	19/09/2019	G	F270S2050	20,0	1,330	125,0	50	WD	Parallel	463	N-S	Downhole
07/08/2019	I	F310SZ041L	20,0	6,470	204,0	50	WOD	Parallel	374	N-S	Up-hole	21/09/2019	J	F270S2032	46,0	3,660	172,5	50	WD	Parallel	585	N-S	Downhole
07/08/2019	J	F310SZ041L	40,1	1,570	204,0	50	WOD	Parallel	526	N-S	Up-hole	21/09/2019	I	F270S2032	20,3	7,350	172,5	50	WD	Parallel	353	E-W	Downhole
14/08/2019	J	F370S2066L	40,0	2,670	164,0	50	WOD	Parallel	423	E-W	Up-hole	21/09/2019	G	F270S2032	50,3	4,870	172,5	50	WD	Parallel	425	E-W	Downhole
14/08/2019	I	F370S2066L	25,5	1,100	164,0	50	WOD	Parallel	580	N-S	Up-hole	22/09/2019	J	F270S2030	60,1	1,450	158,0		WOD	Spiral	633	N-S	Up-hole
15/08/2019	G	F370S2066L	20,0	0,823	164,0	50	WOD	Parallel	691	N-S	Up-hole	22/09/2019	I	F270S2030	20,1	5,620	158,0		WOD	Spiral	384	E-W	Up-hole
15/08/2019	J	F270S2050	40,0	4,180	154,0	50	WOD	Spiral	413	N-S	Up-hole	22/09/2019	G	F270S2030	20,0	2,300	158,0		WOD	Spiral	438	E-W	Up-hole
15/08/2019	I	F270S2050	19,9	5,060	154,0	50	WOD	Spiral	357	N-S	Up-hole	23/09/2019	J	F310SZ041L	40,0	2,330	123,9		WD	Parallel	511	N-S	Downhole
15/08/2019	G	F270S2050	20,0	2,860	154,0	50	WOD	Spiral	466	N-S	Up-hole	23/09/2019	I	F310SZ041L	20,1	6,800	123,9		WD	Parallel	353	E-W	Downhole
16/08/2019	I	F430SZ037A	33,9	2,650	64,3	50	WOD	Parallel	435	E-W	Downhole	24/09/2019	I	F230SZ074L	20,0	1,000	171,0		WOD	Parallel	613	N-S	Up-hole
16/08/2019	G	F430SZ037A	20,0	1,770	64,3	50	WOD	Parallel	462	N-S	Downhole	24/09/2019	J	F230SZ074L	40,0	3,640	171,0		WOD	Parallel	300	E-W	Up-hole
17/08/2019	J	F310SZ041L	40,0	1,940	156,0	50	WOD	Parallel	531	N-S	Up-hole	30/09/2019	I	F270S2030	20,3	4,550	168,0	50	WOD	Parallel	386	E-W	Up-hole
17/08/2019	I	F310SZ041L	20,0	5,740	156,0	50	WOD	Parallel	379	E-W	Up-hole	30/09/2019	G	F270S2030	19,9	0,510	168,0	50	WOD	Parallel	439	E-W	Up-hole
17/08/2019	G	F310SZ041L	20,0	2,370	156,0	50	WOD	Parallel	463	N-S	Up-hole	30/09/2019	J	F270S2030	59,9	1,270	168,0	50	WOD	Parallel	636	N-S	Up-hole
21/08/2019	J	F270S2060	60,0	4,370	169,0	50	WOD	Parallel	403	N-S	Up-hole	30/09/2019	I	F430SZ037	99,8	1,580	23,2	50	WOD	Spiral	448	E-W	Downhole
21/08/2019	I	F270S2060	20,0	5,020	169,0	50	WOD	Parallel	366	N-S	Up-hole	30/09/2019	G	F430SZ037	20,3	0,619	23,2	50	WOD	Spiral	487	N-S	Downhole
21/08/2019	G	F270S2060	20,0	3,240	169,0	50	WOD	Parallel	478	N-S	Up-hole	01/10/2019	I	F310SZ065	20,0	2,800	129,6	50	WD	Parallel	517	N-S	Downhole
23/08/2019	J	F310SZ041L	19,9	1,550	151,0	50	WOD	Parallel	534	N-S	Up-hole	01/10/2019	G	F310SZ065	20,0	1,300	129,6	50	WD	Parallel	648	N-S	Downhole
23/08/2019	I	F310SZ041L	20,0	4,310	151,0	50	WOD	Parallel	377	E-W	Up-hole	01/10/2019	J	F310SZ065	20,0	4,250	129,6	50	WD	Parallel	320	N-S	Downhole
23/08/2019	G	F310SZ041L	20,0	1,770	151,0	50	WOD	Parallel	460	N-S	Up-hole	02/10/2019	I	F430SZ037	20,3	1,570	23,2	50	WOD	Spiral	443	E-W	Downhole
25/08/2019	J	F270S2032	59,8	1,280	233,0	50	WOD	Spiral	608	N-S	Up-hole	02/10/2019	J	F430SZ037	19,8	0,568	23,2	50	WOD	Spiral	643	N-S	Downhole
25/08/2019	I	F270S2032	20,0	1,910	233,0	50	WOD	Spiral	375	E-W	Up-hole	03/10/2019	I	F430SZ037	22,3	0,568	16,1	50	WOD	Spiral	438	E-W	Downhole
25/08/2019	G	F270S2032	39,8	1,300	233,0	50	WOD	Spiral	438	E-W	Up-hole	04/10/2019	J	F370S2066L	46,1	1,930	93,2	65	WD	Parallel	386	N-S	Downhole
26/08/2019	J	F310SZ065	19,9	5,200	133,0	50	WD	Spiral	321	N-S	Downhole	04/10/2019	I	F370S2066L	24,1	0,950	93,2	65	WD	Parallel	550	N-S	Downhole
26/08/2019	I	F310SZ065	19,9	3,280	133,0	50	WD	Spiral	510	N-S	Downhole	04/10/2019	G	F370S2066L	46,1	0,648	93,2	65	WD	Parallel	666	N-S	Downhole
26/08/2019	G	F310SZ065	19,9	1,530	133,0	50	WD	Spiral	639	N-S	Downhole	06/10/2019	J	F310SZ041L	60,0	1,440	153,0		WOD	Parallel	544	N-S	Up-hole
27/08/2019	I	F270S2032	60,0	1,110	187,0		WOD	Parallel	613	N-S	Up-hole	06/10/2019	I	F310SZ041L	20,0	5,360	153,0		WOD	Parallel	379	E-W	Up-hole
27/08/2019	G	F270S2032	20,0	2,900	187,0		WOD	Parallel	371	E-W	Up-hole	06/10/2019	G	F310SZ041L	20,0	2,980	153,0		WOD	Parallel	459	N-S	Up-hole
29/08/2019	J	F310SZ041L	60,0	1,310	159,0	50	WOD	Parallel	540	N-S	Up-hole	08/10/2019	J	F230SZ074L	40,0	3,560	168,0	50	WOD	Parallel	299	E-W	Up-hole
29/08/2019	I	F310SZ041L	20,0	3,360	159,0	50	WOD	Parallel	379	E-W	Up-hole	08/10/2019	G	F230SZ074L	40,5	0,582	168,0	50	WOD	Parallel	610	N-S	Up-hole
29/08/2019	G	F310SZ041L	20,0	1,590	159,0	50	WOD	Parallel	460	N-S	Up-hole	10/10/2019	I	F430SZ037	15,3	2,630	98,2	65	WOD	Parallel	745	N-S	Up-hole
31/08/2019	J	F270S2050	40,0	3,300	146,0		WOD	Parallel	409	N-S	Up-hole	10/10/2019	J	F430SZ037	31,0	0,813	98,2	65	WOD	Parallel	439	E-W	Up-hole
31/08/2019	I	F270S2050	20,0	3,580	146,0		WOD	Parallel	357	N-S	Up-hole	10/10/2019	G	F430SZ037	15,5	1,550	98,2	65	WOD	Parallel	640	N-S	Downhole
31/08/2019	G	F270S2050	20,0	2,670	146,0		WOD	Parallel	466	N-S	Up-hole	11/10/2019	I	F270S2032	16,5	3,280	96,6		WD	Parallel	478	N-S	Downhole
31/08/2019	I	F270S2068L	20,0	2,400	158,0	50	WOD	Parallel	539	N-S	Up-hole	11/10/2019	J	F270S2032	55,6	1,390	96,6		WD	Parallel	350	E-W	Downhole
31/08/2019	G	F270S2068L	20,0	1,000	158,0	50	WOD	Parallel	664	N-S	Up-hole	11/10/2019	G	F270S2032	22,6	1,420	96,6		WD	Parallel	420	E-W	Downhole
01/09/2019	J	F430SZ037A	59,8	1,120	84,0	50	WOD	Parallel	656	N-S	Downhole	12/10/2019	I	F310SZ041L	15,9	3,510	155,0		WOD	Parallel	379	E-W	Up-hole
01/09/2019	I	F430SZ037A	21,6	3,400	84,0	50	WOD	Parallel	437	E-W	Downhole	12/10/2019	J	F310SZ041L	30,8	1,000	155,0		WOD	Parallel	552	N-S	Up-hole
01/09/2019	G	F430SZ037A	41,8	2,480	84,0	50	WOD	Parallel	466	N-S	Downhole	12/10/2019	G	F310SZ041L	30,8	1,390	155,0		WOD	Parallel	456	N-S	Up-hole
02/09/2019	I	F230SZ074L	41,4	4,250	177,0	50	WOD	Spiral	306	E-W	Up-hole	13/10/2019	I	F430SZ037	59,9	3,280	88,6	50	WOD	Parallel	439	E-W	Downhole
02/09/2019	J	F230SZ074L	28,4	2,130	177,0	50	WOD	Spiral	629	N-S	Up-hole	13/10/2019	J	F430SZ037	39,9	0,696	88,6	50	WOD	Parallel	645	N-S	Downhole
02/09/2019	G	F230SZ074L	19,0	0,648	177,0	50	WOD	Spiral	764	N-S	Up-hole	13/10/2019	G	F430SZ037	39,9	1,020	88,6	50	WOD	Parallel	476	N-S	Downhole
03/09/2019	J	F160SZ071R	41,4	10,600	115,0		WOD	Spiral	206	N-S	Up-hole	15/10/2019	I	F270S2060	20,0	3,910	88,6	50	WD	Parallel	350	N-S	Downhole
03/09/2019	I	F160SZ071R	20,0	1,780	115,0		WOD	Spiral	583	N-S	Up-hole	15/10/2019	J	F270S2060	40,0	2,600	88,6	50	WD	Parallel	376	N-S	Downhole

Legend:

Data considered as outliers

WD Data included in models with discontinuity

WOD Data included in models without discontinuity

Date	Monitored structure	Stope	Dominant frequency (Hz)	PVS (mm·s⁻¹)	Maximum charge per delay (kg)	Delay between adjacent holes (ms)	Operational scenario	Initiation pattern geometry	Distance (m)	Orientation	Type of blast	Date	Monitored structure	Stope	Dominant frequency (Hz)	PVS (mm·s⁻¹)	Maximum charge per delay (kg)	Delay between adjacent holes (ms)	Operational scenario	Initiation pattern geometry	Distance (m)	Orientation	Type of blast
15/10/2019	G	F270SZ050	20.0	1.090	88.6	50	WD	Parallel	474	N-S	Downhole	01/12/2019	I	F410SZ046	15.5	1.610	82.5	65	WD	Spiral	425	N-S	Downhole
17/10/2019	I	F410SZ050L	20.0	0.684	107.0		WOD	Spiral	479	N-S	Up-hole	01/12/2019	G	F410SZ046	46.1	1.150	82.5	65	WD	Spiral	492	N-S	Downhole
17/10/2019	J	F410SZ050L	56.0	0.648	107.0		WOD	Spiral	532	N-S	Up-hole	02/12/2019	I	F310SZ041L	23.3	2.440	73.9		WD	Parallel	356	E-W	Downhole
19/10/2019	J	F310SZ041L	40.0	1.120	161.0	50	WOD	Parallel	559	N-S	Up-hole	02/12/2019	G	F310SZ041L	45.9	1.230	73.9		WD	Parallel	437	N-S	Downhole
19/10/2019	I	F310SZ041L	20.0	3.530	161.0	50	WOD	Parallel	382	E-W	Up-hole	05/12/2019	J	F270SZ063	20.0	5.540	97.5	50	WD	Parallel	284	N-S	Downhole
19/10/2019	G	F310SZ041L	20.0	1.200	161.0	50	WOD	Parallel	458	N-S	Up-hole	05/12/2019	I	F270SZ063	20.0	3.010	97.5	50	WD	Parallel	472	N-S	Downhole
21/10/2019	I	F410SZ043AL	19.9	2.330	191.0		WOD	Spiral	450	E-W	Up-hole	05/12/2019	G	F270SZ063	20.1	1.000	97.5	50	WD	Parallel	609	N-S	Downhole
21/10/2019	J	F410SZ043AL	49.6	1.700	191.0		WOD	Spiral	608	N-S	Up-hole	06/12/2019	J	F410SZ046	40.0	0.861	82.5	50	WD	Parallel	540	N-S	Downhole
21/10/2019	G	F410SZ043AL	60.0	1.530	191.0		WOD	Spiral	487	N-S	Up-hole	06/12/2019	I	F410SZ046	20.0	1.580	82.5	50	WD	Parallel	427	N-S	Downhole
24/10/2019	G	F270SZ068L	43.4	1.380	93.2		WD	Parallel	652	E-W	Downhole	06/12/2019	G	F410SZ046	40.0	1.090	82.5	50	WD	Parallel	497	N-S	Downhole
24/10/2019	J	F270SZ068L	43.5	10.200	93.2		WD	Parallel	284	E-W	Downhole	07/12/2019	J	F230SZ074L	40.3	5.450	113.6	50	WD	Parallel	267	E-W	Downhole
24/10/2019	I	F270SZ068L	28.4	2.340	93.2		WD	Parallel	520	N-S	Downhole	07/12/2019	I	F230SZ074L	20.1	1.450	113.6	50	WD	Parallel	600	N-S	Downhole
24/10/2019	G	F310SZ041L	50.3	1.950	154.0	50	WOD	Parallel	458	N-S	Up-hole	07/12/2019	G	F230SZ074L	40.0	0.852	113.6	50	WD	Parallel	739	N-S	Downhole
24/10/2019	J	F310SZ041L	41.1	1.160	154.0	50	WOD	Parallel	562	N-S	Up-hole	08/12/2019	J	F310SZ041L	41.3	1.110	83.0		WD	Parallel	549	N-S	Downhole
24/10/2019	I	F310SZ041L	20.0	4.210	154.0	50	WOD	Parallel	383	E-W	Up-hole	08/12/2019	I	F310SZ041L	22.5	3.620	83.0		WD	Parallel	357	E-W	Downhole
27/10/2019	J	F410SZ043AL	38.5	1.420	175.0		WOD	Parallel	602	N-S	Up-hole	08/12/2019	G	F310SZ041L	25.3	1.660	83.0		WD	Parallel	437	N-S	Downhole
27/10/2019	I	F410SZ043AL	24.3	1.430	175.0		WOD	Parallel	454	E-W	Up-hole	10/12/2019	J	F270SZ068A	46.1	5.450	120.0		WD	Parallel	281	E-W	Downhole
27/10/2019	G	F410SZ043AL	38.5	1.090	175.0		WOD	Parallel	494	N-S	Up-hole	10/12/2019	I	F270SZ068A	15.4	1.210	120.0		WD	Parallel	534	N-S	Downhole
30/10/2019	I	F310SZ041L	40.0	1.110	155.0	50	WOD	Parallel	570	N-S	Up-hole	10/12/2019	G	F270SZ068A	46.0	0.622	120.0		WD	Parallel	669	N-S	Downhole
30/10/2019	I	F310SZ041L	20.0	3.140	155.0	50	WOD	Parallel	384	E-W	Up-hole	11/12/2019	J	F410SZ046	46.1	0.684	87.5		WD	Parallel	541	N-S	Downhole
30/10/2019	G	F310SZ041L	40.0	1.880	155.0	50	WOD	Parallel	457	N-S	Up-hole	11/12/2019	I	F410SZ046	15.4	1.370	87.5		WD	Parallel	427	N-S	Downhole
01/11/2019	J	F270SZ030	61.3	1.200	95.5	65	WD	Spiral	618	N-S	Downhole	11/12/2019	G	F410SZ046	46.1	1.030	87.5		WD	Parallel	498	N-S	Downhole
01/11/2019	I	F270SZ030	17.0	3.990	95.5	65	WD	Spiral	370	E-W	Downhole	14/12/2019	I	F270SZ068A	20.3	1.090	100.0		WD	Parallel	525	N-S	Downhole
01/11/2019	G	F270SZ030	50.5	2.210	95.5	65	WD	Spiral	432	E-W	Downhole	14/12/2019	G	F270SZ068A	12.3	0.568	100.0		WD	Parallel	661	N-S	Downhole
02/11/2019	J	F410SZ043AL	39.9	3.950	112.5		WD	Spiral	582	N-S	Downhole	14/12/2019	J	F270SZ068A	37.9	6.940	100.0		WD	Parallel	279	E-W	Downhole
02/11/2019	I	F410SZ043AL	19.0	5.330	112.5		WD	Spiral	418	E-W	Downhole	16/12/2019	I	F370SZ065	27.1	1.560	93.2		WD	Parallel	542	N-S	Downhole
02/11/2019	G	F410SZ043AL	59.9	4.780	112.5		WD	Spiral	459	N-S	Downhole	16/12/2019	G	F370SZ065	46.3	0.925	93.2		WD	Parallel	657	N-S	Downhole
04/11/2019	J	F270SZ030	60.1	1.020	109.1	50	WD	Parallel	616	N-S	Downhole	16/12/2019	J	F370SZ065	35.8	2.540	93.2		WD	Parallel	389	N-S	Downhole
04/11/2019	I	F270SZ030	20.3	2.520	109.1	50	WD	Parallel	371	E-W	Downhole	17/12/2019	I	F410SZ043AL	19.4	5.290	175.0		WOD	Parallel	458	E-W	Up-hole
04/11/2019	G	F270SZ030	52.5	1.200	109.1	50	WD	Parallel	434	E-W	Downhole	17/12/2019	G	F410SZ043AL	34.4	2.980	175.0		WOD	Parallel	502	N-S	Up-hole
05/11/2019	J	F310SZ041L	40.0	1.710	90.9	50	WD	Parallel	523	N-S	Downhole	17/12/2019	J	F410SZ043AL	34.6	8.760	175.0		WOD	Parallel	589	N-S	Up-hole
05/11/2019	I	F310SZ041L	20.0	7.120	90.9	50	WD	Parallel	353	E-W	Downhole	19/12/2019	I	F310SZ041L	39.5	0.950	85.0	65	WD	Parallel	555	N-S	Downhole
05/11/2019	G	F310SZ041L	20.0	3.210	90.9	50	WD	Parallel	440	N-S	Downhole	19/12/2019	I	F310SZ041L	23.5	2.480	85.0	65	WD	Parallel	398	E-W	Downhole
06/11/2019	J	F230SZ074L	44.9	6.310	210.0		WD	Spiral	279	E-W	Downhole	19/12/2019	G	F310SZ041L	46.8	1.090	85.0	65	WD	Parallel	436	N-S	Downhole
06/11/2019	I	F230SZ074L	29.1	1.140	210.0		WD	Spiral	623	N-S	Downhole	20/12/2019	J	F310SZ053	39.9	2.800	100.0	50	WD	Parallel	386	N-S	Downhole
06/11/2019	G	F230SZ074L	45.0	0.741	210.0		WD	Parallel	762	N-S	Downhole	20/12/2019	I	F310SZ053	17.4	4.190	100.0	50	WD	Parallel	389	N-S	Downhole
08/11/2019	I	F410SZ043AL	45.0	6.600	129.6		WD	Parallel	419	E-W	Downhole	20/12/2019	G	F310SZ053	19.9	1.990	100.0	50	WD	Parallel	503	N-S	Downhole
08/11/2019	G	F410SZ043AL	45.0	4.060	129.6		WD	Parallel	463	N-S	Downhole	21/12/2019	J	F270SZ068A	20.0	3.430	106.8	50	WD	Parallel	279	E-W	Downhole
08/11/2019	I	F410SZ043AL	19.3	4.600	129.6		WD	Parallel	419	E-W	Downhole	21/12/2019	I	F270SZ068A	20.0	0.861	106.8	50	WD	Parallel	535	N-S	Downhole
10/11/2019	I	F310SZ041L	46.3	1.310	118.2		WD	Parallel	354	E-W	Downhole	22/12/2019	J	F370SZ028L	46.3	0.648	154.0		WOD	Spiral	689	N-S	Up-hole
10/11/2019	G	F310SZ041L	46.4	2.000	118.2		WD	Parallel	438	N-S	Downhole	22/12/2019	I	F370SZ028L	30.9	1.670	154.0		WOD	Spiral	459	E-W	Up-hole
10/11/2019	I	F310SZ041L	21.0	4.650	118.2		WD	Parallel	354	E-W	Downhole	22/12/2019	G	F370SZ028L	46.3	1.060	154.0		WOD	Spiral	499	E-W	Up-hole
12/11/2019	I	F270SZ030	42.5	1.990	90.9		WD	Parallel	369	E-W	Downhole	26/12/2019	J	F310SZ041L	46.3	0.783	68.2		WD	Parallel	559	N-S	Downhole
12/11/2019	G	F270SZ030	54.3	1.960	90.9		WD	Parallel	430	E-W	Downhole	26/12/2019	I	F310SZ041L	22.8	1.660	68.2		WD	Parallel	359	E-W	Downhole
12/11/2019	I	F270SZ030	15.6	3.570	90.9		WD	Parallel	369	E-W	Downhole	26/12/2019	G	F310SZ041L	46.0	0.813	68.2		WD	Parallel	435	N-S	Downhole
13/11/2019	I	F270SZ063	30.9	9.520	155.0		WOD	Spiral	494	N-S	Up-hole	28/12/2019	J	F410SZ046	46.3	0.741	89.8		WD	Parallel	534	N-S	Downhole
13/11/2019	G	F270SZ063	13.9	1.050	155.0		WOD	Spiral	624	N-S	Up-hole	28/12/2019	I	F410SZ046	15.4	1.080	89.8		WD	Parallel	430	N-S	Downhole
13/11/2019	I	F270SZ063	30.6	2.700	155.0		WOD	Spiral	494	N-S	Up-hole	29/12/2019	G	F410SZ046	46.3	1.050	89.8		WD	Parallel	504	N-S	Downhole
14/11/2019	I	F310SZ063	36.0	4.070	136.0	65	WOD	Spiral	400	N-S	Up-hole	29/12/2019	J	F310SZ053	38.5	2.010	47.5	65	WD	Spiral	396	N-S	Downhole
14/11/2019	G	F310SZ063	46.1	2.450	136.0	65	WOD	Spiral	499	N-S	Up-hole	29/12/2019	I	F310SZ053	20.5	2.210	47.5	65	WD	Spiral	389	N-S	Downhole
14/11/2019	I	F310SZ063	15.5	3.480	136.0	65	WOD	Spiral	400	N-S	Up-hole	29/12/2019	G	F310SZ053	40.0	1.810	47.5	65	WD	Spiral	498	N-S	Downhole
15/11/2019	I	F410SZ043AL	34.3	4.970	106.8		WD	Parallel	421	E-W	Downhole	31/12/2019	J	F410SZ043A	51.5	0.539	22.5	65	WOD	Spiral	590	N-S	Downhole
15/11/2019	G	F410SZ043AL	34.1	2.470	106.8		WD	Parallel	468	N-S	Downhole	31/12/2019	I	F410SZ043A	21.0	0.959	22.5	65	WOD	Spiral	424	N-S	Downhole
15/11/2019	I	F410SZ043AL	19.3	3.900	106.8		WD	Parallel	421	E-W	Downhole	31/12/2019	G	F410SZ043A	15.8	0.539	22.5	65	WOD	Spiral	472	N-S	Downhole
16/11/2019	I	F230SZ074L	36.4	7.050	90.9		WD	Parallel	614	N-S	Downhole	02/01/2020	J	F410SZ050L	54.0	0.582	105.0		WOD	Spiral	532	N-S	Up-hole
16/11/2019	G	F230SZ074L	23.5	0.925	90.9		WD	Parallel	754	N-S	Downhole	02/01/2020	I	F410SZ050L	30.3	0.852	105.0		WOD	Spiral	480	N-S	Up-hole
16/11/2019	I	F230SZ074L	30.1	1.650	90.9		WD	Parallel	614	N-S	Downhole	02/01/2020	G	F410SZ050L	30.5	0.582	105.0		WOD	Spiral	553	N-S	Up-hole
17/11/2019	I	F310SZ041L	38.9	1.450	97.7		WD	Parallel	354	E-W	Downhole	04/01/2020	I	F370SZ028L	23.0	1.370	166.0	65	WOD	Parallel	455	E-W	Up-hole
17/11/2019	G	F310SZ041L	24.0	2.230	97.7		WD	Parallel	438	N-S	Downhole	04/01/2020	G	F370SZ028L	46.6	0.933	166.0	65	WOD	Parallel	495	E-W	Up-hole
17/11/2019	I	F310SZ041L	22.8	5.210	97.7		WD	Parallel	354	E-W	Downhole	05/01/2020	J	F410SZ043A	51.3	0.554	25.0	50	WOD	Spiral	586	N-S	Downhole
18/11/2019	I	F270SZ030	40.3	1.400	70.0		WD	Parallel	363	E-W	Downhole	05/01/2020	I	F410SZ043A	20.0	0.783	25.0	50	WOD	Spiral	419	N-S	Downhole
18/11/2019	G	F270SZ030	20.3	1.960	70.0	50	WD	Parallel	425	E-W	Downhole	06/01/2020	J	F310SZ053	39.8	1.470	25.0	50	WD	Spiral	391	N-S	Downhole
18/11/2019	I	F270SZ030	20.5	2.670	70.0	50	WD	Parallel	363	E-W	Downhole	06/01/2020	I	F310SZ053	19.8	0.861	25.0	50	WD	Spiral	383	N-S	Downhole
19/11/2019	I	F310SZ053	39.9	3.570	135.0	50	WOD	Parallel	406	N-S	Up-hole	06/01/2020	G	F310SZ053	40.0	0.696	25.0	50	WD	Spiral	494	N-S	Downhole
19/11/2019	G	F310SZ053	20.0	1.980	135.0	50	WOD	Parallel	507	N-S	Up-hole	06/01/2020	I	F410SZ050L	20.0	0.684	105.0		WOD	Parallel	477	N-S	Up-hole
19/11/2019	I	F310SZ053	20.0	1.730	135.0	50	WOD	Parallel	406	N-S	Up-hole	06/01/2020	G	F410SZ050L	20.0	0.539	105.0		WOD	Parallel	549	N-S	Up-hole
20/11/2019	G	F270SZ068A	61.5	4.300	168.0		WOD	Spiral	676	N-S	Up-hole	07/01/2020	I	F310SZ053	20.0	6.100	97.5		WD	Parallel	384	N-S	Downhole
20/11/2019	I	F270SZ068A	30.6	1.400	168.0		WOD	Spiral	545	N-S	Up-hole	07/01/2020	J	F310SZ053	40.0	4.690	97.5		WD	Parallel	390	N-S	Downhole
24/11/2019	G	F310SZ053	36.9	2.670	137.0		WOD	Parallel	510	N-S	Up-hole	07/01/2020	G	F310SZ053	20.0	3.200	97.5		WD	Parallel	495	N-S	Downhole
24/11/2019	I	F310SZ053	15.4	2.900	137.0		WOD	Parallel	407	N-S	Up-hole	08/01/2020	I	F370SZ065	28.3	1.450	186.4		WD	Parallel	538	N-S	Downhole
27/11/2019	I	F230SZ074L	30.0	1.550	90.9		WD	Parallel	606	N-S	Downhole	08/01/2020	J	F370SZ065	31.9	2.360	186.4		WD	Parallel	389	N-S	Downhole
27/11/2019	J	F230SZ074L	34.1	5.320	90.9	269	WD	Parallel	269	E-W	Downhole	08/01/2020	G	F370SZ065	40.0	1.160	186.4		WD	Parallel	653	N-S	Downhole
27/11/2019	G	F230SZ074L	23.6	0.684	90.9		WD	Parallel	745	N-S	Downhole	11/01/2020	J	F230SZ074L	30.6	6.540	168.0		WOD	Parallel	296	E-W	Up-hole
27/11/2019	J	F270SZ068A	30.5	1.330	120.0	65	WOD	Parallel	538	N-S	Up-hole	11/01/2020	G	F230SZ074L	15.9	0.741	168.0		WOD	Spiral	739	N-S	Up-hole
27/11/2019	I	F270SZ068A	30.6	4.080	120.0	65	WOD	Parallel	316	E-W	Up-hole	11/01/2020	J	F410SZ043A	61.6	1.160	125.0		WOD	Spiral	584	N-S	Downhole
27/11/2019	G	F270SZ068A	30.6	0.582	120.0	65	WOD	Parallel	667	N-S	Up-hole	11/01/2020	G	F410SZ043A	46.1	1.640	125.0		WOD	Spiral	461	N-S	Downhole
29/11/2019	I	F310SZ053	30.8	2.460	137.0		WOD	Parallel	410	N-S	Up-hole	12/01/2020	J	F370SZ028L	46.3	0.635	155.0		WOD	Parallel	681	N-S	Up-hole
29/11/2019	G	F310SZ053	46.5	1.630	137.0		WOD	Parallel	515	N-S	Up-hole	12/01/2020	G	F370SZ028L	46.1	1.090	155.0		WOD	Parallel	495	E-W	Up-hole

Legend:

Data considered as outliers

WD — Data included in models with discontinuity

WOD — Data included in models without discontinuity

Date	Monitored structure	Stope	Dominant frequency (Hz)	PVS (mm·s⁻¹)	Maximum charge per delay (kg)	Delay between adjacent holes (ms)	Operational scenario	Initiation pattern geometry	Distance (m)	Orientation	Type of blast	Date	Monitored structure	Stope	Dominant frequency (Hz)	PVS (mm·s⁻¹)	Maximum charge per delay (kg)	Delay between adjacent holes (ms)	Operational scenario	Initiation pattern geometry	Distance (m)	Orientation	Type of blast
16/01/2020	J	F270SZ068	46,3	1,050	22,5	65	WOD	Spiral	288	E-W	Downhole	27/02/2020	I	F410SZ037A	46,3	1,200	32,5		WOD	Spiral	422	E-W	Downhole
16/01/2020	G	F270SZ068	30,6	2,210	22,5	65	WOD	Spiral	681	N-S	Downhole	27/02/2020	G	F410SZ037A	46,5	0,889	32,5		WOD	Spiral	451	N-S	Downhole
16/01/2020	J	F410SZ043A	35,0	1,150	75,0		WOD	Parallel	579	N-S	Downhole	27/02/2020	I	F410SZ050L	18,8	1,590	113,6		WD	Parallel	446	N-S	Downhole
17/01/2020	J	F270SZ068	41,3	1,180	27,5	65	WOD	Spiral	283	E-W	Downhole	27/02/2020	J	F410SZ050L	32,4	1,300	113,6		WD	Parallel	506	N-S	Downhole
18/01/2020	J	F270SZ068	41,5	0,648	12,5	65	WOD	Spiral	278	E-W	Downhole	27/02/2020	G	F410SZ050L	61,3	1,440	113,6		WD	Parallel	523	N-S	Downhole
19/01/2020	G	F270SZ028L	46,6	1,080	156,0	65	WOD	Parallel	494	E-W	Up-hole	28/02/2020	J	F410SZ037A	37,0	0,635	58,9		WOD	Spiral	640	N-S	Downhole
20/01/2020	G	F270SZ068	41,5	0,539	82,5	65	WOD	Spiral	667	N-S	Downhole	28/02/2020	I	F410SZ037A	46,1	3,260	58,9		WOD	Spiral	416	E-W	Downhole
20/01/2020	J	F270SZ068	46,1	4,220	82,5	65	WOD	Spiral	277	E-W	Downhole	28/02/2020	G	F410SZ037A	38,4	1,770	58,9		WOD	Spiral	446	N-S	Downhole
22/01/2020	H	M440SZ004	23,8	0,648	54,7	50	WOD	Parallel	743	N-S	Downhole	02/03/2020	J	F370SZ028L	46,6	0,751	104,8		WD	Parallel	648	N-S	Downhole
23/01/2020	J	M440SZ004	32,6	3,010	81,8		WD	Parallel	395	N-S	Downhole	02/03/2020	I	F370SZ028L	22,6	2,010	104,8		WD	Parallel	417	E-W	Downhole
23/01/2020	I	F310SZ053	20,0	4,080	81,8		WD	Parallel	379	N-S	Downhole	02/03/2020	G	F370SZ028L	38,8	1,140	104,8		WD	Parallel	464	E-W	Downhole
23/01/2020	G	F310SZ053	20,0	1,630	81,8		WD	Parallel	488	N-S	Downhole	03/03/2020	J	F410SZ037A	36,3	0,751	46,4		WOD	Parallel	637	N-S	Downhole
25/01/2020	J	F370SZ028L	46,0	0,582	150,0		WOD	Parallel	665	N-S	Up-hole	03/03/2020	I	F410SZ037A	19,5	2,470	46,4		WOD	Parallel	416	E-W	Downhole
25/01/2020	I	F370SZ028L	15,4	1,400	150,0		WOD	Parallel	447	E-W	Up-hole	03/03/2020	G	F410SZ037A	19,0	1,930	46,4		WOD	Parallel	447	N-S	Downhole
25/01/2020	G	F370SZ028L	46,1	0,933	150,0		WOD	Parallel	492	E-W	Up-hole	04/03/2020	J	F410SZ037A	37,4	0,813	96,0		WOD	Parallel	662	N-S	Up-hole
27/01/2020	J	F270SZ068	46,1	4,530	77,7		WOD	Parallel	278	E-W	Downhole	04/03/2020	I	F410SZ037A	20,0	2,880	96,0		WOD	Parallel	432	E-W	Up-hole
27/01/2020	I	F270SZ068	30,8	0,976	77,7		WOD	Parallel	543	N-S	Downhole	04/03/2020	G	F410SZ037A	40,0	1,690	96,0		WOD	Parallel	457	N-S	Up-hole
27/01/2020	G	F270SZ068	46,1	0,582	77,7		WOD	Parallel	682	N-S	Downhole	06/03/2020	J	F410SZ050L	34,4	2,020	78,4		WD	Parallel	511	N-S	Downhole
02/02/2020	I	F370SZ028L	23,0	1,530	150,0		WOD	Parallel	446	E-W	Up-hole	06/03/2020	I	F410SZ050L	19,8	2,040	78,4		WD	Parallel	442	N-S	Downhole
02/02/2020	J	F370SZ028L	18,1	0,803	150,0		WOD	Parallel	491	E-W	Up-hole	06/03/2020	G	F410SZ050L	25,3	1,660	78,4		WD	Parallel	518	N-S	Downhole
02/02/2020	G	F370SZ028L	18,1	0,803	150,0		WOD	Parallel	491	E-W	Up-hole	09/03/2020	J	F370SZ028L	40,0	0,976	134,1		WD	Parallel	646	N-S	Downhole
05/02/2020	J	F410SZ048	36,9	0,741	82,5		WOD	Spiral	530	N-S	Downhole	09/03/2020	I	F370SZ028L	20,0	2,190	134,1		WD	Parallel	417	E-W	Downhole
05/02/2020	I	F410SZ048	15,6	1,200	82,5		WOD	Spiral	430	N-S	Downhole	09/03/2020	G	F370SZ028L	20,0	1,140	134,1		WD	Parallel	465	E-W	Downhole
05/02/2020	G	F410SZ048	92,3	0,925	82,5		WOD	Spiral	501	N-S	Downhole	10/03/2020	H	M440SZ004	39,8	0,648	105,0		WOD	Parallel	766	N-S	Up-hole
06/02/2020	J	F370SZ028L	32,8	6,160	125,0	65	WD	Parallel	399	N-S	Downhole	13/03/2020	I	F410SZ044	15,6	1,000	60,7		WOD	Parallel	423	N-S	Downhole
06/02/2020	I	F310SZ053	15,4	8,510	125,0	65	WD	Parallel	375	N-S	Downhole	13/03/2020	J	F410SZ065	61,8	1,420	97,5		WD	Spiral	674	N-S	Downhole
06/02/2020	G	F310SZ053	23,1	3,530	125,0	65	WD	Parallel	482	N-S	Downhole	13/03/2020	J	F310SZ027	36,5	1,420	97,5		WD	Parallel	674	N-S	Downhole
07/02/2020	J	F410SZ043AL	35,6	1,940	77,5	65	WD	Parallel	568	N-S	Downhole	14/03/2020	G	F310SZ027	33,4	4,120	97,5		WD	Parallel	441	E-W	Downhole
07/02/2020	I	F410SZ043AL	30,8	2,480	77,5	65	WD	Parallel	423	E-W	Downhole	14/03/2020	I	F310SZ027	22,6	4,940	97,5		WD	Parallel	402	E-W	Downhole
07/02/2020	G	F410SZ043AL	46,1	2,080	77,5	65	WD	Parallel	470	N-S	Downhole	15/03/2020	J	F410SZ050L	34,4	1,910	100,0		WD	Parallel	514	N-S	Downhole
08/02/2020	J	F410SZ048	39,9	0,751	70,0	50	WOD	Parallel	526	N-S	Downhole	15/03/2020	G	F410SZ050L	32,8	1,950	100,0		WD	Parallel	516	N-S	Downhole
08/02/2020	I	F410SZ048	20,0	1,310	70,0	50	WOD	Parallel	432	N-S	Downhole	15/03/2020	I	F410SZ050L	21,0	2,140	100,0		WD	Parallel	439	N-S	Downhole
08/02/2020	G	F410SZ048	60,0	0,852	70,0	50	WOD	Parallel	505	N-S	Downhole	17/03/2020	J	F370SZ028L	123,0	1,440	127,5		WD	Parallel	633	N-S	Downhole
10/02/2020	J	F370SZ028L	40,5	0,648	140,0		WD	Parallel	672	N-S	Downhole	17/03/2020	G	F370SZ028L	18,4	1,300	127,5		WD	Parallel	471	E-W	Downhole
10/02/2020	I	F370SZ028L	16,8	2,340	140,0		WD	Parallel	433	E-W	Downhole	17/03/2020	I	F370SZ028L	30,8	2,230	127,5		WD	Parallel	417	E-W	Downhole
10/02/2020	G	F370SZ028L	20,1	1,260	140,0		WD	Parallel	476	E-W	Downhole	17/03/2020	J	F410SZ065	61,8	0,958	47,5		WD	Spiral	488	N-S	Downhole
11/02/2020	I	F410SZ050L	15,5	0,539	60,0		WD	Spiral	455	N-S	Downhole	17/03/2020	I	F410SZ065	19,5	0,635	47,5		WD	Spiral	479	N-S	Downhole
12/02/2020	H	M440SZ004	24,3	0,696	91,0		WOD	Parallel	757	N-S	Up-hole	18/03/2020	J	F410SZ044	38,8	0,648	65,0		WOD	Parallel	551	N-S	Downhole
14/02/2020	J	F310SZ027	41,4	0,933	146,0		WOD	Parallel	687	N-S	Up-hole	18/03/2020	G	F410SZ044	92,3	1,000	65,0		WOD	Parallel	493	N-S	Downhole
14/02/2020	G	F310SZ027	30,8	1,810	146,0		WOD	Parallel	464	E-W	Up-hole	18/03/2020	I	F410SZ044	15,4	1,710	65,0		WOD	Parallel	424	N-S	Downhole
14/02/2020	I	F310SZ027	15,4	2,720	146,0		WOD	Parallel	427	E-W	Up-hole	19/03/2020	J	F410SZ065	39,6	1,890	100,0		WD	Spiral	481	N-S	Downhole
14/02/2020	J	F410SZ048	46,3	0,582	42,9		WOD	Parallel	522	N-S	Downhole	19/03/2020	G	F410SZ065	45,5	1,090	100,0		WD	Spiral	557	N-S	Downhole
14/02/2020	I	F410SZ048	15,5	0,730	42,9		WOD	Parallel	434	N-S	Downhole	19/03/2020	I	F410SZ065	32,0	1,980	100,0		WD	Spiral	472	N-S	Downhole
15/02/2020	J	F410SZ050L	37,8	1,000	117,5		WD	Parallel	501	N-S	Downhole	21/03/2020	J	F310SZ047	31,0	4,180	100,0		WD	Spiral	444	N-S	Downhole
15/02/2020	G	F410SZ050L	40,1	1,020	117,5		WD	Parallel	529	N-S	Downhole	21/03/2020	G	F310SZ047	19,4	6,390	100,0		WD	Spiral	452	N-S	Downhole
15/02/2020	I	F410SZ050L	17,1	1,660	117,5		WD	Parallel	449	N-S	Downhole	22/03/2020	J	F310SZ027	36,8	1,350	93,2		WD	Parallel	673	N-S	Downhole
16/02/2020	J	F370SZ028L	40,0	0,751	129,1	65	WD	Parallel	667	N-S	Downhole	22/03/2020	G	F310SZ027	45,6	1,530	93,2		WD	Parallel	442	E-W	Downhole
16/02/2020	G	F370SZ028L	40,0	1,400	129,1	65	WD	Parallel	473	E-W	Downhole	22/03/2020	I	F310SZ027	22,8	3,390	93,2		WD	Parallel	403	E-W	Downhole
16/02/2020	I	F370SZ028L	16,4	1,800	129,1	65	WD	Parallel	430	E-W	Downhole	23/03/2020	I	F410SZ044	16,1	1,210	75,0	65	WOD	Parallel	426	N-S	Downhole
17/02/2020	J	F370SZ065	40,0	1,300	99,0		WOD	Parallel	422	N-S	Up-hole	23/03/2020	J	F410SZ044	43,3	0,568	75,0	65	WOD	Parallel	549	N-S	Downhole
17/02/2020	G	F370SZ065	40,0	0,648	99,0		WOD	Parallel	673	N-S	Up-hole	23/03/2020	G	F410SZ044	92,0	0,783	75,0	65	WOD	Parallel	496	N-S	Downhole
17/02/2020	I	F370SZ065	28,8	0,933	99,0		WOD	Parallel	562	N-S	Up-hole	25/03/2020	I	F410SZ065	32,4	1,330	112,5		WD	Parallel	470	N-S	Downhole
19/02/2020	G	F410SZ044	46,5	0,596	45,0	65	WOD	Spiral	493	N-S	Downhole	25/03/2020	J	F410SZ065	36,5	1,790	112,5		WD	Parallel	480	N-S	Downhole
19/02/2020	I	F410SZ044	15,5	0,635	45,0	65	WOD	Spiral	429	N-S	Downhole	25/03/2020	G	F410SZ065	45,0	0,967	112,5		WD	Parallel	556	N-S	Downhole
20/02/2020	J	F410SZ044	61,4	1,820	35,0	65	WOD	Spiral	560	N-S	Downhole	28/03/2020	I	F370SZ028L	20,0	1,940	104,6		WD	Parallel	413	E-W	Downhole
20/02/2020	I	F410SZ044	100,0	0,730	35,0	65	WOD	Spiral	422	N-S	Downhole	28/03/2020	J	F370SZ028L	37,3	0,813	104,6		WD	Parallel	632	N-S	Downhole
20/02/2020	G	F410SZ050L	40,1	1,730	72,7		WD	Parallel	497	N-S	Downhole	28/03/2020	G	F370SZ028L	20,0	1,150	104,6		WD	Parallel	465	E-W	Downhole
20/02/2020	G	F410SZ050L	46,9	1,390	72,7		WD	Parallel	534	N-S	Downhole	02/04/2020	I	F410SZ039A	20,0	4,220	151,0		WOD	Parallel	448	E-W	Up-hole
20/02/2020	I	F410SZ050L	30,6	1,430	72,7		WD	Parallel	454	N-S	Downhole	03/04/2020	I	F370SZ046	20,0	1,850	140,0	50	WOD	Spiral	425	N-S	Up-hole
21/02/2020	J	F410SZ044	44,3	0,648	50,0	65	WOD	Spiral	559	N-S	Downhole	06/04/2020	I	F370SZ046	18,8	2,280	130,0	65	WOD	Parallel	425	N-S	Up-hole
21/02/2020	G	F410SZ044	46,5	1,000	50,0	65	WOD	Spiral	487	N-S	Downhole	07/04/2020	I	F310SZ027	20,0	3,980	161,0	50	WOD	Parallel	431	E-W	Up-hole
21/02/2020	I	F410SZ044	16,5	1,090	50,0	65	WOD	Spiral	422	N-S	Downhole	09/04/2020	I	F370SZ070AR	30,6	1,580	99,0		WOD	Spiral	536	N-S	Up-hole
21/02/2020	J	F410SZ065	37,8	1,640	209,0		WOD	Parallel	512	N-S	Up-hole	09/04/2020	I	F410SZ039A	31,9	1,500	123,0	65	WOD	Parallel	448	E-W	Up-hole
21/02/2020	G	F410SZ065	30,8	0,976	209,0		WOD	Parallel	579	N-S	Up-hole	14/04/2020	I	F310SZ070AR	30,8	1,050	126,0	65	WOD	Parallel	538	N-S	Up-hole
21/02/2020	I	F410SZ065	30,8	1,430	209,0		WOD	Parallel	489	N-S	Up-hole	15/04/2020	I	F370SZ046	15,4	2,160	138,0		WOD	Parallel	426	N-S	Up-hole
22/02/2020	J	F410SZ037A	41,0	0,933	22,5	50	WOD	Spiral	648	N-S	Downhole	17/04/2020	I	F310SZ070AR	30,8	1,280	110,0		WOD	Parallel	550	N-S	Up-hole
23/02/2020	J	F230SZ074L	30,6	5,730	122,5		WD	Parallel	277	E-W	Downhole	18/04/2020	I	F310SZ027	15,5	3,690	88,2		WD	Parallel	404	E-W	Downhole
23/02/2020	G	F230SZ074L	15,4	0,773	122,5		WD	Parallel	762	N-S	Downhole	19/04/2020	I	F370SZ048	17,0	1,620	152,0		WOD	Spiral	428	N-S	Up-hole
23/02/2020	I	F230SZ074L	30,9	1,870	122,5		WD	Parallel	622	N-S	Downhole	21/04/2020	I	F370SZ048	15,5	1,280	138,0		WOD	Parallel	428	N-S	Up-hole
24/02/2020	J	F370SZ028L	40,0	0,925	93,2	50	WD	Parallel	658	N-S	Downhole	24/04/2020	I	F310SZ047	15,9	4,390	135,7	65	WD	Parallel	352	N-S	Downhole
24/02/2020	G	F370SZ028L	20,0	1,310	93,2	50	WD	Parallel	476	E-W	Downhole	24/04/2020	J	F310SZ047	46,8	1,650	135,7	65	WD	Parallel	443	N-S	Downhole
24/02/2020	I	F370SZ028L	20,0	2,120	93,2	50	WD	Parallel	429	E-W	Downhole	25/04/2020	I	F410SZ039A	15,3	4,520	130,0		WD	Spiral	413	E-W	Downhole
24/02/2020	J	F410SZ044	92,3	0,539	67,5		WOD	Parallel	559	N-S	Downhole	25/04/2020	J	F410SZ039A	46,0	1,200	130,0		WD	Spiral	619	N-S	Downhole
24/02/2020	G	F410SZ044	46,3	0,783	67,5		WOD	Parallel	483	N-S	Downhole	28/04/2020	I	F370SZ048	20,0	1,780	141,0		WOD	Parallel	431	N-S	Up-hole
24/02/2020	I	F410SZ044	15,3	1,020	67,5		WOD	Parallel	420	N-S	Downhole	30/04/2020	I	F370SZ046	15,4	2,980	150,0		WD	Parallel	392	N-S	Downhole
27/02/2020	I	F310SZ047	16,0	5,920	140,0		WOD	Parallel	378	N-S	Up-hole	03/05/2020	I	F350SZ028R	21,5	3,650	177,0		WOD	Parallel	426	E-W	Up-hole
27/02/2020	J	F310SZ047	15,9	2,010	140,0		WOD	Parallel	470	N-S	Up-hole	07/05/2020	J	F410SZ039A	31,0	2,110	115,9		WD	Parallel	414	E-W	Downhole
27/02/2020	G	F310SZ047	30,7	3,710	140,0		WOD	Parallel	471	N-S	Up-hole	08/05/2020	J	F370SZ046	15,6	0,751	81,4		WD	Parallel	503	N-S	Downhole

Legend:

Data considered as outliers

WD — Data included in models with discontinuity

WOD — Data included in models without discontinuity

Date	Monitored structure	Stope	Dominant frequency (Hz)	PVS (mm·s⁻¹)	Maximum charge per delay (kg)	Delay between adjacent holes (ms)	Operational scenario	Initiation pattern geometry	Distance (m)	Orientation	Type of blast
08/05/2020	I	F370SZ046	15,6	1.060	81,4		WD	Parallel	393	N-S	Downhole
08/05/2020	G	F370SZ046	46,3	0.889	81,4		WD	Parallel	475	N-S	Downhole
12/05/2020	J	F370SZ046	20,0	1.200	93,2		WD	Parallel	501	N-S	Downhole
12/05/2020	I	F370SZ046	20,0	1.730	93,2		WD	Parallel	395	N-S	Downhole
12/05/2020	G	F370SZ046	20,0	1.180	93,2		WD	Parallel	479	N-S	Downhole
14/05/2020	J	F310SZ071AL	46,1	10.900	154,0		WOD	Spiral	374	E-W	Up-hole
14/05/2020	I	F310SZ071AL	30,8	2,170	154,0		WOD	Spiral	546	N-S	Up-hole
14/05/2020	G	F310SZ071AL	46,1	1,200	154,0		WOD	Spiral	658	N-S	Up-hole
15/05/2020	J	F270SZ034	30,8	1,110	156,0		WOD	Spiral	582	N-S	Up-hole
15/05/2020	I	F270SZ034	15,3	2,330	156,0		WOD	Spiral	367	E-W	Up-hole
15/05/2020	G	F270SZ034	46,0	0,958	156,0		WOD	Spiral	439	E-W	Up-hole
16/05/2020	J	F370SZ048	50,2	0.783	100,0		WD	Spiral	488	N-S	Downhole
16/05/2020	I	F370SZ048	26,9	1,490	100,0		WD	Spiral	398	N-S	Downhole
16/05/2020	G	F370SZ048	86,4	1.220	100,0		WD	Spiral	482	N-S	Downhole
17/05/2020	J	F410SZ039A	20,0	0.898	98,2		WD	Parallel	614	N-S	Downhole
17/05/2020	I	F410SZ039A	31,0	2,460	98,2		WD	Parallel	415	E-W	Downhole
17/05/2020	G	F410SZ039A	32,4	1,650	98,2		WD	Parallel	456	N-S	Downhole
18/05/2020	J	F370SZ046	15,5	0.582	93,2		WD	Parallel	500	N-S	Downhole
18/05/2020	I	F370SZ046	15,5	1.050	93,2		WD	Parallel	396	N-S	Downhole
18/05/2020	G	F370SZ046	15,4	0.889	93,2		WD	Parallel	481	N-S	Downhole
19/05/2020	I	F270SZ034	21,6	2,960	151,0		WOD	Parallel	365	E-W	Up-hole
19/05/2020	J	F270SZ034	30,9	1,470	151,0		WOD	Parallel	578	N-S	Up-hole
19/05/2020	G	F270SZ034	46,1	1,280	151,0		WOD	Parallel	438	N-S	Up-hole
20/05/2020	J	F270SZ073	46,8	2,510	35,0	65	WOD	Spiral	306	E-W	Up-hole
20/05/2020	I	F270SZ073	31,0	0,730	35,0	65	WOD	Spiral	590	N-S	Up-hole
21/05/2020	J	F270SZ073	41,8	1,770	62,5		WOD	Spiral	301	E-W	Downhole
21/05/2020	I	F270SZ073	28,5	0.582	62,5		WOD	Spiral	589	N-S	Downhole
22/05/2020	J	F270SZ073	42,4	4.500	58,9		WOD	Parallel	296	E-W	Downhole
22/05/2020	G	F270SZ073	24,3	0.538	58,9		WOD	Parallel	717	N-S	Downhole
22/05/2020	I	F270SZ073	30,8	1,330	58,9		WOD	Parallel	585	N-S	Downhole
22/05/2020	J	F410SZ039A	52,5	0.648	68,6		WD	Parallel	614	N-S	Downhole
22/05/2020	G	F410SZ039A	46,3	0.933	68,6		WD	Parallel	457	N-S	Downhole
22/05/2020	I	F410SZ039A	30,8	1,470	68,6		WD	Parallel	415	E-W	Downhole
23/05/2020	J	F370SZ046	39,9	6.050	131,0		WOD	Parallel	375	E-W	Up-hole
23/05/2020	I	F310SZ071AL	20,0	1,880	131,0		WOD	Parallel	554	N-S	Up-hole
25/05/2020	J	F310SZ045	61,6	1,880	134,0		WOD	Parallel	492	N-S	Up-hole
25/05/2020	G	F310SZ045	30,6	2,480	134,0		WOD	Parallel	460	N-S	Up-hole
25/05/2020	I	F310SZ045	15,6	5,730	134,0		WOD	Parallel	372	N-S	Up-hole
26/05/2020	J	F370SZ048	44,5	0,813	80,0		WD	Parallel	486	N-S	Downhole
26/05/2020	G	F370SZ048	20,5	0.967	80,0		WD	Parallel	486	N-S	Downhole
26/05/2020	I	F370SZ048	29,0	1.880	80,0		WD	Parallel	400	N-S	Downhole
27/05/2020	J	F270SZ073	47,0	5,260	65,0	65	WOD	Parallel	295	E-W	Downhole
27/05/2020	G	F270SZ073	24,5	0.524	65,0	65	WOD	Parallel	722	N-S	Downhole
27/05/2020	I	F270SZ073	30,5	0.933	65,0	65	WOD	Parallel	588	N-S	Downhole
28/05/2020	J	F270SZ073	46,1	3,630	59,0		WOD	Parallel	295	E-W	Downhole
28/05/2020	I	F270SZ073	15,5	1,230	59,0		WOD	Parallel	596	N-S	Downhole
29/05/2020	J	F310SZ065	30,8	4,220	139,0		WOD	Parallel	412	N-S	Up-hole
29/05/2020	I	F310SZ065	15,4	3,860	139,0		WOD	Parallel	419	N-S	Up-hole
29/05/2020	G	F310SZ065	30,7	2,240	139,0		WOD	Parallel	524	N-S	Up-hole
30/05/2020	J	F370SZ048	45,1	1,080	160,2		WD	Parallel	484	N-S	Downhole
30/05/2020	I	F370SZ048	15,4	2,500	160,2		WD	Parallel	402	N-S	Downhole
30/05/2020	G	F370SZ048	18,0	1,490	160,2		WD	Parallel	490	N-S	Downhole
31/05/2020	J	F310SZ045	15,8	1,140	142,0		WOD	Parallel	486	N-S	Up-hole
31/05/2020	I	F310SZ045	15,8	4,540	142,0		WOD	Parallel	378	N-S	Up-hole
09/06/2020	G	F310SZ045	15,8	1,370	142,0		WOD	Parallel	471	N-S	Up-hole
12/06/2020	J	F310SZ071AL	45,4	9.990	137,5		WD	Spiral	339	E-W	Downhole
12/06/2020	I	F310SZ071AL	15,8	2,080	137,5		WD	Spiral	533	N-S	Downhole
12/06/2020	G	F310SZ071AL	31,4	1,160	137,5		WD	Spiral	652	N-S	Downhole
13/06/2020	J	F270SZ038L	15,4	2,400	165,0		WOD	Spiral	498	N-S	Up-hole
13/06/2020	G	F270SZ038L	30,9	5,810	165,0		WOD	Spiral	449	N-S	Up-hole
16/06/2020	J	F310SZ029	30,8	1,110	135,0		WOD	Spiral	670	N-S	Up-hole
16/06/2020	G	F310SZ029	15,4	2,480	135,0		WOD	Spiral	457	E-W	Up-hole
16/06/2020	I	F310SZ029	10,6	4.420	135,0		WOD	Spiral	416	E-W	Up-hole
17/06/2020	G	F370SZ061L	46,1	1,730	147,0		WOD	Spiral	630	N-S	Up-hole
17/06/2020	I	F370SZ061L	29,5	3,220	147,0		WOD	Spiral	525	N-S	Up-hole
17/06/2020	J	F370SZ061L	40,5	3,820	147,0		WOD	Spiral	433	N-S	Up-hole
18/06/2020	J	F270SZ038L	30,8	1,330	148,0		WOD	Parallel	504	N-S	Up-hole
18/06/2020	G	F270SZ038L	20,8	3,100	148,0		WOD	Parallel	444	N-S	Up-hole
20/06/2020	J	F310SZ071AL	47,8	11.700	114,6		WD	Parallel	340	E-W	Downhole
20/06/2020	G	F310SZ071AL	15,4	1.380	114,6		WD	Parallel	659	N-S	Downhole
21/06/2020	J	F370SZ061L	20,3	1.950	151,0		WOD	Parallel	431	N-S	Up-hole
21/06/2020	G	F370SZ061L	30,0	0.925	151,0		WOD	Parallel	634	N-S	Up-hole
23/06/2020	G	F370SZ061L	30,8	1.020	141,0		WOD	Parallel	617	N-S	Up-hole
24/06/2020	I	F270SZ038L	22,9	5.910	172,0	65	WOD	Parallel	349	E-W	Up-hole
25/06/2020	I	F310SZ045	16,1	9.040	125,0		WOD	Parallel	345	N-S	Downhole
28/06/2020	I	F310SZ029	25,3	3.980	126,4		WD	Parallel	392	E-W	Downhole
28/06/2020	H	M440SZ008	61,4	1,960	50,3	65	WOD	Spiral	550	N-S	Downhole
30/06/2020	I	F370SZ065	26,8	2,740	138,0		WOD	Spiral	462	N-S	Up-hole
02/07/2020	E	F270SZ038L	33,0	0.648	168,0	75	WOD	Parallel	965	E-W	Up-hole
02/07/2020	I	F270SZ038L	26,6	3.450	168,0	75	WOD	Parallel	354	E-W	Up-hole
03/07/2020	J	F310SZ045	40,0	1.430	78,2		WD	Parallel	460	N-S	Downhole
03/07/2020	I	F310SZ045	27,5	3.390	78,2		WD	Parallel	348	N-S	Downhole
05/07/2020	J	F310SZ071AL	46,0	6.320	66,4	75	WD	Parallel	341	E-W	Downhole
05/07/2020	I	F310SZ071AL	26,8	2,110	66,4	75	WD	Parallel	547	N-S	Downhole
10/07/2020	F	F410SZ039	66,6	0.813	144,0		WOD	Spiral	832	E-W	Up-hole
10/07/2020	I	F410SZ039	26,8	2.980	144,0		WOD	Spiral	454	E-W	Up-hole
10/07/2020	E	F410SZ039	53,3	1.060	144,0		WOD	Spiral	1098	E-W	Up-hole
11/07/2020	I	F370SZ065	25,5	2.500	125,0	75	WD	Spiral	1009	E-W	Downhole
11/07/2020	H	M440SZ008	40,0	1.180	55,7	75	WOD	Parallel	554	N-S	Downhole
12/07/2020	E	M440SZ008	53,3	0.660	55,7	75	WOD	Parallel	1477	N-S	Downhole
13/07/2020	I	F310SZ029	27,6	2.450	83,6		WD	Parallel	352	N-S	Downhole
15/07/2020	I	F310SZ029	23,1	2.620	94,1		WD	Parallel	392	E-W	Downhole
15/07/2020	E	F410SZ039	80,0	1.040	94,1		WD	Parallel	904	E-W	Downhole
16/07/2020	I	F370SZ065	19,9	3.830	87,3		WD	Parallel	438	N-S	Downhole
17/07/2020	H	M440SZ008	40,0	1.140	75,9	75	WOD	Parallel	559	N-S	Downhole
18/07/2020	I	F310SZ049	20,0	5.310	138,0		WOD	Spiral	381	N-S	Up-hole
19/07/2020	I	F310SZ045	26,6	2.290	73,6		WD	Parallel	356	N-S	Downhole
21/07/2020	I	F310SZ045	26,6	3.200	47,7		WD	Parallel	359	N-S	Downhole
22/07/2020	I	F270SZ038L	28,0	5.400	100,0		WD	Parallel	333	N-S	Downhole
23/07/2020	E	F270SZ038L	69,3	0.539	100,0		WD	Parallel	950	E-W	Downhole
23/07/2020	I	F410SZ039	13,1	2.560	151,0		WOD	Parallel	456	E-W	Up-hole
23/07/2020	E	F410SZ039	53,3	0.524	151,0		WOD	Parallel	1093	E-W	Up-hole
24/07/2020	I	F370SZ065	26,6	2.560	145,0		WD	Spiral	390	N-S	Downhole
26/07/2020	I	F310SZ065	20,3	3.300	95,9		WD	Parallel	438	N-S	Downhole
26/07/2020	I	F310SZ065	27,4	5.650	124,6		WD	Parallel	398	N-S	Downhole
28/07/2020	I	F310SZ029	25,3	2.920	61,9		WD	Parallel	394	E-W	Downhole
28/07/2020	F	F310SZ029	13,4	0.783	61,9		WD	Parallel	637	N-S	Downhole
28/07/2020	E	F310SZ029	53,4	1.090	61,9		WD	Parallel	900	E-W	Downhole
30/07/2020	F	F410SZ039	13,3	0.596	165,0		WOD	Parallel	834	E-W	Up-hole
30/07/2020	E	F410SZ039	53,5	0.524	165,0		WOD	Parallel	1086	E-W	Up-hole
31/07/2020	I	F410SZ039	26,7	3.060	165,0		WOD	Parallel	458	E-W	Up-hole
31/07/2020	F	F270SZ038L	26,8	1.160	69,1		WD	Parallel	766	N-S	Downhole
31/07/2020	E	F270SZ038L	40,0	0.783	69,1		WD	Parallel	942	E-W	Downhole
31/07/2020	I	F270SZ038L	26,6	6.500	69,1		WD	Parallel	333	E-W	Downhole
31/07/2020	I	F370SZ052	26,9	1.420	158,0		WOD	Parallel	446	N-S	Up-hole
08/08/2020	I	F310SZ049	13,3	3.140	166,0		WOD	Parallel	387	N-S	Up-hole
08/08/2020	F	F310SZ049	13,3	0.783	166,0		WOD	Parallel	917	N-S	Up-hole
10/08/2020	I	F370SZ061L	27,4	1.990	129,1		WD	Parallel	504	N-S	Downhole
12/08/2020	F	F370SZ061L	12,5	0.582	129,1		WD	Parallel	1096	N-S	Downhole
12/08/2020	J	F270SZ038L	40,0	1.350	88,2		WD	Parallel	494	N-S	Downhole
12/08/2020	I	F270SZ038L	26,6	2.800	88,2		WD	Parallel	333	E-W	Downhole
12/08/2020	I	F410SZ039	15,8	0.992	55,0	65	WD	Spiral	429	E-W	Downhole
13/08/2020	I	F410SZ039	15,8	1.400	40,0	65	WD	Spiral	425	E-W	Downhole
17/08/2020	J	F270SZ038L	26,9	2.010	100,0		WD	Parallel	503	N-S	Downhole
18/08/2020	J	F270SZ038L	40,0	2.070	94,1		WD	Parallel	503	N-S	Downhole
18/08/2020	I	F270SZ038L	21,6	4.720	94,1		WD	Parallel	333	E-W	Downhole
22/08/2020	J	F310SZ071	40,0	4.890	158,0		WOD	Parallel	367	E-W	Up-hole
22/08/2020	I	F310SZ071	27,2	2.740	158,0		WOD	Parallel	593	N-S	Up-hole
24/08/2020	I	F370SZ052	20,3	1.210	171,0		WOD	Parallel	448	N-S	Up-hole
29/08/2020	I	F370SZ061L	17,6	1.460	95,9		WD	Parallel	508	N-S	Downhole
29/08/2020	I	F310SZ067	26,6	1.820	157,0		WOD	Parallel	554	N-S	Up-hole
02/09/2020	J	F310SZ071	55,0	1.330	40,0	65	WD	Spiral	347	E-W	Downhole
02/09/2020	I	F310SZ071	26,5	0.568	40,0	65	WD	Spiral	583	N-S	Downhole
04/09/2020	J	F310SZ071	56,5	2.000	82,5	65	WD	Spiral	341	E-W	Downhole
04/09/2020	I	F310SZ071	26,0	0.813	82,5	65	WD	Spiral	580	N-S	Downhole
04/09/2020	J	F410SZ039	26,6	0.813	91,8		WD	Parallel	602	N-S	Downhole
04/09/2020	I	F410SZ039	13,3	2.710	91,8		WD	Parallel	423	E-W	Downhole
06/09/2020	J	F310SZ071	61,5	0.861	17,5		WOD	Spiral	336	E-W	Downhole
11/09/2020	J	F310SZ067	40,0	4.550	167,0	75	WOD	Parallel	357	E-W	Up-hole
11/09/2020	I	F310SZ067	26,6	1.930	167,0	75	WOD	Parallel	553	N-S	Up-hole
11/09/2020	J	F410SZ039	26,6	0.950	91,8		WD	Parallel	598	N-S	Downhole
11/09/2020	I	F410SZ039	26,6	1.990	91,8		WD	Parallel	424	E-W	Downhole
11/09/2020	J	F310SZ071	40,0	4.900	100,0		WD	Spiral	331	E-W	Downhole
12/09/2020	I	F310SZ071	26,8	2.810	100,0		WD	Spiral	573	N-S	Downhole
15/09/2020	J	F310SZ049	53,0	2.790	112,5		WD	Spiral	428	N-S	Downhole
15/09/2020	I	F310SZ049	13,0	5.300	112,5		WD	Spiral	355	N-S	Downhole
18/09/2020	J	F370SZ052	53,0	1.530	100,0		WD	Spiral	464	N-S	Downhole
18/09/2020	I	F370SZ052	28,8	2.150	100,0		WD	Spiral	416	N-S	Downhole
19/09/2020	J	F310SZ031	39,9	0.907	159,0		WOD	Parallel	642	N-S	Up-hole
19/09/2020	I	F310SZ031	13,3	3.060	159,0		WOD	Parallel	402	E-W	Up-hole
25/09/2020	J	F310SZ049	40,0	1.420	80,0		WD	Parallel	423	N-S	Downhole
25/09/2020	I	F310SZ049	17,3	3.240	80,0		WD	Parallel	361	N-S	Downhole
26/09/2020	J	F370SZ052	51,3	2.120	101,4		WD	Parallel	458	N-S	Downhole
26/09/2020	I	F370SZ052	16,6	3.380	101,4		WD	Parallel	419	N-S	Downhole
27/09/2020	J	F310SZ071	40,0	2.130	89,3		WD	Parallel	330	E-W	Downhole

Legend:

Data considered as outliers

WD Data included in models with discontinuity

WOD Data included in models without discontinuity

Date	Monitored structure	Stope	Dominant frequency (Hz)	PVS (mm·s⁻¹)	Maximum charge per delay (kg)	Delay between adjacent holes (ms)	Operational scenario	Initiation pattern geometry	Distance (m)	Orientation	Type of blast
27/09/2020	I	F310SZ071	29.5	1.760	89.3		WD	Parallel	579	N-S	Downhole
29/09/2020	J	F310SZ067	39.9	4.000	125.0		WD	Spiral	322	E-W	Downhole
29/09/2020	I	F310SZ067	26.6	2.010	125.0		WD	Spiral	529	N-S	Downhole
01/10/2020	J	F410SZ047	46.0	0.539	411		WD	Spiral	544	N-S	Downhole
01/10/2020	I	F410SZ047	30.8	1.400	411		WD	Spiral	437	N-S	Downhole
04/10/2020	I	F370SZ042A	26.7	2.450	159.0		WOD	Parallel	409	N-S	Up-hole
04/10/2020	J	F370SZ042A	66.6	0.783	159.0		WOD	Parallel	580	N-S	Up-hole
05/10/2020	I	F370SZ052	26.6	2.400	92.3		WD	Parallel	420	N-S	Downhole
05/10/2020	J	F370SZ052	53.4	1.440	92.3		WD	Parallel	456	N-S	Downhole
07/10/2020	I	F310SZ049	27.0	3.950	91.4		WD	Parallel	363	N-S	Downhole
07/10/2020	J	F310SZ049	67.1	1.630	91.4		WD	Parallel	421	N-S	Downhole
09/10/2020	J	F310SZ067	13.3	3.300	135.5		WD	Parallel	320	E-W	Downhole
09/10/2020	I	F310SZ067	26.6	1.850	135.5		WD	Parallel	537	N-S	Downhole
11/10/2020	I	F410SZ047	26.6	0.898	51.8	75	WD	Spiral	533	N-S	Downhole
11/10/2020	I	F410SZ047	26.6	1.990	51.8	75	WD	Spiral	429	N-S	Downhole
12/10/2020	I	F410SZ050AR	53.4	2.360	167.0	75	WOD	Spiral	523	N-S	Up-hole
12/10/2020	I	F410SZ050AR	26.6	4.960	167.0	75	WOD	Spiral	441	N-S	Up-hole
14/10/2020	I	F410SZ047	26.6	0.596	95.9	75	WD	Parallel	531	N-S	Downhole
14/10/2020	I	F410SZ047	19.9	1.730	95.9	75	WD	Parallel	430	N-S	Downhole
15/10/2020	J	F310SZ031	46.1	0.652	100.0		WD	Spiral	621	N-S	Downhole
15/10/2020	I	F310SZ031	27.6	3.260	100.0		WD	Spiral	375	E-W	Downhole
17/10/2020	J	F370SZ042A	46.1	0.813	152.0		WOD	Parallel	577	N-S	Up-hole
17/10/2020	I	F370SZ042A	30.8	1.400	152.0		WOD	Parallel	411	N-S	Up-hole
20/10/2020	J	F370SZ052	66.6	0.773	91.6		WD	Parallel	456	N-S	Downhole
20/10/2020	I	F370SZ052	20.1	1.310	91.6		WD	Parallel	420	N-S	Downhole
21/10/2020	J	F410SZ050AR	40.0	1.990	160.0	75	WOD	Parallel	528	N-S	Up-hole
21/10/2020	I	F410SZ050AR	20.0	2.750	160.0	75	WOD	Parallel	431	E-W	Up-hole
22/10/2020	I	F310SZ031	22.1	2.230	100.0		WD	Parallel	379	E-W	Downhole
25/10/2020	J	F410SZ050AR	40.0	1.830	156.0		WOD	Parallel	530	N-S	Up-hole
25/10/2020	I	F410SZ050AR	26.8	3.180	156.0		WOD	Parallel	429	E-W	Up-hole
26/10/2020	I	F370SZ044AL	53.4	1.700	160.0	75	WOD	Spiral	570	N-S	Up-hole
26/10/2020	J	F370SZ044AL	26.8	3.100	160.0	75	WOD	Spiral	410	N-S	Up-hole
27/10/2020	I	F410SZ047	66.8	0.554	65.5	75	WD	Parallel	530	N-S	Downhole
27/10/2020	I	F410SZ047	18.9	1.620	65.5	75	WD	Parallel	431	N-S	Downhole
28/10/2020	H	M440SZ004	26.8	0.741	110.0	75	WOD	Parallel	728	N-S	Downhole
29/10/2020	J	F310SZ031	19.8	0.976	101.4		WD	Parallel	622	N-S	Downhole
29/10/2020	I	F310SZ031	20.5	2.430	101.4		WD	Parallel	381	E-W	Downhole
30/10/2020	J	F270SZ038L	40.0	1.330	180.0	75	WOD	Parallel	520	N-S	Up-hole
30/10/2020	I	F270SZ038L	20.0	4.210	180.0	75	WOD	Parallel	354	E-W	Up-hole
31/10/2020	I	F370SZ042A	40.0	0.813	133.0		WOD	Parallel	577	N-S	Up-hole
31/10/2020	I	F370SZ042A	13.3	1.800	133.0		WOD	Parallel	418	N-S	Up-hole
04/11/2020	I	F410SZ047	26.6	0.582	54.1	75	WD	Parallel	528	N-S	Downhole
04/11/2020	I	F410SZ047	26.6	1.360	54.1	75	WD	Parallel	432	N-S	Downhole
05/11/2020	I	F550SZ033AL	3.0	0.596	95.0	75	WOD	Spiral	811	N-S	Downhole
05/11/2020	I	F550SZ033AL	26.8	1.180	95.0	75	WOD	Spiral	570	N-S	Downhole
06/11/2020	I	F310SZ031	40.0	1.030	92.7		WD	Parallel	621	N-S	Downhole
06/11/2020	I	F310SZ031	21.4	3.010	92.7		WD	Parallel	384	E-W	Downhole
08/11/2020	J	F310SZ069	26.6	3.800	159.0		WOD	Parallel	362	E-W	Up-hole
08/11/2020	I	F310SZ069	26.6	5.020	159.0		WOD	Parallel	576	N-S	Up-hole
09/11/2020	I	F550SZ033AL	26.6	2.500	50.5	75	WOD	Parallel	567	N-S	Downhole
20/11/2020	I	F210SZ074	26.5	1.000	64.3	75	WD	Spiral	583	N-S	Downhole
20/11/2020	I	F370SZ044AL	15.6	1.840	65.0	65	WD	Spiral	386	N-S	Downhole
21/11/2020	I	F310SZ069	13.4	1.360	165.0	75	WOD	Parallel	575	N-S	Up-hole
22/11/2020	I	F230SZ072	26.6	1.230	159.0		WOD	Parallel	580	N-S	Up-hole
26/11/2020	I	F310SZ031	20.6	2.560	104.1		WD	Parallel	386	E-W	Downhole
27/11/2020	I	F370SZ042A	20.0	2.520	100.9	75	WD	Parallel	377	N-S	Downhole
28/11/2020	I	F270SZ065	13.3	2.480	171.0		WOD	Parallel	519	N-S	Up-hole
28/11/2020	A	F270SZ065	13.5	0.524	171.0		WOD	Parallel	1670	E-W	Up-hole
29/11/2020	I	F230SZ072	26.6	0.933	148.0	75	WOD	Parallel	583	N-S	Up-hole
02/12/2020	I	F550SZ033AL	26.7	2.080	54.5		WOD	Parallel	565	N-S	Downhole
02/12/2020	I	F210SZ074	26.6	1.080	75.9		WOD	Parallel	593	N-S	Downhole
04/12/2020	J	F550SZ024L	70.8	1.380	30.0		WD	Spiral	879	N-S	Downhole
06/12/2020	J	F310SZ069	40.1	3.190	100.0	75	WD	Spiral	326	E-W	Downhole
06/12/2020	I	F310SZ069	26.8	2.010	100.0	75	WD	Spiral	553	N-S	Downhole
07/12/2020	J	F370SZ042A	66.6	0.933	100.9		WD	Parallel	551	N-S	Downhole
07/12/2020	I	F370SZ042A	13.3	2.230	100.9		WD	Parallel	377	N-S	Downhole
09/12/2020	J	F230SZ072	46.0	1.560	27.5	65	WD	Spiral	260	E-W	Downhole
09/12/2020	I	F550SZ024L	79.9	0.852	60.7	75	WD	Spiral	608	E-W	Downhole
11/12/2020	J	F230SZ072	40.3	6.170	50.0	75	WD	Spiral	255	N-S	Downhole
11/12/2020	I	F230SZ072	26.8	0.533	50.0	75	WD	Spiral	576	N-S	Downhole
11/12/2020	J	F310SZ069	40.0	2.740	160.0		WOD	Parallel	358	E-W	Up-hole
11/12/2020	I	F310SZ069	13.4	1.157	160.0		WOD	Parallel	577	N-S	Up-hole
15/12/2020	I	F550SZ024L	21.5	1.710	62.5	75	WD	Parallel	599	E-W	Downhole
17/12/2020	J	F370SZ040A	18.9	0.741	148.0		WOD	Parallel	608	N-S	Up-hole
17/12/2020	I	F370SZ040A	17.8	3.270	148.0		WOD	Parallel	408	E-W	Up-hole
18/12/2020	J	F310SZ069	19.5	2.130	100.0		WD	Parallel	324	E-W	Downhole
18/12/2020	I	F310SZ069	26.6	1.280	100.0		WD	Parallel	556	N-S	Downhole
20/12/2020	J	F270SZ065	53.3	4.570	104.6		WD	Spiral	279	N-S	Downhole
20/12/2020	I	F270SZ065	26.6	2.360	104.6		WD	Spiral	322	N-S	Downhole
22/12/2020	J	F310SZ061	40.0	2.500	142.0		WOD	Parallel	440	N-S	Up-hole
23/12/2020	I	F310SZ061	26.6	3.990	142.0		WOD	Parallel	393	N-S	Up-hole
27/12/2020	I	F550SZ024L	26.6	1.280	55.7	75	WD	Parallel	597	E-W	Downhole
27/12/2020	J	F270SZ065	40.0	4.730	100.9		WD	Parallel	278	N-S	Downhole
27/12/2020	I	F270SZ065	11.3	1.250	100.9		WD	Parallel	502	N-S	Downhole
28/12/2020	J	F210SZ078L	108.0	1.050	25.0	65	WOD	Spiral	288	E-W	Downhole
28/12/2020	J	F310SZ069	13.3	1.780	100.9		WD	Parallel	323	E-W	Downhole
28/12/2020	I	F310SZ069	26.8	0.933	100.9		WD	Parallel	559	N-S	Downhole
28/12/2020	J	F270SZ065	40.3	4.490	10.7	65	WOD	Spiral	285	E-W	Downhole
28/12/2020	I	F210SZ078L	27.5	0.933	10.7	65	WOD	Spiral	648	N-S	Downhole
28/12/2020	J	F230SZ072	40.0	8.690	125.0		WD	Parallel	253	N-S	Downhole
29/12/2020	I	F230SZ072	25.9	1.360	125.0		WD	Parallel	582	N-S	Downhole
30/12/2020	H	M440SZ007	39.9	0.773	69.6		WOD	Spiral	575	N-S	Downhole
30/12/2020	I	F370SZ040A	20.4	1.730	132.0		WOD	Parallel	409	E-W	Up-hole
30/12/2020	I	F270SZ065	26.8	1.450	80.5		WD	Parallel	503	N-S	Downhole
06/01/2021	J	F270SZ065	40.0	5.240	80.5		WD	Parallel	278	N-S	Downhole
07/01/2021	I	F560SZ037AL	51.0	0.582	47.5		WD	Spiral	564	N-S	Downhole
09/01/2021	I	F370SZ040A	20.6	2.070	141.0		WOD	Parallel	410	E-W	Up-hole
09/01/2021	J	F210SZ078L	53.4	2.120	40.0		WOD	Parallel	269	E-W	Downhole
10/01/2021	J	F230SZ072	40.1	6.490	92.3		WD	Parallel	252	E-W	Downhole
10/01/2021	I	F230SZ072	12.8	1.510	92.3		WD	Parallel	575	N-S	Downhole
12/01/2021	I	F560SZ037AL	26.6	1.440	97.5		WD	Spiral	558	N-S	Downhole
13/01/2021	J	F310SZ061	19.6	1.530	126.0		WOD	Parallel	394	N-S	Up-hole
13/01/2021	J	F310SZ061	53.4	1.470	126.0		WOD	Parallel	439	N-S	Up-hole
14/01/2021	I	F370SZ040A	17.9	1.660	131.0		WOD	Parallel	411	E-W	Up-hole
15/01/2021	H	M440SZ007	40.0	0.684	92.7		WOD	Parallel	580	N-S	Downhole
16/01/2021	I	F370SZ040A	13.4	1.670	131.0	75	WOD	Parallel	412	E-W	Up-hole
17/01/2021	J	F310SZ061	13.4	1.730	129.0	75	WOD	Parallel	437	N-S	Up-hole
17/01/2021	I	F310SZ061	18.4	3.000	129.0	75	WOD	Parallel	395	N-S	Up-hole
18/01/2021	I	F230SZ072	40.0	4.770	92.7		WD	Parallel	251	E-W	Downhole
18/01/2021	I	F230SZ072	27.5	1.590	92.7		WD	Parallel	569	N-S	Downhole
20/01/2021	J	F370SZ060	53.4	1.020	190.0		WOD	Parallel	508	N-S	Up-hole
20/01/2021	I	F370SZ060	13.4	1.540	190.0		WOD	Parallel	433	N-S	Up-hole
21/01/2021	J	F310SZ061	13.3	1.530	162.0		WOD	Parallel	434	N-S	Up-hole
21/01/2021	I	F310SZ061	26.6	1.910	162.0		WOD	Parallel	398	N-S	Up-hole
23/01/2021	J	F370SZ060	66.6	0.622	163.0	75	WOD	Parallel	503	N-S	Up-hole
23/01/2021	I	F370SZ060	20.5	1.210	163.0	75	WOD	Parallel	436	N-S	Up-hole
24/01/2021	J	F230SZ072	53.4	5.040	87.7		WD	Parallel	252	E-W	Downhole
24/01/2021	I	F230SZ072	26.6	1.370	87.7		WD	Parallel	565	N-S	Downhole
25/01/2021	J	F370SZ040A	31.0	0.751	100.0	65	WD	Spiral	570	N-S	Downhole
25/01/2021	I	F370SZ040A	15.6	3.080	100.0	65	WD	Spiral	375	N-S	Downhole
26/01/2021	J	F210SZ078L	33.4	2.520	36.9	75	WOD	Parallel	266	E-W	Downhole
26/01/2021	I	F210SZ078L	21.5	1.730	36.9	75	WOD	Parallel	625	N-S	Downhole
28/01/2021	J	F310SZ061	13.1	1.320	151.0		WOD	Parallel	403	N-S	Up-hole
28/01/2021	I	F310SZ061	20.5	1.940	151.0		WOD	Parallel	433	N-S	Up-hole
29/01/2021	J	F370SZ044AL	50.0	0.598	50.0		WD	Spiral	545	N-S	Downhole
29/01/2021	I	F370SZ044AL	30.8	1.110	50.0		WD	Spiral	389	N-S	Downhole
29/01/2021	J	F370SZ061L	40.0	1.800	114.6		WD	Parallel	383	N-S	Downhole
29/01/2021	I	F370SZ061L	20.4	1.770	114.6		WD	Parallel	513	N-S	Downhole
31/01/2021	I	F550SZ027L	26.6	1.390	86.4		WD	Parallel	590	E-W	Downhole
02/02/2021	J	F230SZ066	46.1	5.290	161.0	75	WOD	Parallel	330	N-S	Up-hole
02/02/2021	I	F230SZ066	30.8	3.850	161.0	75	WOD	Parallel	376	N-S	Up-hole
04/02/2021	J	F370SZ040A	53.3	0.684	71.7		WD	Parallel	576	N-S	Downhole
04/02/2021	I	F370SZ040A	13.4	2.580	71.7		WD	Parallel	377	E-W	Downhole
05/02/2021	J	F230SZ056	53.4	3.280	153.0		WOD	Parallel	323	N-S	Up-hole
05/02/2021	I	F230SZ056	26.6	2.080	153.0		WOD	Parallel	383	N-S	Up-hole
07/02/2021	J	F550SZ027L	26.6	1.630	70.5		WD	Parallel	588	E-W	Downhole
07/02/2021	I	F210SZ078L	53.4	3.540	42.8		WOD	Parallel	259	E-W	Downhole
07/02/2021	I	F210SZ078L	26.6	0.813	42.8		WOD	Parallel	613	N-S	Downhole
09/02/2021	J	F370SZ060	61.6	0.950	112.5		WD	Spiral	474	N-S	Downhole
09/02/2021	I	F370SZ060	15.1	1.580	112.5		WD	Spiral	406	N-S	Downhole
10/02/2021	J	F230SZ066	53.4	2.650	139.0	75	WOD	Parallel	323	N-S	Up-hole
10/02/2021	I	F230SZ066	26.6	1.420	139.0	75	WOD	Parallel	383	N-S	Up-hole
11/02/2021	J	F560SZ037AL	53.3	0.803	78.2		WD	Parallel	774	N-S	Downhole
11/02/2021	I	F560SZ037AL	26.6	1.970	78.2		WD	Parallel	559	N-S	Downhole
12/02/2021	J	F210SZ078L	40.1	3.790	118.0		WOD	Parallel	292	E-W	Up-hole
12/02/2021	I	F210SZ078L	26.5	1.080	118.0		WOD	Parallel	653	N-S	Up-hole
13/02/2021	I	F310SZ061	30.8	0.524	32.5		WD	Spiral	381	N-S	Downhole
14/02/2021	I	F550SZ027L	26.6	1.360	92.1		WD	Parallel	582	E-W	Downhole
14/02/2021	H	M440SZ007	40.8	0.813	93.6		WOD	Parallel	590	N-S	Downhole
14/02/2021	H	M440SZ007	40.8	0.751	93.6		WOD	Parallel	590	N-S	Downhole
15/02/2021	I	F310SZ061	15.5	0.698	25.0		WD	Spiral	376	N-S	Downhole
17/02/2021	I	F210SZ075	13.3	1.350	132.0		WOD	Parallel	609	N-S	Up-hole
17/02/2021	J	F210SZ075	40.0	5.820	132.0		WOD	Parallel	263	E-W	Up-hole
17/02/2021	I	F370SZ060	19.3	1.820	113.2		WD	Parallel	408	N-S	Downhole
17/02/2021	J	F370SZ060	13.4	0.684	113.2		WD	Parallel	471	N-S	Downhole

Legend:

Data considered as outliers

WD Data included in models with discontinuity

WOD Data included in models without discontinuity

Date	Monitored structure	Stope	Dominant frequency (Hz)	PVS (mm·s⁻¹)	Maximum charge per delay (kg)	Delay between adjacent holes (ms)	Operational scenario	Initiation pattern geometry	Distance (m)	Orientation	Type of blast	Date	Monitored structure	Stope	Dominant frequency (Hz)	PVS (mm·s⁻¹)	Maximum charge per delay (kg)	Delay between adjacent holes (ms)	Operational scenario	Initiation pattern geometry	Distance (m)	Orientation	Type of blast
18/02/2021	J	F310S2051	20,4	0,833	20,0	65	WD	Spiral	404	N-S	Downhole	12/05/2021	J	F270S2045L	31,0	0,582	30,0	65	WD	Spiral	427	N-S	Downhole
18/02/2021	I	F370S2044AL	15,5	2,110	75,0	65	WD	Spiral	379	N-S	Downhole	12/05/2021	I	F270S2045L	15,8	1,000	30,0	65	WD	Spiral	346	N-S	Downhole
19/02/2021	I	F550S2037AL	26,6	2,700	94,1		WD	Parallel	561	N-S	Downhole	13/05/2021	J	F230S2070	53,3	6,180	93,2		WD	Parallel	243	E-W	Downhole
19/02/2021	J	F550S2037AL	53,3	1,030	94,1		WD	Parallel	782	N-S	Downhole	13/05/2021	I	F230S2070	26,6	1,210	93,2		WD	Parallel	542	N-S	Downhole
20/02/2021	I	F550S2027L	26,6	1,910	86,8		WD	Parallel	582	E-W	Downhole	14/05/2021	J	F270S2034	67,0	0,783	141,5	75	WOD	Parallel	582	N-S	Up-hole
22/02/2021	I	F310S2051	27,4	5,400	110,0		WD	Spiral	372	N-S	Downhole	14/05/2021	I	F270S2034	26,5	1,450	141,5	75	WOD	Parallel	372	E-W	Up-hole
22/02/2021	J	F310S2051	13,5	2,080	110,0		WD	Spiral	404	N-S	Downhole	14/05/2021	I	F370S2040	13,4	2,080	104,1	75	WD	Parallel	391	E-W	Downhole
23/02/2021	I	F550S2037AL	26,6	1,890	102,7		WD	Parallel	562	N-S	Downhole	15/05/2021	J	F270S2045L	61,3	0,696	62,5	65	WD	Spiral	421	N-S	Downhole
23/02/2021	J	F550S2037AL	53,3	0,783	102,7		WD	Parallel	787	N-S	Downhole	15/05/2021	I	F270S2045L	31,3	1,530	62,5	65	WD	Spiral	342	N-S	Downhole
25/02/2021	I	F550S2027L	26,5	1,700	82,3	75	WD	Parallel	578	E-W	Downhole	16/05/2021	J	F230S2066L	30,8	8,460	110,0		WD	Parallel	237	N-S	Downhole
26/02/2021	I	F230S2054	26,7	3,120	162,0		WOD	Parallel	357	N-S	Up-hole	16/05/2021	I	F230S2066L	30,8	1,400	110,0		WD	Parallel	498	N-S	Downhole
26/02/2021	J	F230S2054	26,7	4,420	162,0		WOD	Parallel	345	N-S	Up-hole	18/05/2021	I	F230S2070	26,6	1,150	70,5	75	WD	Parallel	539	N-S	Downhole
27/02/2021	I	F370S2050	19,6	1,200	85,9	75	WD	Parallel	409	N-S	Downhole	19/05/2021	J	F270S2045L	53,3	2,390	125,0		WD	Spiral	414	N-S	Downhole
27/02/2021	J	F370S2050	13,3	0,539	85,9	75	WD	Parallel	470	N-S	Downhole	19/05/2021	I	F270S2045L	20,8	3,010	125,0		WD	Spiral	336	N-S	Downhole
01/03/2021	I	F230S2054	26,6	2,300	136,0		WOD	Parallel	363	N-S	Up-hole	20/05/2021	J	F370S2040	53,8	0,539	114,6	75	WD	Parallel	556	N-S	Downhole
01/03/2021	J	F230S2054	53,4	3,690	136,0		WOD	Parallel	340	N-S	Up-hole	20/05/2021	I	F370S2040	27,8	2,360	114,6	75	WD	Parallel	393	E-W	Downhole
02/03/2021	I	F550S2037AL	26,6	2,620	98,6		WD	Parallel	565	N-S	Downhole	22/05/2021	J	F230S2066L	40,0	10,900	91,8		WD	Parallel	237	N-S	Downhole
03/03/2021	I	F230S2056	26,7	3,130	100,0		WD	Parallel	360	N-S	Downhole	22/05/2021	I	F230S2038L	26,6	2,160	91,8		WD	Spiral	499	N-S	Downhole
03/03/2021	J	F230S2056	53,3	4,190	100,0		WD	Parallel	295	N-S	Downhole	23/05/2021	J	F230S2038L	46,1	1,530	82,5		WD	Spiral	489	N-S	Downhole
04/03/2021	I	F370S2044AL	31,1	2,520	167,5		WD	Parallel	379	N-S	Downhole	23/05/2021	I	F230S2038L	30,8	2,950	82,5		WD	Spiral	326	E-W	Downhole
04/03/2021	J	F370S2044AL	66,8	1,110	167,5		WD	Parallel	536	N-S	Downhole	23/05/2021	A	F230S2038L	2,5	0,539	82,5		WD	Spiral	1251	E-W	Downhole
05/03/2021	I	F310S2051	13,0	3,470	86,8		WD	Parallel	370	N-S	Downhole	25/05/2021	J	F310S2026R	40,0	0,992	166,0	75	WOD	Parallel	676	N-S	Up-hole
05/03/2021	J	F310S2051	12,5	1,200	86,8		WD	Parallel	407	N-S	Downhole	25/05/2021	A	F310S2026R	28,6	3,500	166,0	75	WOD	Parallel	405	E-W	Up-hole
10/03/2021	I	F230S2056	26,6	1,770	98,2		WD	Parallel	366	N-S	Downhole	25/05/2021	A	F310S2026R	13,5	0,582	166,0	75	WOD	Parallel	1123	E-W	Up-hole
10/03/2021	J	F230S2056	53,4	3,790	98,2		WD	Parallel	291	N-S	Downhole	26/05/2021	J	F270S2045L	53,3	2,200	78,5	75	WD	Parallel	420	N-S	Downhole
11/03/2021	I	F370S2044AL	18,6	3,360	105,0		WD	Parallel	381	N-S	Downhole	26/05/2021	I	F270S2045L	19,6	3,390	78,5	75	WD	Parallel	337	N-S	Downhole
11/03/2021	J	F370S2044AL	51,0	1,300	105,0		WD	Parallel	529	N-S	Downhole	27/05/2021	I	F370S2040	19,9	1,820	77,1	75	WD	Parallel	395	E-W	Downhole
12/03/2021	I	F310S2046R	30,8	2,410	84,0	65	WOD	Parallel	343	N-S	Up-hole	29/05/2021	D	F230S2038L	31,3	0,648	120,0		WD	Parallel	850	E-W	Downhole
12/03/2021	J	F310S2046R	61,5	1,980	84,0	65	WOD	Parallel	450	N-S	Up-hole	29/05/2021	J	F230S2038L	40,0	1,530	120,0		WD	Parallel	484	N-S	Downhole
15/03/2021	I	F310S2051	13,3	3,450	84,6	75	WD	Parallel	365	N-S	Downhole	29/05/2021	I	F230S2038L	52,0	2,400	120,0		WD	Parallel	324	E-W	Downhole
15/03/2021	J	F310S2051	13,1	1,050	84,6	75	WD	Parallel	411	N-S	Downhole	31/05/2021	J	F370S2042	48,8	0,741	154,0	65	WOD	Parallel	568	N-S	Up-hole
16/03/2021	J	F230S2054	53,8	6,620	71,4		WD	Spiral	312	N-S	Downhole	31/05/2021	I	F370S2042	30,8	1,840	154,0	65	WOD	Parallel	418	N-S	Up-hole
16/03/2021	I	F230S2054	19,5	5,320	71,4		WD	Spiral	340	N-S	Downhole	01/06/2021	I	F270S2045L	46,1	1,840	90,7		WD	Parallel	428	N-S	Downhole
17/03/2021	J	F230S2066	53,4	3,280	105,0		WD	Parallel	291	N-S	Downhole	01/06/2021	I	F270S2045L	15,4	3,790	90,7		WD	Parallel	336	N-S	Downhole
17/03/2021	I	F230S2066	26,8	1,200	105,0		WD	Parallel	367	N-S	Downhole	02/06/2021	J	F230S2066L	40,1	11,500	96,6		WD	Parallel	237	N-S	Downhole
19/03/2021	J	F230S2054	54,0	2,450	66,0		WD	Parallel	308	N-S	Downhole	02/06/2021	I	F230S2066L	26,6	3,560	96,6		WD	Parallel	492	N-S	Downhole
19/03/2021	I	F230S2054	20,6	1,310	66,0		WD	Parallel	345	N-S	Downhole	02/06/2021	I	F550S2030L	22,8	1,210	30,0	65	WOD	Spiral	587	E-W	Downhole
19/03/2021	J	F230S2070	53,4	5,280	164,0		WOD	Parallel	278	E-W	Up-hole	04/06/2021	H	M440S2007	67,1	1,661	86,8		WOD	Parallel	609	N-S	Up-hole
19/03/2021	I	F230S2070	26,7	1,310	164,0		WOD	Parallel	553	N-S	Up-hole	05/06/2021	D	F310S2026R	53,4	0,813	149,8	75	WOD	Parallel	751	E-W	Up-hole
20/03/2021	J	F370S2061L	18,6	3,780	100,9		WD	Parallel	392	N-S	Downhole	05/06/2021	J	F310S2026R	40,0	0,833	149,8	75	WOD	Parallel	670	N-S	Up-hole
20/03/2021	I	F370S2061L	24,9	2,980	100,9		WD	Parallel	519	N-S	Downhole	05/06/2021	I	F310S2026R	66,6	3,340	149,8	75	WOD	Parallel	405	E-W	Up-hole
21/03/2021	J	F230S2056	120,0	2,180	42,3	75	WD	Parallel	290	N-S	Downhole	05/06/2021	A	F310S2026R	26,5	0,539	149,8	75	WOD	Parallel	1127	E-W	Up-hole
21/03/2021	I	F230S2056	26,8	0,730	42,3	75	WD	Parallel	369	N-S	Downhole	06/06/2021	I	F370S2042	26,6	2,380	135,8		WOD	Parallel	421	N-S	Up-hole
23/03/2021	J	F370S2044AL	20,0	1,280	128,7		WD	Parallel	524	N-S	Downhole	08/06/2021	D	F230S2038L	22,9	0,730	106,8		WD	Parallel	863	E-W	Downhole
23/03/2021	I	F370S2044AL	29,8	4,450	128,7		WD	Parallel	382	N-S	Downhole	08/06/2021	D	F230S2038L	30,5	0,730	106,8		WD	Parallel	863	E-W	Downhole
25/03/2021	J	F230S2070	40,0	2,920	159,0		WOD	Parallel	277	E-W	Up-hole	08/06/2021	I	F230S2038L	24,4	4,940	106,8		WD	Parallel	324	E-W	Downhole
25/03/2021	I	F230S2070	26,6	0,822	159,0		WOD	Parallel	554	N-S	Up-hole	09/06/2021	J	F230S2038L	40,0	2,820	106,8		WD	Parallel	471	N-S	Downhole
19/04/2021	J	F230S2038L	40,0	1,400	196,0		WOD	Parallel	500	N-S	Up-hole	09/06/2021	A	F230S2038L	20,0	0,648	106,8		WD	Parallel	1271	E-W	Downhole
20/04/2021	J	F270S2045L	66,6	2,720	139,8		WOD	Parallel	444	N-S	Up-hole	09/06/2021	I	F550S2030L	30,9	1,510	66,0	65	WOD	Parallel	578	E-W	Downhole
21/04/2021	J	F230S2066L	26,6	7,480	154,6		WOD	Parallel	272	N-S	Up-hole	10/06/2021	I	F370S2040	27,6	2,760	98,4		WD	Parallel	386	E-W	Downhole
21/04/2021	I	F230S2066L	26,6	1,710	154,6		WOD	Parallel	518	N-S	Up-hole	11/06/2021	I	F230S2066L	27,3	3,010	98,9		WD	Parallel	488	N-S	Downhole
22/04/2021	J	F230S2070	46,3	1,710	30,0	65	WD	Spiral	257	N-S	Downhole	11/06/2021	J	F230S2066L	50,6	11,700	98,9		WD	Parallel	237	N-S	Downhole
23/04/2021	J	F230S2070	46,0	2,480	55,0	65	WD	Spiral	249	E-W	Downhole	11/06/2021	A	F230S2066L	3,0	0,524	98,9		WD	Parallel	1647	E-W	Downhole
23/04/2021	I	F230S2070	30,5	0,648	55,0	65	WD	Spiral	553	N-S	Downhole	12/06/2021	I	F310S2026R	26,6	4,220	148,4	75	WOD	Parallel	416	E-W	Up-hole
24/04/2021	J	F370S2053	48,4	1,400	110,9		WD	Parallel	453	N-S	Downhole	12/06/2021	J	F310S2026R	26,6	0,648	148,4	75	WOD	Parallel	683	N-S	Up-hole
24/04/2021	I	F370S2053	26,6	1,470	110,9		WD	Parallel	424	N-S	Downhole	12/06/2021	A	F310S2026R	3,0	0,539	148,4	75	WOD	Parallel	1111	E-W	Up-hole
29/04/2021	J	F310S2026R	46,1	1,100	158,0	75	WOD	Parallel	683	N-S	Up-hole	14/06/2021	I	F370S2042	26,6	1,920	140,3	75	WOD	Parallel	423	N-S	Up-hole
29/04/2021	I	F310S2026R	15,4	3,480	158,0	75	WOD	Parallel	408	E-W	Up-hole	17/06/2021	J	F370S2040	18,1	0,730	92,7		WD	Parallel	555	N-S	Downhole
29/04/2021	A	F310S2026R	15,5	0,696	158,0	75	WOD	Parallel	1116	E-W	Up-hole	17/06/2021	I	F370S2040	29,1	2,118	92,7		WD	Parallel	399	E-W	Downhole
30/04/2021	J	F230S2070	46,2	7,750	95,0		WD	Spiral	242	N-S	Downhole	18/06/2021	J	F410S2049	15,3	0,783	67,8	65	WOD	Parallel	523	N-S	Downhole
30/04/2021	I	F230S2070	31,2	2,670	95,0		WD	Spiral	548	N-S	Downhole	18/06/2021	I	F410S2049	21,9	1,727	67,8	65	WOD	Parallel	434	N-S	Downhole
02/05/2021	J	F230S2038L	40,0	1,980	175,0	75	WOD	Parallel	499	N-S	Up-hole	21/06/2021	A	F230S2038L	3,0	0,539	109,1		WD	Parallel	1275	E-W	Downhole
02/05/2021	I	F230S2038L	26,6	3,310	175,0	75	WOD	Parallel	328	E-W	Up-hole	21/06/2021	J	F230S2038L	41,0	2,691	109,1		WD	Parallel	467	N-S	Downhole
04/05/2021	J	F230S2066L	45,1	0,976	30,0	65	WD	Spiral	246	N-S	Downhole	21/06/2021	I	F230S2038L	27,0	5,305	109,1		WD	Parallel	323	E-W	Downhole
04/05/2021	I	F230S2066L	31,0	0,648	30,0	65	WD	Spiral	504	N-S	Downhole	21/06/2021	I	F550S2030L	28,6	2,178	177,2	75	WOD	Parallel	590	E-W	Up-hole
04/05/2021	J	F370S2040	61,8	2,350	117,5		WD	Spiral	561	N-S	Downhole	23/06/2021	H	M440S2007	39,9	1,024	105,0	75	WOD	Parallel	613	N-S	Downhole
04/05/2021	I	F370S2040	53,4	2,280	117,5		WD	Spiral	388	E-W	Downhole	23/06/2021	J	F410S2049	40,1	0,568	53,6	75	WOD	Parallel	519	N-S	Downhole
05/05/2021	J	F310S2026R	53,4	1,630	152,6	75	WOD	Parallel	684	N-S	Up-hole	23/06/2021	I	F410S2049	26,6	1,055	53,6	75	WOD	Parallel	436	N-S	Downhole
05/05/2021	I	F310S2026R	26,6	2,890	152,6	75	WOD	Parallel	413	E-W	Up-hole	26/06/2021	J	F370S2039	19,8	0,741	171,0		WOD	Parallel	576	N-S	Up-hole
08/05/2021	A	F230S2070	3,0	0,539	97,7	75	WD	Parallel	1718	E-W	Downhole	26/06/2021	I	F370S2039	19,8	2,879	171,0		WOD	Parallel	404	E-W	Up-hole
08/05/2021	J	F230S2070	53,3	4,930	97,7	75	WD	Parallel	242	E-W	Downhole	28/06/2021	I	F410S2049	19,4	1,276	53,0	75	WOD	Parallel	437	N-S	Downhole
08/05/2021	I	F230S2070	26,6	1,370	97,7	75	WD	Parallel	547	N-S	Downhole	29/06/2021	I	F550S2030L	26,6	1,535	110,9	75	WOD	Parallel	588	E-W	Up-hole
09/05/2021	A	M440S2007	13,3	0,524	105,0	75	WOD	Parallel	973	E-W	Downhole	01/07/2021	H	M440S2007	73,5	0,916	66,0	75	WOD	Parallel	614	N-S	Downhole
10/05/2021	J	F370S2040	20,0	3,650	87,5		WD	Parallel	389	E-W	Downhole	02/07/2021	J	F370S2042	27,0	2,479	107,5		WD	Parallel	385	N-S	Downhole
11/05/2021	J	F230S2066L	54,5	3,440	36,4	65	WD	Spiral	237	N-S	Downhole	02/07/2021	I	F370S2042	40,0	0,524	107,5		WD	Parallel	541	N-S	Downhole
11/05/2021	I	F230S2066L	25,8	1,120	36,4	65	WD	Spiral	499	N-S	Up-hole	05/07/2021	I	F310S2026R	16,2	6,702	157,0	75	WOD	Parallel	395	E-W	Up-hole
12/05/2021	J	F270S2034	66,8	0,813	153,0		WOD	Parallel	581	N-S	Up-hole	05/07/2021	A	F310S2026R	12,0	1,143	157,0	75	WOD	Parallel	1138	E-W	Up-hole
12/05/2021	I	F270S2034	26,5	2,130	153,0		WOD	Parallel	369	E-W	Up-hole	05/07/2021	J	F310S2026R	26,6	0,992	157,0	75	WOD	Parallel	662	N-S	Up-hole

Legend:

Data considered as outliers

WD Data included in models with discontinuity

WOD Data included in models without discontinuity

Date	Monitored structure	Stope	Dominant frequency (Hz)	PVS (mm·s⁻¹)	Maximum charge per delay (kg)	Delay between adjacent holes (ms)	Operational scenario	Initiation pattern geometry	Distance (m)	Orientation	Type of blast	Date	Monitored structure	Stope	Dominant frequency (Hz)	PVS (mm·s⁻¹)	Maximum charge per delay (kg)	Delay between adjacent holes (ms)	Operational scenario	Initiation pattern geometry	Distance (m)	Orientation	Type of blast
06/07/2021	H	M420SZ008	61.5	1,092	21,4	65	WOD	Spiral	525	N-S	Downhole	15/09/2021	I	F410SZ039AR	26,6	2,805	100,0	75	WOD	Parallel	409	E-W	Up-hole
06/07/2021	J	F370SZ039	26,8	0,660	160,8	75	WOD	Parallel	578	N-S	Up-hole	16/09/2021	I	F550SZ032L	26,6	1,178	119,1	75	WOD	Parallel	580	E-W	Up-hole
06/07/2021	I	F370SZ039	26,6	3,013	160,8	75	WOD	Parallel	404	E-W	Up-hole	18/09/2021	I	F370SZ044	16,9	1,465	137,0	75	WOD	Spiral	419	N-S	Up-hole
07/07/2021	H	M420SZ008	61,8	0,959	30,3	65	WOD	Spiral	521	N-S	Downhole	22/09/2021	J	F230SZ068	50,0	0,811	25,0	75	WD	Spiral	242	N-S	Downhole
10/07/2021	A	F230SZ073	13,0	0,539	125,0	WOD	Parallel	1764	E-W	Downhole	22/09/2021	I	F230SZ068	26,6	1,403	25,0	75	WD	Spiral	531	N-S	Downhole
11/07/2021	I	F370SZ042	20,0	1,805	96,6	WD	Parallel	387	N-S	Downhole	24/09/2021	H	M420SZ008	40,0	1,875	103,2	75	WOD	Parallel	538	N-S	Downhole
12/07/2021	I	F410SZ049	26,8	1,403	125,0	75	WOD	Parallel	440	N-S	Downhole	25/09/2021	I	F410SZ039AR	33,1	2,286	102,7	75	WOD	Parallel	410	E-W	Up-hole
13/07/2021	H	M420SZ008	66,6	2,071	53,6	WOD	Spiral	515	N-S	Downhole	26/09/2021	J	F230SZ068	40,0	11,860	200,0		WD	Spiral	238	N-S	Downhole
14/07/2021	I	F370SZ042	13,4	1,581	90,5	WD	Parallel	394	N-S	Downhole	26/09/2021	I	F230SZ068	24,9	2,155	200,0		WD	Spiral	533	N-S	Downhole
16/07/2021	J	F230SZ066L	53,3	6,507	134,6	WOD	Parallel	274	N-S	Up-hole	30/09/2021	I	F370SZ044	26,8	1,426	129,0	75	WOD	Parallel	420	N-S	Up-hole
16/07/2021	I	F230SZ066L	26,6	2,189	134,6	WOD	Parallel	479	N-S	Up-hole	01/10/2021	J	F370SZ058AL	44,5	7,127	127,5		WD	Spiral	427	N-S	Downhole
17/07/2021	J	F370SZ039	53,4	0,718	184,0	75	WOD	Parallel	580	N-S	Up-hole	01/10/2021	I	F370SZ058AL	21,4	9,162	127,5		WD	Spiral	473	N-S	Downhole
17/07/2021	A	F370SZ039	13,5	0,524	184,0	75	WOD	Parallel	1332	E-W	Up-hole	02/10/2021	I	F410SZ039AR	33,4	2,290	102,0	75	WOD	Parallel	409	E-W	Up-hole
17/07/2021	I	F370SZ039	26,6	3,401	184,0	75	WOD	Parallel	404	E-W	Up-hole	04/10/2021	J	F230SZ068	51,0	8,560	94,1		WD	Parallel	238	E-W	Downhole
18/07/2021	H	M420SZ008	40,0	3,657	64,3	75	WOD	Parallel	517	N-S	Downhole	04/10/2021	I	F230SZ068	21,8	2,885	94,1		WD	Parallel	528	N-S	Downhole
18/07/2021	A	M420SZ008	26,5	0,635	64,3	75	WOD	Parallel	860	E-W	Downhole	07/10/2021	J	F370SZ049	50,0	1,679	192,0		WOD	Parallel	510	N-S	Up-hole
20/07/2021	A	F310SZ026R	13,5	0,524	150,0	75	WOD	Parallel	1112	E-W	Up-hole	07/10/2021	I	F370SZ049	15,9	3,334	192,0		WOD	Parallel	433	N-S	Up-hole
20/07/2021	J	F310SZ026R	40,0	0,906	150,0	75	WOD	Parallel	683	N-S	Up-hole	07/10/2021	I	F410SZ039AR	26,5	1,838	82,0	75	WOD	Parallel	409	E-W	Up-hole
20/07/2021	I	F310SZ026R	26,6	2,882	150,0	75	WOD	Parallel	415	E-W	Up-hole	08/10/2021	I	F510SZ037AL	49,9	0,907	115,0		WD	Spiral	725	N-S	Downhole
24/07/2021	J	F270SZ055	40,0	6,748	161,3	WOD	Parallel	369	N-S	Up-hole	09/10/2021	J	F270SZ028L	50,0	0,684	147,0		WOD	Parallel	660	N-S	Up-hole
24/07/2021	J	F270SZ055	40,0	6,438	161,3	WOD	Parallel	369	N-S	Up-hole	09/10/2021	I	F270SZ028L	26,7	3,892	147,0		WOD	Parallel	409	E-W	Up-hole
24/07/2021	I	F270SZ055	26,7	5,118	161,3	WOD	Parallel	396	N-S	Up-hole	11/10/2021	J	F230SZ068	40,1	8,060	101,1		WD	Parallel	238	E-W	Downhole
25/07/2021	I	F370SZ042	13,4	1,596	96,8	75	WD	Parallel	392	N-S	Downhole	11/10/2021	I	F230SZ068	18,9	1,314	101,1		WD	Parallel	520	N-S	Downhole
27/07/2021	I	F410SZ049	26,6	1,388	94,6	75	WOD	Parallel	441	N-S	Downhole	11/10/2021	I	F370SZ044	26,7	1,380	113,0	75	WOD	Parallel	424	N-S	Up-hole
27/07/2021	J	F410SZ049	26,8	0,582	94,6	75	WOD	Parallel	510	N-S	Downhole	14/10/2021	I	F410SZ039AR	13,3	2,860	96,0	75	WOD	Parallel	410	E-W	Up-hole
29/07/2021	I	F370SZ042	28,0	2,004	69,6	WD	Parallel	393	N-S	Downhole	15/10/2021	J	F370SZ058AL	53,4	5,891	114,8		WD	Parallel	422	N-S	Downhole
29/07/2021	J	F370SZ042	19,5	0,751	69,6	WD	Parallel	536	N-S	Downhole	15/10/2021	I	F370SZ058AL	28,4	5,140	114,8		WD	Parallel	480	N-S	Downhole
30/07/2021	J	F230SZ066L	53,4	5,261	135,0	75	WOD	Parallel	273	N-S	Up-hole	15/10/2021	A	F370SZ058AL	19,0	0,582	114,8		WD	Parallel	1637	E-W	Downhole
30/07/2021	J	F230SZ066L	53,4	5,063	135,0	75	WOD	Parallel	273	N-S	Up-hole	17/10/2021	I	F230SZ068	18,0	1,943	91,4		WD	Parallel	519	N-S	Downhole
30/07/2021	I	F230SZ066L	26,6	1,670	135,0	75	WOD	Parallel	496	N-S	Up-hole	18/10/2021	J	F510SZ037AL	50,0	0,709	110,0		WD	Parallel	733	N-S	Downhole
31/07/2021	H	M420SZ008	40,0	2,012	64,3	75	WOD	Parallel	522	N-S	Downhole	18/10/2021	I	F510SZ037AL	27,0	0,835	110,0		WD	Parallel	517	N-S	Downhole
02/08/2021	J	F230SZ068	40,0	3,598	101,7	75	WOD	Parallel	273	E-W	Up-hole	19/10/2021	J	F510SZ062L	50,0	0,933	129,1		WOD	Parallel	579	N-S	Up-hole
02/08/2021	J	F230SZ068	40,0	3,799	101,7	75	WOD	Parallel	273	E-W	Up-hole	19/10/2021	I	F510SZ062L	20,8	0,933	129,1		WOD	Parallel	643	N-S	Up-hole
02/08/2021	I	F230SZ068	26,6	1,092	101,7	75	WOD	Parallel	532	N-S	Up-hole	21/10/2021	J	F370SZ049	50,0	0,829	147,0	75	WOD	Parallel	508	N-S	Up-hole
07/08/2021	J	F230SZ066L	26,6	7,857	129,7	75	WOD	Parallel	271	N-S	Up-hole	21/10/2021	I	F370SZ049	16,4	2,400	147,0	75	WOD	Parallel	434	N-S	Up-hole
07/08/2021	J	F230SZ066L	53,4	7,210	129,7	75	WOD	Parallel	271	N-S	Up-hole	21/10/2021	I	F410SZ039AR	26,7	1,426	111,0		WOD	Parallel	409	E-W	Up-hole
07/08/2021	I	F230SZ066L	26,6	2,694	129,7	75	WOD	Parallel	513	N-S	Up-hole	23/10/2021	I	F550SZ032L	19,9	1,382	90,0	50	WOD	Spiral	565	E-W	Up-hole
09/08/2021	H	M420SZ008	40,0	1,875	51,0	75	WOD	Parallel	525	N-S	Downhole	25/10/2021	J	F510SZ062L	50,0	0,948	133,0	75	WOD	Parallel	579	N-S	Up-hole
09/08/2021	A	M420SZ008	3,0	0,539	51,0	75	WOD	Parallel	868	E-W	Downhole	25/10/2021	I	F510SZ062L	26,8	1,280	133,0	75	WOD	Parallel	638	N-S	Up-hole
10/08/2021	I	F230SZ068	26,6	0,861	102,3	75	WOD	Parallel	532	N-S	Up-hole	28/10/2021	H	M440SZ001	26,5	0,684	102,5		WOD	Spiral	875	E-W	Downhole
10/08/2021	I	F230SZ068	53,3	3,774	102,3	75	WOD	Parallel	272	E-W	Up-hole	31/10/2021	J	F370SZ049	53,4	0,886	162,0	75	WOD	Parallel	508	N-S	Up-hole
11/08/2021	I	F370SZ039	26,6	3,758	175,0	75	WOD	Parallel	404	E-W	Up-hole	31/10/2021	I	F370SZ049	13,4	2,048	162,0	75	WOD	Parallel	435	N-S	Up-hole
11/08/2021	J	F370SZ039	50,0	1,006	175,0	75	WOD	Parallel	583	N-S	Up-hole	01/11/2021	J	F370SZ058AL	32,0	4,491	98,4		WD	Parallel	428	N-S	Downhole
16/08/2021	J	F370SZ058AL	53,3	2,513	165,5	WOD	Parallel	463	N-S	Up-hole	01/11/2021	I	F370SZ058AL	27,4	4,581	98,4		WD	Parallel	463	N-S	Downhole
16/08/2021	I	F370SZ058AL	26,6	2,456	165,5	WOD	Parallel	496	N-S	Up-hole	01/11/2021	A	F370SZ058AL	3,0	0,534	98,4		WD	Parallel	1609	E-W	Downhole
16/08/2021	I	F550SZ032L	26,6	1,301	119,1	WOD	Parallel	584	E-W	Up-hole	03/11/2021	J	F370SZ044	50,0	0,606	102,5	75	WD	Parallel	524	N-S	Downhole
17/08/2021	H	M420SZ008	40,1	2,800	50,0	75	WOD	Parallel	513	N-S	Downhole	03/11/2021	I	F370SZ044	16,0	1,858	102,5	75	WD	Parallel	387	N-S	Downhole
18/08/2021	J	F230SZ068	40,0	4,770	103,4	WOD	Parallel	271	E-W	Up-hole	04/11/2021	J	F370SZ049	50,0	0,553	152,0	75	WOD	Parallel	503	N-S	Up-hole
18/08/2021	I	F230SZ068	26,8	0,950	103,4	WOD	Parallel	541	N-S	Up-hole	04/11/2021	I	F370SZ049	20,0	1,611	152,0	75	WOD	Parallel	435	N-S	Up-hole
19/08/2021	J	F270SZ055	40,0	5,246	107,5	75	WD	Spiral	345	N-S	Downhole	06/11/2021	J	F270SZ028L	40,1	1,185	145,2		WOD	Parallel	655	N-S	Up-hole
19/08/2021	I	F270SZ055	26,6	3,694	107,5	75	WD	Spiral	367	N-S	Downhole	06/11/2021	I	F270SZ028L	26,6	3,420	145,2		WOD	Parallel	407	E-W	Up-hole
20/08/2021	J	F370SZ058AL	53,4	1,825	158,0	75	WOD	Parallel	465	N-S	Up-hole	09/11/2021	A	F270SZ028L	13,4	0,539	145,2		WOD	Parallel	1136	E-W	Up-hole
20/08/2021	I	F370SZ058AL	26,6	1,926	158,0	75	WOD	Parallel	490	N-S	Up-hole	09/11/2021	I	F370SZ044	19,8	2,036	95,6	75	WD	Parallel	388	N-S	Downhole
22/08/2021	I	F550SZ032L	26,6	1,143	118,0	75	WOD	Parallel	581	E-W	Up-hole	10/11/2021	D	F270SZ028L	29,0	0,950	147,0	75	WOD	Parallel	758	E-W	Up-hole
23/08/2021	J	F230SZ066L	40,0	7,039	82,3	75	WD	Parallel	238	N-S	Downhole	10/11/2021	J	F270SZ028L	50,0	1,514	147,0	75	WOD	Parallel	657	N-S	Up-hole
23/08/2021	I	F230SZ066L	26,8	1,374	82,3	75	WD	Parallel	482	N-S	Downhole	10/11/2021	I	F270SZ028L	13,3	7,851	147,0	75	WOD	Parallel	403	E-W	Up-hole
27/08/2021	J	F370SZ058AL	40,0	1,803	172,3	WOD	Parallel	467	N-S	Up-hole	10/11/2021	A	F270SZ028L	12,5	0,823	147,0	75	WOD	Parallel	1138	E-W	Up-hole
27/08/2021	I	F370SZ058AL	13,3	1,699	172,3	WOD	Parallel	485	N-S	Up-hole	12/11/2021	J	F230SZ052	40,1	4,504	160,6		WOD	Parallel	349	N-S	Up-hole
28/08/2021	J	F270SZ055	40,0	5,822	96,4	WD	Parallel	340	N-S	Downhole	12/11/2021	I	F230SZ052	13,3	2,670	160,6		WOD	Parallel	355	N-S	Up-hole
28/08/2021	I	F270SZ055	13,3	2,338	96,4	WD	Parallel	372	N-S	Downhole	13/11/2021	J	F370SZ049	13,3	1,225	125,0	75	WD	Spiral	479	N-S	Downhole
30/08/2021	I	F370SZ038	26,6	2,785	142,0	75	WOD	Parallel	408	E-W	Up-hole	13/11/2021	I	F370SZ049	13,1	3,434	125,0	75	WD	Spiral	403	N-S	Downhole
02/09/2021	I	F370SZ058AL	18,8	1,675	138,3	WOD	Parallel	478	N-S	Up-hole	13/11/2021	A	F370SZ049	13,0	0,524	125,0	75	WD	Spiral	1475	E-W	Downhole
02/09/2021	J	F370SZ058AL	40,1	1,659	138,3	WOD	Parallel	470	N-S	Up-hole	14/11/2021	H	M440SZ001	40,1	0,582	80,0	75	WOD	Parallel	870	E-W	Downhole
02/09/2021	I	F550SZ032L	26,8	0,933	115,0	WOD	Parallel	581	E-W	Up-hole	15/11/2021	J	F270SZ028L	50,0	1,014	182,0	75	WOD	Parallel	644	N-S	Up-hole
03/09/2021	J	F270SZ055	53,3	3,575	98,6	WD	Parallel	338	N-S	Downhole	15/11/2021	I	F270SZ028L	26,6	4,665	182,0	75	WOD	Parallel	401	E-W	Up-hole
03/09/2021	I	F270SZ055	13,3	1,875	98,6	WD	Parallel	374	N-S	Downhole	15/11/2021	A	F270SZ028L	40,0	0,539	182,0	75	WOD	Parallel	1152	E-W	Up-hole
04/09/2021	H	M420SZ008	40,0	1,550	49,4	75	WOD	Parallel	534	N-S	Downhole	17/11/2021	I	F370SZ058AL	23,0	2,649	165,0		WD	Parallel	462	N-S	Downhole
05/09/2021	I	F370SZ038	26,6	3,533	130,0	75	WOD	Parallel	409	E-W	Up-hole	17/11/2021	J	F370SZ058AL	40,0	2,899	165,0		WD	Parallel	427	N-S	Downhole
06/09/2021	I	F230SZ068	50,0	3,724	30,0	65	WD	Spiral	258	N-S	Downhole	18/11/2021	I	F370SZ044	26,6	1,571	109,6	75	WD	Parallel	391	N-S	Downhole
06/09/2021	I	F230SZ068	30,9	1,426	30,0	65	WD	Spiral	538	N-S	Downhole	21/11/2021	I	F370SZ049	20,3	1,231	91,8		WD	Parallel	404	N-S	Downhole
08/09/2021	J	F410SZ039AR	50,0	0,608	101,5	WOD	Spiral	616	N-S	Up-hole	21/11/2021	J	F370SZ049	50,0	0,720	91,8		WD	Parallel	478	N-S	Downhole
08/09/2021	I	F410SZ039AR	30,8	2,670	101,5	WOD	Spiral	408	E-W	Up-hole	23/11/2021	I	F370SZ044	26,9	1,836	100,0	75	WD	Parallel	395	N-S	Downhole
09/09/2021	J	F230SZ068	50,0	3,978	27,5	65	WD	Spiral	254	N-S	Downhole	23/11/2021	J	F370SZ044	50,0	0,652	100,0	75	WD	Parallel	515	N-S	Downhole
10/09/2021	J	F230SZ068	50,0	1,970	20,0	65	WD	Spiral	250	N-S	Downhole	23/11/2021	H	M440SZ001	2,1	0,582	98,9	75	WOD	Parallel	855	E-W	Downhole
11/09/2021	J	F230SZ068	50,0	2,563	35,0	65	WD	Spiral	246	N-S	Downhole	25/11/2021	H	M420SZ004	20,4	0,773	92,0	75	WOD	Parallel	737	N-S	Up-hole
13/09/2021	H	M420SZ008	40,1	1,814	98,6	75	WOD	Parallel	537	N-S	Downhole	25/11/2021	J	F470SZ049L	49,9	0,805	147,0		WOD	Parallel	631	N-S	Up-hole
13/09/2021	I	F510SZ037AL	26,6	1,276	143,0	75	WOD	Parallel	552	N-S	Up-hole	25/11/2021	I	F470SZ049L	26,7	2,865	147,0		WOD	Parallel	526	E-W	Up-hole

Legend:

Data considered as outliers

WD Data included in models with discontinuity

WOD Data included in models without discontinuity

Date	Monitored structure	Stope	Dominant frequency (Hz)	PVS (mm·s⁻¹)	Maximum charge per delay (kg)	Delay between adjacent holes (ms)	Operational scenario	Initiation pattern geometry	Distance (m)	Orientation	Type of blast	Date	Monitored structure	Stope	Dominant frequency (Hz)	PVS (mm·s⁻¹)	Maximum charge per delay (kg)	Delay between adjacent holes (ms)	Operational scenario	Initiation pattern geometry	Distance (m)	Orientation	Type of blast
28/11/2021	J	F370S2049	50,0	0,737	92,1		WD	Parallel	475	N-S	Downhole	02/02/2022	I	F470S2049	26,6	4,639	94,1		WD	Parallel	486	E-W	Downhole
28/11/2021	I	F370S2049	13,5	1,513	92,1		WD	Parallel	407	N-S	Downhole	04/02/2022	J	F230S2050	40,4	2,466	99,6		WD	Parallel	342	N-S	Downhole
29/11/2021	I	F270S2028	49,9	1,388	142,5		WD	Spiral	639	N-S	Downhole	04/02/2022	I	F230S2050	19,9	1,778	99,6		WD	Parallel	359	N-S	Downhole
29/11/2021	I	F270S2028	11,8	4,854	142,5		WD	Spiral	387	E-W	Downhole	05/02/2022	D	F230S2041LR	40,0	0,684	173,0	75	WOD	Parallel	878	E-W	Up-hole
29/11/2021	A	F270S2028	19,1	0,660	142,5		WD	Spiral	1125	E-W	Downhole	05/02/2022	A	F230S2041LR	3,0	0,524	173,0	75	WOD	Parallel	1288	E-W	Up-hole
02/12/2021	J	F230S2062	49,9	5,416	156,8	75	WD	Spiral	320	N-S	Downhole	05/02/2022	J	F230S2041LR	40,0	2,600	173,0	75	WOD	Parallel	450	E-W	Up-hole
02/12/2021	I	F230S2062	53,3	4,327	156,8	75	WD	Spiral	341	N-S	Downhole	05/02/2022	I	F230S2041LR	53,3	2,765	173,0	75	WOD	Parallel	326	N-S	Up-hole
02/12/2021	J	F470S2049	50,0	0,819	136,0		WOD	Parallel	638	N-S	Up-hole	06/02/2022	J	F230S2056B	46,3	1,836	35,0	65	WOD	Spiral	276	N-S	Downhole
02/12/2021	I	F470S2049	13,3	1,270	136,0		WOD	Parallel	522	E-W	Up-hole	06/02/2022	I	F210S2056B	26,8	0,696	35,0	65	WOD	Spiral	385	N-S	Downhole
03/12/2021	J	F510S2137AL	50,0	0,840	95,9		WD	Parallel	735	N-S	Downhole	08/02/2022	I	F610S2024L	26,6	3,100	73,2	75	WD	Parallel	564	E-W	Downhole
03/12/2021	I	F510S2137AL	12,6	4,058	95,9		WD	Parallel	517	N-S	Downhole	09/02/2022	J	F210S2056B	46,4	1,611	50,0	65	WOD	Spiral	271	N-S	Downhole
03/12/2021	A	F510S2137AL	3,0	0,508	95,9		WD	Parallel	1391	E-W	Downhole	09/02/2022	I	F210S2056B	30,8	0,684	50,0	65	WOD	Spiral	383	N-S	Downhole
04/12/2021	D	F270S2028	53,0	0,524	95,9		WD	Parallel	747	E-W	Downhole	10/02/2022	D	F230S2041LR	66,6	1,171	191,1		WOD	Parallel	862	E-W	Up-hole
04/12/2021	J	F270S2028	50,0	1,093	95,9		WD	Parallel	631	N-S	Downhole	10/02/2022	A	F230S2041LR	26,8	0,539	191,1		WOD	Parallel	1270	E-W	Up-hole
04/12/2021	I	F270S2028	28,4	4,588	95,9		WD	Parallel	380	E-W	Downhole	10/02/2022	J	F230S2041LR	40,0	3,074	191,1		WOD	Parallel	467	N-S	Up-hole
04/12/2021	A	F270S2028	2,3	0,539	95,9		WD	Parallel	1135	E-W	Downhole	10/02/2022	I	F230S2041LR	26,6	2,765	191,1		WOD	Parallel	321	E-W	Up-hole
05/12/2021	I	F370S2049	13,0	1,397	95,9		WD	Parallel	407	N-S	Downhole	11/02/2022	D	F510S2137AL	18,6	0,582	97,5		WD	Parallel	1041	E-W	Downhole
06/12/2021	J	F270S2056A	50,0	1,815	17,9	65	WOD	Spiral	285	N-S	Downhole	11/02/2022	J	F510S2137AL	18,6	0,823	97,5		WD	Parallel	745	N-S	Downhole
06/12/2021	I	F270S2056A	16,8	0,696	17,9	65	WOD	Spiral	356	N-S	Downhole	11/02/2022	I	F510S2137AL	20,0	5,127	97,5		WD	Parallel	519	N-S	Downhole
07/12/2021	J	F210S2056A	50,0	1,136	27,5	65	WOD	Spiral	282	N-S	Downhole	11/02/2022	A	F510S2137AL	21,3	0,582	97,5		WD	Parallel	1375	E-W	Downhole
08/12/2021	J	F230S2052	53,4	4,917	106,4	75	WD	Parallel	325	N-S	Downhole	15/02/2022	J	F310S2073	40,0	3,198	129,6	75	WD	Spiral	335	E-W	Downhole
08/12/2021	I	F230S2052	13,4	2,667	106,4	75	WD	Parallel	340	N-S	Downhole	15/02/2022	I	F310S2073	26,5	1,380	129,6	75	WD	Spiral	599	N-S	Downhole
10/12/2021	I	F370S2044	27,3	2,899	145,7		WD	Parallel	385	N-S	Up-hole	17/02/2022	I	F370S2047	26,6	3,471	142,0		WOD	Parallel	425	N-S	Up-hole
10/12/2021	A	F370S2044	10,8	0,539	145,7		WD	Parallel	1405	E-W	Downhole	17/02/2022	J	F370S2047	40,0	2,345	142,0		WOD	Parallel	526	N-S	Up-hole
10/12/2021	I	F510S2137AL	11,5	4,663	91,4		WD	Parallel	517	N-S	Downhole	17/02/2022	A	F370S2047	3,0	0,648	142,0		WOD	Parallel	1463	E-W	Up-hole
10/12/2021	A	F510S2137AL	20,5	0,539	91,4		WD	Parallel	1385	E-W	Downhole	19/02/2022	I	F270S2069	26,7	2,556	268,3	75	WOD	Spiral	549	N-S	Up-hole
11/12/2021	I	F370S2049	20,9	4,098	92,5	75	WD	Parallel	403	N-S	Downhole	19/02/2022	J	F270S2069	46,0	5,607	268,3	75	WOD	Spiral	318	E-W	Up-hole
12/12/2021	D	F270S2028	52,5	0,622	95,9		WD	Parallel	751	E-W	Downhole	19/02/2022	A	F270S2069	3,0	0,539	268,3	75	WOD	Spiral	1721	E-W	Up-hole
12/12/2021	I	F270S2028	27,5	4,808	95,9		WD	Parallel	378	E-W	Downhole	21/02/2022	I	F210S2056B	26,7	2,083	92,5	75	WOD	Spiral	385	N-S	Downhole
12/12/2021	A	F270S2028	27,5	0,648	95,9		WD	Spiral	1139	E-W	Downhole	21/02/2022	J	F210S2056B	53,4	5,235	92,5	75	WOD	Spiral	267	N-S	Downhole
14/12/2021	I	F210S2056A	26,8	1,645	64,3	75	WOD	Spiral	347	N-S	Downhole	22/02/2022	D	F230S2041LR	66,6	0,907	198,0		WOD	Parallel	858	E-W	Up-hole
16/12/2021	I	F230S2052	53,4	2,304	78,2	75	WD	Parallel	342	N-S	Downhole	22/02/2022	I	F230S2041LR	26,6	3,288	198,0		WOD	Parallel	321	E-W	Up-hole
19/12/2021	I	F270S2034	22,1	3,821	105,0		WD	Spiral	347	E-W	Downhole	22/02/2022	J	F230S2041LR	40,0	2,598	198,0		WOD	Parallel	472	N-S	Up-hole
19/12/2021	D	F510S2024L	30,8	0,539	161,0		WOD	Spiral	919	E-W	Up-hole	22/02/2022	A	F230S2041LR	26,6	0,539	198,0		WOD	Parallel	1285	E-W	Up-hole
19/12/2021	I	F510S2024L	76,9	1,508	161,0		WOD	Spiral	599	E-W	Up-hole	24/02/2022	H	M420S2007	49,9	1,159	162,5		WOD	Parallel	559	N-S	Downhole
21/12/2021	I	F470S2049	26,9	3,298	142,5		WD	Spiral	491	E-W	Downhole	24/02/2022	J	F370S2047	38,9	0,925	148,9	75	WOD	Parallel	525	N-S	Up-hole
21/12/2021	J	F470S2049	50,0	1,287	142,5		WD	Spiral	601	N-S	Downhole	24/02/2022	I	F370S2047	20,9	1,913	148,9	75	WOD	Parallel	426	N-S	Up-hole
27/12/2021	J	F210S2056	50,0	1,326	22,5	65	WOD	Spiral	280	N-S	Downhole	24/02/2022	A	M420S2007	8,5	0,539	162,5		WOD	Parallel	914	E-W	Downhole
28/12/2021	H	M440S2003	39,9	0,660	140,0		WOD	Spiral	827	E-W	Downhole	25/02/2022	J	F470S2049	26,6	1,809	103,9		WD	Parallel	620	N-S	Downhole
29/12/2021	I	F470S2049	26,8	2,700	109,6		WD	Parallel	488	E-W	Downhole	25/02/2022	I	F470S2049	26,6	3,408	103,9		WD	Parallel	483	E-W	Downhole
29/12/2021	A	F470S2049	13,5	0,539	109,6		WD	Parallel	1529	E-W	Downhole	27/02/2022	J	F270S2069	21,6	4,982	168,0	75	WOD	Parallel	314	E-W	Up-hole
29/12/2021	J	F470S2049	50,0	1,330	109,6		WD	Parallel	609	N-S	Downhole	27/02/2022	I	F270S2069	13,3	2,600	168,0	75	WOD	Parallel	557	N-S	Up-hole
30/12/2021	I	F210S2056	26,8	2,071	32,5	65	WOD	Spiral	365	N-S	Downhole	27/02/2022	A	F270S2069	3,0	0,582	168,0	75	WOD	Parallel	1723	E-W	Up-hole
30/12/2021	A	F210S2056	2,3	0,539	32,5	65	WOD	Spiral	1518	E-W	Downhole	28/02/2022	J	F370S2047	13,4	0,925	158,0	75	WOD	Parallel	520	N-S	Up-hole
30/12/2021	J	F210S2056	50,0	1,220	32,5	65	WOD	Spiral	276	N-S	Downhole	28/02/2022	I	F370S2047	20,6	1,814	158,0	75	WOD	Parallel	427	N-S	Up-hole
31/12/2021	A	F270S2034	2,3	0,539	105,9	75	WD	Parallel	1213	E-W	Downhole	02/03/2022	I	F410S2041	19,5	0,696	25,0	65	WOD	Spiral	442	E-W	Downhole
31/12/2021	D	F270S2034	40,0	0,588	105,9	75	WD	Parallel	821	E-W	Downhole	03/03/2022	I	F410S2041	15,3	0,751	40,0	65	WOD	Spiral	437	N-S	Downhole
31/12/2021	I	F270S2034	26,6	3,343	105,9	75	WD	Parallel	342	E-W	Downhole	05/03/2022	J	F510S2024L	40,0	0,582	142,7	75	WOD	Parallel	849	N-S	Up-hole
31/12/2021	J	F270S2034	49,9	1,411	105,9	75	WD	Parallel	561	N-S	Downhole	05/03/2022	I	F510S2024L	26,6	3,892	142,7	75	WOD	Parallel	569	E-W	Up-hole
02/01/2022	D	F210S2066	26,8	0,730	95,0	75	WOD	Spiral	1107	E-W	Downhole	05/03/2022	A	F510S2024L	13,3	0,648	142,7	75	WOD	Parallel	1247	E-W	Up-hole
02/01/2022	I	F210S2066	53,3	2,694	95,0	75	WOD	Spiral	369	N-S	Downhole	06/03/2022	J	F270S2069	40,5	2,581	170,0	75	WOD	Parallel	315	E-W	Up-hole
02/01/2022	J	F210S2066	53,3	9,740	95,0	75	WOD	Spiral	267	N-S	Downhole	06/03/2022	I	F270S2069	26,6	1,611	170,0	75	WOD	Parallel	561	N-S	Up-hole
07/01/2022	J	F210S2066	53,4	7,694	67,5	75	WOD	Spiral	269	N-S	Downhole	08/03/2022	J	F470S2049	26,8	1,631	115,0	75	WD	Parallel	622	N-S	Downhole
07/01/2022	I	F210S2066	26,8	2,159	67,5	75	WOD	Parallel	367	N-S	Downhole	08/03/2022	I	F470S2049	26,6	2,948	115,0	75	WD	Parallel	482	E-W	Downhole
11/01/2022	A	F470S2049	3,0	0,539	133,0	75	WOD	Parallel	1535	E-W	Up-hole	10/03/2022	D	F125S2050	26,7	1,100	182,0	75	WOD	Parallel	1018	E-W	Up-hole
11/01/2022	J	F470S2049	53,4	0,992	133,0	75	WOD	Parallel	644	N-S	Up-hole	10/03/2022	J	F125S2050	39,9	8,547	182,0	75	WOD	Parallel	274	E-W	Up-hole
11/01/2022	I	F470S2049	26,6	2,012	133,0	75	WOD	Parallel	520	E-W	Up-hole	10/03/2022	I	F125S2050	26,7	4,961	182,0	75	WOD	Parallel	402	N-S	Up-hole
14/01/2022	J	F510S2024L	50,0	0,565	141,8	75	WOD	Parallel	858	N-S	Up-hole	10/03/2022	A	F125S2050	13,3	0,751	182,0	75	WOD	Parallel	1446	E-W	Up-hole
14/01/2022	I	F510S2024L	26,6	4,372	141,8	75	WOD	Parallel	594	E-W	Up-hole	11/03/2022	A	M420S2007	3,0	0,582	67,5	75	WOD	Parallel	927	E-W	Downhole
14/01/2022	A	F510S2024L	13,3	0,588	141,8	75	WOD	Parallel	1237	E-W	Up-hole	12/03/2022	J	F470S2049	40,0	1,481	154,0	75	WOD	Parallel	656	N-S	Up-hole
18/01/2022	J	F160S2074	40,0	9,874	175,0		WOD	Parallel	241	N-S	Up-hole	12/03/2022	I	F470S2049	26,6	2,106	154,0	75	WOD	Parallel	515	E-W	Up-hole
18/01/2022	I	F160S2074	26,7	1,326	175,0		WOD	Parallel	595	N-S	Up-hole	16/03/2022	J	F510S2027L	26,6	1,626	158,0	75	WOD	Parallel	984	E-W	Up-hole
19/01/2022	I	F470S2049	26,6	1,555	147,0	75	WOD	Parallel	518	E-W	Up-hole	16/03/2022	J	F510S2027L	26,8	0,582	158,0	75	WOD	Parallel	837	N-S	Up-hole
19/01/2022	A	F470S2049	50,0	0,963	147,0	75	WOD	Parallel	647	N-S	Up-hole	16/03/2022	A	F510S2027L	3,0	0,539	158,0	75	WOD	Parallel	1261	E-W	Up-hole
19/01/2022	A	F470S2049	3,0	0,524	147,0	75	WOD	Parallel	1528	E-W	Up-hole	18/03/2022	I	F160S2074	15,7	3,914	30,0	65	WD	Spiral	590	N-S	Downhole
22/01/2022	A	F510S2137AL	2,3	0,648	102,7	75	WD	Parallel	1390	E-W	Downhole	18/03/2022	J	F160S2074	46,3	3,610	30,0	65	WD	Spiral	218	N-S	Downhole
24/01/2022	J	F230S2050	53,4	3,682	105,0	75	WD	Spiral	343	N-S	Downhole	18/03/2022	I	F160S2086L	30,8	0,933	140,0		WOD	Spiral	731	N-S	Up-hole
24/01/2022	I	F230S2050	53,3	3,808	105,0	75	WD	Spiral	333	N-S	Downhole	18/03/2022	J	F160S2086L	39,9	1,888	140,0		WOD	Spiral	340	N-S	Up-hole
25/01/2022	I	F160S2074	26,6	0,842	167,0		WOD	Parallel	597	N-S	Up-hole	18/03/2022	A	F160S2086L	12,6	0,539	140,0		WOD	Spiral	1922	E-W	Up-hole
26/01/2022	I	F470S2049	26,6	1,205	151,0	75	WOD	Parallel	516	E-W	Up-hole	18/03/2022	J	F370S2047	46,3	5,421	110,0		WD	Spiral	496	N-S	Up-hole
27/01/2022	I	F510S2024L	30,8	1,550	100,0	65	WD	Spiral	571	E-W	Up-hole	19/03/2022	I	F125S2050L	40,0	4,290	173,5	75	WOD	Parallel	396	N-S	Up-hole
27/01/2022	A	F510S2024L	2,5	0,568	100,0	65	WD	Spiral	1205	E-W	Downhole	19/03/2022	J	F125S2050L	40,0	8,123	173,5	75	WOD	Parallel	285	E-W	Up-hole
28/01/2022	I	F310S2073	26,6	1,746	173,0	75	WOD	Spiral	615	N-S	Up-hole	19/03/2022	A	F125S2050L	40,0	0,568	173,5	75	WOD	Parallel	1431	E-W	Up-hole
30/01/2022	I	F230S2050	26,8	2,440	97,7	75	WD	Parallel	336	N-S	Downhole	21/03/2022	J	F470S2049	26,6	3,412	83,2	65	WD	Spiral	213	N-S	Downhole
31/01/2022	I	F510S2024L	53,3	2,373	78,4	75	WD	Parallel	566	E-W	Downhole	21/03/2022	I	F470S2049	26,6	3,139	30,0	65	WD	Spiral	493	E-W	Downhole
31/01/2022	A	F510S2024L	13,3	0,539	78,4	75	WD	Parallel	1216	E-W	Downhole	21/03/2022	J	F470S2049L	26,6	1,308	83,2		WD	Parallel	617	N-S	Downhole
01/02/2022	D	F230S2041LR	66,8	0,568	157,2	75	WOD	Parallel	871	E-W	Up-hole	24/03/2022	J	F410S2041	26,8	2,275	97,5		WOD	Parallel	432	N-S	Downhole
01/02/2022	I	F230S2041LR	66,4	2,865	157,2	75	WOD	Parallel	326	E-W	Up-hole	24/03/2022	I	F410S2041	15,1	0,889	97,5		WOD	Parallel	621	N-S	Downhole

Legend:

Data considered as outliers

WD — Data included in models with discontinuity

WOD — Data included in models without discontinuity

Date	Monitored structure	Stope	Dominant frequency (Hz)	PVS (mm·s⁻¹)	Maximum charge per delay (kg)	Delay between adjacent holes (ms)	Operational scenario	Initiation pattern geometry	Distance (m)	Orientation	Type of blast
24/03/2022	A	F410S2041	15,0	0,539	97,5		WOD	Parallel	1404	E-W	Downhole
25/03/2022	I	F160S2086L	26,6	0,861	162,0	75	WOD	Parallel	724	N-S	Up-hole
25/03/2022	J	F160S2086L	40,0	5,153	162,0	75	WOD	Parallel	335	N-S	Up-hole
25/03/2022	I	F510S2037AL	26,7	2,655	154,0		WOD	Parallel	561	N-S	Up-hole
25/03/2022	J	F510S2037AL	26,6	0,823	154,0		WOD	Parallel	786	N-S	Up-hole
27/03/2022	H	M420S2007	40,0	0,760	69,1	75	WOD	Parallel	569	N-S	Up-hole
28/03/2022	I	F410S2041	13,3	1,205	90,2	75	WOD	Parallel	432	N-S	Up-hole
28/03/2022	J	F410S2041	40,0	0,635	90,2	75	WOD	Parallel	618	N-S	Up-hole
31/03/2022	I	F160S2086L	26,6	0,823	164,0	75	WOD	Parallel	717	N-S	Up-hole
31/03/2022	J	F160S2086L	40,0	3,937	164,0	75	WOD	Parallel	330	N-S	Up-hole
01/04/2022	D	F125S2050L	26,8	0,568	185,0	75	WOD	Parallel	1001	E-W	Up-hole
01/04/2022	I	F125S2050L	40,0	2,997	185,0	75	WOD	Parallel	395	N-S	Up-hole
01/04/2022	J	F125S2050L	40,0	6,934	185,0	75	WOD	Parallel	287	E-W	Up-hole
02/04/2022	I	F370S2047	26,6	0,950	91,4	75	WD	Parallel	397	N-S	Downhole
02/04/2022	J	F370S2047	13,3	0,660	91,4	75	WD	Parallel	493	N-S	Downhole
04/04/2022	I	F270S2069	17,5	0,508	25,0	65	WD	Spiral	547	N-S	Downhole
04/04/2022	J	F270S2069	34,0	1,143	25,0	65	WD	Spiral	299	E-W	Downhole
04/04/2022	I	F370S2052AL	26,7	3,343	188,0		WOD	Parallel	437	N-S	Up-hole
04/04/2022	J	F370S2052AL	53,3	1,901	188,0		WOD	Parallel	510	N-S	Up-hole
05/04/2022	I	F270S2069	13,3	2,355	50,0	65	WD	Spiral	546	N-S	Downhole
05/04/2022	J	F270S2069	46,1	1,922	50,0	65	WD	Spiral	294	E-W	Downhole
05/04/2022	J	F410S2041	13,3	0,852	100,0	75	WOD	Parallel	614	N-S	Downhole
07/04/2022	J	F160S2074	46,3	5,039	90,0	65	WD	Spiral	208	N-S	Downhole
07/04/2022	J	F270S2069	45,9	1,257	27,5	65	WD	Spiral	288	E-W	Downhole
08/04/2022	I	F510S2027L	26,6	1,905	163,0	75	WOD	Parallel	580	E-W	Up-hole
08/04/2022	J	F510S2027L	19,8	0,582	163,0	75	WOD	Parallel	830	N-S	Up-hole
09/04/2022	I	F230S2141LR	26,6	5,120	163,0	75	WOD	Parallel	325	N-S	Up-hole
09/04/2022	J	F230S2141LR	56,1	2,472	163,0	75	WOD	Parallel	443	E-W	Up-hole
11/04/2022	I	F160S2074	26,6	1,397	100,0		WD	Spiral	583	N-S	Downhole
12/04/2022	I	F370S2047	21,8	1,492	114,1		WD	Parallel	389	N-S	Downhole
12/04/2022	J	F370S2047	13,3	0,925	114,1		WD	Parallel	491	N-S	Downhole
16/04/2022	J	F270S2069	39,9	7,494	125,0		WD	Spiral	284	E-W	Downhole
18/04/2022	I	F270S2069	18,1	2,222	125,0		WD	Spiral	539	N-S	Downhole
18/04/2022	J	F125S2050L	39,9	8,173	223,0	75	WOD	Parallel	300	E-W	Up-hole
18/04/2022	I	F125S2050L	26,6	5,507	223,0	75	WOD	Parallel	377	N-S	Up-hole
18/04/2022	D	F125S2050L	26,8	0,823	223,0	75	WOD	Parallel	985	E-W	Up-hole
18/04/2022	A	F125S2050L	40,0	0,648	223,0	75	WOD	Parallel	1411	E-W	Up-hole
19/04/2022	J	F160S2074	40,0	11,770	128,7	75	WD	Parallel	202	N-S	Downhole
19/04/2022	I	F160S2074	27,6	1,391	128,7	75	WD	Parallel	587	N-S	Downhole
24/04/2022	I	F270S2069	18,4	1,947	87,3	75	WD	Parallel	281	E-W	Downhole
24/04/2022	I	F270S2069	16,6	1,092	87,3	75	WD	Parallel	543	N-S	Downhole
26/04/2022	J	F160S2086L	39,9	4,920	180,9	75	WD	Parallel	328	N-S	Downhole
26/04/2022	D	F160S2086L	3,0	0,568	180,9	75	WD	Parallel	1502	E-W	Downhole
27/04/2022	J	F125S2050L	40,0	4,685	124,0	75	WOD	Parallel	267	E-W	Up-hole
27/04/2022	J	F125S2050L	40,0	4,685	124,0	75	WOD	Parallel	267	E-W	Up-hole
27/04/2022	I	F125S2050L	26,6	2,492	124,0	75	WOD	Parallel	386	N-S	Up-hole
30/04/2022	H	M420S2007	50,0	0,578	70,6	75	WOD	Parallel	578	N-S	Downhole
02/05/2022	I	F510S2027L	20,3	0,539	72,5	65	WD	Spiral	556	E-W	Downhole
03/05/2022	J	F270S2069	40,0	2,694	92,3	75	WD	Parallel	280	E-W	Downhole
03/05/2022	I	F270S2069	26,8	0,813	92,3		WD	Parallel	545	N-S	Downhole
04/05/2022	J	F370S2052AL	58,6	1,836	100,0		WD	Spiral	486	N-S	Downhole
04/05/2022	I	F370S2052AL	21,0	2,943	100,0		WD	Spiral	401	N-S	Downhole
06/05/2022	J	F510S2027L	20,0	0,554	100,0		WD	Parallel	810	N-S	Downhole
06/05/2022	I	F510S2027L	22,4	3,008	100,0		WD	Spiral	551	E-W	Downhole
06/05/2022	D	F510S2027L	59,9	0,813	100,0		WD	Spiral	925	E-W	Downhole
06/05/2022	A	F510S2027L	2,3	0,582	100,0		WD	Spiral	1248	E-W	Downhole
07/05/2022	I	F350S2058AL	48,5	1,024	25,0	65	WOD	Spiral	406	N-S	Downhole
07/05/2022	J	F350S2058AL	30,8	0,582	25,0	65	WOD	Spiral	488	N-S	Downhole
08/05/2022	J	F370S2052AL	53,3	4,072	108,0		WD	Parallel	479	N-S	Downhole
08/05/2022	I	F370S2052AL	21,3	3,718	108,0		WD	Parallel	407	N-S	Downhole
08/05/2022	D	F370S2052AL	2,8	0,524	108,0		WD	Parallel	1129	E-W	Downhole
09/05/2022	J	F350S2058AL	48,5	1,283	27,5	65	WOD	Spiral	402	N-S	Downhole
10/05/2022	J	F125S2064L	45,9	9,972	151,0		WOD	Parallel	179	E-W	Up-hole
10/05/2022	I	F125S2064L	30,9	1,391	151,0		WOD	Parallel	462	N-S	Up-hole
10/05/2022	J	F350S2058AL	61,4	5,511	87,5		WOD	Spiral	395	N-S	Downhole
11/05/2022	I	F350S2058AL	26,9	3,321	87,5		WOD	Spiral	484	N-S	Downhole
11/05/2022	J	F160S2086L	40,0	6,605	96,4	75	WD	Parallel	313	N-S	Downhole
11/05/2022	I	F160S2086L	26,6	1,840	96,4	75	WD	Parallel	721	N-S	Downhole
11/05/2022	J	F270S2027	58,9	0,741	71,4	65	WD	Spiral	653	N-S	Downhole
11/05/2022	I	F270S2027	17,5	2,186	71,4	65	WD	Spiral	375	E-W	Downhole
11/05/2022	A	F160S2086L	2,3	0,539	96,4	75	WD	Parallel	1913	E-W	Downhole
12/05/2022	I	F125S2064L	20,5	1,867	157,0	75	WOD	Parallel	470	N-S	Up-hole
14/05/2022	J	F350S2058AL	53,3	7,792	105,0	75	WOD	Parallel	398	N-S	Downhole

Date	Monitored structure	Stope	Dominant frequency (Hz)	PVS (mm·s⁻¹)	Maximum charge per delay (kg)	Delay between adjacent holes (ms)	Operational scenario	Initiation pattern geometry	Distance (m)	Orientation	Type of blast
24/03/2022	I	F350S2058AL	53,3	5,287	105,0	75	WOD	Parallel	473	N-S	Downhole
25/03/2022	I	F410S2041	60,3	0,568	25,0	65	WOD	Spiral	448	N-S	Downhole
25/03/2022	I	F410S2041	55,8	0,582	45,0	65	WOD	Spiral	443	N-S	Downhole
25/03/2022	J	F270S2069	40,0	3,603	99,6		WD	Parallel	280	E-W	Downhole
25/03/2022	I	F270S2069	26,4	1,454	99,6		WD	Parallel	548	N-S	Downhole
27/03/2022	I	F125S2064L	40,0	0,524	185,5	75	WOD	Parallel	1176	E-W	Up-hole
28/03/2022	I	F125S2064L	26,6	2,008	185,5	75	WOD	Parallel	473	N-S	Up-hole
28/03/2022	J	F410S2041	40,0	0,648	90,0	75	WOD	Spiral	597	N-S	Downhole
31/03/2022	I	F410S2041	26,8	1,836	90,0	75	WOD	Spiral	439	N-S	Downhole
31/03/2022	J	F410S2041	2,8	0,524	90,0	75	WOD	Spiral	1017	E-W	Downhole
01/04/2022	D	F160S2086L	40,0	2,800	94,1	75	WD	Parallel	305	N-S	Downhole
01/04/2022	I	F160S2086L	26,6	1,055	94,1	75	WD	Parallel	712	N-S	Downhole
01/04/2022	J	F360S2058AL	53,1	4,639	88,2	75	WOD	Parallel	399	N-S	Downhole
02/04/2022	I	F360S2058AL	26,6	5,256	88,2	75	WOD	Parallel	471	N-S	Downhole
02/04/2022	J	F360S2058AL	8,0	0,524	88,2	75	WOD	Parallel	1637	E-W	Downhole
04/04/2022	I	F125S2064L	27,8	2,342	176,4		WOD	Parallel	477	N-S	Up-hole
04/04/2022	J	F125S2064L	50,0	0,527	50,5	75	WOD	Parallel	588	N-S	Downhole
04/04/2022	I	M420S2007	50,0	0,568	93,2		WOD	Parallel	596	N-S	Downhole
04/04/2022	J	F410S2041	18,3	0,568	93,2		WOD	Parallel	441	N-S	Downhole
05/04/2022	I	F410S2041	26,6	2,118	93,2		WOD	Parallel	1293	E-W	Downhole
05/04/2022	J	F410S2041	21,5	0,696	93,2		WOD	Parallel	1010	E-W	Downhole
05/04/2022	J	F360S2058AL	40,0	4,107	89,3	75	WOD	Parallel	400	N-S	Downhole
05/04/2022	I	F360S2058AL	26,6	5,256	89,3	75	WOD	Parallel	466	N-S	Downhole
07/04/2022	J	F125S2064L	40,0	9,160	179,3	75	WOD	Parallel	181	E-W	Up-hole
07/04/2022	I	F125S2064L	26,6	1,276	179,3	75	WOD	Parallel	489	N-S	Up-hole
08/04/2022	I	F270S2069	53,4	2,898	75,0	75	WD	Parallel	280	E-W	Downhole
08/04/2022	J	F270S2069	26,6	1,892	75,0	75	WD	Parallel	549	N-S	Downhole
09/04/2022	I	F270S2069	2,8	0,568	75,0	75	WD	Parallel	1293	E-W	Downhole
09/04/2022	J	F410S2041	26,6	1,675	99,6	75	WOD	Parallel	441	N-S	Downhole
11/04/2022	I	F410S2041	2,1	0,568	99,6	75	WOD	Parallel	1009	E-W	Downhole
12/04/2022	I	F270S2053	39,9	5,355	180,0		WOD	Spiral	381	N-S	Up-hole
12/04/2022	J	F270S2053	26,6	5,342	180,0		WOD	Spiral	383	N-S	Up-hole
16/04/2022	J	F370S2051	13,2	2,071	187,4		WOD	Parallel	498	N-S	Up-hole
18/04/2022	I	F410S2041	26,9	1,283	92,7	75	WOD	Parallel	443	N-S	Downhole
18/04/2022	J	F370S2051	13,3	0,783	187,4		WOD	Parallel	1519	E-W	Up-hole
18/04/2022	I	F370S2051	14,0	0,696	187,4		WOD	Parallel	1134	E-W	Up-hole
18/04/2022	D	F270S2053	26,6	2,254	180,0		WOD	Parallel	381	N-S	Up-hole
18/04/2022	A	F270S2053	13,3	4,342	180,0		WOD	Parallel	382	N-S	Up-hole
19/04/2022	J	F270S2053	13,3	0,582	180,0		WOD	Parallel	1510	E-W	Up-hole
19/04/2022	I	F270S2053	13,4	0,648	180,0		WOD	Parallel	1109	E-W	Up-hole
24/04/2022	I	F370S2051	13,4	1,283	174,8		WOD	Parallel	496	N-S	Up-hole
24/04/2022	I	F370S2051	19,1	2,879	174,8		WOD	Parallel	442	N-S	Up-hole
26/04/2022	J	F370S2051	13,3	0,539	174,8		WOD	Parallel	1514	E-W	Up-hole
26/04/2022	D	F370S2051	13,4	0,648	174,8		WOD	Parallel	1128	E-W	Up-hole
27/04/2022	J	F125S2064L	26,8	2,102	125,0		WD	Parallel	452	N-S	Downhole
27/04/2022	J	M420S2007	50,0	0,556	55,0	75	WOD	Parallel	597	N-S	Downhole
27/04/2022	I	F125S2064L	40,0	0,554	125,0		WD	Parallel	1160	E-W	Up-hole
30/04/2022	I	F510S2027L	26,6	3,061	166,0	75	WOD	Parallel	576	E-W	Up-hole
02/05/2022	I	F125S2050L	61,3	3,441	85,0		WD	Spiral	391	N-S	Downhole
03/05/2022	J	F125S2050L	49,4	5,951	85,0		WD	Spiral	250	E-W	Downhole
03/05/2022	I	F125S2050L	3,0	0,582	85,0		WD	Spiral	1020	E-W	Downhole
04/05/2022	J	F270S2053	13,3	3,035	186,0	75	WOD	Parallel	377	N-S	Up-hole
04/05/2022	I	F270S2053	53,3	1,858	186,0	75	WOD	Parallel	387	N-S	Up-hole
06/05/2022	J	F370S2051	66,4	3,343	112,5		WD	Spiral	413	N-S	Downhole
06/05/2022	I	F125S2050L	13,1	4,540	92,5		WD	Parallel	399	N-S	Downhole
06/05/2022	D	F370S2051	12,9	1,972	112,5		WD	Spiral	466	N-S	Downhole
06/05/2022	A	F125S2050L	39,9	7,245	92,5		WD	Parallel	254	E-W	Downhole
07/05/2022	I	F125S2050L	12,5	0,539	92,5		WD	Parallel	1448	E-W	Downhole
07/05/2022	J	F370S2051	13,5	0,582	112,5		WD	Spiral	1120	E-W	Downhole
08/05/2022	J	F370S2051	13,4	1,024	114,6	75	WD	Parallel	462	N-S	Downhole
08/05/2022	I	F370S2051	13,4	1,746	114,6	75	WD	Parallel	415	N-S	Downhole
08/05/2022	D	F370S2051	3,0	0,582	114,6	75	WD	Parallel	1117	E-W	Downhole
09/05/2022	J	F125S2050L	40,0	5,047	80,5	75	WD	Parallel	263	E-W	Downhole
10/05/2022	J	F125S2050L	26,8	2,843	80,5	75	WD	Parallel	398	N-S	Downhole
10/05/2022	I	F370S2051	25,4	1,513	130,0	75	WD	Parallel	416	N-S	Downhole
10/05/2022	J	F370S2051	13,4	1,024	130,0	75	WD	Parallel	460	N-S	Downhole
11/05/2022	I	F125S2064L	46,3	4,246	30,0		WOD	Spiral	173	E-W	Up-hole
11/05/2022	J	F125S2064L	26,6	1,947	100,0		WD	Parallel	397	N-S	Downhole
11/05/2022	I	F270S2067	13,3	4,072	178,5		WOD	Parallel	537	N-S	Up-hole
11/05/2022	J	F270S2067	13,3	4,072	178,5		WOD	Parallel	314	E-W	Up-hole
11/05/2022	I	F125S2064L	31,1	4,423	35,0		WD	Spiral	168	E-W	Downhole
11/05/2022	J	F125S2064L	46,0	6,332	32,5		WD	Spiral	162	E-W	Downhole
11/05/2022	I	F125S2050L	26,6	1,947	100,0		WD	Parallel	397	N-S	Downhole
12/05/2022	I	F125S2050L	66,8	0,730	92,3	75	WD	Parallel	910	E-W	Downhole
14/05/2022	I	F510S2027L	40,0	0,355	176,0	75	WOD	Parallel	1132	E-W	Up-hole
	C	F370S2051	50,0	0,302	100,0	75	WD	Parallel	1217	E-W	Downhole

Database compiling information relative to the discarded monitored events:

Date	Monitored structure	Stope	Dominant frequency (Hz)	PVS (mm·s⁻¹)	Note	Date	Monitored structure	Stope	Dominant frequency (Hz)	PVS (mm·s⁻¹)	Note
08/02/2018	G	F430SZ036A	77,3	0,696	Trim blast	18/04/2019	G	F410SZ038	99,9	1,310	No Q determined
08/02/2018	I	F430SZ036A	58,3	1,180	Trim blast	28/04/2019	I	F370SZ024L	20,0	2,860	No Q determined
09/02/2018	I	F430SZ036A	29,0	0,582	Trim blast	28/04/2019	G	F370SZ024L	40,0	2,040	No Q determined
15/02/2018	I	F430SZ036A	48,0	0,635	Trim blast	09/05/2019	I	F310SZ030	20,0	2,050	No Q determined
21/03/2018	I	F410SZ038A	29,8	5,190	No Q determined	09/05/2019	I	F310SZ032	80,0	0,823	No Q determined
21/03/2018	G	F410SZ038A	31,0	4,360	No Q determined	09/05/2019	G	F310SZ030/32	20,0	1,030	No Q determined
27/04/2018	J	F310SZ054	33,8	0,696	No Q determined	15/05/2019	I	F410SZ063	21,0	1,280	Trim blast
29/04/2018	I	F310SZ044	20,0	4,730	No Q determined	15/05/2019	G	F410SZ063	21,0	0,596	Trim blast
29/04/2018	J	F310SZ044	60,0	2,080	No Q determined	22/07/2019	G	F270SZ068L	39,8	1,400	No Q determined
29/04/2018	G	F310SZ044	20,0	3,470	No Q determined	22/07/2019	I	F270SZ068L	27,3	2,540	No Q determined
30/04/2018	I	F310SZ064	20,0	2,110	No Q determined	02/10/2019	I	F270SZ050	19,8	2,190	Trim blast
30/04/2018	J	F310SZ064	40,2	7,190	No Q determined	02/10/2019	G	F270SZ050	20,3	1,220	Trim blast
30/04/2018	G	F310SZ064	20,0	1,700	No Q determined	02/10/2019	J	F270SZ050	40,0	2,090	Trim blast
04/05/2018	G	F410SZ038A	78,0	3,040	Trim blast	07/10/2019	J	F270SZ050	40,0	2,390	No Q determined
04/05/2018	I	F410SZ038A	21,5	1,980	Trim blast	07/10/2019	I	F270SZ050	24,9	4,100	No Q determined
04/05/2018	J	F410SZ038A	39,8	1,050	Trim blast	07/10/2019	G	F270SZ050	40,0	2,230	No Q determined
14/05/2018	J	F310SZ062L	40,0	6,430	No Q determined	08/11/2019	G	F270SZ030	45,0	0,539	Trim blast
14/05/2018	G	F310SZ062L	38,3	1,570	No Q determined	08/11/2019	I	F270SZ030	17,3	0,660	Trim blast
14/05/2018	I	F310SZ062L	21,3	2,230	No Q determined	26/11/2019	G	F270SZ063	22,8	1,580	No Q determined
15/05/2018	J	F310SZ062L	2,8	1,540	Trim blast	26/11/2019	I	F270SZ063	17,1	2,870	No Q determined
15/05/2018	G	F310SZ062L	42,0	0,596	Trim blast	26/11/2019	J	F270SZ063	36,8	8,080	No Q determined
15/05/2018	I	F310SZ062L	29,1	1,050	Trim blast	15/01/2020	J	F270SZ063	18,5	5,370	Trim blast
23/05/2018	J	F310SZ054	44,0	0,833	Trim blast	15/01/2020	G	F270SZ063	13,0	1,390	Trim blast
27/05/2018	J	F310SZ042	60,1	2,570	No Q determined	24/01/2020	J	F270SZ068	19,0	2,480	Trim blast
27/05/2018	I	F310SZ042	20,0	4,760	No Q determined	24/01/2020	I	F270SZ068	20,0	0,751	Trim blast
27/05/2018	G	F310SZ042	20,0	3,390	No Q determined	24/01/2020	G	F270SZ068	41,0	0,524	Trim blast
01/06/2018	G	F310SZ058L	32,8	1,450	Trim blast	06/03/2020	I	F410SZ044	76,8	0,852	Trim blast
01/06/2018	J	F310SZ058L	66,9	3,100	Trim blast	16/04/2020	I	F310SZ047	19,5	2,600	Trim blast
13/06/2018	J	F310SZ054	2,3	0,751	Trim blast	29/05/2020	J	F310SZ070AR	39,9	4,440	Trim blast
21/06/2018	I	F310SZ066	30,6	1,370	No Q determined	29/05/2020	G	F310SZ070AR	79,9	0,823	Trim blast
21/06/2018	J	F310SZ066	45,4	7,130	No Q determined	29/05/2020	I	F310SZ070AR	25,8	1,220	Trim blast
21/06/2018	G	F310SZ066	16,0	1,250	No Q determined	26/08/2020	I	F310SZ049	16,5	0,582	Trim blast
29/06/2018	G	F310SZ058L	32,3	1,490	No Q determined	27/08/2020	I	F370SZ061L	25,3	0,684	Trim blast
29/06/2018	J	F310SZ058L	40,1	2,400	No Q determined	09/09/2020	J	F310SZ071	3,0	0,648	Trim blast
29/06/2018	I	F310SZ058L	30,0	1,550	No Q determined	22/09/2020	I	F310SZ049	3,0	0,648	Trim blast
04/07/2018	G	F410SZ062	30,8	2,390	No Q determined	23/09/2020	I	F410SZ039	21,5	1,410	Trim blast
04/07/2018	J	F410SZ062	46,1	3,210	No Q determined	19/10/2020	I	F270SZ038L	22,3	0,950	Trim blast
04/07/2018	I	F410SZ062	30,5	1,930	No Q determined	30/10/2020	J	F410SZ050AR	40,0	0,741	Trim blast
17/07/2018	I	F310SZ054	31,0	2,700	No Q determined	30/10/2020	I	F410SZ050AR	26,8	0,648	Trim blast
17/07/2018	G	F310SZ054	30,6	1,580	No Q determined	02/11/2020	J	F410SZ050AR	3,0	0,568	Trim blast
23/07/2018	I	F310SZ070	27,3	0,582	Trim blast	02/11/2020	I	F410SZ050AR	3,0	0,554	Trim blast
23/07/2018	G	F310SZ070	116,0	1,450	Trim blast	03/11/2020	I	F410SZ047	20,8	1,000	Trim blast
29/08/2018	G	F310SZ072	22,6	0,684	No Q determined	16/12/2020	J	F370SZ044AL	53,3	1,570	Trim blast
29/08/2018	J	F310SZ072	123,0	8,360	No Q determined	16/12/2020	I	F370SZ044AL	26,6	2,820	Trim blast
29/08/2018	I	F310SZ072	30,8	1,100	No Q determined	21/12/2020	J	F230SZ072	59,5	1,970	Trim blast
01/09/2018	J	F310SZ072	69,8	4,820	Trim blast	30/12/2020	J	F230SZ072	47,0	1,430	Trim blast
01/09/2018	I	F310SZ072	20,0	0,751	Trim blast	19/01/2021	J	F210SZ076L	33,4	4,160	Trim blast
03/09/2018	J	F310SZ070	53,0	1,920	Trim blast	19/01/2021	I	F210SZ076L	26,6	1,120	Trim blast
03/09/2018	I	F310SZ070	27,5	0,635	Trim blast	30/01/2021	J	F370SZ044AL	140,0	0,524	Trim blast
11/09/2018	J	F310SZ042	120,0	3,590	No Q determined	30/01/2021	I	F370SZ044AL	15,8	0,773	Trim blast
12/09/2018	J	F310SZ070	44,0	3,320	Trim blast	03/02/2021	H	M440SZ007	40,0	0,696	No Q determined
19/09/2018	I	F430SZ038	18,0	1,000	Trim blast	03/02/2021	I	F370SZ044AL	16,5	1,050	Trim blast
19/09/2018	B	F430SZ038	2,5	0,762	Trim blast	22/03/2021	I	F370SZ044AL	28,8	1,390	Trim blast
19/09/2018	J	F430SZ038	98,5	0,762	Trim blast	26/03/2021	J	F310SZ051	13,3	0,959	Trim blast
19/09/2018	G	F430SZ038	18,8	0,959	Trim blast	26/03/2021	I	F310SZ051	16,5	1,280	Trim blast
02/10/2018	B	F270SZ064	60,0	4,040	No Q determined	01/05/2021	A	F310SZ026R	3,0	0,524	No Q determined
02/10/2018	I	F270SZ064	19,0	1,800	No Q determined	03/06/2021	D	F230SZ038L	167,0	0,813	Trim blast
02/10/2018	G	F270SZ064	21,3	0,898	No Q determined	03/06/2021	J	F230SZ038L	50,0	0,813	Trim blast
02/10/2018	J	F270SZ064	60,0	9,580	No Q determined	03/06/2021	I	F230SZ038L	20,0	1,300	Trim blast
14/10/2018	G	F410SZ042	46,1	2,510	No Q determined	19/09/2021	I	F230SZ073	27,5	1,024	Trim blast
14/10/2018	I	F410SZ042	30,8	3,240	No Q determined	23/09/2021	J	F230SZ068	50,0	2,132	Trim blast
14/10/2018	J	F410SZ042	92,3	1,420	No Q determined	23/09/2021	J	F230SZ073	50,0	1,161	Trim blast
16/10/2018	J	F310SZ046	100,0	2,640	No Q determined	23/09/2021	I	F230SZ068	25,0	0,539	Trim blast
16/10/2018	G	F310SZ046	20,0	3,810	No Q determined	11/10/2021	I	F370SZ058AL	26,3	3,438	Trim blast
16/10/2018	I	F310SZ046	20,0	5,810	No Q determined	11/10/2021	J	F370SZ058AL	50,0	4,734	Trim blast
06/11/2018	J	F430SZ038	52,8	0,648	Trim blast	12/10/2021	I	F370SZ039	26,6	1,555	Trim blast
06/11/2018	G	F430SZ038	20,5	0,741	Trim blast	23/12/2021	I	F370SZ058AL	20,3	1,675	Trim blast
06/11/2018	I	F430SZ038	30,0	1,110	Trim blast	23/12/2021	J	F370SZ058AL	50,0	1,303	Trim blast
11/11/2018	J	F310SZ068	46,1	4,690	No Q determined	03/01/2022	J	F210SZ056	50,0	1,513	Trim blast
11/11/2018	G	F310SZ068	16,1	0,751	No Q determined	14/01/2022	D	F510SZ037AL	23,8	0,568	No Q determined
11/11/2018	I	F310SZ068	30,9	1,210	No Q determined	29/01/2022	A	F510SZ037AL	27,0	0,696	Trim blast
12/12/2018	J	F410SZ060	32,3	2,600	No Q determined	29/01/2022	I	F510SZ037AL	26,6	4,420	Trim blast
12/12/2018	I	F410SZ060	20,0	1,570	No Q determined	16/03/2022	J	F210SZ056B	53,5	1,055	Trim blast
12/12/2018	G	F410SZ060	29,1	1,310	No Q determined	23/04/2022	J	F510SZ037AL	26,3	0,539	Trim blast
02/01/2019	I	F270SZ074	31,0	1,080	No Q determined	23/04/2022	I	F510SZ037AL	26,5	1,529	Trim blast
02/01/2019	J	F270SZ074	60,1	7,040	No Q determined	18/05/2022	J	F125SZ050L	40,0	5,839	Trim blast
02/01/2019	G	F270SZ074	60,1	0,660	No Q determined	18/05/2022	D	F125SZ050L	26,6	0,582	Trim blast
15/01/2019	I	F410SZ023L	3,0	0,539	Trim blast	18/05/2022	I	F125SZ050L	53,4	3,429	Trim blast
25/01/2019	J	F410SZ054	40,1	1,710	No Q determined	18/05/2022	D	F125SZ050L	26,6	0,582	Trim blast
25/01/2019	I	F410SZ054	19,9	1,650	No Q determined	27/05/2022	I	F510SZ027L	46,8	4,050	Trim blast
25/01/2019	G	F410SZ054	39,9	1,160	No Q determined	27/05/2022	D	F510SZ027L	33,0	0,582	Trim blast
18/02/2019	I	F270SZ054	27,0	0,684	Trim blast	30/05/2022	I	F510SZ037AL	27,0	1,492	No Q determined
18/02/2019	J	F270SZ054	108,0	1,110	Trim blast	01/06/2022	J	F510SZ037AL	19,3	0,539	Trim blast
19/02/2019	G	F310SZ043	30,5	1,700	Trim blast	01/06/2022	I	F510SZ037AL	26,6	2,565	Trim blast
19/02/2019	J	F310SZ043	44,3	1,000	Trim blast	07/06/2022	J	F370SZ061L	26,6	0,950	Trim blast
19/02/2019	I	F310SZ043	30,0	3,290	Trim blast	07/06/2022	I	F370SZ061L	17,0	0,861	Trim blast
21/02/2019	J	F310SZ032	108,0	1,030	No Q determined	17/06/2022	D	F510SZ027L	40,0	0,539	Trim blast
21/02/2019	G	F310SZ032	46,1	1,060	No Q determined	25/06/2022	J	F125SZ064L	114,3	3,021	Trim blast
21/03/2019	I	F410SZ040A	60,0	1,400	Trim blast	28/06/2022	H	M420SZ007	50,0	0,522	Trim blast
21/03/2019	G	F410SZ040A	60,0	0,783	Trim blast	30/06/2022	J	F125SZ064L	39,9	4,410	Trim blast
07/04/2019	J	F310SZ034	100,0	1,350	No Q determined	30/06/2022	I	F125SZ064L	66,5	0,741	Trim blast
07/04/2019	G	F310SZ034	40,0	1,820	No Q determined	14/07/2022	J	F125SZ064L	39,5	10,210	Trim blast
07/04/2019	I	F310SZ034	60,0	2,650	No Q determined	14/07/2022	I	F125SZ064L	40,3	1,503	Trim blast
18/04/2019	I	F410SZ038	16,0	2,040	No Q determined						

Annex C - Example of Event and FFT reports from a monitored vibration event

The considered records were measured at structure E and generated after a blast at stope F510SZ027L on August 1st, 2022.

Event report:

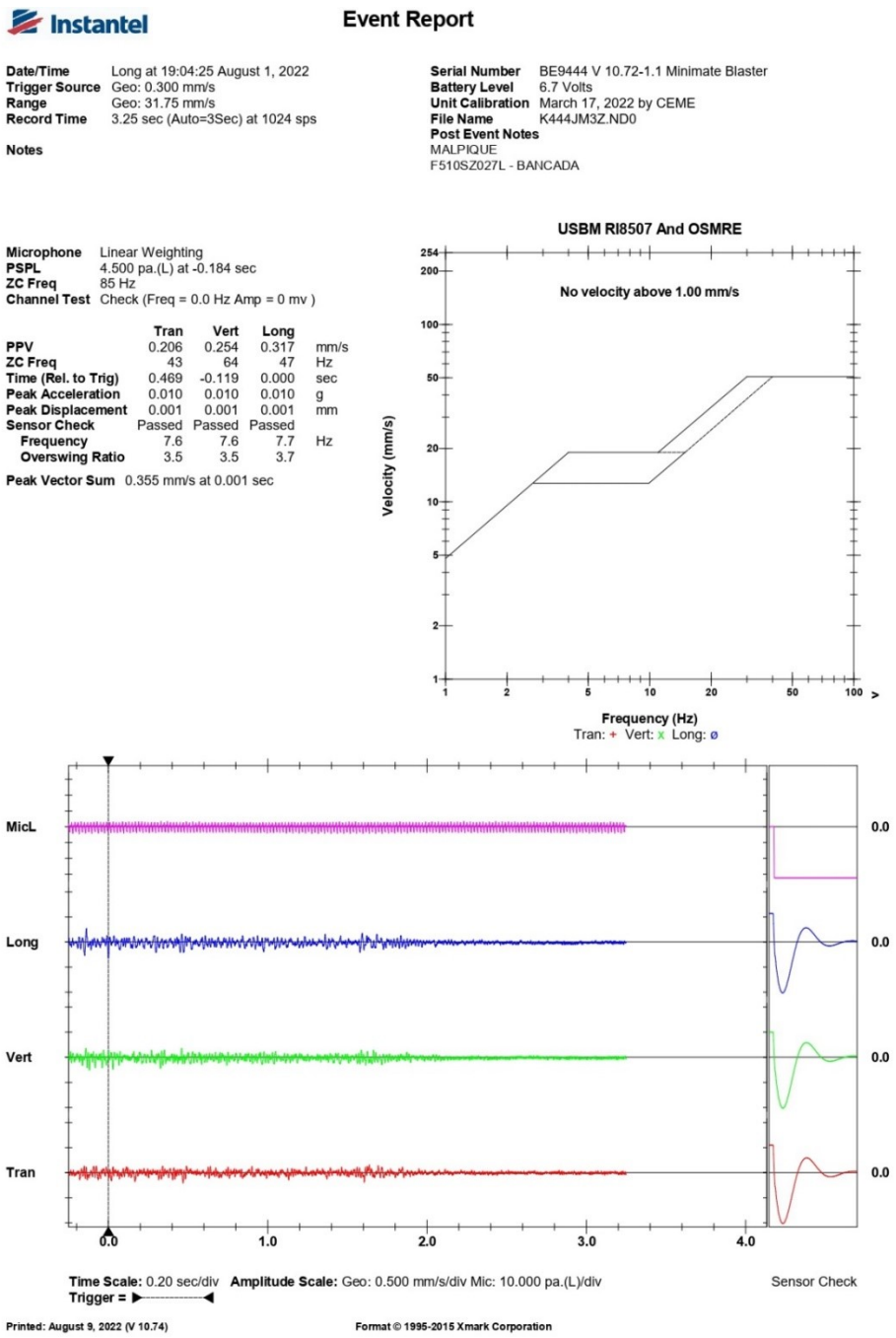

FFT report:

Instantel

FFT Report

Date/Time	Long at 19:04:25 August 1, 2022	**Serial Number**	BE9444 V 10.72-1.1 Minimate Blaster
Trigger Source	Geo: 0.300 mm/s	**Battery Level**	6.7 Volts
Range	Geo: 31.75 mm/s	**Unit Calibration**	March 17, 2022 by CEME
Record Time	3.25 sec (Auto=3Sec) at 1024 sps	**File Name**	K444JM3Z.ND0

Notes

Post Event Notes
MALPIQUE
F510SZ027L - BANCADA

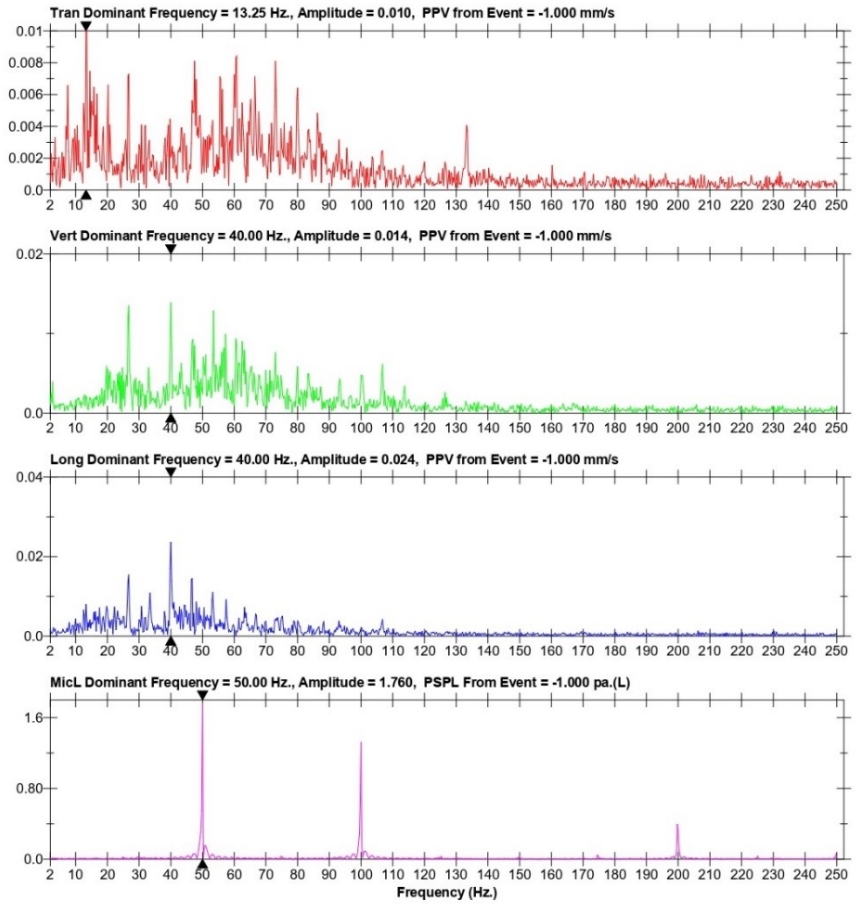

Printed: August 9, 2022 (V 10.74)

In this event, the dominant frequency is equal to 40 Hz.

Annex D - Structures porosity and building materials' propagation velocity results

This section compiles data measured at the four studied structures, essential to estimate the respective porosity and building materials' propagation velocity. The volume of structural elements at each building is calculated by the sum of the volumes equivalent to the existing pillars at the respective floor and to the slab corresponding to the ceiling.

Structure A:

Travel time (µs)	Distance (cm)	C_P (m·s^{-1})	$\overline{C_P}$ (m·s^{-1})
38,8	5	1.288,7	3.152,2
34,2	10	2.924,0	
34,9	15	4.298,0	
48,8	20	4.098,4	
11,4	25	-	
27,6	30	-	

Total structure volume (m³)	911,7
Volume of structural elements (m³)	331,7
Porosity	0,64

Structure C:

Travel time (µs)	Distance (cm)	C_P (m·s^{-1})	$\overline{C_P}$ (m·s^{-1})
25	5	2.000,0	2.189,7
45,7	10	2.188,2	
56,3	15	2.664,3	
82,3	20	2.430,1	
128,8	25	1.941,0	
156,7	30	1.914,5	

Cellar	**Floor volume (m³)**	1.132,8
	Structural elements volume (m³)	164,4
First floor	**Floor volume (m³)**	990,9
	Structural elements volume (m³)	92,4
Second floor	**Floor volume (m³)**	452,7
	Structural elements volume (m³)	41,1
Total structure volume (m³)		2.576,4
Volume of structural elements (m³)		297,9
Porosity		0,88

Structure D:

Travel time (µs)	Distance (cm)	C_P (m·s^{-1})	$\overline{C_P}$ (m·s^{-1})
30,5	5	1.639,3	2.030,9
53,4	10	1.872,7	
70,4	15	2.130,7	
91,8	20	2.178,6	
118,2	25	2.115,1	
133,4	30	2.248,9	

Cellar	**Floor volume (m³)**	1.720,9
	Structural elements volume (m³)	120,3
First floor	**Floor volume (m³)**	1.018,0
	Structural elements volume (m³)	130,1
Second floor	**Floor volume (m³)**	887,5
	Structural elements volume (m³)	230,0
Total structure volume (m³)		3.626,3
Volume of structural elements (m³)		480,4
Porosity		0,87

Structure E:

Travel time (µs)	Distance (cm)	C_P (m·s^{-1})	$\overline{C_P}$ (m·s^{-1})
25,3	5	1.976,3	2.383,0
49,6	10	2.016,1	
64,7	15	2.318,4	
73,3	20	2.728,5	
92,7	25	2.696,9	
117,1	30	2.561,9	

Total structure volume (m³)	2,3
Volume of structural elements (m³)	216,9
Porosity	0,99